Title
Cobalt and Nickel-Based Organometallic Chemistry of the [N]Phenylenes

Author
Padilla, Robin

Publication Date
2010

Peer reviewed|Thesis/dissertation

Cobalt and Nickel-Based Organometallic Chemistry of the [*N*]Phenylenes

by

Robin Padilla

A dissertation submitted in partial satisfaction of the

requirements for the degree of

Doctor of Philosophy

in

Chemistry

in the

Graduate Division

of the

University of California, Berkeley

Committee in Charge:

Professor K. Peter C. Vollhardt, Chair
Professor Jonathan A. Ellman
Professor Yuri Suzuki

Spring 2010

Cobalt and Nickel-Based Organometallic Chemistry of the [*N*]Phenylenes

by Robin Padilla

Abstract

Cobalt and Nickel-Based Organometallic Chemistry of the [*N*]Phenylenes

by

Robin Padilla

Doctor of Philosophy in Chemistry

University of California, Berkeley

Professor K. Peter C. Vollhardt, Chair

This dissertation explores the synthesis and study of linear [*N*]phenylene cobalt complexes and the reactions of angular [*N*]phenylenes with nickel catalysts. Chapter 1 contains a general introduction to the properties of the [*N*]phenylenes as well as a brief overview of earlier organometallic [*N*]phenylene chemistry with an emphasis on work directly related to that presented in the subsequent chapters.

Chapter 2 presents studies regarding first ever examples of photo-induced, thermally reversible haptotropic shifts in linear [3]phenylene cyclopentadienyl cobalt (CpCo) complexes. In these reactions, the CpCo fragment migrates from one cyclobutadiene ring to another upon exposure to UV irradiation. Heating the photoisomer complexes causes the metal fragment to return to its original position. Aside from the novelty of an η^4:η^4 cyclobutadiene migration, the photo-induced, thermally reversible nature of these systems makes them attractive as candidates for photostorage devices and/or molecular switches. The syntheses and structural studies of the linear phenylene(CpCo) complexes are discussed. In addition to the experimental work, computational studies on the haptotropic shift are also included. Closely related work, such as the observation of an intermediate haptotropic species at low temperature and the preparation of a linear [3]phenylene complex containing two CpCo units bound to the ligand, is also discussed.

Chapter 3 describes nickel-catalyzed insertion reactions with angular phenylenes as a method for preparing derivatives of [N]phenacenes, a class of polycyclic aromatic hydrocarbons that are of interest in organic electronic applications. Previous work regarding nickel insertion reactions with biphenylene is mentioned. Nickel-catalyzed insertion reactions with angular [3]- and [4]phenylene are then described. Mechanistic studies, both experimental and computational, are discussed. The results from these studies were used to optimize the reaction to produce [N]phenacenes as the major products of these insertion reactions.

Chapter 4 contains experimental details relating to chapters two and three. General experimental considerations, synthetic procedures, crystallographic, and computation data are presented. Relevant references are also included in this chapter.

Table of Contents

Acknowledgements

"Where would I find leather enough to cover the surface of the earth?
The Earth is covered over merely with the leather of my sandals".
-Shāntideva in the Bodhicaryāvatārah: Ch. 4., v.13

Five years ago, I arrived in Berkeley with a rather clear objective: get (or rather survive) a Ph.D. Though the goal never changed, the all paths (scientific, personal, professional, and spiritual) I traversed were often quite unlike anything I could have anticipated. I have had the great fortune to stand on the shoulders of many giants during these past few years and it is to them that I owe my deepest gratitude. First and foremost, I would like to thank my advisor, Peter Vollhardt, for all of his support and patience. The things I have learned from him are far too numerous to list but certainly the two most important are clarity and rigor, two qualities that extend far beyond the chemical realm.

Working with so many different people was another interesting, challenging, and ultimately highly rewarding experience. I am particularly indebted to "The Old Gang", consisting, in part, of Phil Leonard and Ken Windler. These two gentlemanly, pyromaniacal firearms enthusiasts, aside from showing me the ins and outs when I was a new arrival (and teaching me more than I will ever need to know about guns and explosives), soon became good and close friends. No mention of The Gang would be complete without Jordan Rose Figura. Despite being a chemical biologist and not actually a member of the Vollhardt Group, she nonetheless (somehow?) managed to fit in perfectly. My life has been forever changed by her introducing me to "Doctor Who".

Many others also deserve special mention. Sabine Amslinger has and will continue to provide a near endless amount of legendary stories that often border on mythological. Tom Gadek was just plain awesome. Vince Gandon, aside from being one the best experimentalists I've seen, also happened to have a rather fine taste in films and music. Dominik Hager excelled at getting me out of the lab for an occasional weekend of fun. The elegant and refined chocolate cakes of Aude Hubaud were a rare yet very welcome occurrence. Her sassy, chic comments on all aspects of life, however, were quite copious. Greg Boursalian performed an excellent job of filling the "cool undergrad" spot and I wish him the best for his own graduate school journey. Steve Meier managed the Herculean task of (legally) disposing of all those old, empty gas cylinders. It is my great hope that Prof. Sgt. Meier will share many (but certainly not all) of his Berkeley experiences with the next generation of chemists that he will educate. Explaining the strange and quirky aspects of American culture and the English language to Kerstin Weiß made for a fair number of humorous conversations. Learning the stranger and quirkier aspects of German language and culture made for many more. Similarly, much time was spent meticulously examining the lyrics and slang expressions of assorted hip-hop songs with Sander Oldenhof. Practicing kindergarten level German while sharing a fairly constant supply of Ritter Sport bars with Verena Engelhardt was another fine example of cultural exchange. Despite his best efforts, Kasper Moth-Poulsen has yet to convince me that Volvo is the greatest vehicle manufacturer in the known universe. My cultural exposure was not limited to European interactions, however, and I managed to learn a little Chinese as well. Apparently "Hao Shen"

means “MacGyver” in Mandarin.

I would also like to thank the rest of my co-workers, past and present, for all of their support. They are, in rough chronological order: Thomas Carl, Miles Carter, Kaspar Schärer, Ingo Janser, Romy Michiels, Elisa Paredes, Thilo Heckrodt, Nicholas Cheron, Alex Lee, Anais Geny, Samer Al-Gharabli, Nicole Franssen, Vladislav Kulikov, Alexandra Romek, Isaac Ho, Zhenhua Gu, Florian Montermini, Nikolai Vinokurov, Robert Zitterbart, and Cedric Ghellamallah.

Bonnie Kirk skillfully handled the various arcane, administrative procedures but also provided many interesting and memorable early morning conversations. The finer points of NMR spectroscopy were taught to me by the indomitable Rudi Nunlist. His wry humor and outlook on life were often the perfect supplement to the rigors of graduate school life. Working with Chris Canlas, Rudi’s able successor, has also been a pleasure. I was encouraged when he was so quick to remind me that I have the same name as a bad-boy Filipino action-movie star.

Teaching, while always quite time consuming, proved to be an invaluable experience. Teaching under the direction of Peter, the man who wrote the book on organic chemistry, was quite an adventure. His passion and talent for teaching are immediately obvious and inspiring, even without flipping through the Basque translation of his textbook. Jon Ellman’s ability to write exams that are easy to grade but difficult for students to take is similarly awe inspiring. There is no doubt in my mind that Heino Nitsche has taken teaching of general chemistry to new levels of eccentricity and excitement. Jean Fréchet’s impressive aptitude for lecturing is, perhaps, surpassed only by the impressiveness of his wine collection.

Looking down the academic chain, I have to acknowledge many of the brilliant and wonderful students that made teaching such a fantastic experience. Special thanks goes to Steve Seyedin, Nellie Ekmejian, Jessie Zhang, Yao Yue, Ashley Johnson, Brent Jellen, Zarina Khan, and Mojgan Rastegar, all of whom were extraordinary students that I hope will do their part to save the world.

No acknowledgement could be complete without recognizing the love and support of my family, in particular my mother. Her love, though always tough, was always there.

My various housemates also provided me with some great times. Chris Trinh, my first housemate in Berkeley, was a superb fellow to live with, and I will always fondly remember our conversations on life, love, and quantum gravity. Cory McLitus, when he wasn’t slaving away in the architecture studio, also became a good friend. I feel no need to apologize for getting him hopelessly addicted to “The Big Bang Theory”. The awesome Samra Kasim was always ready for chai, good food, and hearty discussions on Bollywood and all things South Asian. The housemates of 1505 Oxford St. are also great people. Though we rarely cross paths, Vicky Zhuang’s highly entertaining biology lab adventures are much appreciated. Vannamaria Kalafonos always has something wonderful going on in the kitchen and I aspire to learn the Greek specialty of cooking for a zillion people from her. The cats, Pink, Tuffy, and especially Floyd, are nice companions even though they sleep a combined 60 hours per day.

Many *kalyānamitras* helped me get through the toughest times and to them, I am especially grateful. A large number of my Saturday evenings were spent in the calm environs of the Berkeley Monastery, where Rev. Heng Sure’s Avataṃsaka Sūtra

lectures gave me much to think about. The monthly lectures by Ajahn Amaro, Ajahn Passano, and the Abhayagiri Sangha were also a wonderful learning experience. Chats about long-dead ancient languages and obscure texts with Sean Kerr, a fellow survivor of Dagmar Theison's German class, will also be fondly remembered. The NY Sangha, though far away, always supported me and welcomed me warmly whenever I returned home. Frank Yao, Hai-Dee Lee, Sheila Sussman, Fred Ng, Martin Applebaum, Josephine Verceles, Tiffany Taulton, Phung Tran, and especially Aaron Vederman repeatedly reminded me to "smile, breath deep, and go slowly". The many visits to Bodhi Monastery were always the high points of my summers. Michael Roehm, Bhikkhu Bodhi, Jane Berry, Henry and Lily Teoh, Marcie Barth, Mahendra Sagar, the dearly departed Felicia Miller, Ven. Guo Jun, Susan Chastain, and the polygot Bhikkhu Analayo made every visit an unforgettable experience and never failed to remind me why I get out of bed in the morning.

Chapter One

Properties of the [*N*]Phenylenes and Their Organometallic Chemistry

1.1 General Discussion of [*N*]Phenylene Properties

Polycyclic aromatic hydrocarbons (PAHs) are a class of molecules that have occupied the minds of chemists for generations.[1] Their essential feature, aromaticity, is the unusual stabilization that arises from having a 4n+2 number of π-electrons in a cyclical array. This seemingly simple definition obscures the fact that aromaticity continues to be one of the most scrutinized topics in modern organic chemistry[2] and more rigorous definitions[3] have remained elusive. Much of the early work[4] with PAHs was aimed at investigating theoretical issues surrounding aromaticity. There has been renewed interest in these systems in recent years because they are increasingly attractive as functional materials in organic-based electronics.[5] Of the many different kinds of PAHs known, e.g., **1**–**6** (Figure 1.1), one subclass is of particular interest: the [*N*]phenylenes.[6]

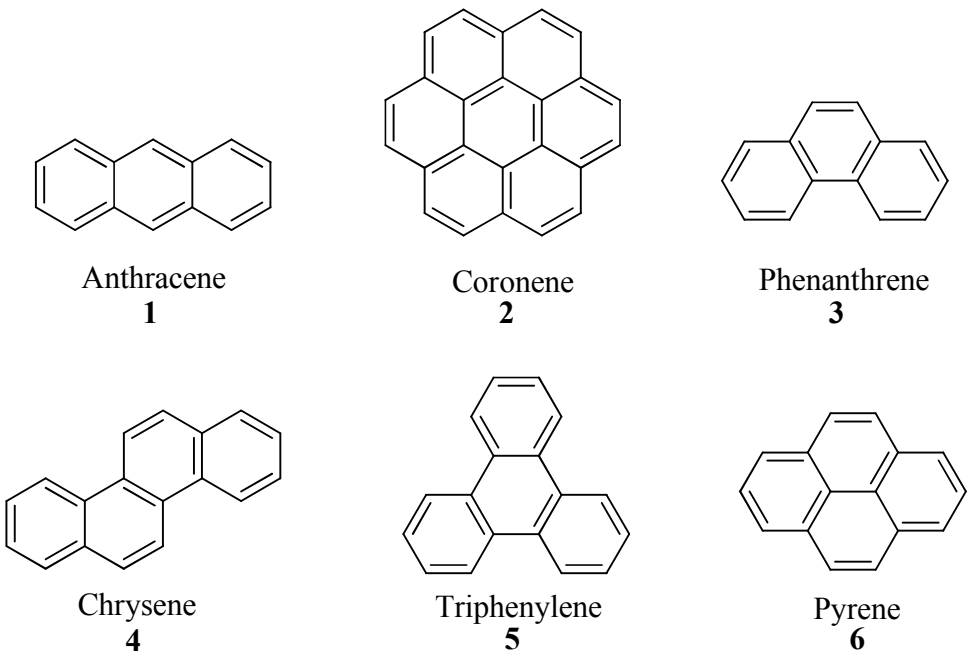

Figure 1.1. Some examples of polycyclic aromatic hydrocarbons.

The [*N*]phenylenes (where *N* = the number of benzene rings) are PAHs in which benzene and cyclobutadiene rings are fused in an alternating manner. The cyclobutadiene ring imparts very unusual structural and electronic properties, as seen in the simplest molecule in the series, biphenylene (**7**). It can be described by several resonance forms (Figure 1.2, a–e) in which the major contributor **7c** avoids formation of the highly destabilizing, antiaromatic cyclobutadiene (**7a**, **7e**) and benzocyclobutadiene circuit (**7b**, **7d**). This preference is manifest in the significant bond alternation[7] seen in

the crystal structure of biphenylene (Figure 1.2), which shows a clear difference in bond lengths between the formal single bonds (~1.43 Å) and the shorter formal double bonds (~1.37 Å).

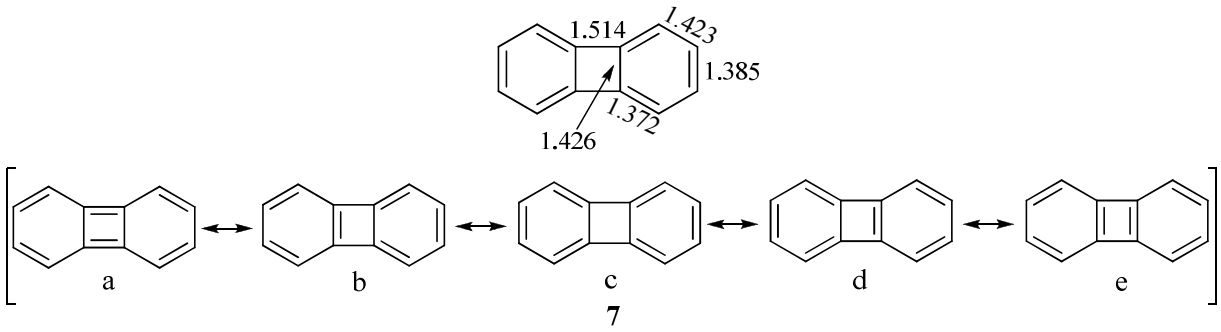

Figure 1.2. Biphenylene bond lengths (top; Å) and resonance contributors (bottom).

An extreme example of [*N*]phenylene π-bond localization is triangular [4]phenylene (**8**) (Scheme 1.1), in which the three-fold peripheral fusion imparts complete cyclohexatriene character on the central ring.[8,9a] This property is reflected in the reactivity of the system, e.g., catalytic hydrogenation (**9**),[8b] epoxidation (**10**),[8c] and cyclopropanation (**11**).[8c]

Scheme 1.1. Reactions Illustrating the Fully Bond Localized Character of the Central Benzene Ring in Triangular [4]Phenylene **8**. Bond lengths are in Å

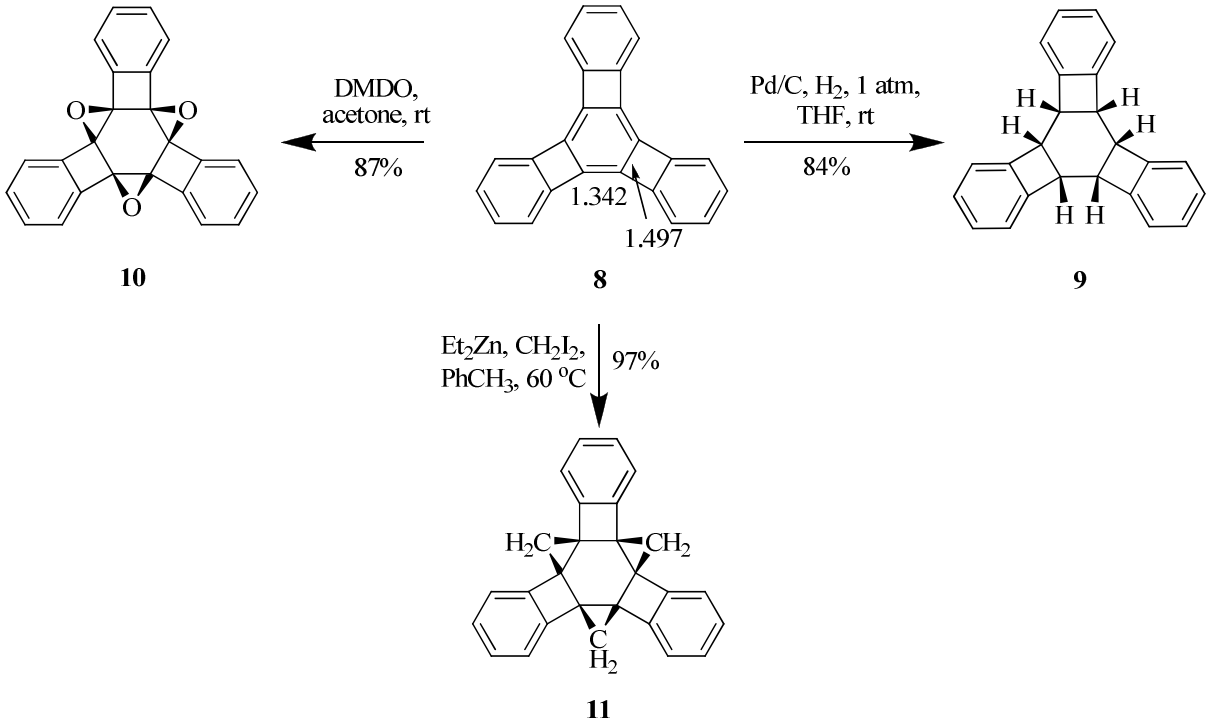

Phenylenes exhibit another interesting structural feature in contrast to other PAHs: sizable deviations from planarity (Figure 1.3).[9a,b] The flexibility of the phenylene framework arises from the combined effect of π- and σ-strain.[9a,b] By adopting a nonplanar geometry, overlap between the π-orbitals is diminished and in turn leads to a decrease in destabilizing, antiaromatic character. Pyramidalization of the four-membered ring carbons also reduces σ-strain,[9a,b] a phenomenon observed in highly strained alkene systems.[9c]

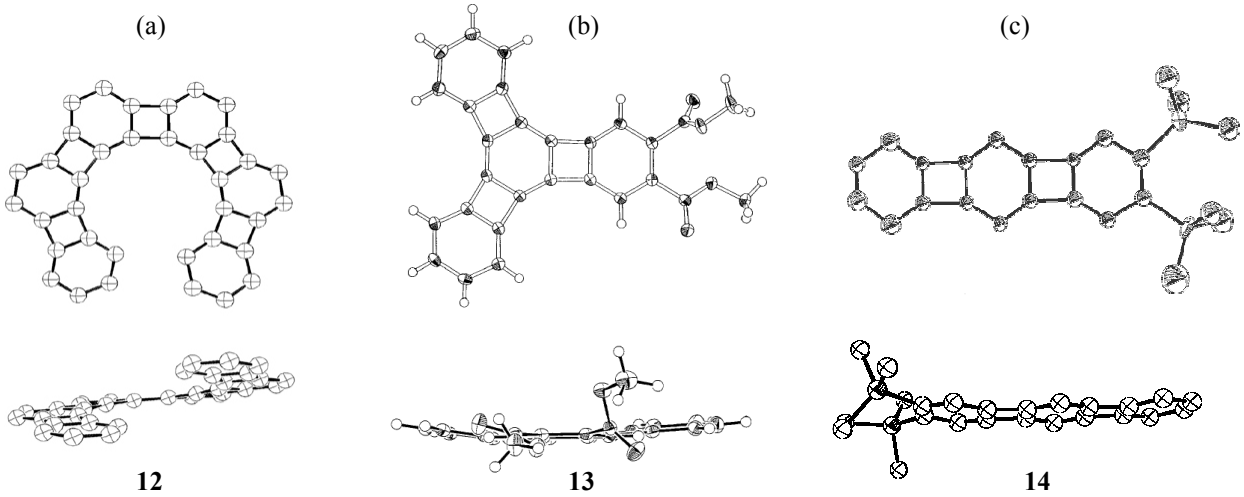

Figure 1.3. Crystal structures showing deviations from planarity in (a) helical [6]phenylene (**12**),[10] (b) dimethyl triangular [4]phenylene-2,3-dicarboxylate (**13**),[9a] and (c) 2,3-bis(tri-methylsilyl) linear [3]phenylene (**14**).[9a]

The fusion of aromatic benzene rings with antiaromatic cyclobutadiene units in the same molecule has prompted numerous experimental and theoretical discussions[6] regarding the magnetic and electronic properties of the phenylenes. ^{1}H-NMR spectroscopy is one typical measure of aromaticity. Protons on the exterior of aromatic rings (e.g., **15**) show relatively low field resonances, while their interior counterparts resonate at relatively high field, due to the presence of a diamagnetic ring current. Conversely, antiaromatic rings with 4n π-electrons are paratropic and reveal the opposite disposition of the two respective types of protons (e.g., **16**). The interplay between aromatic and antiaromatic character in the phenylenes is evident in their chemical shifts, which tend to show weakly aromatic resonances (Figure 1.5) relative to benzene (7.36 ppm).

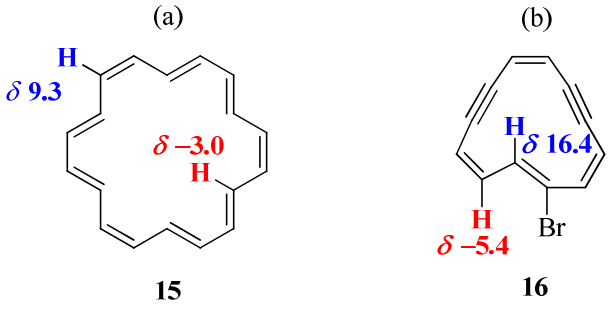

Figure 1.4. Observed ^{1}H-NMR resonances in (a) the aromatic [18]annulene (**15**)[11] and (b) the antiaromatic 5-bromo-1,9-bisdehydro-[12]annulene (**16**).[12]

Aside from NMR spectroscopy, nucleus independent chemical shift (NICS)[13] calculations have also proven to be useful measures of aromaticity. The NICS technique works by calculating the magnetic shielding of a "ghost nucleus" that can be positioned anywhere around a molecule. For probing aromaticity, the calculated point is in the center of the π-electron circuit to be examined. Calculations placing the ghost nucleus 1 Å above the plane of the molecule are often used to minimize local anisotropy and are referred to as NICS(1).[14] NICS data are given in ppm and are thus comparable to experimental ^{1}H-NMR measurements. Negative NICS values indicate aromatic character, while positive values suggest antiaromatic character. For example, the NICS(1) of benzene[15] is –12.5 ppm, whereas for cyclobutadiene[15] it is 15.1 ppm. NICS calculations for various phenylenes have been carried out[6] and are shown in Figure 1.5, alongside the experimentally measured ^{1}H-NMR chemical shifts. The attenuated aromatic character of the benzene and the relatively weak antiaromatic character of the cyclobutadiene rings in phenylenes, such as biphenylene (**7**), triangular [4]phenylene (**8**), and angular [4]phenylene (**17**), are apparent from both sets of data.

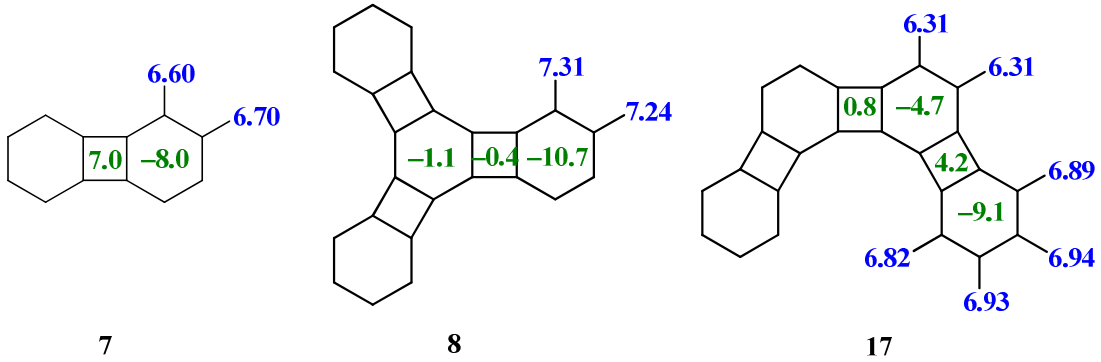

Figure 1.5. ^{1}H-NMR (blue) and NICS(1) (green) data for selected phenylene topologies (ppm).[6]

The phenylenes possess multiple modes of reactivity,[7] as illustrated by biphenylene (**7**) in Scheme 1.2. It can undergo electrophilic aromatic substitution like other PAHs, but does so selectively at the 2-position to avoid the formation of intermediates with antiaromatic character. Biphenylene does not readily undergo Diels-

Alder reactions, but was shown to react with electron-deficient benzynes to give the corresponding cycloadducts.[16] Opening of the highly strained four-membered ring is another prominent aspect of phenylene reactivity.

Scheme 1.2. Illustrative Reaction Pathways of Biphenylene[6]

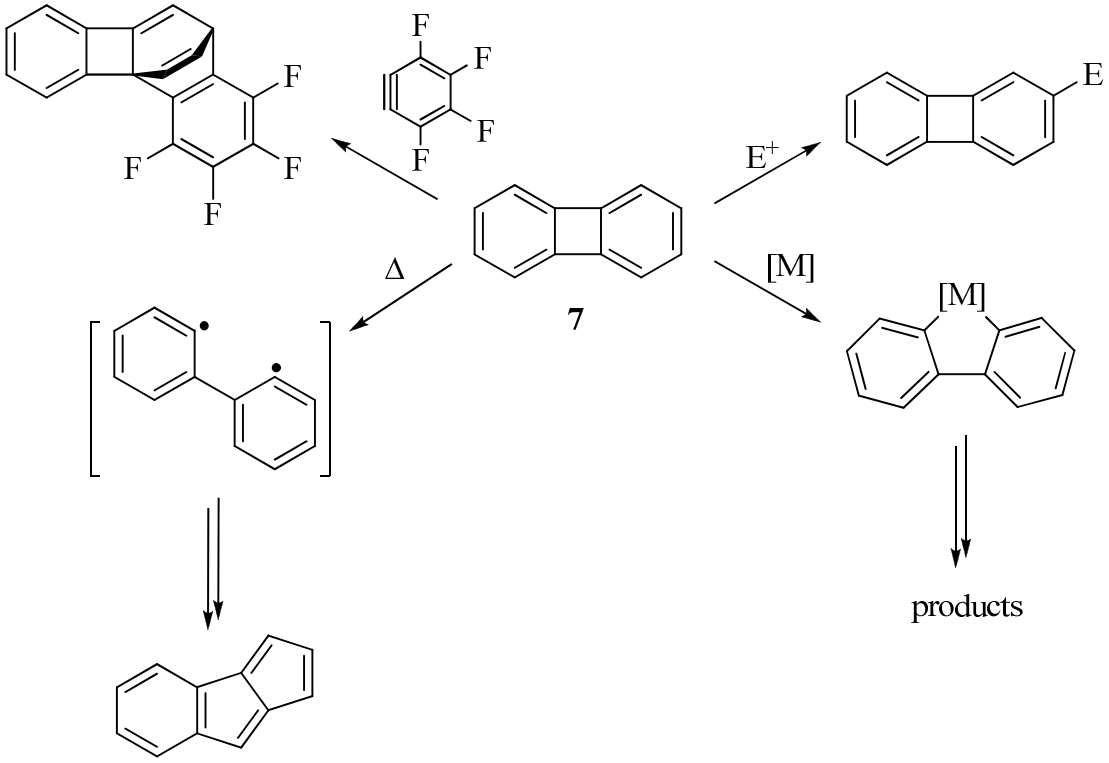

Early work[17] showed that it was possible to cleave the aryl-aryl C-C bonds via thermolysis in the neat state. Rupture of the four-membered ring is a key step in the rearrangement of phenylenes into other PAHs and has been observed typically under flash vacuum pyrolytic conditions[18] (e.g., 10^{-3}–10^{-6} torr, 800–1000 °C). Strained ring opening on exposure to metal complexes to give metallacycles[19] is discussed in further detail in Section 1.2.

1.2 Overview of Phenylene Organometallic Chemistry

As mentioned above, the weakly aromatic character of the phenylenes dominates their structure and reactivity. In the linear phenylenes, the antiaromatic contribution to structure and reactivity becomes increasingly significant. A simple, yet instructive explanation for this phenomenon can be seen in the various resonance structures of linear [3]phenylene (**18**), a selection of which is depicted in Figure 1.6. Even the most favorable forms **a** and **b** feature double bonds in the four-membered rings. The cumulative increase in cyclobutadienoid circuits should therefore lead to an increase in antiaromatic character. The relative augmentation in

cyclobutadienoid/antiaromatic character of the linear phenylenes was confirmed[6] by NMR, NICS calculations, and HOMO-LUMO measurements.[20]

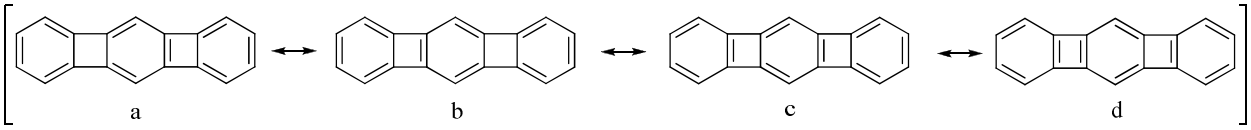

18

Figure 1.6. Resonance contributors to linear [3]phenylene.

Cyclobutadiene is often invoked as the typical example of a highly destabilized, antiaromatic system. Indeed, the difficulties[21] in preparing and isolating it confirm theoretical predictions regarding its instability.[22] Attachment of a metal, however, is known to produce aromatic organometallic molecules of high stability.[23] The increased antiaromatic character of the linear phenylenes thus makes them amenable to metal complexation. Cyclopentadienylcobalt cyclobutadiene complexes of linear [3]- (**19**),[24] linear [4]- (**20**),[25] and linear [5]phenylene (**21**)[26] have been prepared using the well-developed, cobalt-based [2+2+2] alkyne cyclotrimerization methods (Scheme 1.3).[27] Compounds **19**–**21** constitute the only linear CpCo phenylene systems known so far.

Scheme 1.3. Synthesis of Linear Phenylene(CpCo) Cyclobutadiene Complexes

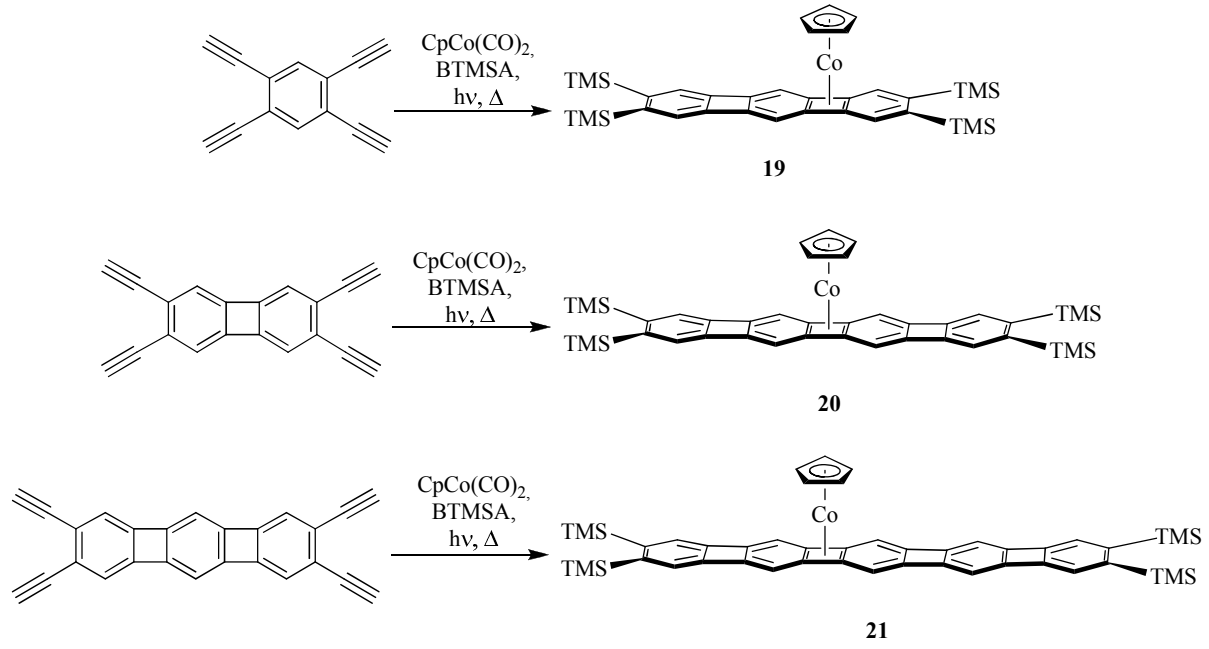

19

20

21

In the metallated linear [4]- and [5]phenylene **20** and **21,** respectively, the CpCo unit is located on the inner cyclobutadiene ring. This is curious, as one would have expected the metal fragment to be bound to its outside counterpart, close to the center of reactivity during the cyclotrimerization step. The position of the CpCo unit was established by NMR spectroscopy.[26,28] In addition, a crystal structure of a tetrahexyl

substituted linear [5]phenylene[28] (Figure 1.7) clearly reveals the inside position of the metal fragment. Difficulties in obtaining high quality crystals, however, precluded a detailed bond analysis of the complex. The unexpected location of the CpCo unit in **20** and **21** suggested the occurrence of CpCo migration under the conditions of their preparation. Detailed experiments verifying this hypothesis will be the subject of Chapter 2.

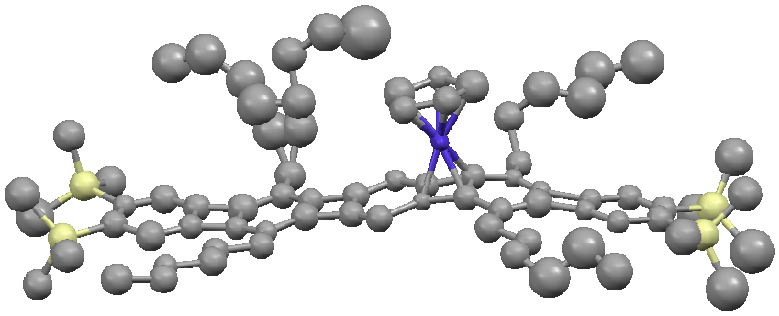

Figure 1.7. Disordered crystal structure for the 2,3,9,10-tetrakis(trimethylsilyl)-5,7,12,14-tetrahexyl linear [5]phenylene(CpCo).

In contrast to the linear phenylenes, their angular relatives undergo π-metallation at the cyclohexatrienoid moieties (Figure 1.8). For example, angular [3]phenylene (**22**) reacts with $Cp^*Co(C_2H_4)_2$ to form the η^4-Cp*Co complex **23**.[29] Similar treatment with $Cr(CO)_3(NH_3)_3$ yields the η^6-$Cr(CO)_3$ analog **24**.[30]

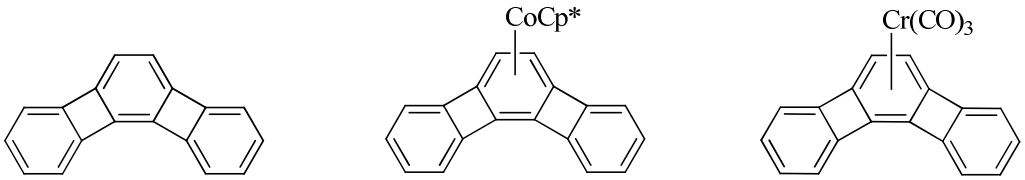

Figure 1.8. η^4-Cp*Co (**23**) and η^6-$Cr(CO)_3$ (**24**) complexes of angular [3]phenylene (**22**).

In addition to **24**, related chromium complexes of the triangular [4]phenylene frame, e.g. **25**, have been prepared (Scheme 1.4).[31] Interestingly, regioisomer **26,** generated at relatively lower temperatures, is the kinetic product of monocomplexation and rearranges thermally to **27**. Double metallation is possible, as illustrated in the conversion of **27** to **28** with added (naphthalene)$Cr(CO)_3$.

Scheme 1.4. Synthesis and Reactions of Triangular [4]Phenylene($Cr(CO)_3$) Complexes

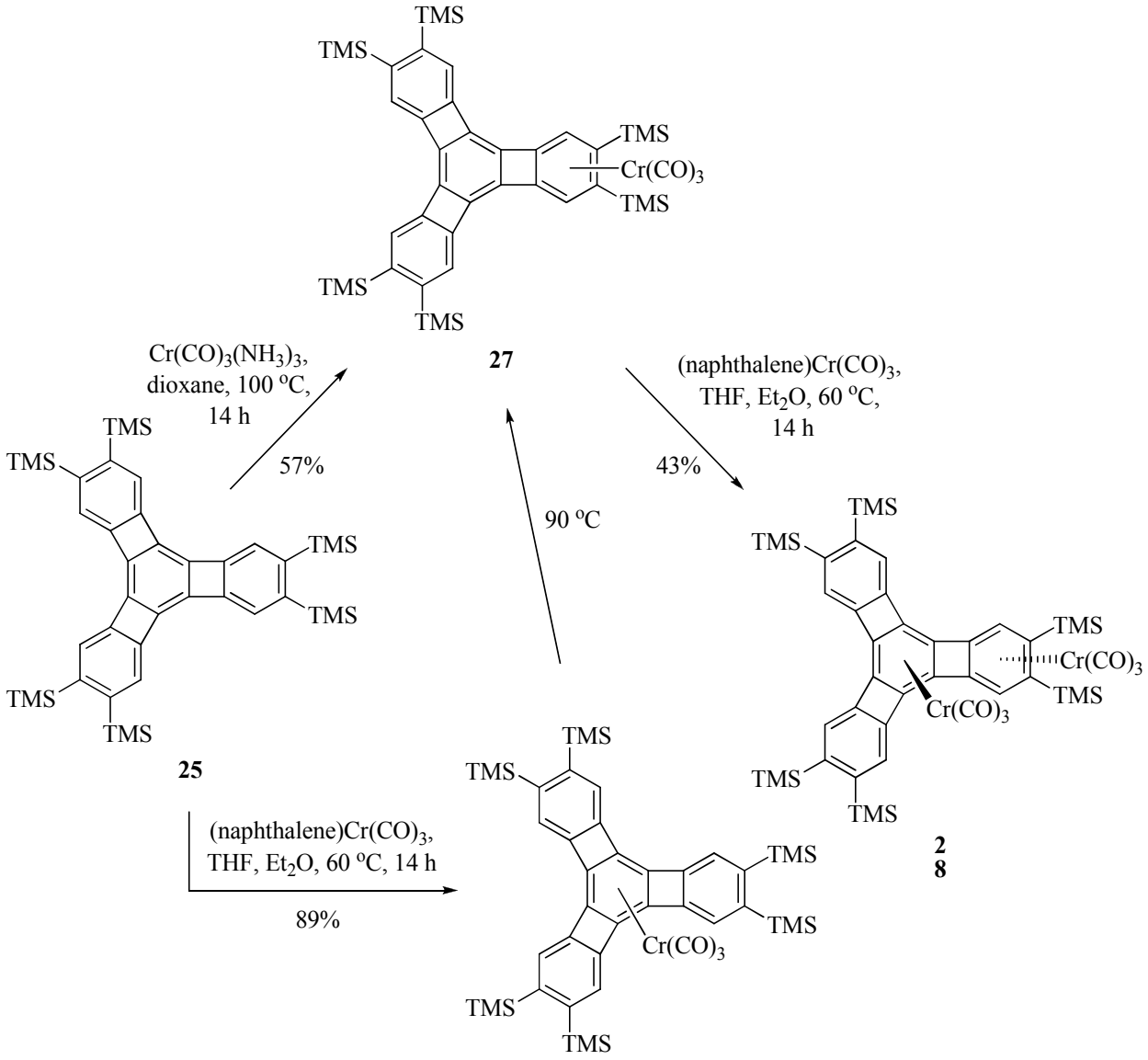

In contrast to CpCo, which attaches itself exclusively to the four-membered ring in the linear phenylenes, including the linear [3]phenylene frame, as in **19** (Scheme 1.3), $Fe_2(CO)_9$ gives a plethora of complexes with the tetrasilyl derivative **29**, among which the iron tricarbonyl cyclobutadiene complex **30** is only minor (Scheme 1.5).[27] Instead, other organometallic molecules, such as arene complex **31**, were isolated. This compound contains two $Fe(CO)_3$ units coordinated to the central benzene ring. An iron-iron bond was proposed for this molecule (**31a**), although the spectral data are also consistent with a structure in which the $Fe(CO)_3$ fragments are located on opposite faces (**31b**). Because a crystal structure could not be obtained, the structural identity of **31** remains ambiguous. The major products of this reaction, **32** and **33**, illustrate another important aspect of phenylene reactivity: metal insertion into the strained ring,

in this case involving the dinuclear $Fe_2(CO)_6$ unit. Complex **33**, probably originating from **32**, contains an additional $Fe(CO)_3$ moiety coordinated to the terminal benzene ring closest to the $Fe_2(CO)_6$ fragment.

Scheme 1.5. Reaction of Linear [3]Phenylene with $Fe_2(CO)_9$

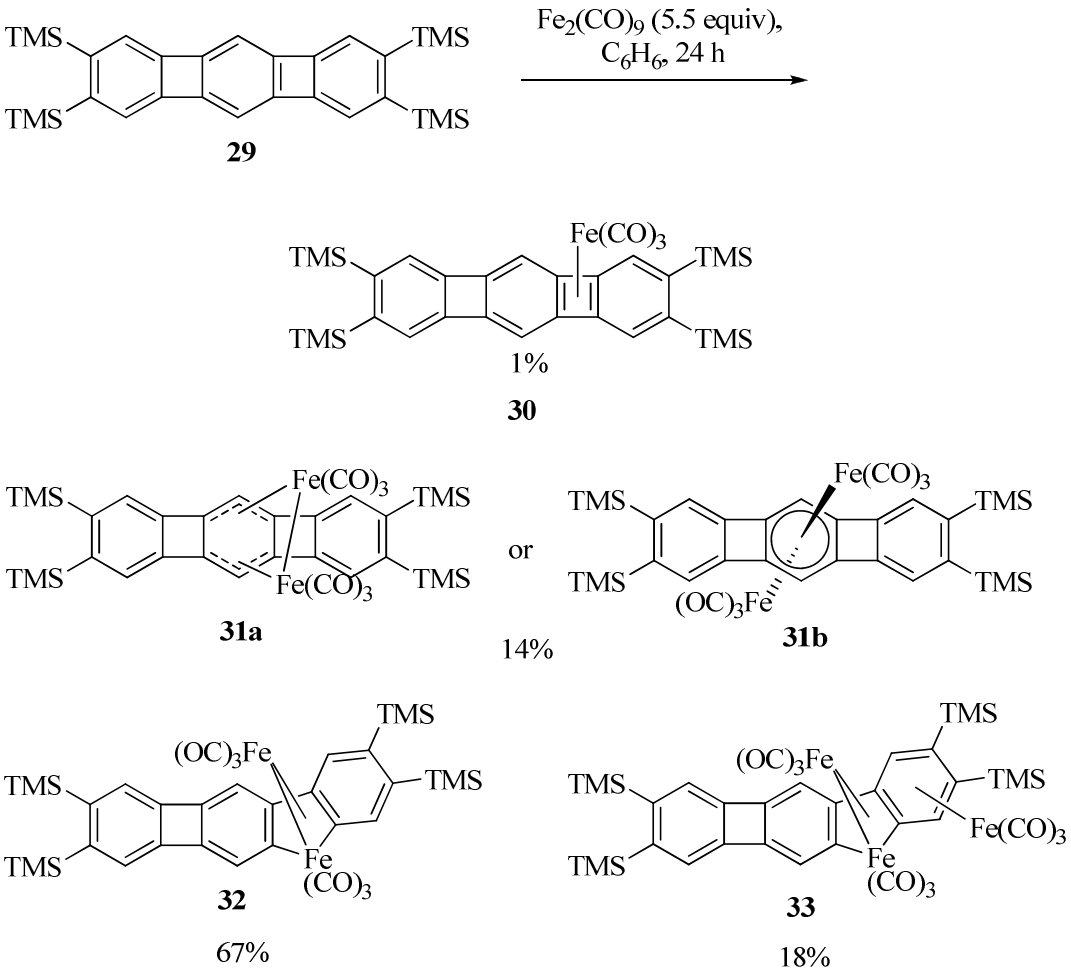

While as yet absent in the linear series, a cobalt insertion product analogous to iron compounds **32** and **33** was isolated when angular phenylene **22** was exposed to excess CpCo(ethene)$_2$ (Figure 1.9).[32] In this case, double insertion of two (CpCo)$_2$

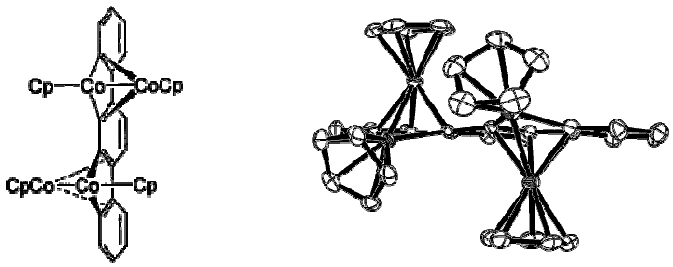

34

Figure 1.9. Tetranuclear CpCo-terphenylene complex **34** and its crystal structure.

fragments occurred to give **34** in 71% yield. Notably, neither **23** nor analogs of the type **31** were detected.

As alluded to in Scheme 1.2, biphenylene (**7**) itself also undergoes metal insertions into the four-membered ring. This type of reactivity has been observed with a range of transition metals, including Co.[19] Mechanistically best delineated is the attack of Ni and Pt species. Thus, $Ni(PEt_3)_4$[33a] and $Ni(COD)(PMe_3)_2$,[33b] begin with insertion of the nickel fragment into the four-membered ring to give a metallacycle of the type **35** (Scheme 1.6). Subsequent dimerization assembles **36**, from which Ni is extruded to furnish tetraphenylene **37** as the final product. A similar reaction pathway was proposed for $Pt(PEt)_4$,[19] but proceeding via **38** to a monometallacycle **40**, possibly through the intermediacy of **39**.

In summary, the σ- and π-activation of the phenylenes endows them with rich organometallic chemical potential. The synthetic and mechanistic exploration of one aspect of it, namely the Ni-catalyzed cycloaddition of alkynes to the four-membered rings in angular phenylenes, will be discussed in Chapter 3.

Scheme 1.6. Reaction of Biphenylene with Nickel and Platinum Complexes

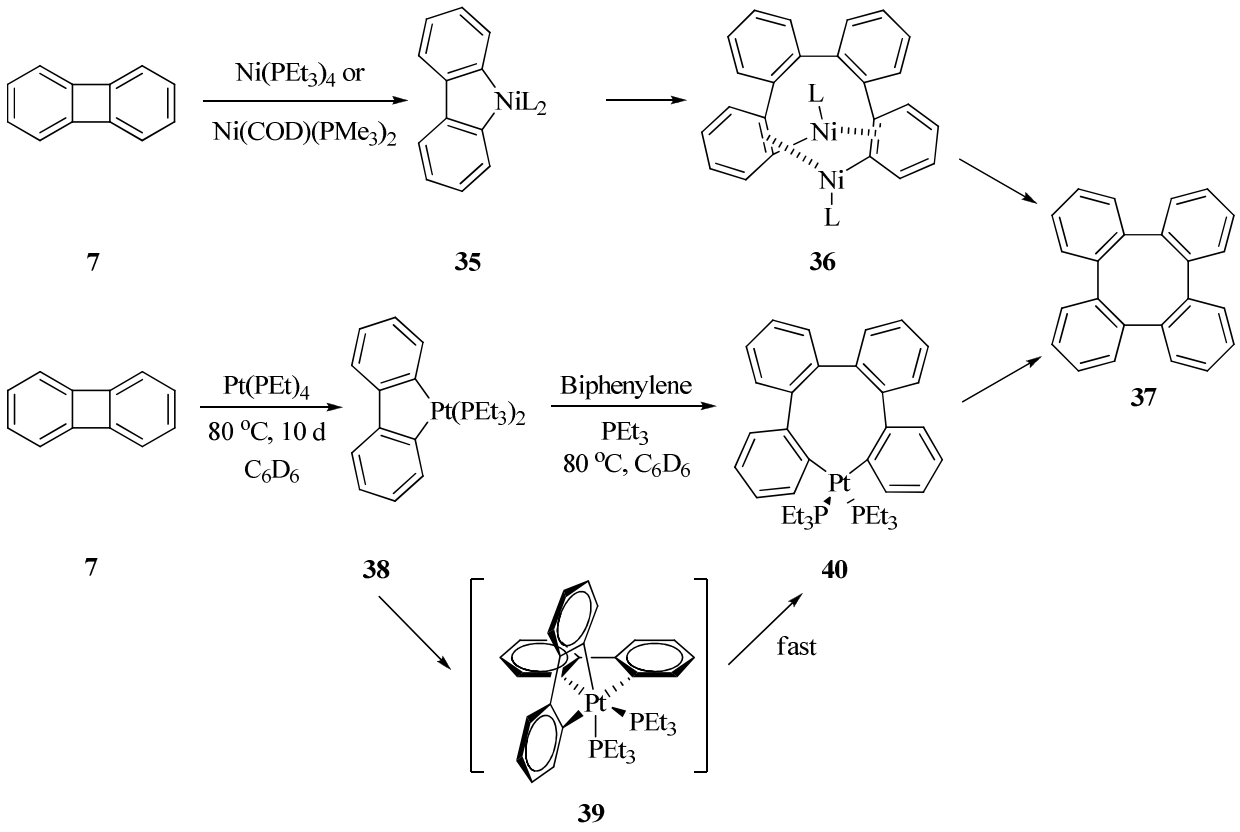

1.3 Direction of Work

The discussions in Sections 1.1 and 1.2 have provided a brief overview of phenylene properties and their previously studied organometallic chemistry,

respectively. The aim of this thesis was to advance two aspects of prior investigations.

The first area examines the chemistry of the linear phenylene(CpCo) complexes. In particular, experiments are presented addressing the question of a possible migration of the CpCo fragment along their framework. The revocable movement of a metal fragment between cyclobutadiene rings is a highly noteworthy discovery as this process has never before been reported. On a practical level, this mode of reactivity places linear phenylene(CpCo) complexes in the increasingly appealing class of organometallic arrays that can serve as the basis for various molecular electronic systems. The reversible isomerizations described in the second chapter can potentially be employed in molecular machines and switches, data storage, and, as will be detailed, photostorage devices. Experimental work, in the form of detailed solid state and spectroscopic analyses, is provided. Computational studies are also employed to further scrutinize the novel chemistry of the abovementioned Co-based molecules.

The second topic of this thesis examines nickel-catalyzed insertions into the four-membered rings of angular phenylene systems. Specifically, the application of this reactivity to the synthesis of a class of PAHs known as [N]phenacenes is discussed. Phenacenes (polyphenanthrenes) have recently shown great promise as organic transistors and conductors but advancement of this field has been hampered due to few practical syntheses. The insolubility of these molecules has also been a substantial barrier to the development of phenacene-based applications. The content of the third chapter explores the preparation of soluble phenacene derivatives using a tandem Ni-insertion, alkyne cycloaddition reaction. This new process provides an efficient, widely applicable, and practical synthesis of larger phenacenes using correspondingly larger angular phenylene systems. Detailed mechanistic studies of this reaction are presented. Experimental data are used in conjunction with computational studies to gain further insight with the optimization of the reaction by reduction of side product formation being a crucial milestone.

Chapter Two

Photo–Thermal Haptotropism in Cyclopentadienylcobalt Complexes of Linear Phenylenes: Intercyclobutadiene Metal Migration

2.1 Introduction

As previewed in Section 1.2, the unexpected position of the metallic unit in the linear [4]- and [5]phenylene(CpCo) systems **20** and **21** constituted the background for the studies presented in this chapter. Specifically, it was hypothesized that its origin was due to the migration of the metal fragment from one cyclobutadiene ring to another, a process that would constitute an unprecedented type of haptotropic shift.[34-36] However, a prerequisite for studying such a rearrangement would be the generation of the haptoisomers of **20** and **21** (Scheme 1.3), bearing the CpCo appendage at the respective terminal four-membered rings, a possibility obviated by their thermal method of synthesis. The following describes the history that led to the discovery of photochemical conditions that circumvented this thermodynamic problem.

The story begins with a prior attempt to stabilize the linear phenylene frame by alkyl substitution, the ultimate aim being the synthesis of members of the series with *N*>5. Such substitution was also hoped to improve solubility, a facet exploited in the corresponding zigzag series.[37] The synthetic strategy followed that used in the preparation of the largest known linear phenylene, **41**, namely the CpCo-catalyzed cyclization to **21**, followed by careful oxidative demetallation, as shown in Scheme 2.1. The initial target chosen was the tetrahexyl system **43**, approached via the synthesis of complex **42** (Scheme 2.2).[28] Demetallation was thought to be facile to provide the free ligand, but this anticipation proved to be erroneous.

Scheme 2.1. Oxidative Decomplexation of Linear [5]Phenylene Complex **21**

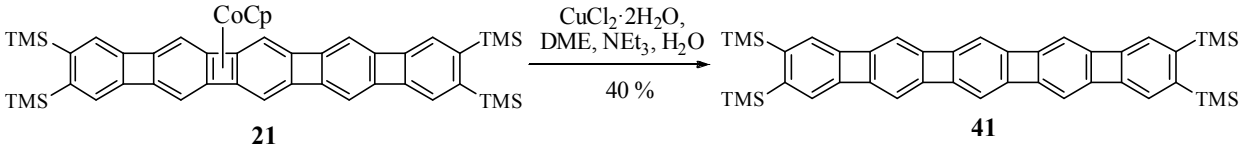

Scheme 2.2. Preparation of Tetrahexyl Linear [5]Phenylene Complex **42**

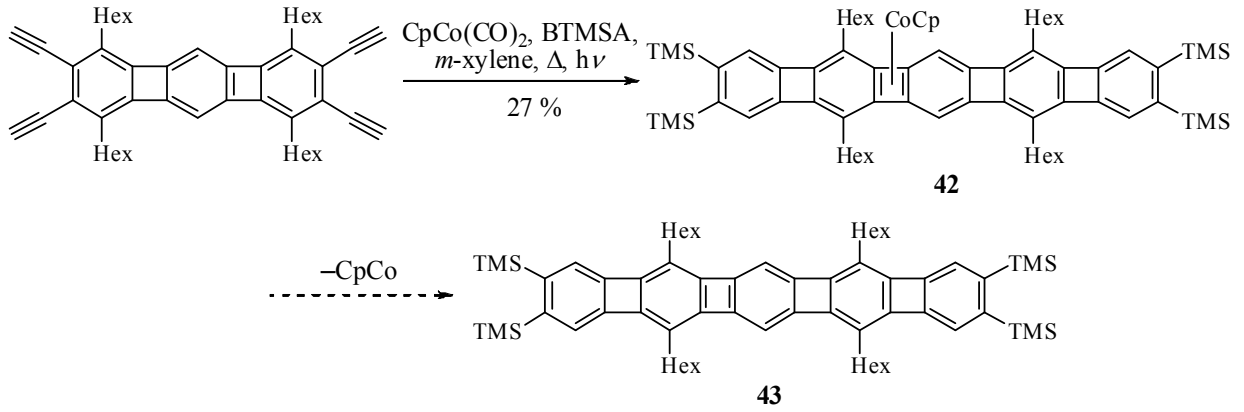

The demetallation of **42** under numerous conditions was unattainable. However, in one of these attempts, an NMR sample of **42** was exposed to UV-irradiation, leading to the evolution of new signals, eventually assigned to originate from rearranged compound **45** (Scheme 2.3).[28] This molecule is also a linear [5]phenylene(CpCo) complex, but now has the metal fragment bound to the outer cyclobutadiene ring, an arrangement that was suspected to be the initial product of the preparation of **42** (Scheme 2.2). That this conjecture was correct was established by heating, which caused photoisomer **45** to revert to **42**. An indication of the generality of this phenomenon was gleaned from **21**, which underwent the same photoinduced, thermally reversible haptotropic migration (Scheme 2.3).[38] A detailed discussion of the spectral properties of these haptomers is provided in Sections 2.3 and 2.4.

Scheme 2.3. Photoinduced, Thermally Reversible Haptotropic Migration of the CpCo Fragment in Linear [5]Phenylene(CpCo) Complexes

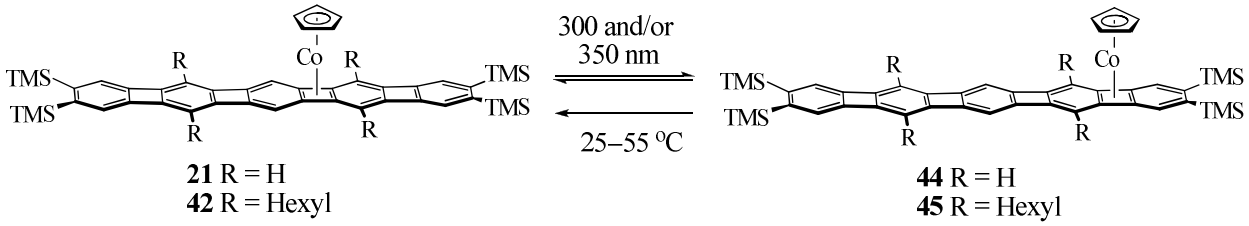

This discovery was deemed significant for two reasons: 1. it constitutes the first observation of intercyclobutadiene metallohaptotropism and 2. there are only two previously known examples of mononuclear,[39] additive-free,[40] photothermal, reversible haptotropic shifts, both of which are based on $Mo(PMe_3)_3$ complexes (Scheme 2.4).[41] Systems capable of undergoing this type of reaction are of much practical importance because of their potential employment as photostorage devices and/or molecular switches.[42] The development and application of functional organometallic materials[43] has proceeded at a relatively slow pace when compared to their non-metallated counterparts.[5c] Thus, the great prospects for discovery and advancement make this area of study particularly attractive.

Scheme 2.4. Photothermal, Reversible Metallohaptotropism in (a) Molybendum-Indole,[41a] and (b) Molybendum-Isoquinoline Complexes[41b]

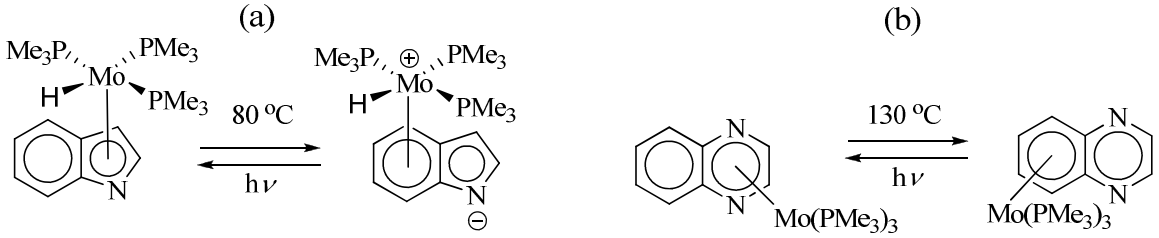

Having confirmed that an η^4:η^4 cyclobutadiene haptotropic migration was indeed occurring, mechanistic investigations[28,38] were begun. Interestingly, full conversion of the inner bound CpCo complexes to their photoisomers was never achieved. The maximum ratio obtained for **21**:**44** and **42**:**45** was 88:12. Variations of solvent (e.g., benzene, THF, $CHCl_3$) and temperature (0–30°C) had no effect on this ratio. Added ligands, such as 1,5-cyclooctadiene, CO, and phosphines, were also inconsequential. Of further significance was the robustness of the photothermal cycle, which could be run multiple times without decomposition.

Kinetic experiments were carried out to determine the activation parameters for the thermal reversal of **44** and **45** to **21** and **42**, respectively. These data are shown in Table 2.1. The isomerizations are cleanly first order, a finding that was unaffected by changes in concentration.[22] The enthalpy of activation ($\Delta H^{\neq}$) increased only slightly with hexyl substitution (**44** vs. **45**). The near zero entropy of activation values ($\Delta S^{\neq}$) was consistent with the occurrence of an intramolecular process.

Table 2.1. Activation Parameters for the Conversion of Outer to Inner CpCo Complexes Under Thermal Conditions. $\Delta S^{\neq}$ Values are in Entropy Units (1 eu = cal/mol·K)

Reaction	Solvent	$\Delta H^{\neq}$ (kcal/mol)	$\Delta S^{\neq}$ (eu)
44 to **21**	C_6D_6	25.9 ± 0.4	1.6 ± 1.4
44 to **21**	THF-d_8	25.6 ± 0.9	0.1 ± 3.0
45 to **42**	THF-d_8	27.6 ± 0.8	7.7 ± 2.7

Consideration of the relative facility of the above haptotropic shifts made it likely that migration was occurring along the entire phenylene frame, including the "hopping" across the central six-membered ring (Scheme 2.5). This degenerate equilibration should be detectable by NMR spectroscopy,[44] if it were sufficiently fast. Unfortunately, but perhaps not surprisingly, considering the data in Table 2.1, coalescence of the spectrum of **21** could not be achieved, even at temperatures as high as 120 °C. Spin saturation transfer experiments (e.g., EXSY) also failed.[44] These data allowed an estimate of the lower limit for the activation energy of the internal shift of $\Delta G^{\neq} \geq 22$ kcal/mol.[28]

Scheme 2.5. Proposed Internal η^4:η^4 Cyclobutadiene CpCo Migration.

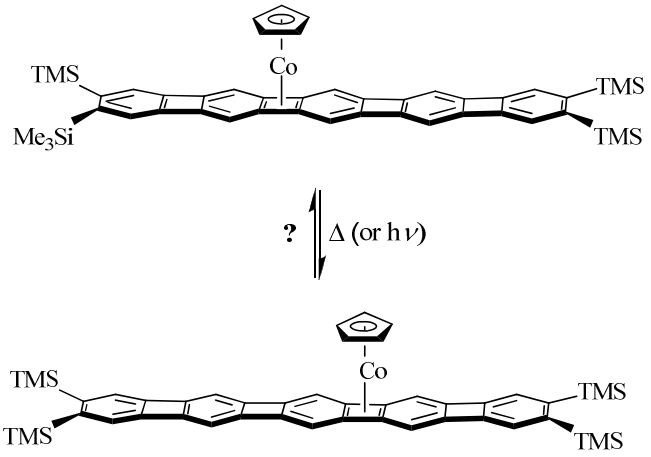

The failure of the above experiments inspired a different approach based on the following arguments. The antiaromatic character of the linear phenylenes has been shown by theory and experiment to increase with size.[6,45] Consequently, the effect of metalloaromatization[46] makes linear [5]phenylene a better (and hence more strongly bound) ligand for CpCo than a smaller system (e.g., linear [3]phenylene). Indeed, the enthalpy of the homodesmotic in Scheme 2.6 was computed by DFT methods to be

Scheme 2.6. Calculated Homodesmotic Reaction Showing Preferential Binding of CpCo to Linear [5]Phenylene

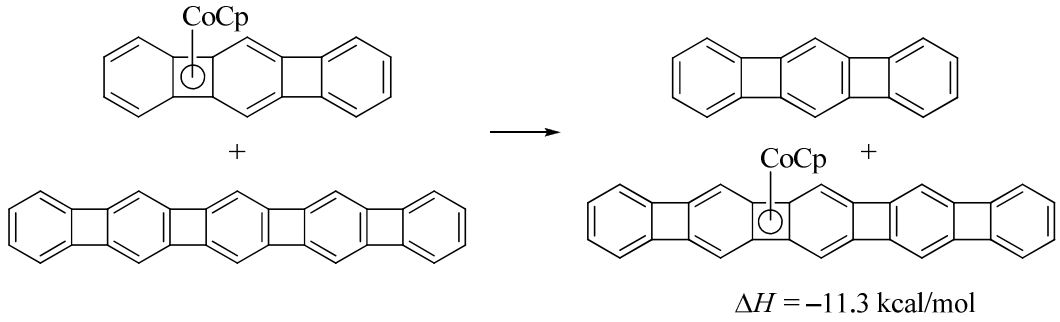

11.3 kcal/mol.[47] If the barrier to intercyclobutadiene hopping were related to the binding energy of the metal, one would expect a more loosely bound metal fragment to migrate faster. The hope was therefore that the degenerate haptotropism in Scheme 2.7 would be observable by VT NMR methods. Unfortunately, these efforts failed again,[38] either because the anticipated acceleration was not sufficient to be observable by NMR or because the argument above (which rests solely on ground state considerations) is flawed.

Scheme 2.7. Proposed Degenerate Haptotropic Shift in Linear [3]Phenylene Complex **19**

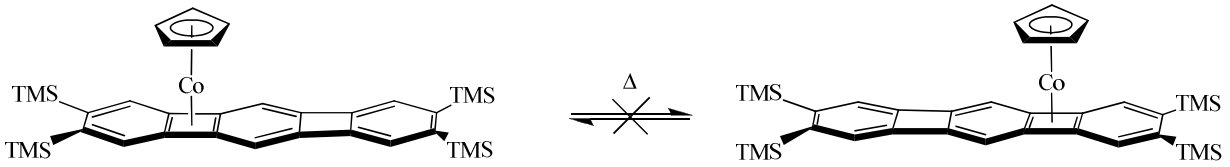

19

The preceding discussion summarizes some of the quantitative aspects of this new type of haptotropic shift. Many fundamental questions, however, remained to be answered. Is it possible to observe the photothermal shift in other systems, such as linear [3]- and [4]phenylene? What is the exact mechanism of metal migration between cyclobutadiene rings? In what way, if any, does attachment of CpCo alter the structure of the phenylene scaffold? Related to these questions was the long-standing quest for an accurate crystal structure of any linear phenylene(CpCo) complex. The answers are addressed in the following sections.

2.2 Studies of the Haptrotropic Shift in the Linear [3]Phenylene(CpCo) Complexes

As recounted in Section 2.1, the degenerate, internal haptotropic shift could not be seen by NMR in the symmetrical **19**. Therefore, recourse had to be taken to chemical methods involving an isomerization of the sort shown in Scheme 2.8.

Scheme 2.8. Isomerization of a Desymmetrized Linear [3]Phenylene(CpCo) Complex

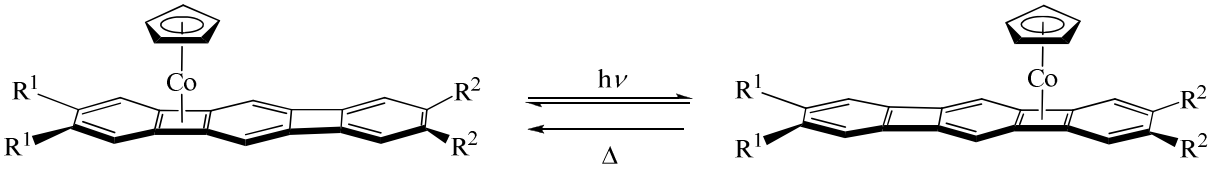

Initial efforts focused on attempts to desymmetrize compound **19** directly by selective electrophilic desilylation, specifically protodesilylation. Earlier studies[48] had shown that such selectivity was possible in the reactions of bis(trimethylsilyl)benzocycloalkenes, such as the benzocyclobutene depicted in Scheme 2.9. In this case, loss of the first TMS group is approximately forty times faster than that of the second. Along these lines, it was thought that exposing **19** to acidic conditions would selectively remove one (or perhaps two) TMS groups before attacking the remaining silylarene positions. In the event, treating compound **19** with trifluoroacetic acid in carbon tetrachloride did induce protodesilylation, but with no selectivity. A mixture of products was obtained and its separation proved impossible (Scheme 2.10). In light of this setback, a new synthetic scheme had to be considered that would generate a desymmetrized system directly in the CpCo-catalyzed cyclization step.

Scheme 2.9. Selective Desymmetrizing Reactions of 1,2-Bis(trimethylsilyl)benzocyclobutene with Electrophiles

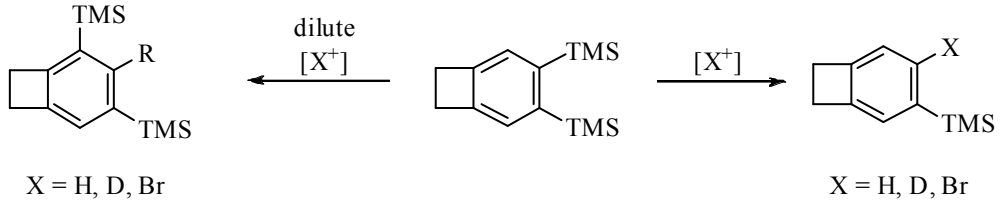

Scheme 2.10. Attempted Selective Protodesilylation of **19**

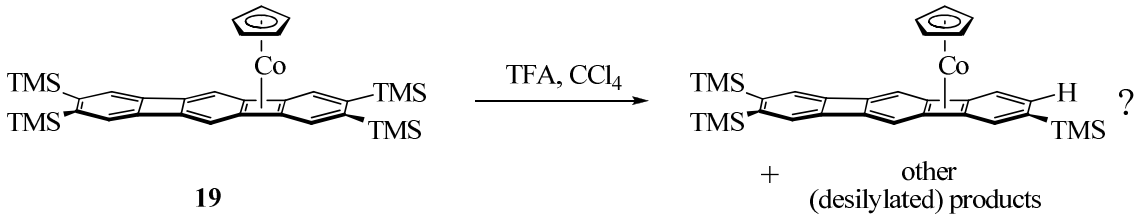

Fortunately, such a strategy had already been executed successfully in the creation of 2,3-bis(trimethylsilyl) linear [3]phenylene (**46**) and employed the iterative

Scheme 2.11. Iterative Cyclotrimerization Route in the Synthesis of Linear [3]Phenylene **46**

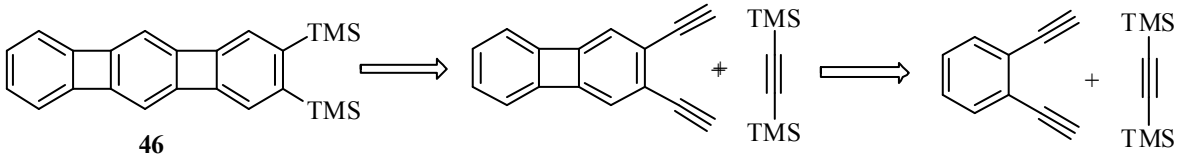

cyclization depicted in Scheme 2.11.[27] Its specific execution (Scheme 2.12) started with a Sonogashira reaction between trimethylsilylacetylene (TMSA) and 1,2-diiodobenzene (**47**), to give diyne **48** in high yield. Deprotection of **48** with K_2CO_3, immediately followed by standard $CpCo(CO)_2$-catalyzed alkyne cyclotrimerization[6,49] with bis(trimethylsilyl)acetylene (BTMSA), afforded 2,3-bis(trimethylsilyl)biphenylene (**49**). Iododesilylation was then performed using pure ICl to give 2,3-diiodobiphenylene (**50**). A Sonogashira coupling between TMSA and **50** produced diyne **51** in good yield. The use of a slightly modified cyclization procedure provided the new 2,3-bis(trimethylsilyl) linear [3]phenylene(CpCo) (**52**) in 57 % yield. This protocol employed THF as a cosolvent to BTMSA, thus reducing the reaction temperature, in turn allowing for the CpCo to remain attached in the final product and preventing catalytic turnover.[25,26,38]

Scheme 2.12. Synthesis of Asymmetric Linear [3]Phenylene(CpCo) **52**

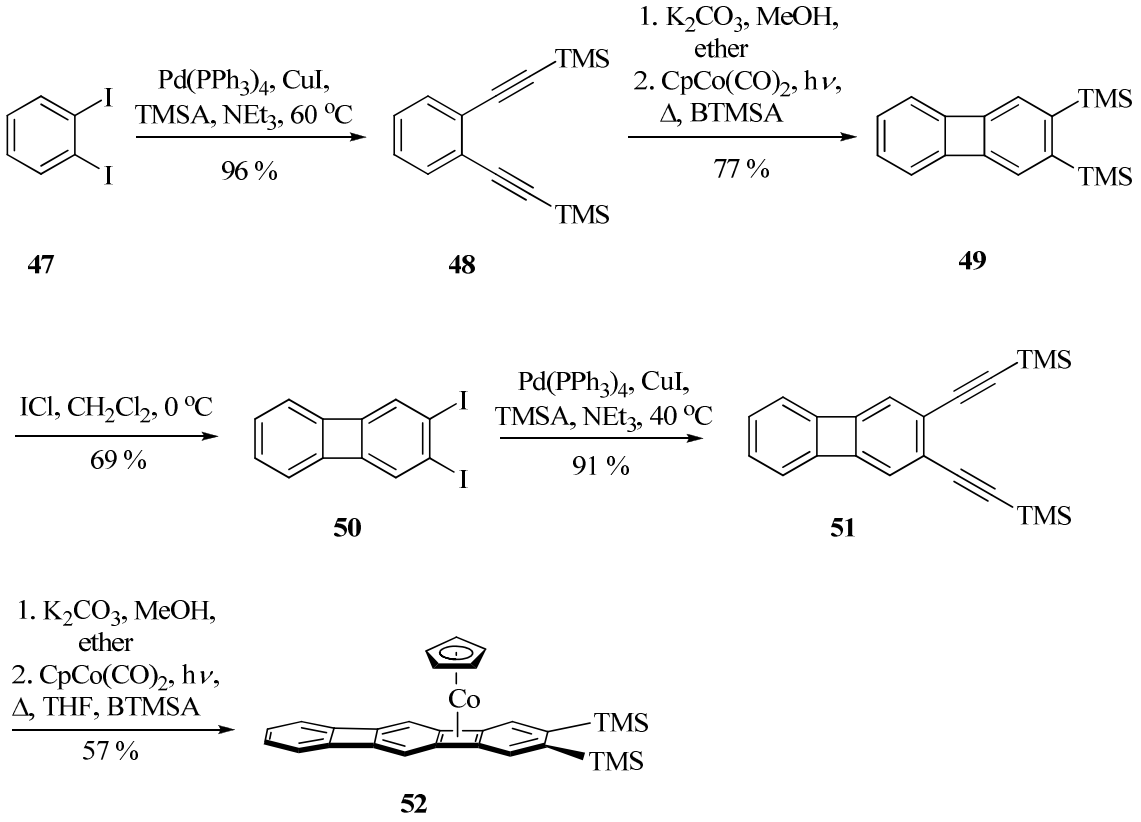

High dilution conditions also helped to suppress formation of cyclobutadiene(CpCo) complexes, a well known side reaction in alkyne cyclization chemistry.

Compound **52**, like its tetrasilylated analogue **19**, is a black, air-sensitive solid. Although it can be handled in air for brief periods of time, complete decomposition occurs within 24 hours if left exposed to the ambient atmosphere. Purification must always be done with neutral activity III alumina, as lower activities (and silica gel) cause decomplexation to give the deep red ligand **46** as the only isolable product.

Critically, exposing molecule **52** to UV irradiation induced the desired haptotropic shift, giving its photoisomer **53** (Scheme 2.13). Heating **53** converted it back to **52**, thus completing the photothermal cycle. Interestingly, close inspection of the NMR spectra of this experiment revealed that a small amount of **53** (2%) always remained even on prolonged heating. That this observation signaled a thermodynamic equilibrium was confirmed by dissolution of pure crystalline **52** and NMR analysis. From the equilibrium constant, the ΔG°_{298} was calculated to be 2.3 kcal/mol in favor of **52**. The reasons for this energetic preference and a discussion of the NMR spectral properties of these and related complexes are presented in Section 2.3.

Scheme 2.13. The Photoinduced, Thermally Reversible, Haptropic Shift in Linear

[3]Phenylene-(CpCo) **52** to Give Photoisomer Complex **53**

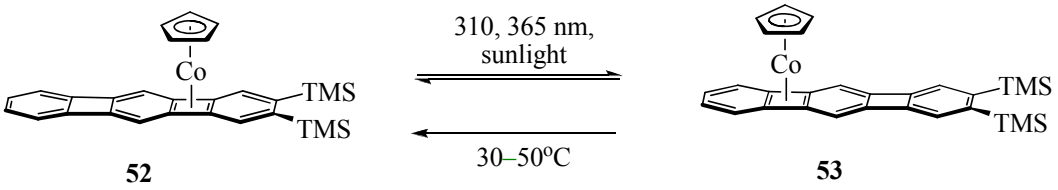

52 **53**

The investigations of the equilibration depicted in Scheme 2.13 were all carried out in sealed, Pyrex NMR tubes (J-Young or flame-sealed), using benzene-d_6 and/or toluene-d_8 as the solvent. As for the linear [5]phenylene(CpCo) system, the cycle could be run multiple times without decomposition and was unaffected by changes in solvent and temperature. The maximum ratio of **53**:**52** that could be obtained on irradiation was 1:1 after ten hours. This value is larger than that observed for its linear [5] analogs **21**/**44** and **42**/**45**. Photoisomerization also occurs with sunlight, leading to the photostationary equilibrium of **52**:**53** = 1:0.5. Consequently, care must be taken to shield **52** from direct and/or indirect sunlight. Indoor fluorescent lighting, however, did not induce CpCo migration.

Attempts to monitor the photoisomerization and its thermal reverse by UV-Vis spectroscopy failed because of minimal changes in the absorptions due to **52** during these processes. This finding implies that the absorption spectra of **52** and **53** are, not unexpectedly, very similar and offers a possible explanation for the maximum photostationary ratio of 1:1.

The activation parameters for the thermal reversal reaction (**53** to **52**) in Scheme 2.13 were obtained in the manner described in Section 2.1 and are shown in Table 2.2. The relatively high activation barriers (with respect to the NMR time scale) explain why the degenerate isomerization in **19** could not be verified by NMR experiments. Qualitatively, the $\Delta H^{\neq}$ values agree with the hypothesis that the more loosely bound CpCo unit in the linear [3]phenylene is relatively more mobile: they are approximately 3 kcal/mol lower than those of the [5]phenylene system. On the other hand, the $\Delta S^{\neq}$ values, especially in C_6D_6, are positive and relatively high, although still within the range acceptable for intramolecular reactions. Nevertheless, a crossover experiment was devised to provide a definite answer.

Table 2.2. Activation Parameters for the Thermal Conversion of Complex **53** to **52**

Solvent	$\Delta H^{\neq}$ (kcal/mol)	$\Delta S^{\neq}$ (eu)
C_6D_6	20.4 ± 1.4	15.8 ± 2.2
Toluene-d_8	23.1 ± 0.7	6.0 ± 1.3

For this purpose, two new linear [3]phenylene(CpCo) derivatives were required. One would carry a marker on the Cp ring, while the other would be labeled at the phenylene frame. Execution of Scheme 2.13 would involve an equimolar mixture of both compounds. An intramolecular mechanism would retain the integrity of the labeling, while a dissociative path would lead to label scrambling. The outcome of this experiment should be ascertainable by NMR spectroscopy and, more rigorously, by

Scheme 2.14. Preparation of MeCp- (**54**) and Deuterium Labeled (**55**) [3]Phenylene Complexes

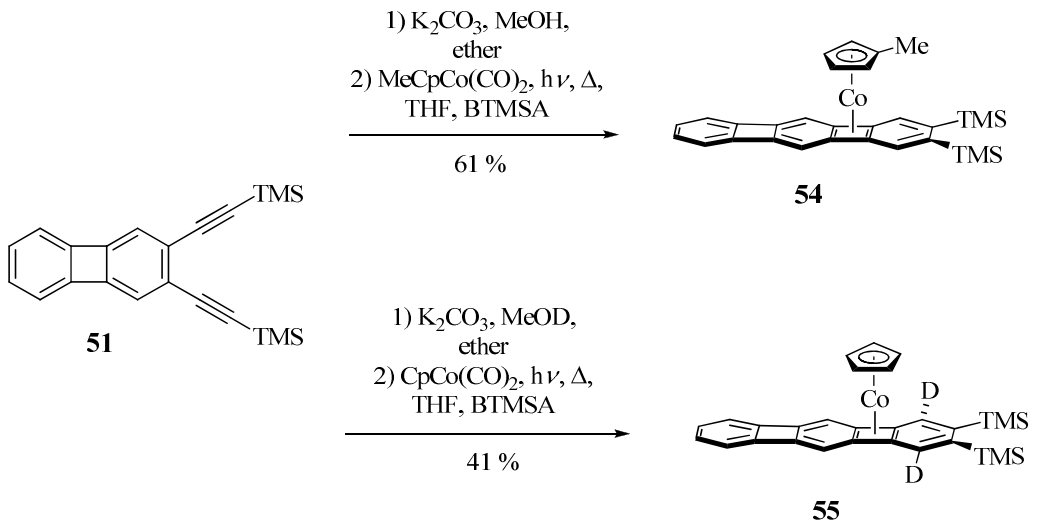

mass spectrometry. To this end, methyl-Cp complex **54** and dideuterio compound **55** were targeted for synthesis (Scheme 2.14). Compound **54** was prepared by carrying out the modified cyclotrimerization reaction with $MeCpCo(CO)_2$,[50] while **55** was made using methanol-OD in the desilylation of **51**. The amount of deuterium incorporation in **55** was found to be 63 %, as gleaned from its proton NMR spectrum.

Scheme 2.15. Crossover Experiment with Labeled Linear [3]Phenylene(CpCo) Complexes

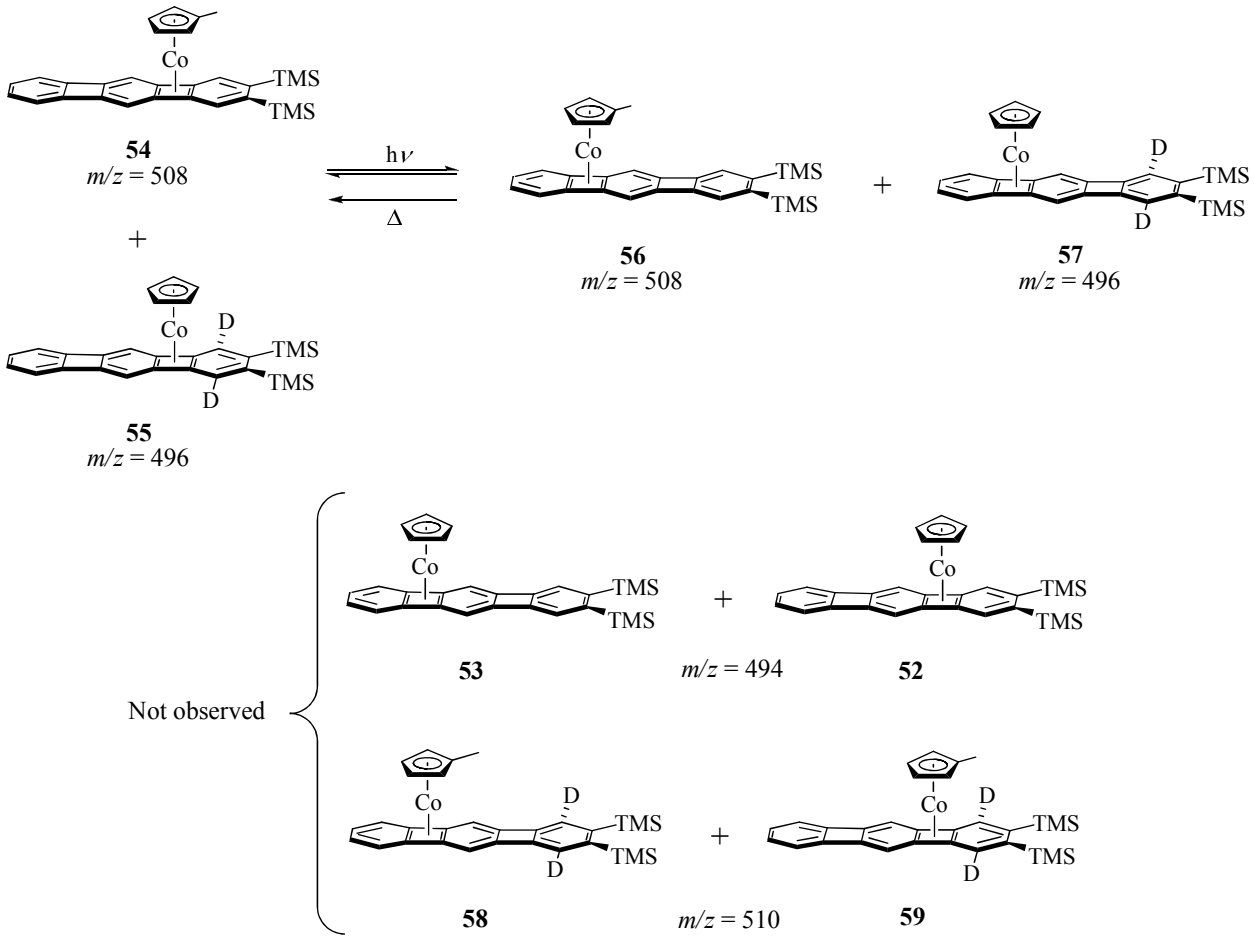

Six distinct products are possible in the crossover experiment using **54** and **55** (Scheme 2.15). Compounds **56** and **5** would arise as a consequence of an intramolecular shift. Molecules **53** and **58** and their photoisomers **52** and **59**, respectively, would be the result of metal fragment dissociation. Mass spectrometry would readily verify the occurrence of crossover, as the masses (given in *m/z* in Scheme 2.15) of the products with scrambled labels (**52**, **53**, **58**, **59**) are distinct from the masses of the starting materials (**54**, **55**) and their photoisomers (**56**, **57**).

In the first part of the experiment, equal amounts of **54** and **55** were mixed (shielded from light) and allowed to stand for 2 hours at room temperature. The resulting ^{1}H-NMR spectrum consisted of only the signals for **54** and **55**. Similarly, the mass spectrum showed molecular ion peaks matching the masses of **55** and **56** (Figure 2.1). The second step was irradiation. Analysis of the photolyzed mixture showed new peaks due to complex **56** (the resonances of which had been obtained in a separate photothermal experiment with pure **54**), with the expected integration ratio, and a second set assigned to **57**, identical with the spectrum of **53**, but with the expected attenuated absorption for the silyl bearing arene hydrogens. The relative integrations for all compounds observed were consistent with a mixture of **54**/**55** and **56**/**57**. Mass spectral analysis of the irradiated mixture showed a pattern that was identical to that collected before irradiation (Figure 2.1). Finally, the thermal reversal reaction was carried out by heating the photolyzed mixture at 80 °C. After 30 hours, the resulting

NMR spectrum matched that of the initial mixture of **54** and **56**, in particular confirming the full protonation of **54** and the unchanged level of deuterium incorporation in the silyl

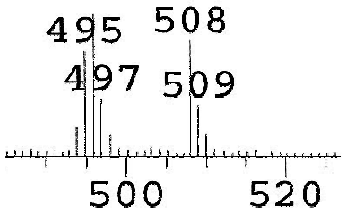

Figure 2.1. Molecular ion peaks for **54**/**56** (*m/z* = 508) and **55**/**57** (*m/z* = 496).

bearing arene ring of **55**. The corresponding mass spectrum contained no evidence for the presence of scrambled products. To conclude: The haptotropic shift is non-dissociative. The exact manner in which the metal traverses from one cyclobutadiene ring to the other will be examined in greater detail in Section 2.4.

2.3 X-Ray Structural and Comparative NMR Analysis of Linear [3]Phenylene(CpCo) Complexes

The results described in Sections 2.1 and 2.2 pose some fundamental questions beyond those concerned with the immediate details of the observed haptotropism and addressing the basic novelty of the complexes involved. What actually happens to the phenylene ligand when it is ligated via a cyclobutadienoid ring? This section will address this question from a structural and (NMR) magnetic point of view.

Only one crystal structure of a linear phenylene(CpCo) complex was known at the outset of this work, namely that of [5]phenylene(CpCo) **42** (Figure 1.7), and its acquisition required extensive efforts at crystallization.[28] Unfortunately, extensive disorder obviated a detailed analysis. It was hoped that some of the complexes employed in the chemistry disclosed in Section 2.2 would be more forthcoming in this respect. The challenge lay in finding the right conditions for crystal growth. We began with tetrasilyl linear [3]phenylene(CpCo) **19**, which had been crystallized previously by slow cooling in acetone.[38] These conditions, and numerous others (Table 2.3), did not provide material suitable for X-ray diffraction. Success entailed slow cooling a solution of **19** to –10 °C in a mixture of methanol-diethyl ether (4:1). The ensuing sample allowed the determination of the first high quality crystal structure of a linear phenylene (CpCo) complex, obtained in collaboration with the group of Professor Tatiana Timofeeva of New Mexico Highlands University (Figure 2.2).

Table 2.3. Trial Crystallization Conditions for Linear [3]Phenylene(CpCo)**19**

Solvent (Ratio)	Conditions	Result
Acetone	Slow Cooling	Heterocrystalline Solid
Acetone-Pentane (3:1)	Slow Cooling	Heterocrystalline Solid
Pentane-Acetone (10:1)	Solvent Diffusion	Amorphous Solid
Chlorobenzene	Slow Cooling	Amorphous Solid

Acetone-Methanol (1:10	Slow Cooling	Amorphous Solid
Diethyl Ether-Methanol	Slow Cooling	Small Needles
Acetonitrile	Slow Cooling	Powder
Ethyl Acetate	Slow Cooling	No Crystals
Ethyl Acetate-Methanol (1:1)	Slow Cooling	Amorphous Solid
Methanol-Diethyl Ether (4:1)	Slow Cooling	Large, Fine Needles

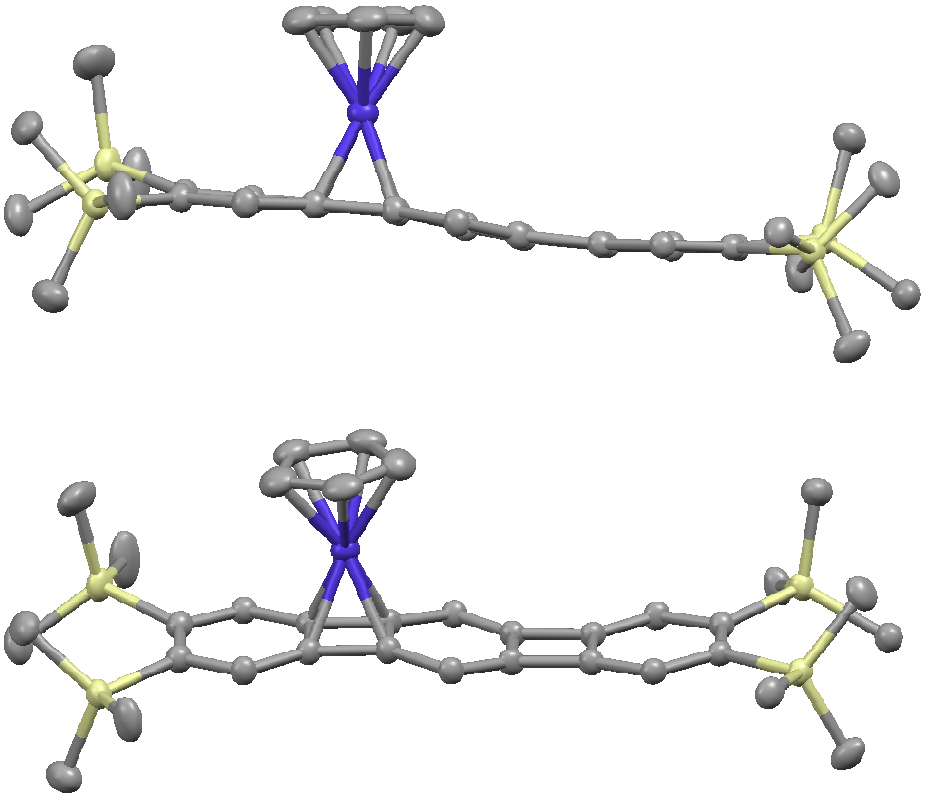

Figure 2.2. X-ray crystal structure of 2,3,7,8-tetrakis(trimethylsilyl) linear [3]phenylene(CpCo) (**19**). Carbon atoms are labeled grey, silicon atoms beige, and cobalt blue. Hydrogen atoms are omitted for clarity.

Expectedly, the CpCo unit is bound in an η^4 fashion to the cyclobutadiene ring. Also prominent is the deviation from planarity (Section 1.1) in the linear [3]phenylene, a facet typical of the phenylenes themselves (Section 1.1).[9a] Of greater importance than these general observations, however, is the effect of metal complexation on the linear [3] framework. The bond lengths for **19** are shown in Figure 2.3 and, as is typical for the phenylenes,[6] show a certain degree of bond π-localization with measurable differences between single and double bonds. However, the extent of this phenomenon and its direction varies significantly when compared to the free ligand **60**. A quantitative

comparison of the structural data for **19** with those of its ligand **60** is shown in Figure 2.3.[27]

In **60**, the terminal rings adopt bond alternation similar to that in biphenylene (Section 1.1) and the central benzene takes on a "bis-allyl" configuration, both ostensibly to minimize electron density (and therefore antiaromaticity) in the four-membered rings. As dictated by symmetry, the two bonds spanning the central ring are of equal length (1.385 Å). Ligation by CpCo alters this picture profoundly, in as much as bond alternation across the entire phenylene frame, including the four-membered rings, is strongly reduced (Figure 2.3). Generally all relatively long bonds in **60** shorten in **19**, while all short bonds lengthen. Some residual, but attenuated biphenylene type

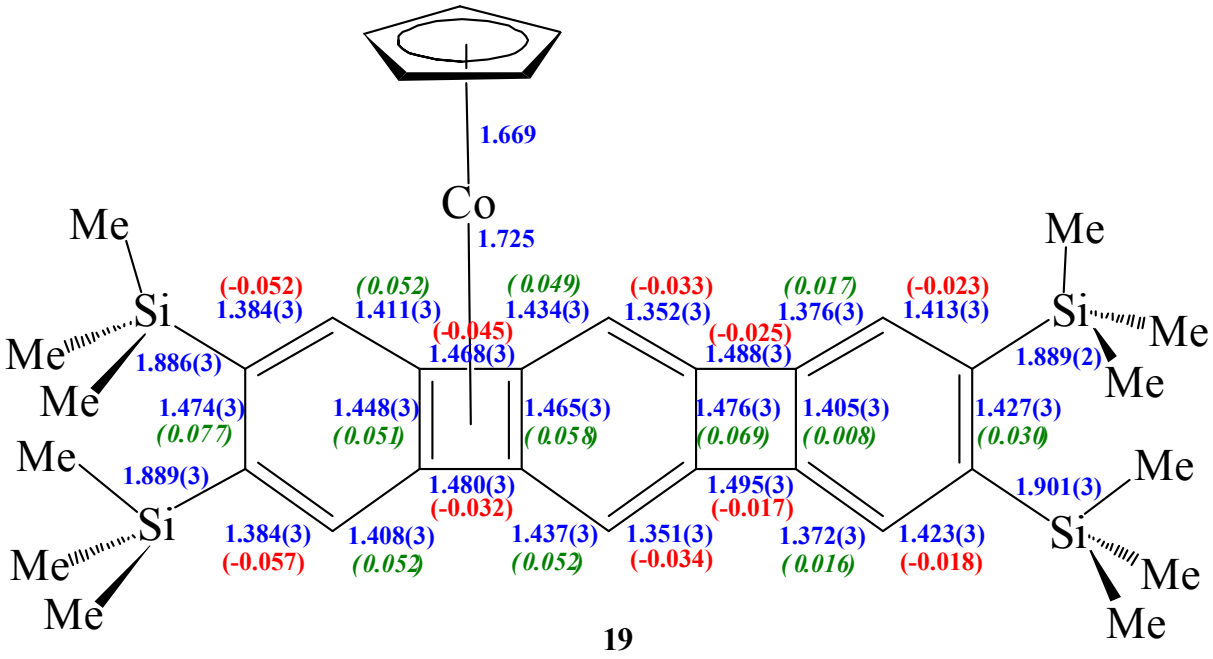

19

(x) = **(19)** - **(60)**
increase
decrease

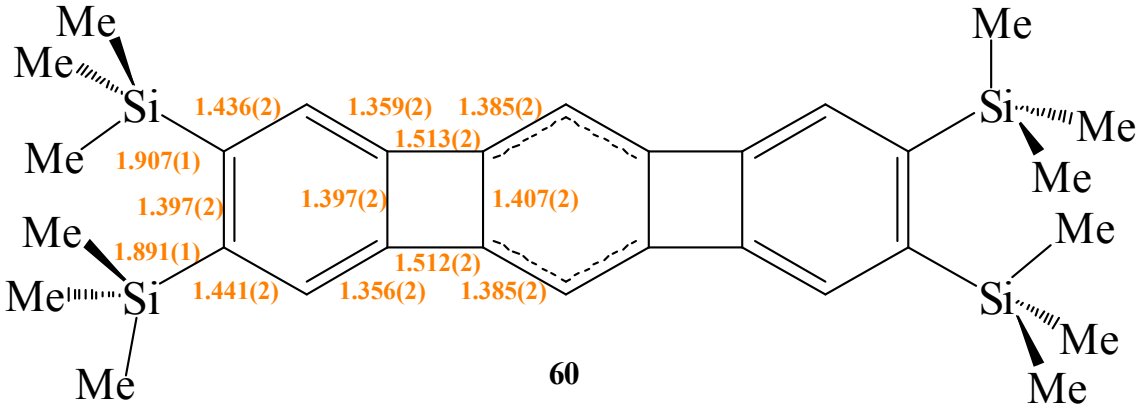

60

Figure 2.3. Comparison of bond lengths (in Å) between linear [3]phenylene(CpCo)complex **19** and 2,3,7,8-tetrakis(trimethylsilyl) linear [3]phenylene (**60**). The bond distances in **19** are shown in blue. Increases in bond length in going from **60** to **19** are marked in green, decreases in red.

"bond fixation" (Figure 1.2) remains in the vicinity of the uncomplexed cyclobutadiene. Compound **19** thus provides a prime demonstration of the powerful effect of metalloaromatization,[46] in which the bonds of a cyclobutadiene-metal system attempt to adopt the equalized bond lengths that are a classic hallmark of aromaticity.[2–4]

Encouraged by the successful development of a procedure to obtain X-ray quality crystals of **19**, these techniques were applied to bis(trimethylsilyl) linear [3]phenylene(CpCo) **52**. Gratifyingly, with acetone as the solvent, the results depicted in Figure 2.4 were ultimately obtained.

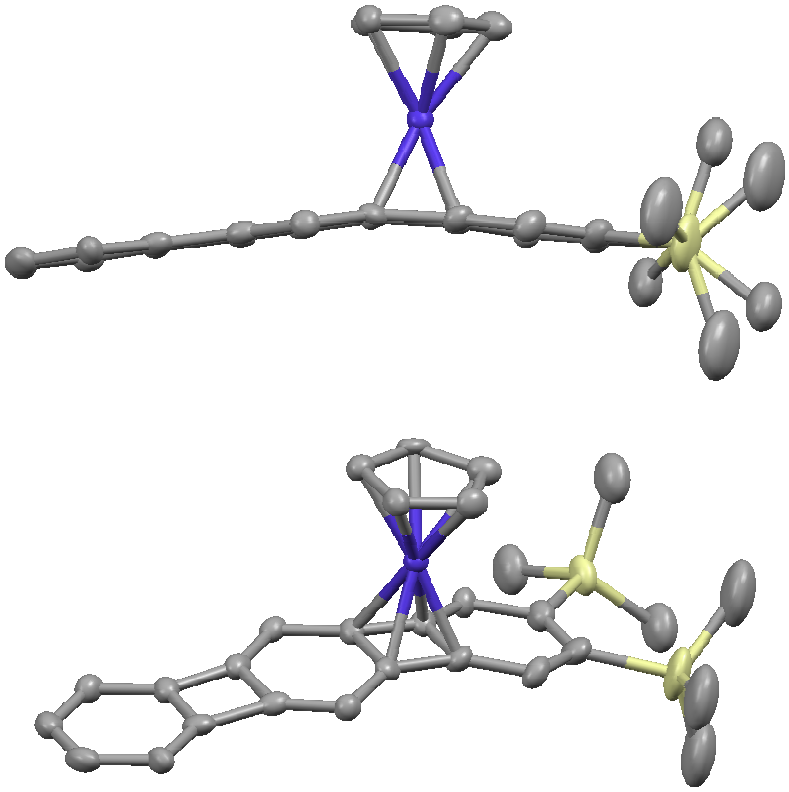

Figure 2.4. X-ray crystal structure of 2,3-bis(trimethylsilyl) linear [3]phenylene(CpCo) (**52**). Carbon atoms are labeled grey, silicon atoms beige, and cobalt blue. Hydrogen atoms are omitted for clarity.

A comparison of the bond lengths of **52** with those of its corresponding linear [3]phenylene ligand **46**[9a] is given in Figure 2.5. Comparison with Figure 2.3 reveals the same type of aromatization of the ligand on attachment of the metal.

With these structures in hand, an attempt was made to rationalize structurally the

thermodynamic preference for **52**, in which the CpCo is located proximal to the silylated terminus, in its equilibrium with **53**, in which the metal is located close to the unsilylated benzene ring. Focusing on the desymmetrizing ortho-bis(trimethylsilyl) unit, one notes that the SiC–CSi bond in **52** is elongated by 0.05 Å on attaching the metal in **46**, thus providing steric relief. On the other hand, the symmetry equivalent remote C7–C8 distance is unchanged. The same effect is seen in the tetrasilyl complex **19**.

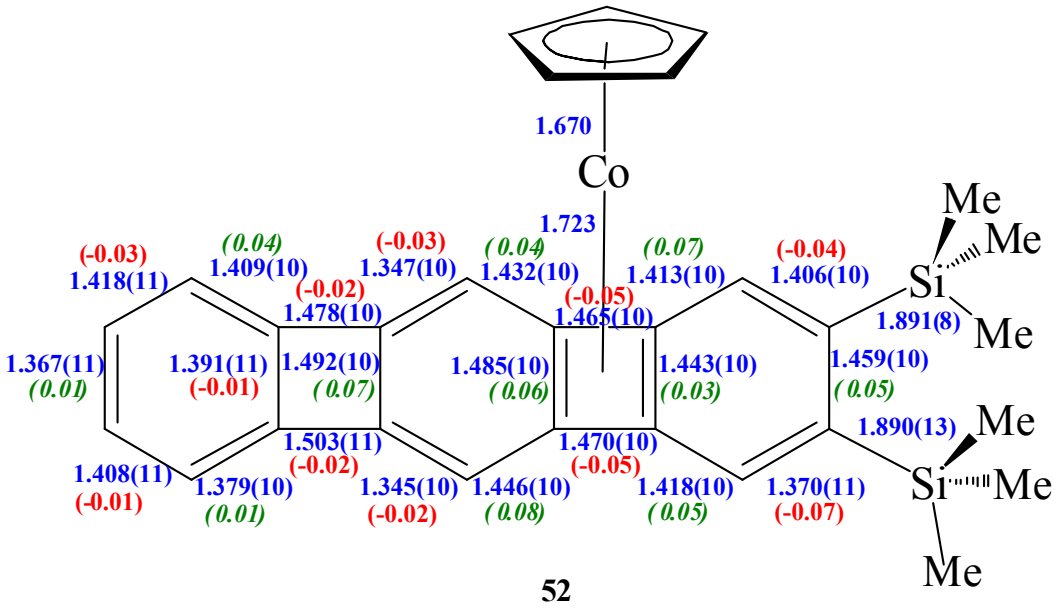

52

(x) = **(53)** - **(62)**
increase
decrease

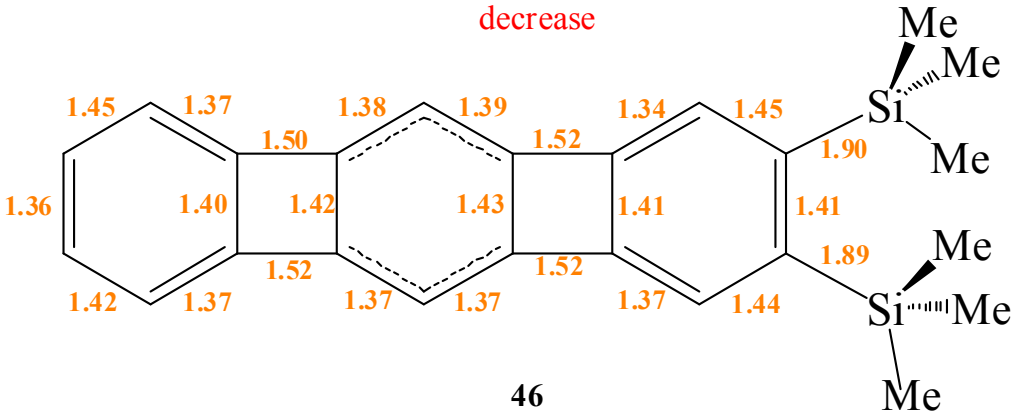

46

Figure 2.5. Comparison of bond lengths (in Å) between bis(trimethylsilyl) linear [3]phenylene(CpCo) complex **52** and 2,3-bis(trimethylsilyl) linear [3]phenylene (**46**). Bond lengths for **46** are the average of four molecules in the unit cell (standard deviation = ±0.02). Increases in bond length going from **46** to **52** are marked in green, decreases in red.

The observed structural changes make sense in a simple resonance picture

(Scheme 2.16). Metalloaromatization alters the dominant resonance forms during intercyclobutadiene hopping such that the essentially single SiC–CSi bond in **52** transforms into an essential double bond in **53**, increasing unfavorable repulsion between the TMS groups.

Scheme 2.16. A Resonance Picture Rationale for the Preference of **52** in its Equilibrium with **53**

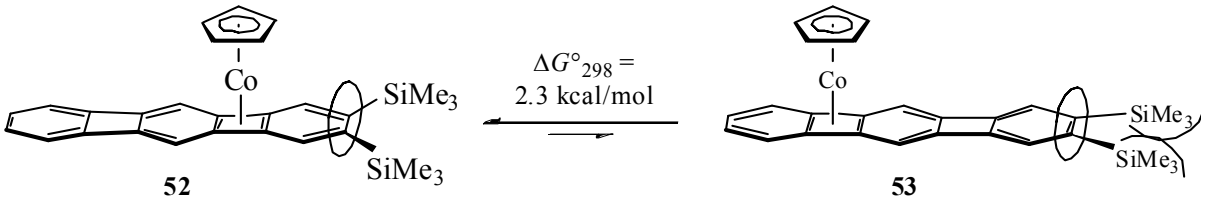

52 **53**

The aromatization effect of metal complexation on the phenylene nucleus, described structurally in the preceding text, can also be demonstrated powerfully through the measurement of ring currents with ^{1}H-NMR spectroscopy, both by experiment and computation (NICS;[13] see Section 1.1). A relevant simple example is depicted in Figure 2.6(a), featuring the changes occurring when 1,2-bis(trimethylsilyl)benzocyclobutadiene (**61**) is complexed by CpCo, as in **62**.[51] The paratropic antiaromatic 8π system **61**, exhibiting relatively shielded six-membered ring hydrogens, turns diatropic in **62**. Equally importantly and focusing on the ring current contributions of the individual cycles, the paratropism of the four-membered ring in **63** shields the adjacent hydrogens more than the remote ones. Conversely, aromatization of this ring and the ensuing diatropism inverts this order.

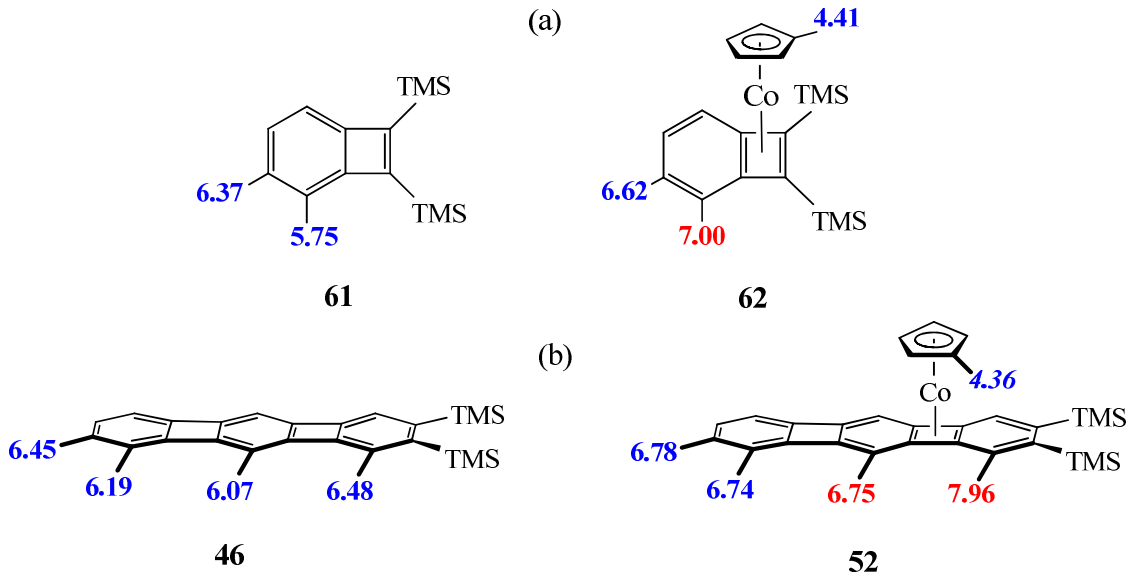

61 **62**

46 **52**

Figure 2.6. The effect CpCo complexation (a) on benzocyclobutadiene **61** and (b) linear [3]phenylene **46**. Chemicals shifts are in ppm.

Turning to a phenylene system, comparison of the NMR data for complex **52** with those for ligand **46** (Figure 2.6(b)) reveals the same changes, not only in the vicinity of the ligated ring, but also in the remote parts of the molecule. Thus, the hydrogens closest to the metal fragment are shifted downfield by 1.25 ppm in **62** and 1.48/0.68 ppm in **52**, when compared with **61** and **46**, respectively. The observed relatively large chemical shifts of the arene hydrogens proximal to the metal unit are not due to its anisotropy, since its value in this area of space is (if anything) shielding.[51,52] In addition, the remote hydrogens in **52** are deshielded by 0.55/0.33 ppm relative to the corresponding nuclei in **46**, clearly substantiating the aromatization of the overall system upon metal complexation that was seen by structural analysis. These pronounced chemical shift changes are diagnostic and greatly aided the spectral interpretations of the photochemically induced haptotropic shift experiments described in Sections 2.1 and 2.2, as illustrated for the isomerization between **52** and **53** (Scheme 2.17).

Scheme 2.17. Chemical Shift Changes in the Isomerization of **52** to **53**

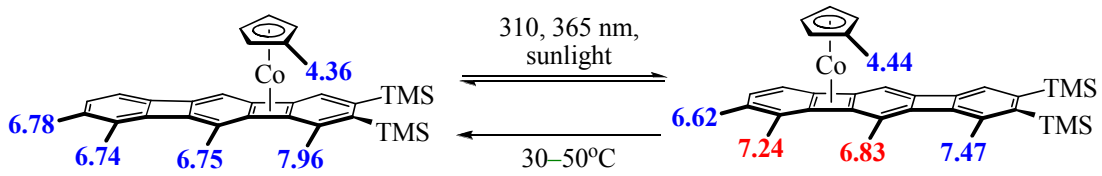

52 **53**

These NMR measurements were augmented by NICS calculations carried out in collaboration with Professor Amnon Stanger at the Technion in Haifa. NICS data have the advantage that they indicate the extent of (anti)aromaticity even in rings for which the molecule has no hydrogen probe in the classical NMR experiment, in this case the cyclobutadienes. Computational details are given in Chapter 4. The experimentally determined proton NMR data for the series of silylated linear phenylenes from [2] to [5] and their metallated analogues, in addition to the corresponding NICS(1) values of the respective parent phenylenes, are shown in Figure 2.7. All compounds in Figure 2.7 are known except for the hypothetical biphenylene(CpCo) **64**, which is included for comparative purposes. Metalloaromatization is pronounced, as all rings of the phenylene exhibit diminished or more negative NICS numbers, signaling increasing aromatic and decreasing antiaromatic character, respectively. Again, the effect is most pronounced on the rings closest to the metal bound unit, tapering off (but never disappearing) with distance. Most illustrative in this respect is **44**, in which the penultimate and ultimate rings away from the Co still show decreases in the NICS values of 0.6 and 0.5 ppm, respectively. Interestingly, the sum of all NICS values of **44** ("total NICS"[13c]), –9.1, is less negative than that of **21**, –13.2, suggesting that **21** is more aromatic, hence more stable, as observed experimentally. This may be fortuitous, and the issue is addressed further in Section 2.4.

Finally, a caveat regarding the unusually large negative NICS values associated with the CpCo-complexed cyclobutadiene rings. As pointed out by Solà in connection with a related study of (benzene)$Cr(CO)_3$, which produced similar numbers,[53] there are local ring currents associated with the extra electrons involved in the metal to π-ligand

bonding that lead to an overestimation of aromaticity. Therefore, to corroborate the general conclusions of metalloaromatization of this (and all other rings) in Figure 2.7, Stanger's NICS scan method was applied.[54] This procedure is indicative of para- and diamagnetic ring currents in carbocycles and consists of: (a) dissection of NICS values into in-plane ($NICS_{XY}$) and out-of-plane components ($NICS_{ZZ}$), in which the latter is the π ring current diagnostic, and (b) composition of graphical plots of the values of the NICS components versus distance r (from the ring centroid under scrutiny) and their

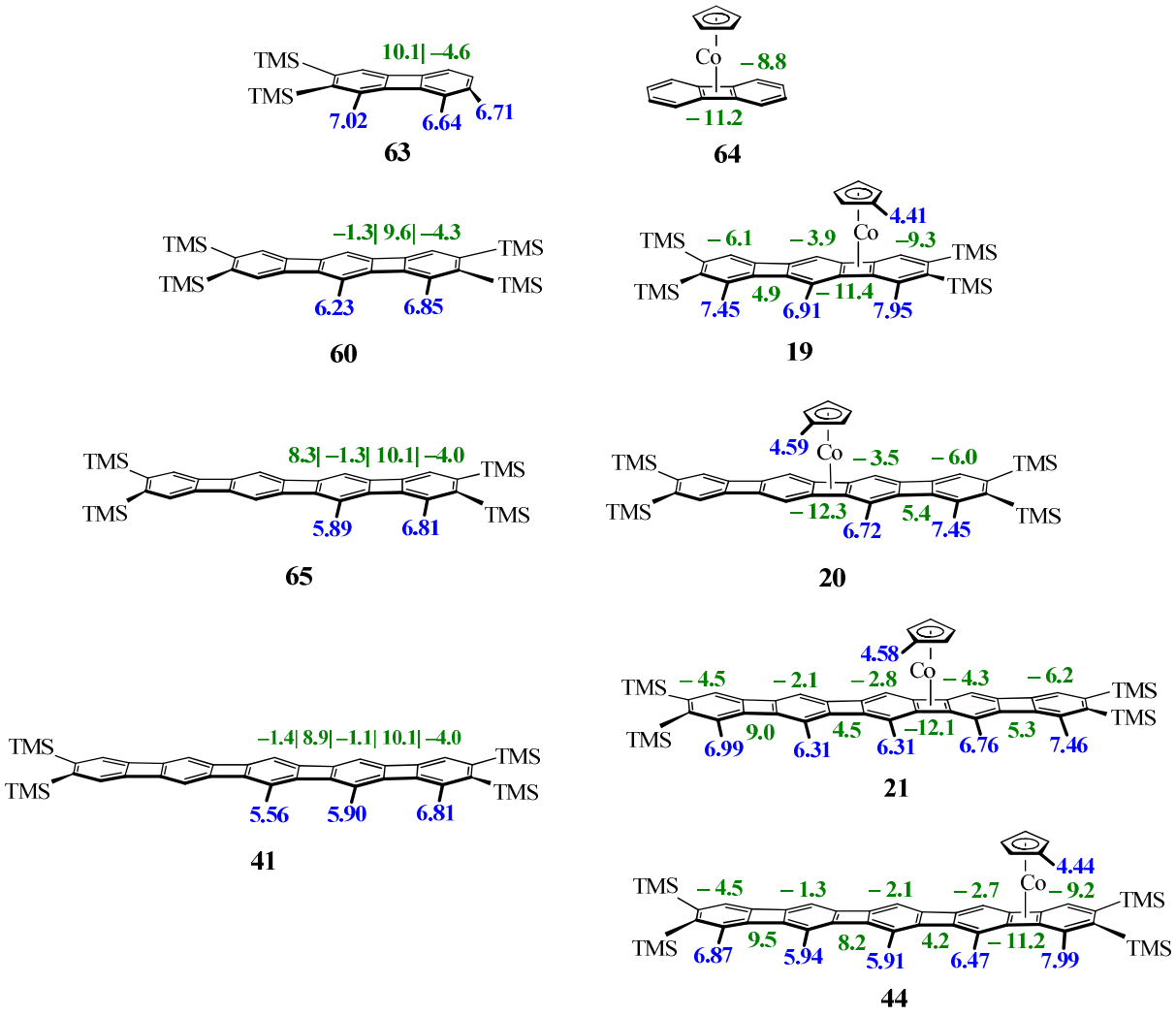

Figure 2.7. Experimental ^{1}H-NMR (C_6D_6; blue) and computed NICS(1) (green) values for linear phenylenes and their corresponding CpCo complexes. The experimental data are for the silylated derivatives shown. The NICS data are for the parent systems.

interpretation. The data, presented in Chapter 4, confirm the conclusions of this section.

While not reflective of ring current effects, the values of the ^{13}C chemical shifts for the linear phenylene(CpCo)complexes do provide some insight into the nature of the

σ-framework. Comparing complex **19** with parent ligand **60**, one observes two general phenomena (Figure 2.8). The most apparent is the upfield values for the cobalt-bound cyclobutadiene carbons (~74–78 ppm) in **19**, arising from the local, anisotropic shielding effect of the metal (*vide supra*). Secondly, the carbon atoms in the four-membered ring not bound to the metal exhibit large, deshielded values (144–149 ppm). This effect, also seen in ligand **60**, arises from the rehybridization[6] of the cyclobutadiene sp^2 orbitals and is observed in all phenylene topologies. A comparison of the ^{13}C-NMR data for the linear [3]-, [4]-, and [5]phenylene(CpCo)complexes with their respective parent ligands is given in Chapter 4.

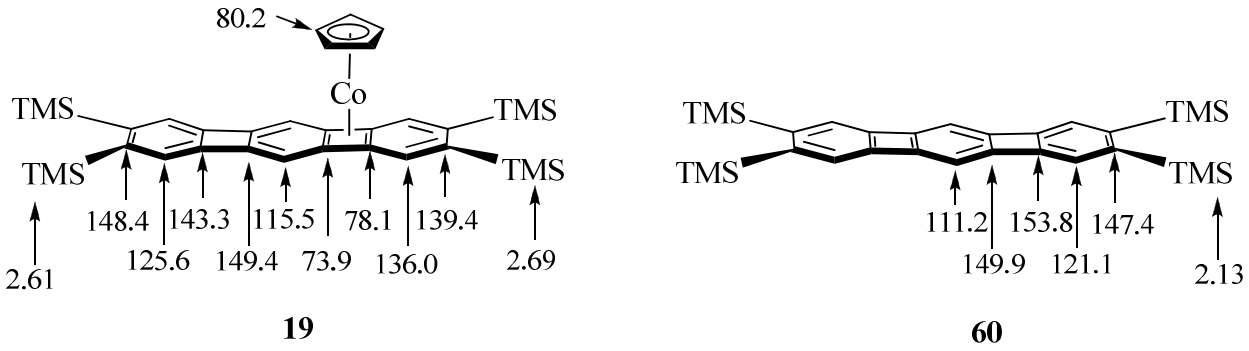

Figure 2.8. ^{13}C-NMR data for complex **19** and parent silylated ligand **60**. Values are in ppm.

2.4 Computational Mechanistic Studies of the η^4:η^4 Cyclobutadiene Haptotropic Shift

How does the CpCo moiety migrate from one cyclobutadiene unit to the next? Two extreme alternatives present themselves: a least-motion movement across the intervening arene unit or a more circuitous pathway along the periphery. The latter is prevalent in other computed haptotropic shifts,[56-57] in particular those occurring in (arene)$Cr(CO)_3$ complexes, all of which choose peripheral trails.[56] In these, the metal typically moves straight to the edge to adopt an η^4 (often described as η^1) trimethylenemethane-like transition state on the way to a neighboring ring, as illustrated for the η^6-η^6 hopping in naphthalene$Cr(CO)_3$ summarized in Scheme 2.18. More relevant is the computed course of the η^6-η^6 interconversion of (biphenylene)$Cr(CO)_3$ (Scheme 2.19).[57] The metal slides from the (near)center of one benzene ring to the quaternary (four-membered) ring carbon to reach a distorted trimethylenemethane maximum, and then proceeds to the edge of the bridging cyclobutadiene bond. This species represents a minimum on the potential energy curve and adopts an η^2-like complexed cyclobutadiene topology ("quasi-η^4"), from which it continues by the microscopic reverse on to the other benzene nucleus. The relevance of these findings with respect to the intercyclobutadiene hopping of CpCo along the phenylene frame was not clear at the outset of the work described in this section. The CpCo fragment has a different electronic requirement from $Cr(CO)_3$, and interring migration in arenes (and related systems) involves aromatic electron counts of all intervening circuits.

Scheme 2.18. Migration of $Cr(CO)_3$ Across Naphthalene

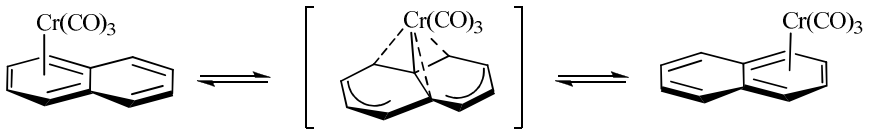

Scheme 2.19. Migration of $Cr(CO)_3$ Across Biphenylene

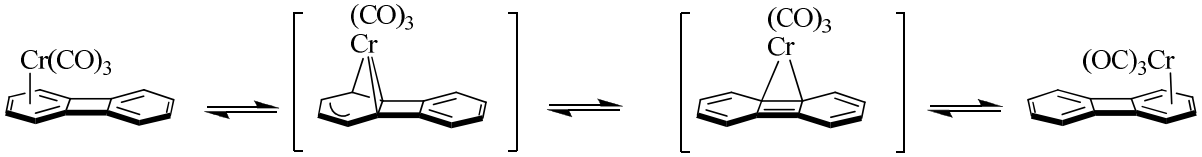

DFT calculations were carried out in collaboration with Professor Thomas Albright at the University of Houston. In these studies, using B3LYP 3-21G (carbon/hydrogen) and LANL2DZ (cobalt) basis sets, the metal fragment was placed 1.8 Å above the π system with energy minimizations carried out every 0.2 Å along the frame of the parent linear phenylene in question. When transition states and local minima were located, their structures were refined with the B3LYP 6-31G (hydrogen), 6-113G (carbon), and LANL2DZ (with inclusion of cobalt f-orbitals) basis sets. More computational details are given in Chapter 4.

The resulting potential energy surface for the thermal rearrangement in the parent linear [3]phenylene(CpCo)system is shown in Figure 2.9. Figure 2.10 contains enlarged images of the transition states and intermediate structures. The haptotropic shift begins with the (η^4-cyclobutadiene)CpCo global minimum (labeled ground state, GS), assigned a relative value of 0.00 kcal/mol. An η^2-cyclobutadiene transition state (TS 1), 26.9 kcal/mol higher in energy than GS, is passed before reaching a local minimum (LM) that lies 10.9 kcal/mol above GS. LM features CpCo coordinated unsymmetrically η^4 to the central benzene ring, thus avoiding an unstable 20 electron η^6-benzene configuration (not shown), which, when explicitly calculated, proved to lie 36 kcal/mol above LM. From LM, a symmetry-related second η^4 structure is reached via an η^3-benzene transition state (TS 2; barrier 14 kcal/mol) that symmetrizes the "left" with the "right" half of the molecule. LM is 24.9 kcal/mol higher in energy than GS. The shift is completed through the reverse of the initial two movements, through LM and TS 1 on the other side of the ligand to reach the second cyclobutadiene ring. Thus, as for $Cr(CO)_3$ (Scheme 2.19), CpCo migrates along the edge of the linear phenylene, but, because of its differing electronic needs, through distinctly different intermediates and transition states. Most obvious is the internal η^2-cyclobutadiene TS 1, which, for Cr, changes to a peripheral η^2-intermediate. The calculated rate determining barrier of 26.9 kcal/mol (GS to TS 1) is slightly higher than that measured for the reversal of **53** to **52** (~23 kcal/mol). Part of this discrepancy may be due to ground state activation of **53**, which is ~2 kcal/mol less stable than **52**.

The LM structure has some resemblance to the isolated η^4-Cp*Co angular [3]phenylene **23** (Section 1.2). Its location in an energetic well of ~14–16 kcal/mol (TS 1 and TS 2) suggested that it may be observable at low temperature. This investigation is detailed in Section 2.5.

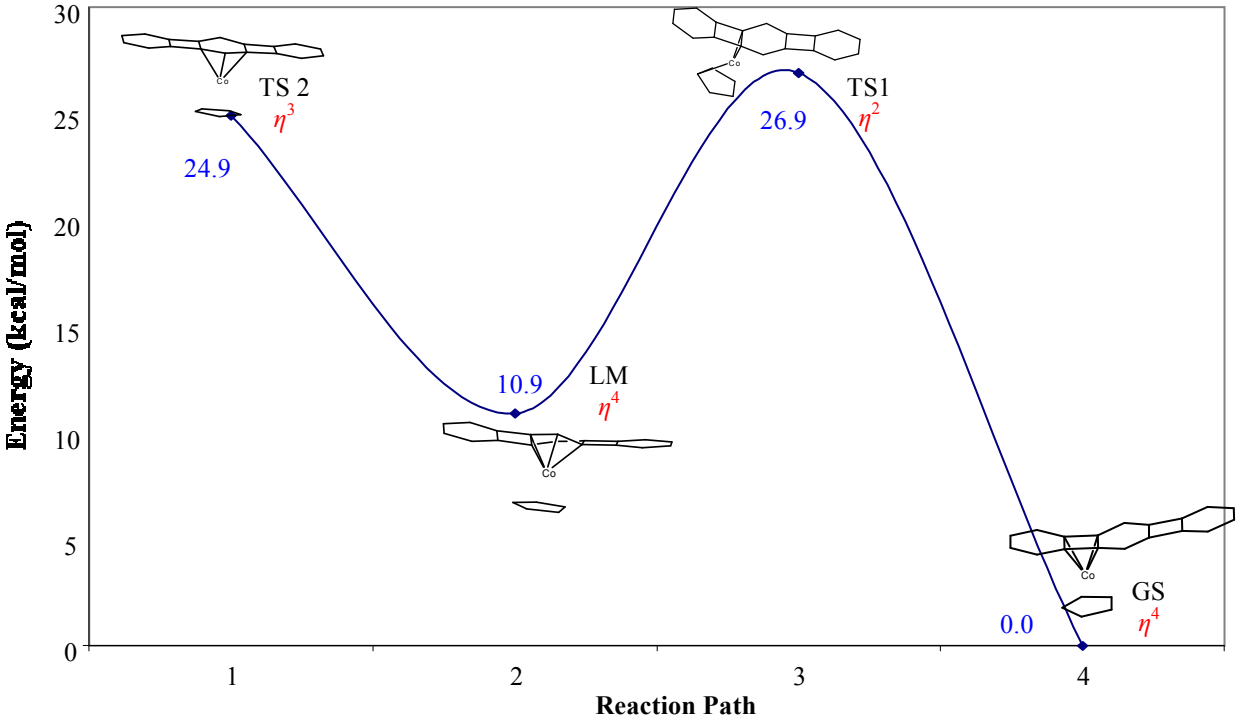

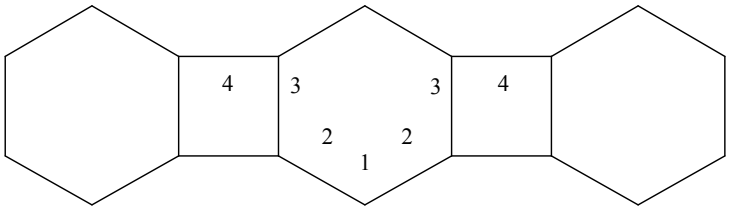

Key
- Global Minimum/Ground State (GS)
- Local Minimum (LM)
- Transition State (TS)

Figure 2.9. Calculated potential energy profile for the thermal η^4:η^4 haptotropic shift in linear [3]phenylene(CpCo). Relative energies are shown in blue and are given in kcal/mol. Structure labels and hapticity are highlighted in black and red, respectively.

(a) Global minimum: η^4-cyclobutadiene (0.0 kcal/mol)

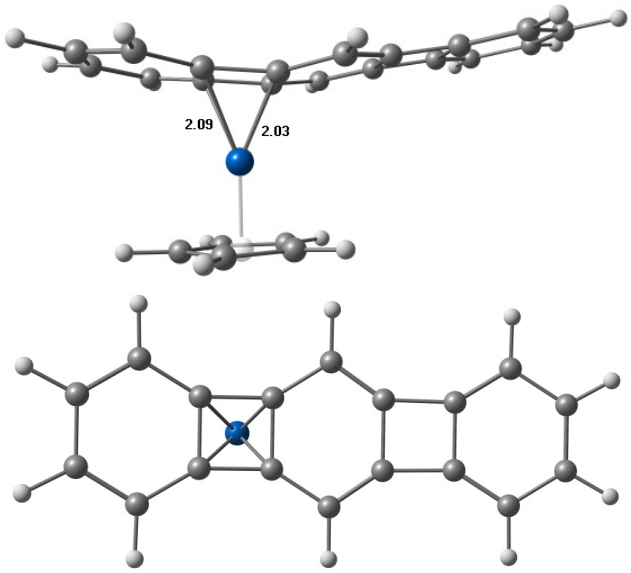

(b) Transition state 1: η^2-cyclobutadiene (26.9 kcal/mol)

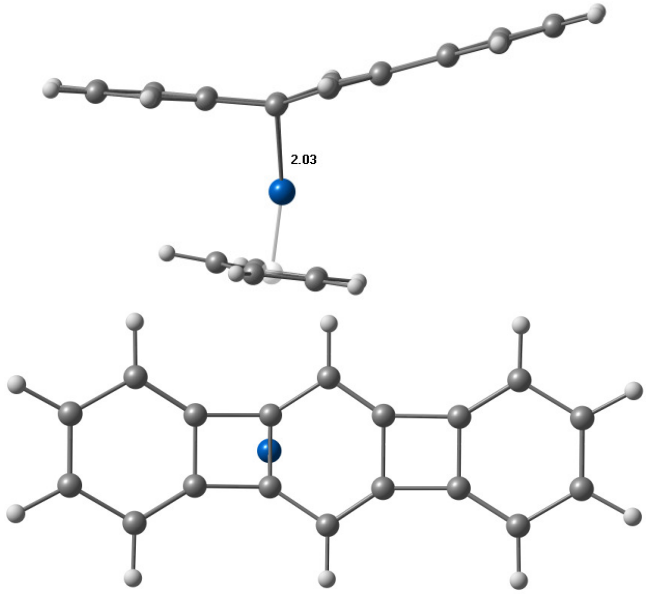

(c) Local minimum 1: η^4-benzene (10.9 kcal/mol)

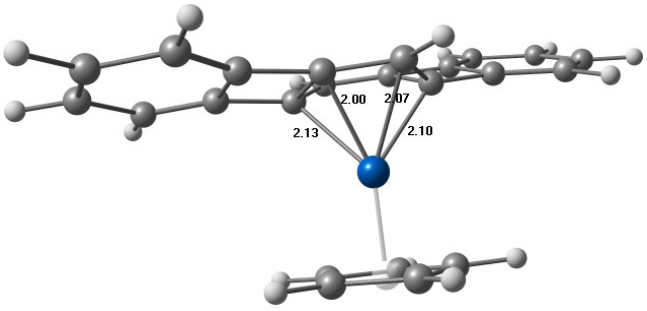

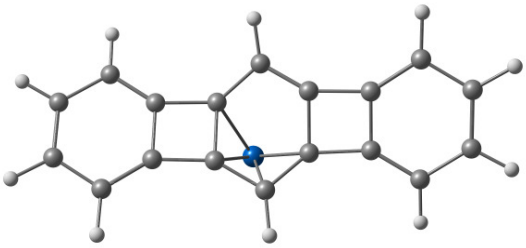

(d) Transition state 2: η^3-benzene (24.9 kcal/mol)

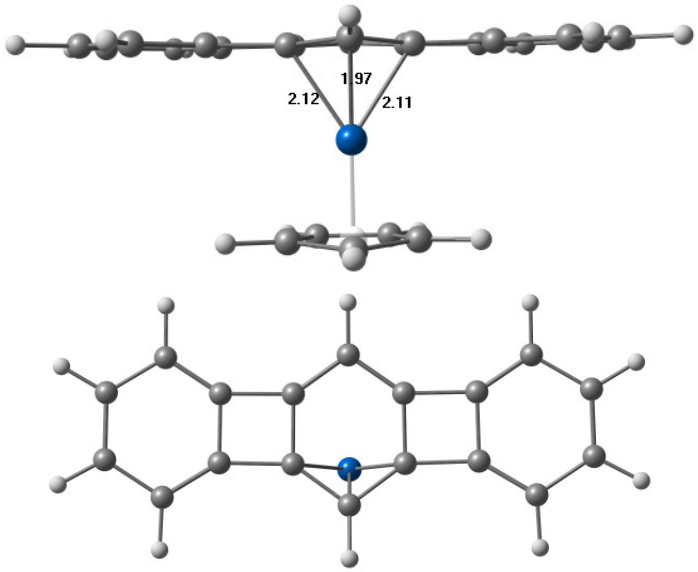

Figure 2.10. Optimized structures and relative energies for the linear [3]phenylene(CpCo) haptotropic shift. Carbon atoms are shaded grey, hydrogens light grey, and cobalt blue. Bond lengths are in Å.

The potential energy profile for the thermal shift in the linear [5]phenylene(CpCo) system was calculated in the same manner and is shown in Figure 2.11. Images of the intermediates and transition states are depicted in Figure 2.12.

Placing the metal fragment on the inner cyclobutadiene ring resulted in the lowest energy structure and was therefore set as the global minimum (GS). Two distinct haptotropic migrations, inner-to-inner and inner-to-outer cyclobutadiene, are now possible (Section 2.1). Beginning at GS, the metal can proceed in the direction of TS 2 or TS 3, respectively, both of which are η^2 with similar barrier heights (~36 kcal/mol). The former pathway is degenerate and continues from TS 2 to η^4-LM 1, and then via η^3 central benzene TS 1 to the symmetry related corresponding LM 1, TS 2, and finally GS involving the opposite inner four-membered ring. The rate determining barrier for this process is 35.9 kcal/mol, clearly too high to be measurable by NMR techniques, as found for **21**.[28,38] Interior-to-exterior shifting of the cobalt continues from TS 3 on to η^4-benzene LM 2. The η^3-TS 3 is traversed before the second η^4:η^2 sequence (LM3 and TS 5, respectively), ultimately leading to LM 4, which is the outer

cyclobutadiene coordinated structure and represents the photoisomeric species observed experimentally in Scheme 2.3. The computed rate-determining barrier (TS 3) of 26.3 kcal/mol for the reverse reaction of LM 4 to GS is close to the experimentally measured values of 25.6–27.6 kcal/mol for the derivatives in Table 2.1.

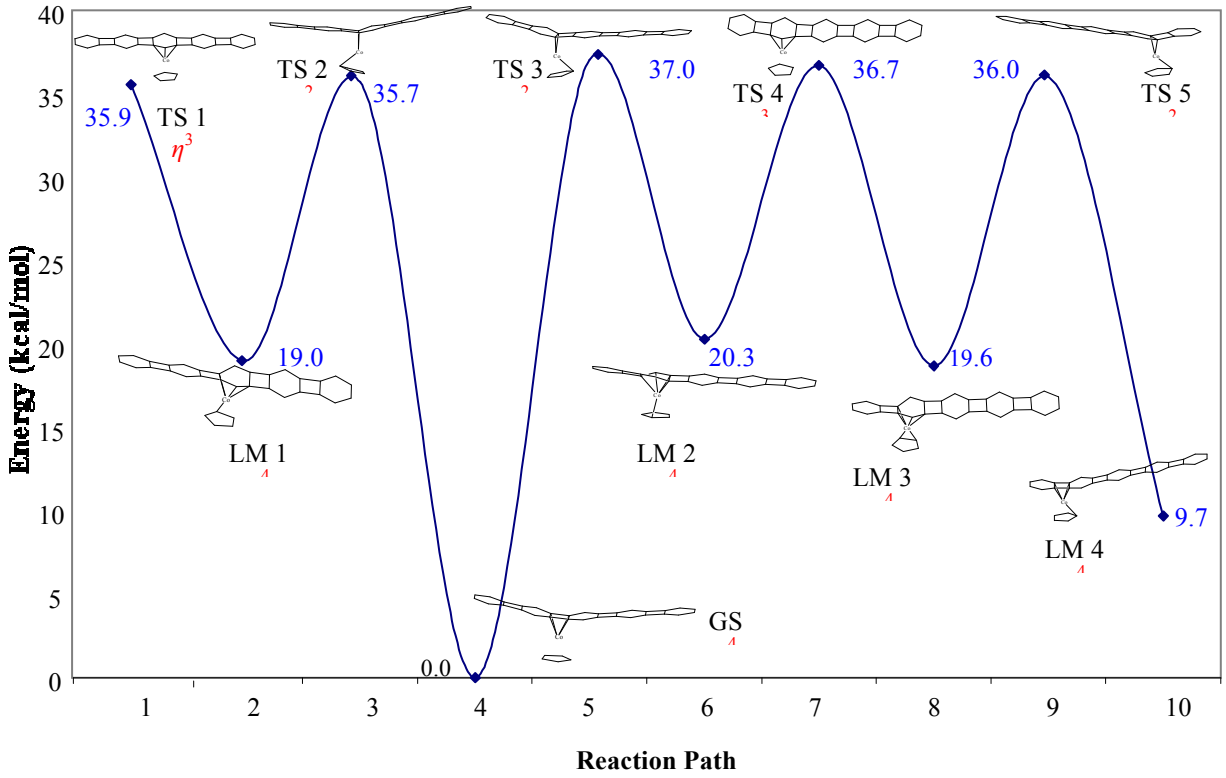

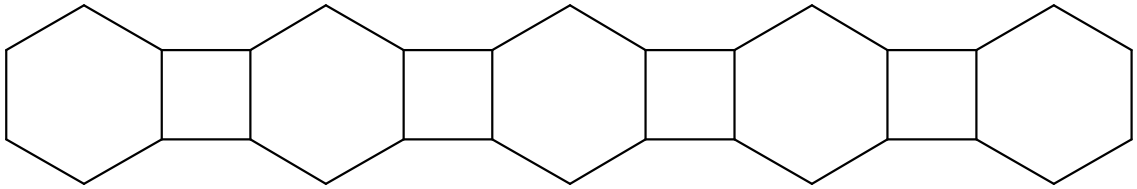

Key

- Global Minimum/Ground State (GS)
- Local Minimum (LM)
- Transition State (TS)

Figure 2.11. Calculated potential energy profile for the η^4:η^4 haptotropic shift in linear [5]phenylene(CpCo). Relative energies are shown in blue and are given in kcal/mol. Structure labels and hapticity are highlighted in black and red, respectively.

(a) Global minimum: η^4-cyclobutadiene (0.00 kcal/mol)

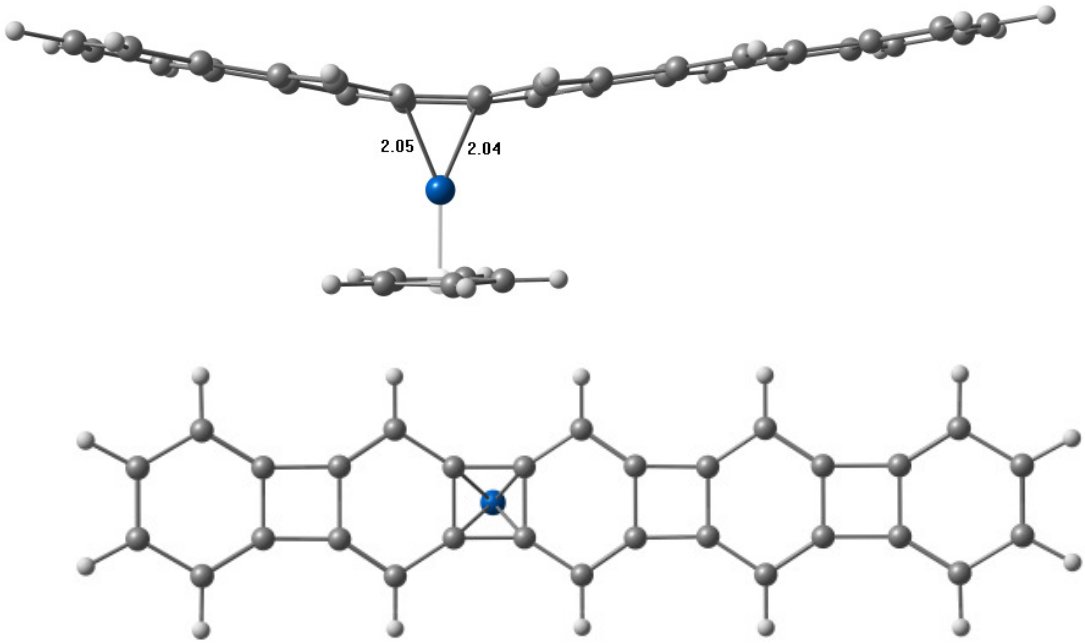

(b) Transition state 3: η^2-cyclobutadiene (37.0 kcal/mol)

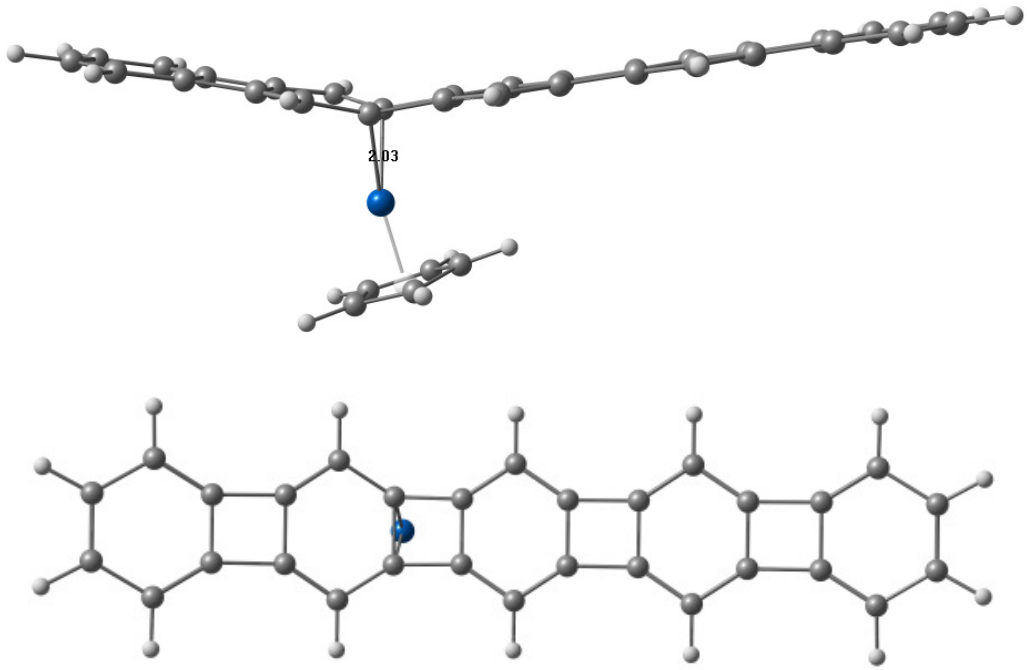

(c) Local minimum 2: η^4-benzene (20.3 kcal/mol)

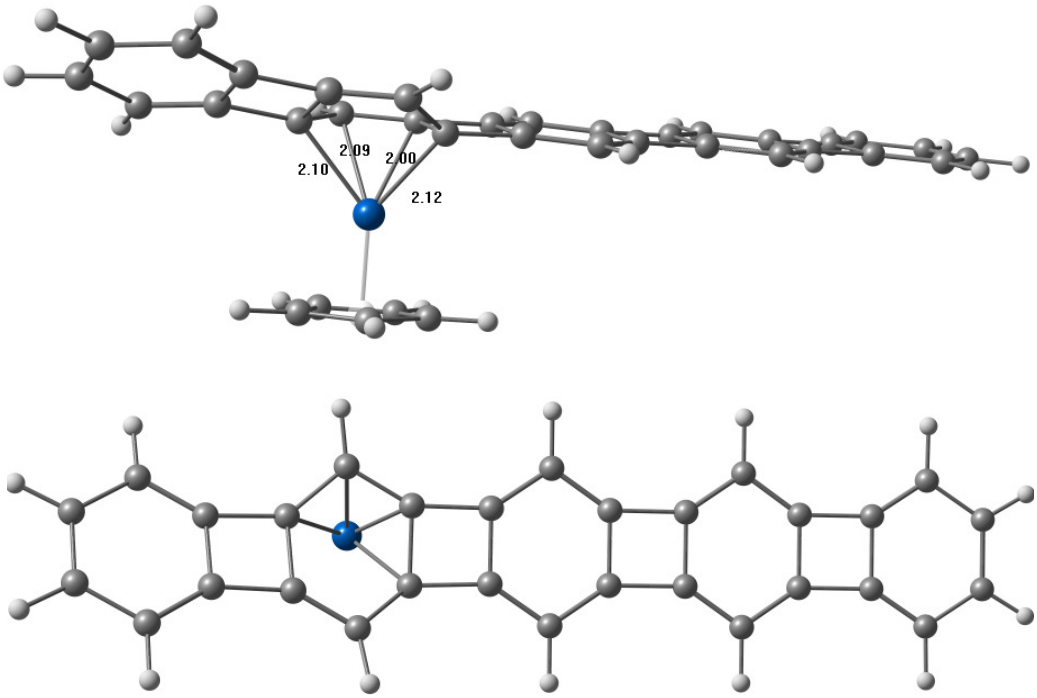

(d) Transition state 4: η^3-benzene (36.7 kcal/mol)

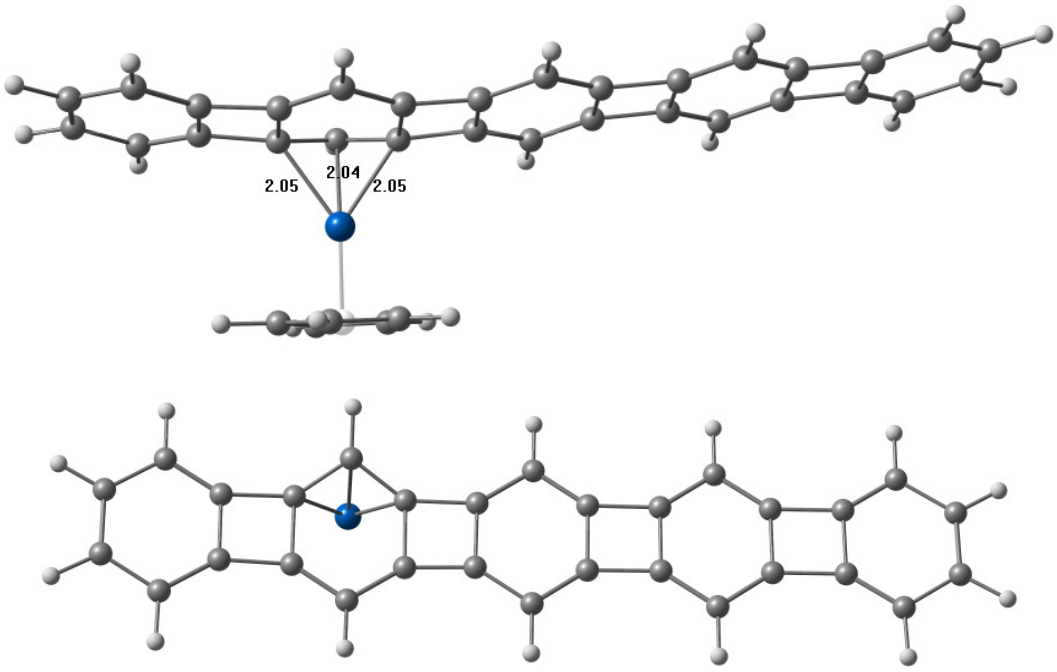

(e) Local minimum 3: η^4-benzene (19.0 kcal/mol)

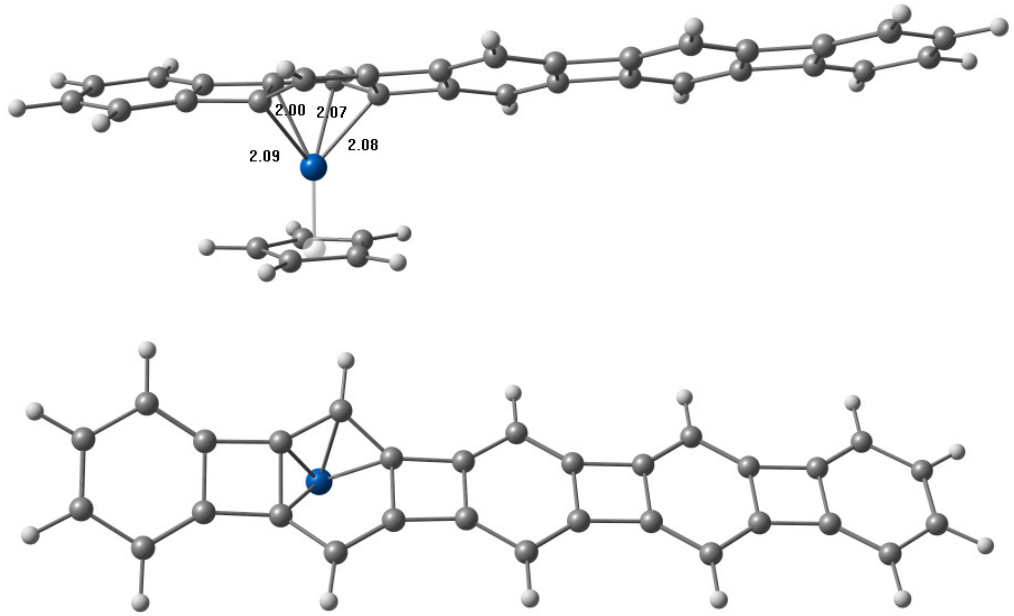

(f) Transition state 5: η^2-cyclobutadiene (36.0 kcal/mol)

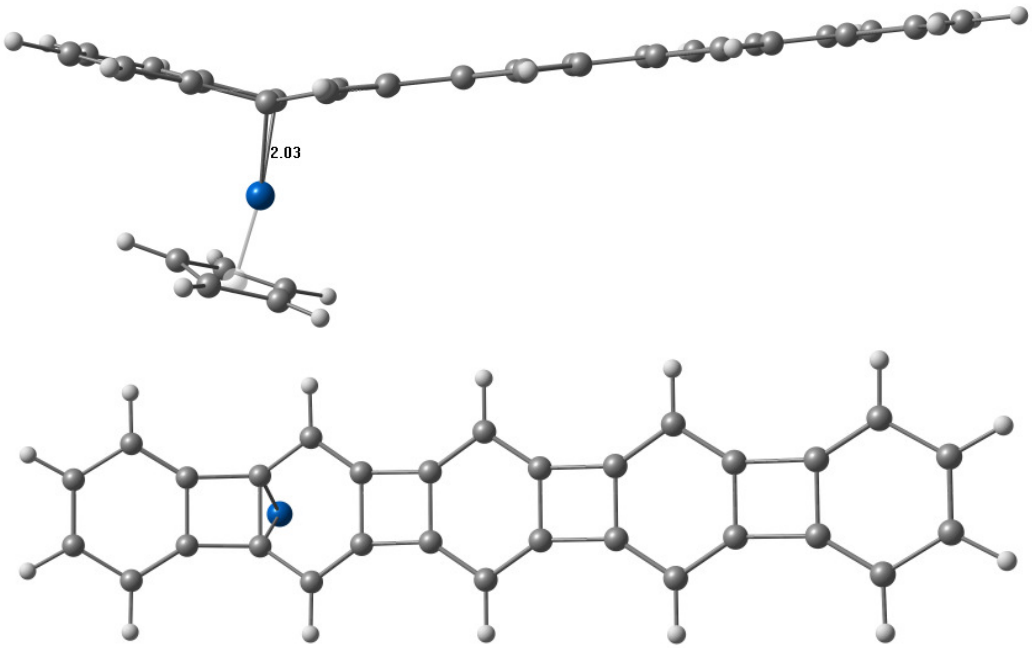

(g) Local minimum 4: η^4-cyclobutadiene (9.7 kcal/mol)

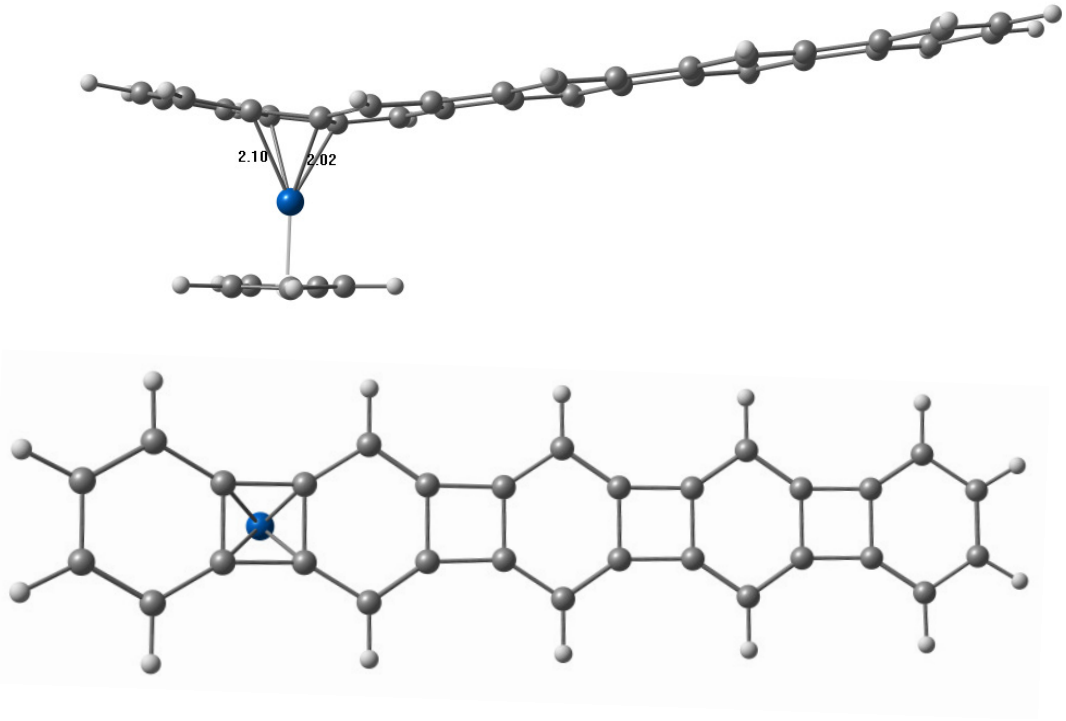

(h) Transition state 2: η^2-cyclobutadiene (35.7 kcal/mol)

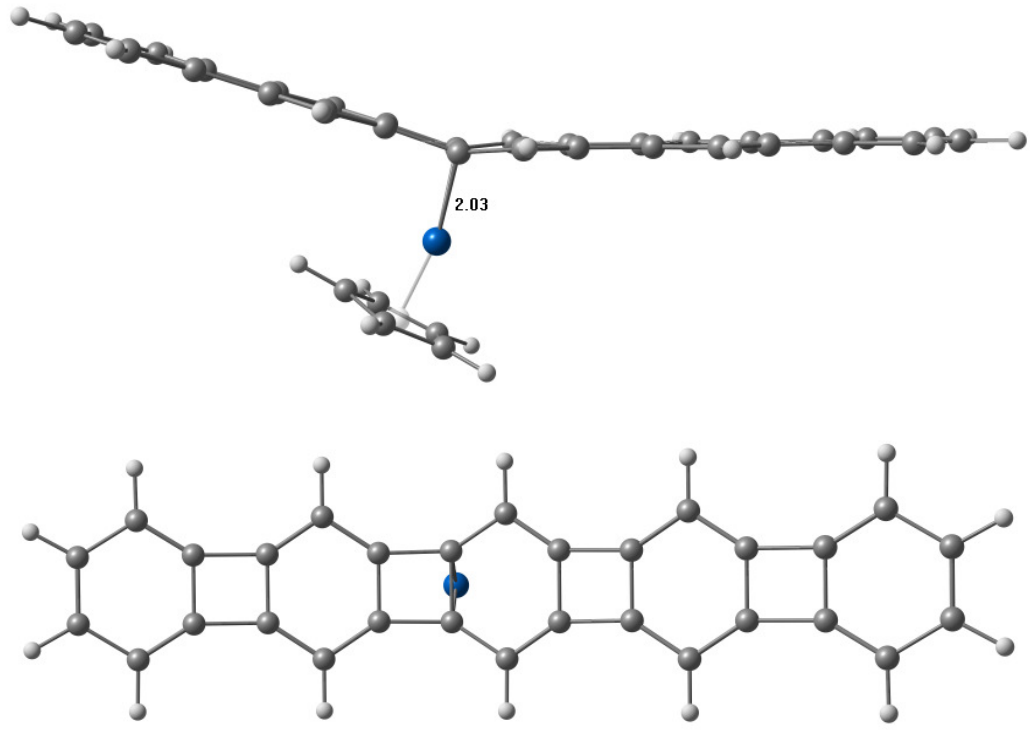

(i) Local minimum 1: η^4-benzene (19.0 kcal/mol)

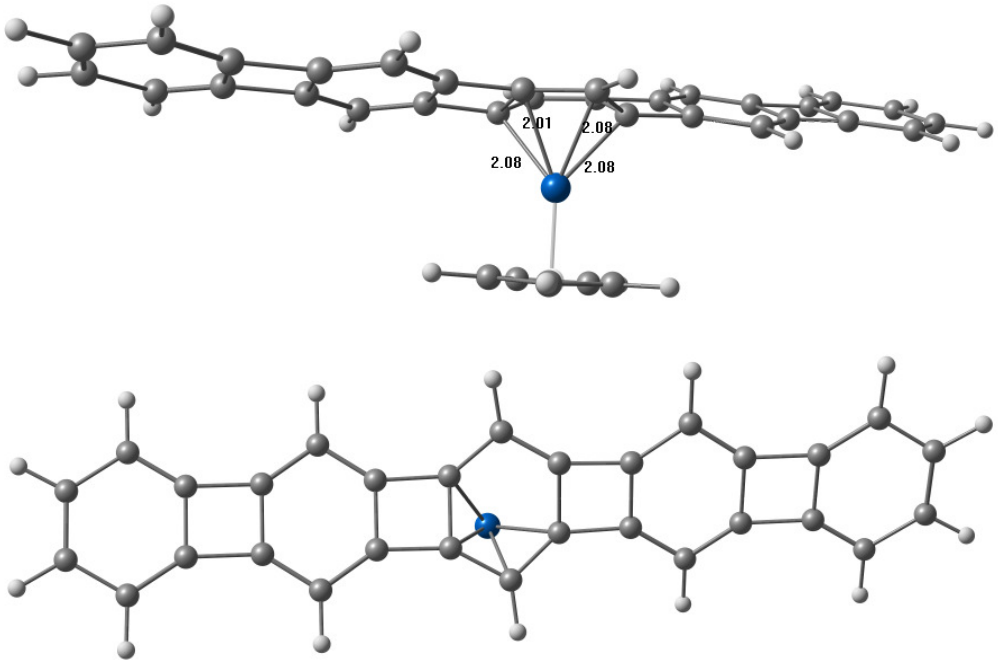

(j) Transition state 1: η^3-cyclobutadiene (35.6 kcal/mol)

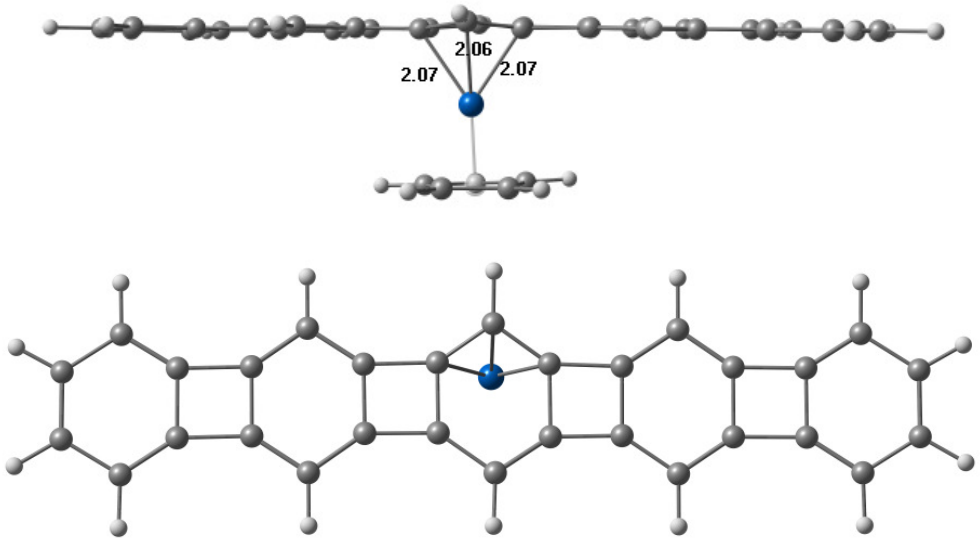

Figure 2.12. Optimized structures and relative energies for the linear [5]phenylene(CpCo) haptotropic shift. Structures for the inner-to-outer cyclobutadiene migration are given by (a)–(g). Species (h)–(j) are involved in the interior-to-interior four-membered ring pathway. Carbon atoms are shaded grey, hydrogen atoms light grey, and cobalt blue. Bond lengths are in Å.

Why does CpCo prefer complexation to the internal cyclobutadiene, that is GS (as represented by **21** and **42**) over LM 4 (as represented by **44** and **45**)? Calculations show that the energies required to distort linear [5]phenylene to the geometries found in

the complexed isomers are very similar (16 versus 14 kcal/mol). Hence the answer must rest on electronic grounds. Indeed, extended Hückel calculations reveal that the overlap populations between the frontier orbitals on the CpCo fragment and the HOMO and the LUMO of the π system are greater for GS (0.0793 and 0.0745, respectively) than for LM 4 (0.0556 and 0.0517, respectively). A didactically more instructive valence bond view recognizes that metalloaromatization of the inside four-membered ring allows the formulation of more resonance forms that avoid antiaromatic cyclobutadiene circuits. A full list of these resonance forms as well as details of the EHMO calculations are given in Chapter 4.

2.5 Low Temperature Photochemical Studies of the Haptotropic Shift in Linear [3]Phenylene(CpCo) Complexes

Of the various participating species in the mechanism for intercyclobutadiene migration (Section 2.4), specific attention was focused on the η^4-benzene intermediates that occur in both the linear [3]- and [5]phenylene haptotropic shifts. These structures are energetic local minima on the reaction profiles for both systems and were of considerable intrinsic interest, not only as reactive intermediates in this manifold, but also because of their relationship to the isolable angular [3]phenylene(Cp*Co) complex **23**[29] (Figure 2.13).

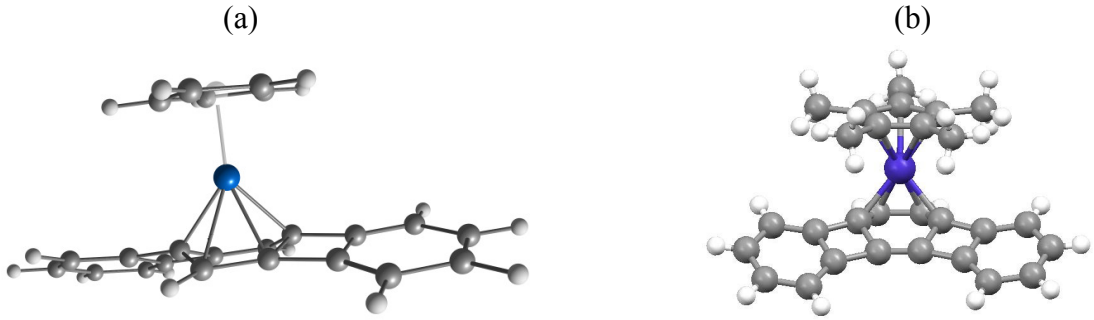

Figure 2.13. (a) Calculated structure for the η^4-benzene linear [3]phenylene(CpCo)intermediate in the haptotropic migration. (b) Crystal structure of η^4 angular [3]phenylene (Cp*Co) **23**.

While rare, a handful of other η^4-benzene-metal complexes have been isolated (Figure 2.14). For example, two related iridium based systems, benzene(CpIr) **66**[58] and benzene triphos(Ir) **67**,[59] are known. As expected, ligation causes significant shielding of the hydrogens in the η^4 portion of the ligand, especially the terminal positions.

The η^4 intermediates in the haptotropic shift are situated in wells on the potential energy surface that are ~17 kcal/mol deep for the linear [5]- and ~15 kcal/mol for the linear [3]phenylene complexes. These values are large enough that such species might be observable by NMR spectroscopy if irradiation of the starting materials were performed at low temperature and if the excited state would relax selectively to these intermediates. As a suitable candidate with which to explore this possibility, the partly symmetric tetrasilyl complex **19** was chosen. The generation of anticipated desymmetrized **68** would be readily detected by the appearance of 11 new singlets in the ^{1}H- and 23 new peaks in the ^{13}C-NMR spectra (Scheme 2.20).

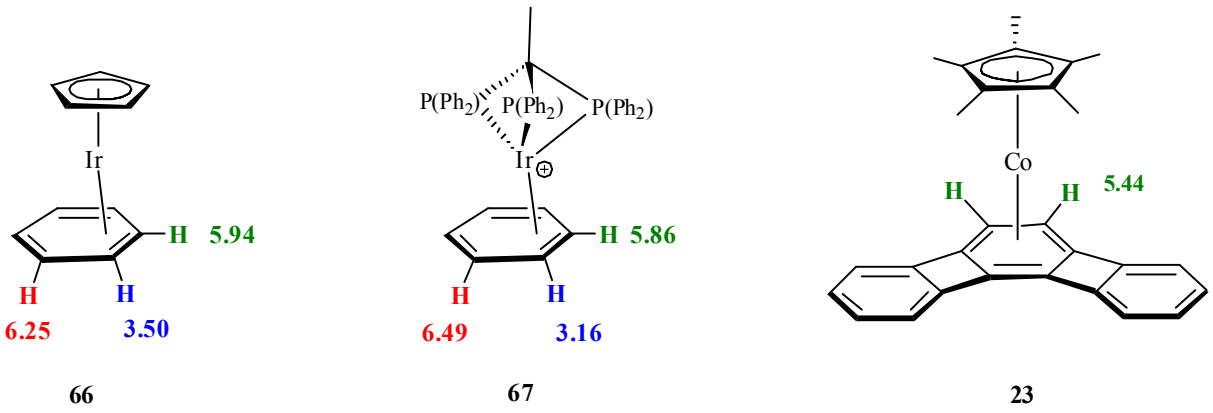

66 **67** **23**

Figure 2.14. Selected relevant examples of isolated η^4-benzene complexes and their proton NMR chemical shifts (ppm).

Scheme 2.20. Low Temperature Irradiation Experiment Designed to Generate η^4-Benzene Intermediate **68**

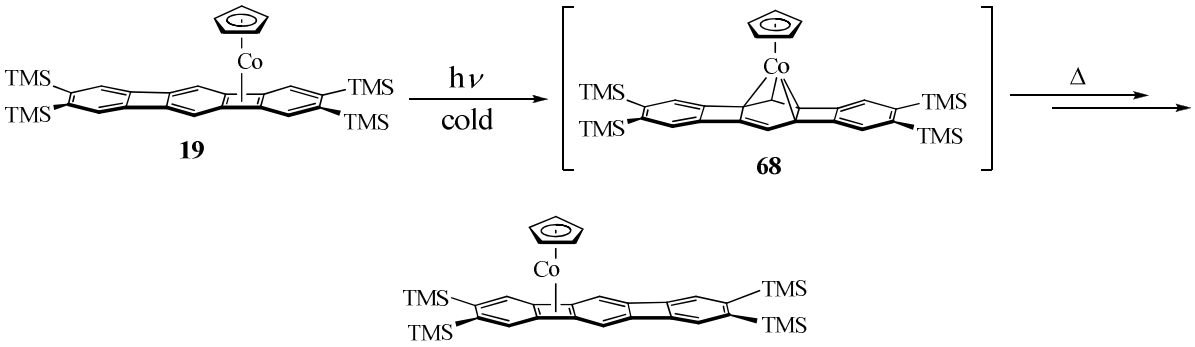

Construction of a satisfactory setup to allow for the planned low temperature irradiation was not trivial. An optimal experimental configuration, however, was devised utilizing three pieces of equipment, each of which is shown in Figure 2.15. The first was a custom-made Pyrex Dewar flask small enough to adequately contain an NMR tube. Cooling was achieved by means of a Neslab refrigerated circulating bath. Thirdly, a Rayonet Photochemical Reactor was used as the light source. The sample was first placed inside of the Dewar flask and cooled to the required temperature inside of the Rayonet. Once cold, irradiation was carried out for the desired length of time. When complete, the sample was transported cold to the NMR laboratory, and *very quickly* placed inside of a pre-cooled NMR probe for analysis.

A solution of complex **19** was irradiated at –65 °C as described and its ^{1}H-NMR spectrum recorded at –30 °C, revealing a dramatic change. The signals for **19** had almost entirely vanished, and a set of new peaks appeared. The new aromatic resonances were comprised of two sharp singlets at δ = 7.08 and 6.44 ppm and a broad singlet at δ = 5.58 ppm, all of which integrated for 2 hydrogens each. Another broad

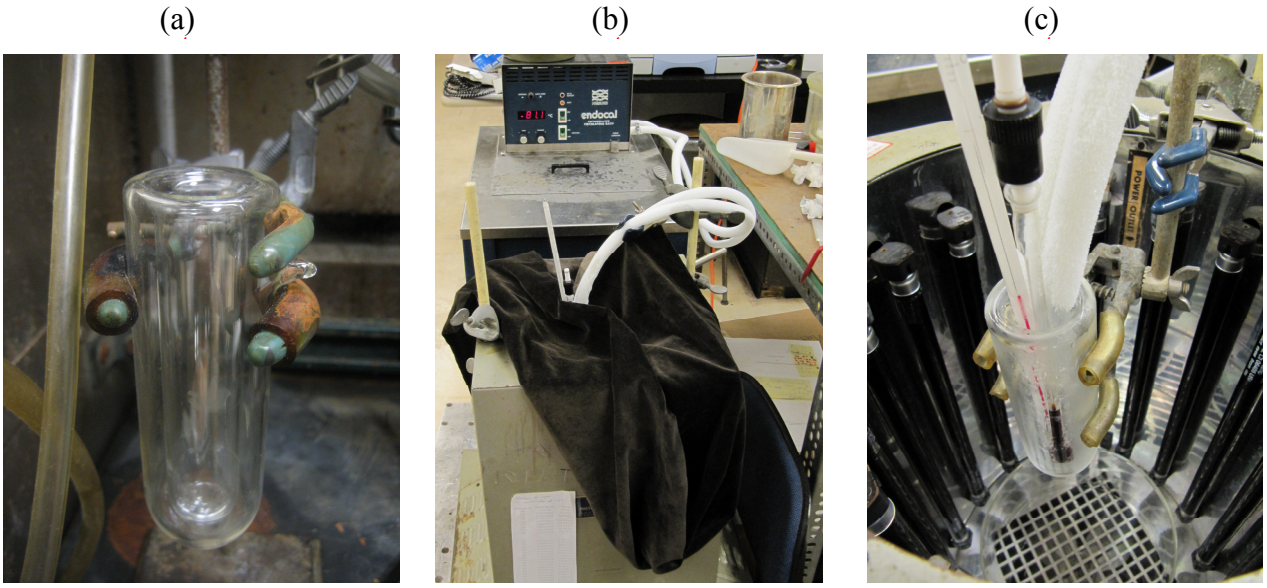

Figure 2.15. Cold irradiation experimental setup consisting of (a) Pyrex Dewar flask, (b) refrigerated circulating bath, (c) Rayonet Photochemical Reactor with Pyrex Dewar vessel placed inside.

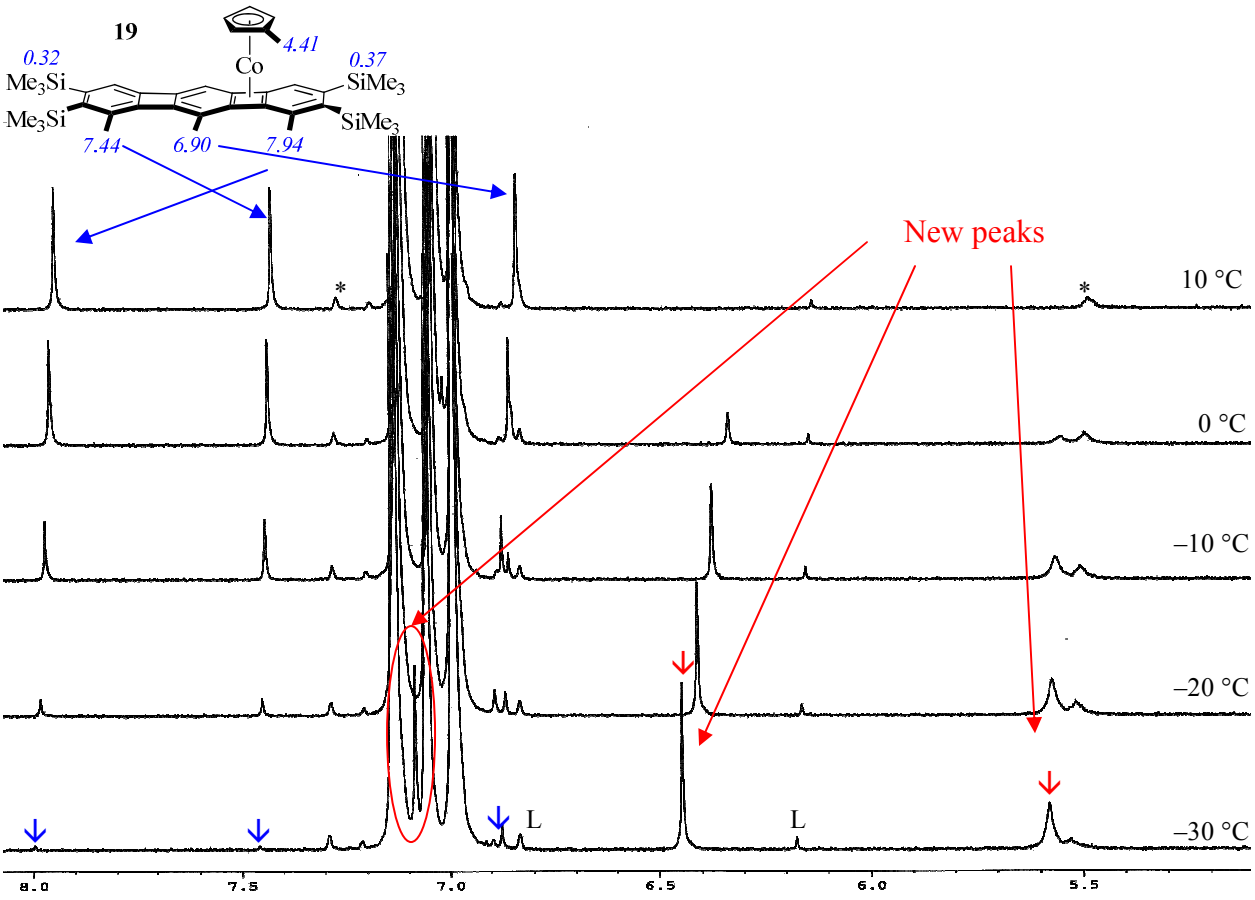

Figure 2.16. Stacked plot of the aromatic ^{1}H-NMR spectral region recorded after the cold irradiation of **19** in toluene-d_8. Peaks for **19** are indicated by blue, new peaks by red arrows. Impurities are marked with * and traces of free ligand **60** with L. The scale is in ppm.

singlet at δ = 3.98 ppm (5 H) was assigned to a new Cp group (Figure 2.17), and two new TMS singlets (9 H each, not shown) were also present. The new, broad Cp absorption displayed peculiar behavior, gradually moving to higher field ($\Delta\delta$ ~ 0.8 ppm for Cp-H) on warming from –30 °C to 10 °C (Figure 2.17). The broadened singlet at δ = 5.58 ppm showed similar, albeit much attenuated, behavior. At room temperature, all new peaks had disappeared, leading to regeneration of the original spectrum of **19.**

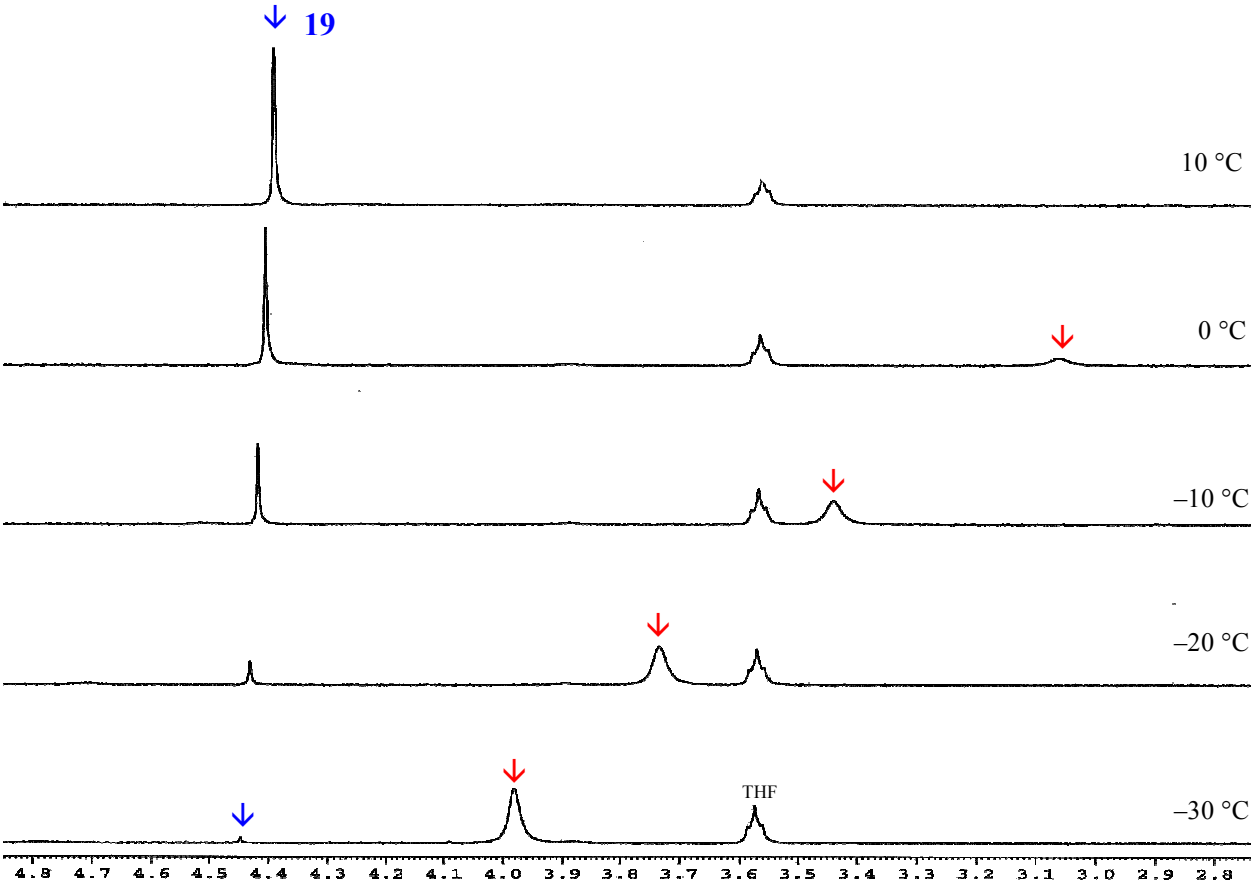

Figure 2.17. Stacked plot of the Cp spectral region in the cold irradiation of **19** in toluene-d_8. Peaks for molecule **19** are indicated by blue, the new peaks by red arrows. The scale is in ppm.

In addition to these NMR observations, a remarkable change in color from the red/maroon of **19** to olive green took place during the course of this experiment (Figure 2.18). Indeed, the UV-Vis spectrum of the low temperature species is strikingly different from that of **19**, showing a large, broad absorbance band centered in the visible region

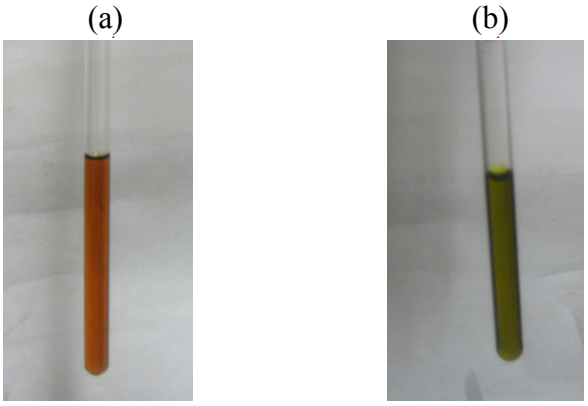

Figure 2.18. Color change during the low temperature irradiation of **19**. (a) Before irradiation. (b) After irradiation.

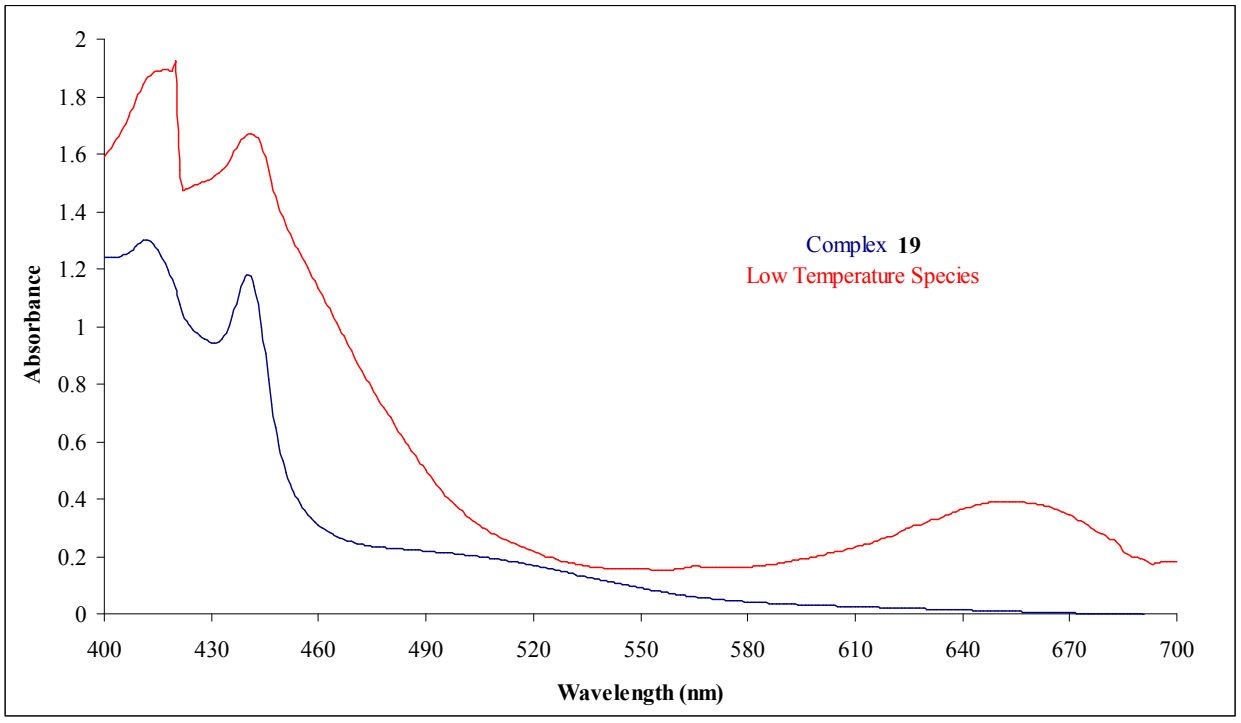

Figure 2.19. UV-Vis spectra (toluene) of **19** (at rt), shown in blue, and the new compound (at ~ –30 °C), shown in red.

at 654 nm (Figure 2.19). Warming the sample to room temperature restored its original red color.

While the observation of a new species was gratifying, the NMR data posed a puzzle, as they were clearly incompatible with (a static) structure **68**. Instead, they pointed to a molecule exhibiting mirror (or "top-down") symmetry along the long molecular axis, as in **19** itself. The two most obvious candidates, **69** and **70** (Figure

2.20), were ruled out, as the first could not be found during the computations underlying Figure 2.9, and the second actually constitutes the transition state TS 1 for the thermal reverse process.

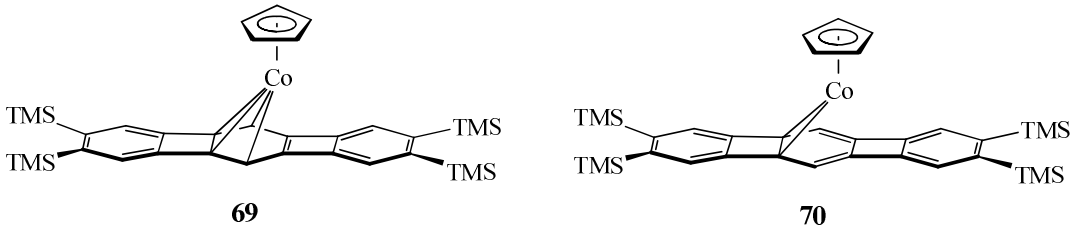

Figure 2.20. Possible (but unlikely) structures of correct symmetry for the low temperature photoisomer of **19**.

In the hope to shed further light on the nature of purported **68**, low temperature ^{13}C in conjunction with 2-D NMR (HSQC, HMBC) experiments were carried out. These data led to the tentative assignments shown in Figure 2.21. Assuming the presence of top-down symmetry, as surmised by the proton spectra, one would have expected to observe nine phenylene carbon signals. The actual spectrum, however, contains only six peaks. The Cp line was broadened to the point of being barely visible, and no crosspeaks for the absorption at δ = 5.56 ppm were seen by 2-D NMR spectroscopy.

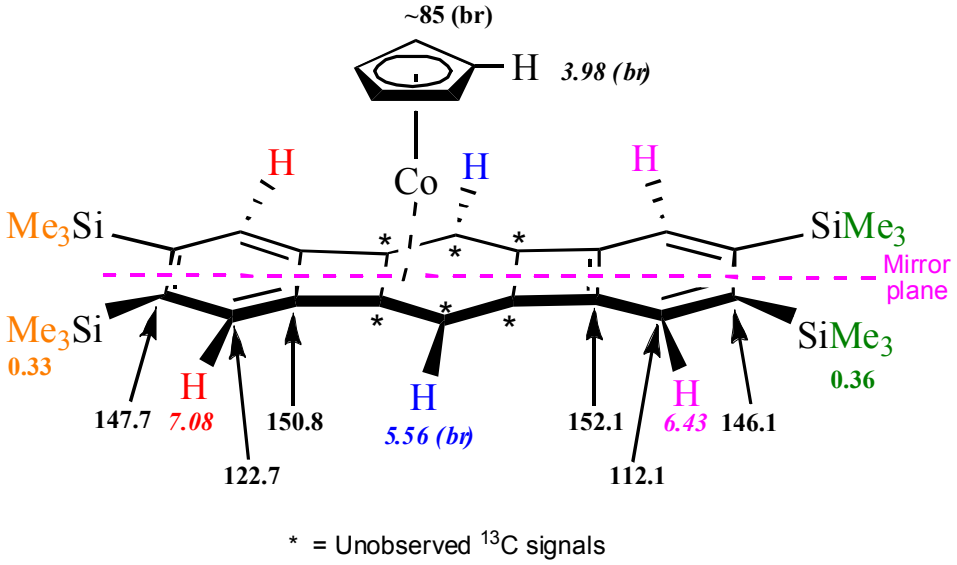

Figure 2.21. Partial assignments of ^{1}H-(italicized) and ^{13}C-NMR signals of **68**. The "top-down" plane of symmetry is indicated by the dashed purple line. HMBC: δ = 6.43 ppm correlates with δ = 146.1 and 152.1 ppm, δ = 7.08 ppm correlates with δ = 147.7 and 150.8 ppm, δ = 0.33 ppm correlates with δ = 147.7 ppm, and δ = 0.36 ppm correlates with δ = 146.1 ppm; HSQC: δ = 6.43 ppm correlates with δ = 112.1 ppm, δ = 7.08 ppm correlates with δ = 122.7 ppm, and δ = 3.98 ppm correlates with δ = 85 ppm. The connectivity of the CpCo to the central ring is left intentionally unspecified and the choice of positioning it to the left of the center hydrogens (blue)

arbitrary. Similarly, the assignments of the groups of "left" and "right" benzene signals are tentative and might be inverted. The carbons marked * could not be observed.

It is thus clear that we are dealing with an unusual species and, if it is **68**, the molecule must be partly (but not completely) fluxional around the central ring. Returning to the computed energy profile in Figure 2.9, one notes that central η^4:η^4-benzene fluxionality via TS 2 with a barrier of 14.0 kcal/mol is presaged. This process, which causes "left"-"right", but not "top"-"bottom" symmetrization, is unlikely to be responsible for the above data, as it should have given rise to two ^{1}H-NMR singlets for the central hydrogens. However, considering the expected relative closeness in the respective chemical shifts of the anticipated signals (see Figure 2.14), accidental isochronism could not be ruled out. Consequently, low temperature irradiation experiments were executed with **52**, in which the "left"-"right" option of symmetrization was obviated by the substitution pattern, while leaving the "top"-"bottom" option intact (Scheme 2.21). As

Scheme 2.21. Low Temperature Irradiation of **52** and Possible Pathways for Fluxionality of Intermediate **71**

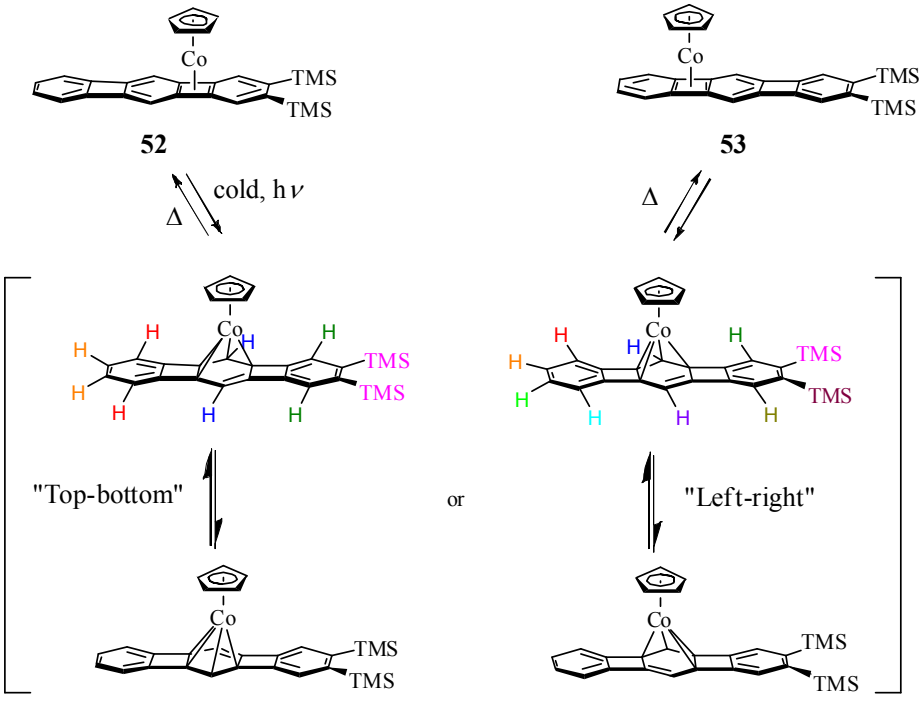

71

indicated in color, the latter would provide a diagnostically simple proton spectrum of only four phenylene signals. The former, on the other hand, should show eight such peaks. A potential complication of this experiment was the possibility of two regioisomeric (and non-interconverting) cobalt species located on either side of the central six-membered ring (Scheme 2.22).

In the event, the spectra shown in Figure 2.22 were obtained. At –60 °C, in

addition to unreacted **52** and photoisomer **53**, a new species formed, the spectral features of which implicate **71** as a "top-bottom" symmetrizing species. Specifically, the

Scheme 2.22. The Two Possible Regioisomers of **71**: "Left" and "Right"

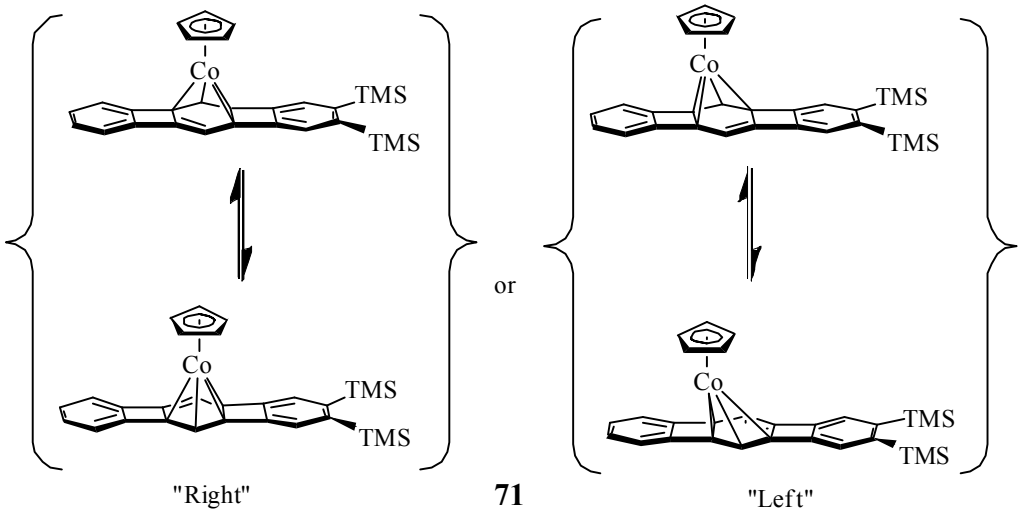

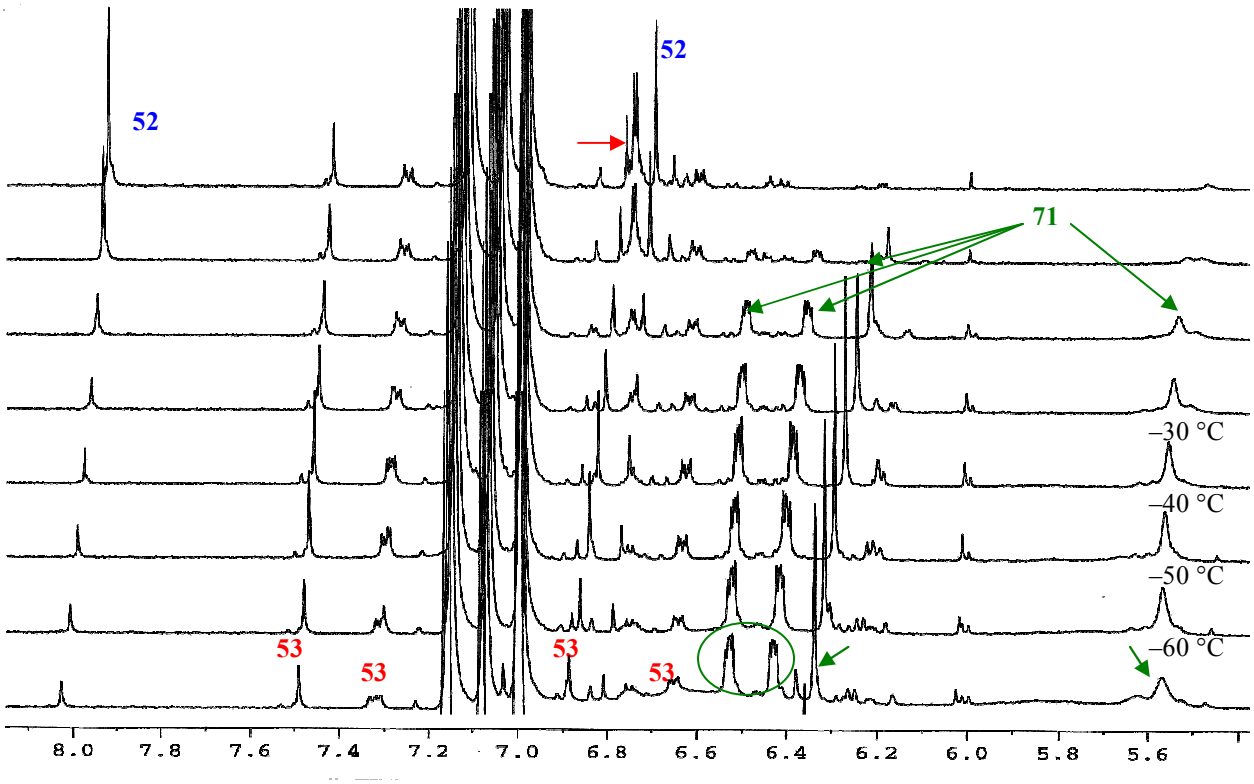

Figure 2.22. Stacked plot of the aromatic spectral region in the cold irradiation of **52** in toluene-d_8. Peaks for molecule **52** are marked by blue arrows, **53** in red, and **71** in green. Trace amounts of free ligand, bis(trimethylsilyl) linear [3]phenylene] **46**, are denoted with L. The scale is in ppm.

unsubstituted benzene terminus hydrogens exhibit an AA'BB' pattern at δ = 6.47 ppm which integrate for 4 hydrogens. The central ring hydrogens appear as a broad singlet at δ = 5.57 ppm (2H) and the silylated terminus as a singlet at δ = 6.32 ppm (2H). Warming the reaction mixture to 10 °C led to the gradual disappearance of **71**, with a concomitant increase of the signals assigned to **52** and **53**. This experiment confirms the conclusions drawn as a result of the low temperature irradiation of **19**, namely that a "top-bottom" symmetrizing species is generated.

Remarkably, in view of the possibility of two regioisomers (Scheme 2.22), only one set of peaks is observed, indicating that the excited state of **53** relaxes to settle on only one side of the central ring. Which side is a matter of speculation. Figure 2.23 compares the ^{1}H chemical shifts of **71** with those of **68** and, for calibration, **52**, **53**, and free ligands **46** and **60**. For the first pair, it is clear that the two species are very similar, with almost identical chemical shifts of the relevant hydrogens, taking into account the considerable deshielding effect of TMS substitution on the unsubstituted terminus in **73** (~0.7 ppm; cf. **52** vs. **53**, **46** vs. **60**). Arguably, placing the CpCo moiety to the "left", as depicted in **68** and **71**, aromatizes the proximal benzene by η^2-complexation of the adjacent four-membered ring, leaving considerable benzocyclobutadiene character on the "right", consistent with the associated chemical shifts.

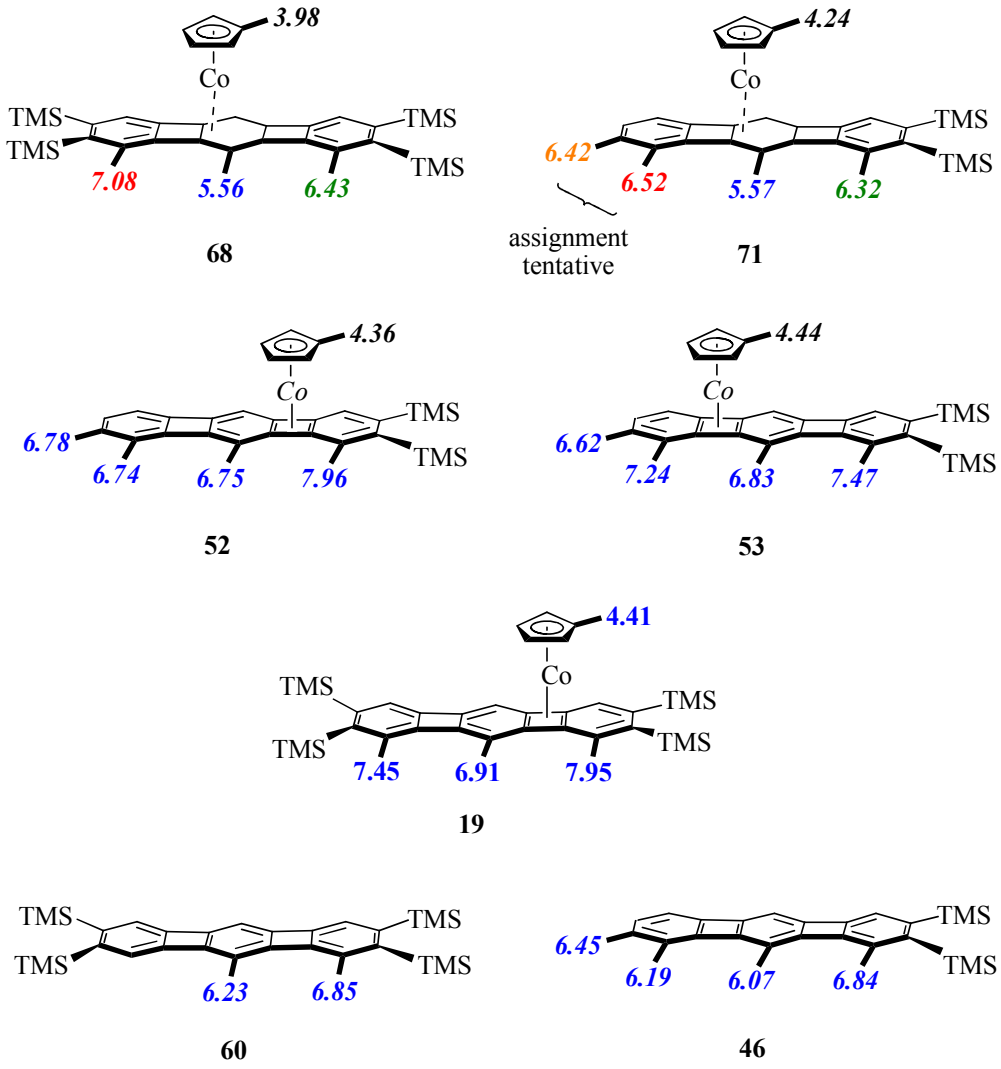

Figure 2.23. [1]H-NMR chemical shift comparison of **68** and **71** with other relevant species.

A plot of the changes in concentration of **52**, **53**, and **71** with temperature is shown in Figure 2.24. Within (the considerable) error, and considering the unusual magnetic behavior of **71** (vide infra), it appears that the latter converts mainly to **52** in the temperature regime in which **53** is stable with respect to its thermal reverse to **52**. This observation may be interpreted as indicating a lower barrier for Co migration from the center ring to the more stable cyclobutadiene haptomer.

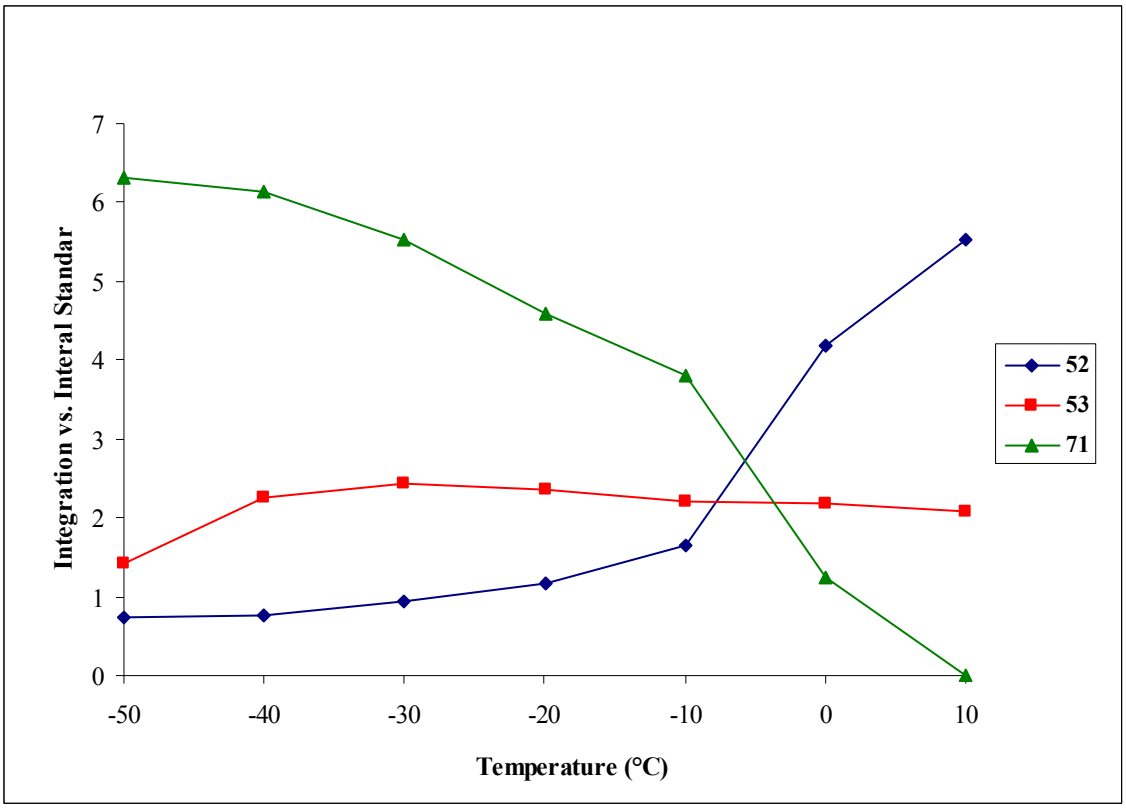

Figure 2.24. Plot of the concentration changes of **52**, **53**, and **71** with temperature, measured by the relative integrations of the peaks at δ = 7.96 (**52**), 7.47 (**53**), and 6.32 ppm (**71**), respectively. The $-CD_3$ peak of toluened-d_8 was used as the internal standard (set to 100).

Another plot, this one showing the ratios of **52**, **53**, and **71** with respect to each other, is given in Figure 2.25. The disappearance of **71** with rising temperature is illustrated by the increase in the ratios of **52**/**71** and **53**/**71**. As indicated by the steep slopes, the conversion of **71** into **52** and **53** is particularly fast between –10 and 0 °C. That complex **52** is preferentially formed is again confirmed by the escalating **52**/**53** ratio. While these data do not provide a definitive answer for the location of the CpCo, they are consistent with the plots shown in Figure 2.24 and the above discussions.

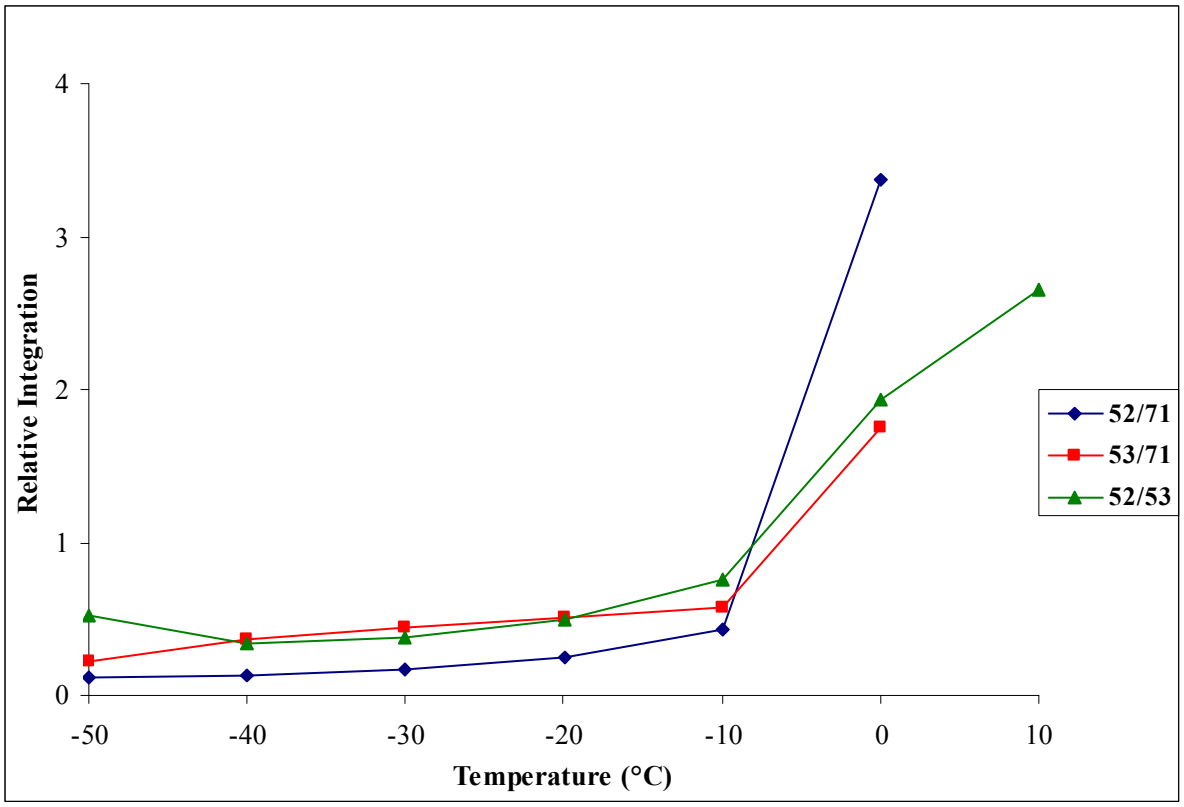

Figure 2.25. Plot of the ratios of **52**, **53**, and **71** against each other with temperature, measured by the integrations of the peaks at δ = 7.96 (**52**), 7.47 (**53**), and 6.32 ppm (**71**), respectively. The $-CD_3$ peak of toluened-d_8 was used as the internal standard (set to 100).

Having established the topological aspects of **68** and **71**, attention was turned to their peculiar NMR characteristics in the vicinity of the metal, i.e., the broad peaks for the central hydrogens and the CpHs, the broad Cp-carbon line, the inability to observe ^{13}C signals for the central benzene ring, and the temperature dependent drifting of (particularly) the Cp absorption. A trivial (and ultimately unsatisfying) explanation for at least peak broadening was the presence of trace paramagnetic, metallic impurities[60] that might have been generated during the irradiation process. Spin exchange, preferentially Co-based, might affect the center atoms in **68** and **71** more than the remainder of the molecule, although it should also cause line broadening in the isomers **19**, and **52** and **53**, respectively. Experimentally, the presence of such species was made unlikely by executing the cold irradiation experiment of **19** in the presence of the radical trap 1,3-cyclohexadiene, which produced spectra identical to those described earlier. An attractive alternative that might explain the data and, in addition, provide a mechanism for "top-down" exchange is of the intervention of triplet state cobalt species.

The ability of metals to change their electronic spin state and the consequences of this phenomenon on organometallic structure and reactivity are well documented.[61] 18-Electron CpCo complexes are ground state singlets, but their 16-electron counterparts, accessed typically by ligand dissociation, have more stable triplet configurations.[62] A number of CpCo and related Co species have also been reported in

which singlets are in thermal equilibrium with paramagnetic triplets by intersystem crossing.[63] Such complexes display spectral behavior very similar to that seen for **68** and **71**. For example, **72**,[63b] exists as a mixed spin state system in which the singlet predominates at room temperature in solution (Figure 2.26). On heating, the triplet becomes increasingly populated, shifting and broadening its NMR signals. Cooling the solution back to room temperature reverses these spectral changes. In addition to complexes of cobalt, analogous observations have been reported for other metals, such those based on hafnium,[64] copper,[65] ruthenium,[66] and tungsten.[67]

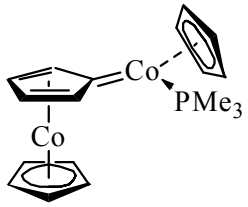

72

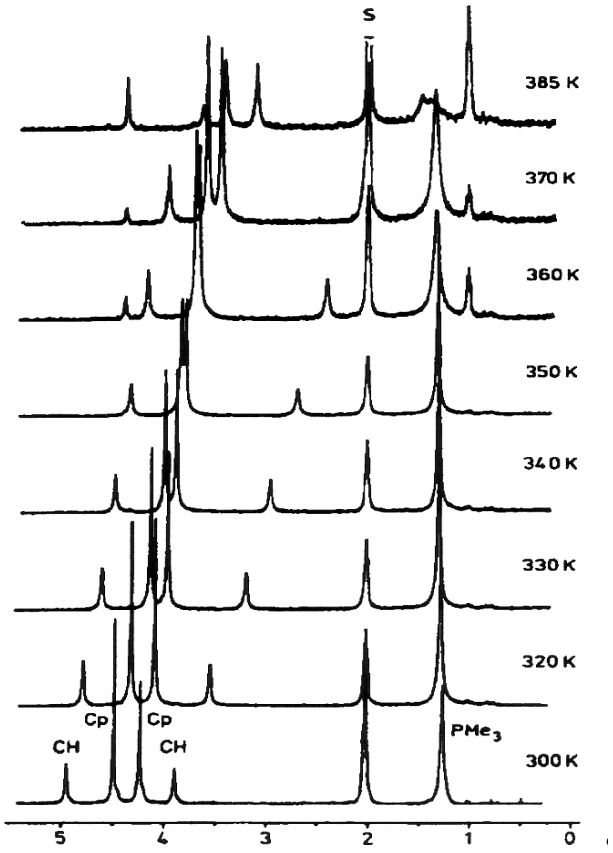

Figure 2.26. Temperature dependent chemical shifts in CpCo derivative **72** in toluene-d_8 (marked as S on the plot). The scale is in ppm.

Consideration of these examples would then suggest that **68**/**71** undergo "top-down" equilibration through a triplet 16-electron intermediate, or that **68**/**71** themselves are triplets or have thermally accessible triplet states, from which fluxionality might occur. Since the relaxation times (T_1) of paramagnetic systems[60a] are much shorter compared to their diamagnetic counterparts, measurement of this property was thought to be informative. The T_1 values for the proton in **68** were determined via a standard inversion recovery experiment[44] and are given in Table 2.4 (cf. Figure 2.20), in comparison to *p*-terphenyl.[60b]

Table 2.4. ^{1}H-NMR Relaxation Times in Intermediate **68** at –30 °C

Resonance (ppm)	T_1(s)
7.11	2.309
6.46	0.997
5.56	0.05
3.98	0.108

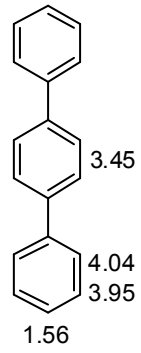

p-Terphenyl

In consonance with the associated line broadening, the relaxation times of the Cp (δ = 3.98 ppm, 0.108 s) and central ring hydrogens (5.56 ppm, 0.05 s) are much smaller than those of the remaining phenylene ligand (7.11 and 6.46 ppm, 2.309 and 0.997 s, respectively), the latter in turn comparing well with the values in *p*-terphenyl. With this corroborative evidence in hand, the question whether the species is itself a triplet or is in thermal equilibrium with such was addressed.

The answer can be obtained by using a Curie-like graph,[68] in which chemical shifts are plotted as a function of temperature.[65] A linear relationship corresponds to the presence of a triplet compound, while curved behavior is indicative of a singlet-triplet equilibrium. Plotting the chemical shifts of the Cp hydrogen of **68** and **71** against the inverse of temperature (Figure 2.27) gave distinctly curved lines, supporting the notion that these species are in thermal equilibrium with their triplets. The exact nature of these species, however, remains to be determined.

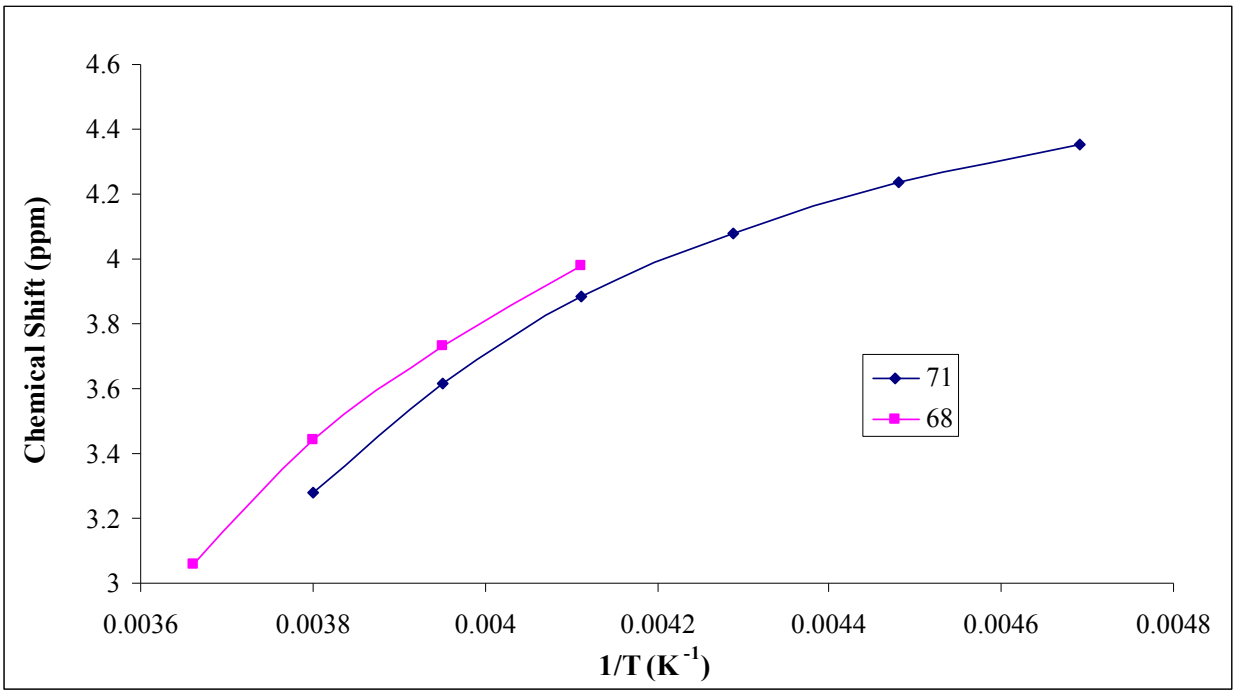

Figure 2.27. Plot of the Cp chemical shift (toluene-d_8) of **68** and **71** versus the inverse of temperature.

DFT calculations have commenced in an attempt to find a plausible structure for such a triplet cobalt species and, with it, possibly arrive at a mechanism for the fluxional behavior of **68** and **71**. These studies are being carried out in collaboration with Professors Tom Albright of the University of Houston and Vincent Gandon of the Université Paris-Sud 11. Preliminary results, at the B3LYP/6-31G(d,p) and BP86/6-31G(d,p) levels, suggest the η^2-cyclobutadiene structure depicted in Figure 2.28. It is apparent that this species corresponds topologically to singlet TS 1 in Figure 2.9 and **70** in Figure 2.20, endowed with the symmetrical requirements dictated by the experiments.

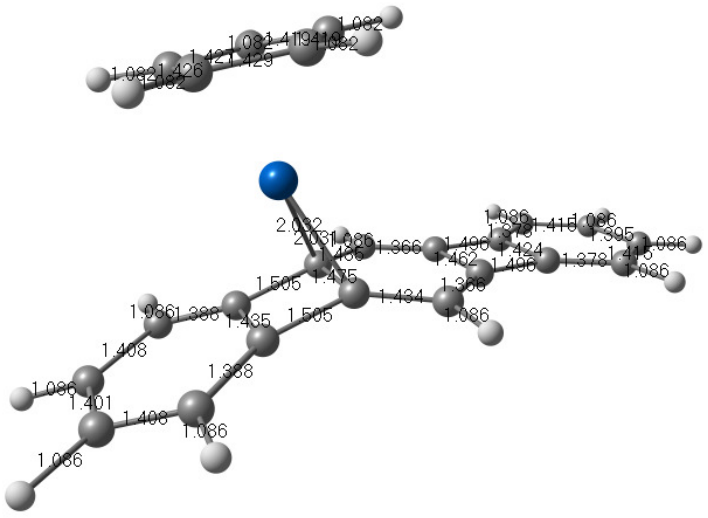

Figure 2.28. Calculated structure of a triplet η^2-cyclobutadiene linear [3]phenylene(CpCo).

One can therefore envision fluxionality between the two "top" and "down" η^4-benzene structures via the intermediacy of a triplet η^2-cyclobutadiene (Scheme 2.23). Further

Scheme 2.23. Conversion of "Top-Down" η^4-Haptomers of **68** Via a Triplet, η^2-Cyclobutadiene Intermediate

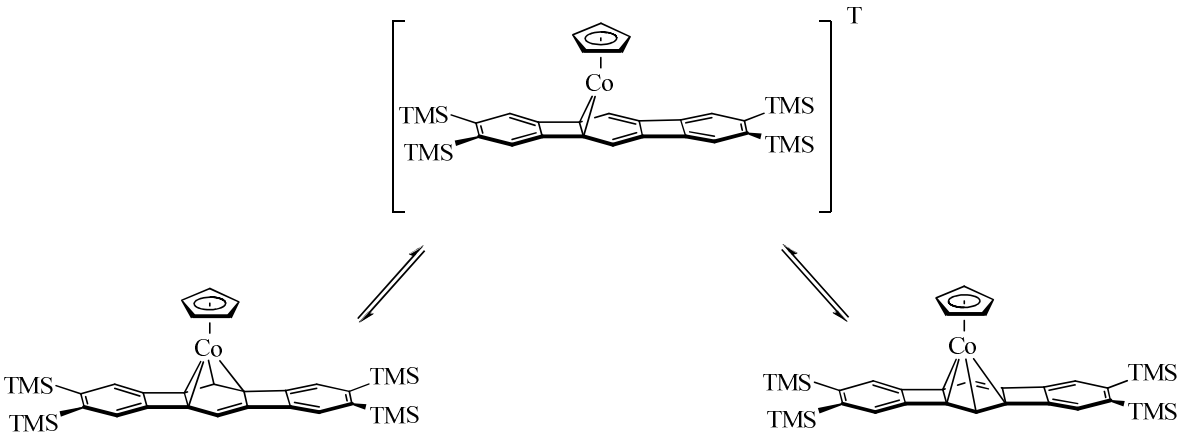

68

computations are required to pinpoint the minimum energy crossing points between the singlet η^4 and triplet η^2 structures and to explain why this triplet does not collapse to the CpCo cyclobutadiene isomer. This work is in progress.

2.6 Synthesis of Tetrakis(trimethylsilyl) Linear [3]Phenylene(CpCo)$_2$

All of the linear phenylene(CpCo) complexes mentioned thus far share one common feature: a single CpCo unit bound to the phenylene scaffold. However, since there are one or more additional cyclobutadienoid rings in the series, the question arises whether it might be possible to bind more than one metal fragment to the ligand. If so, what would be the structural consequences? Would be there further metalloaromatization? Would such systems be capable of light-induced haptotropism and, if so, how would the metals move relative to the ligand and to each other? Finally, would such complexes mimic structurally the variety of arrays obtained in the reaction of **29** with $Fe_2(CO)_9$ (Scheme 1.5)?

Since the linear phenylenes become increasingly more antiaromatic with size, the optimal candidates for preparing such multi-metallic systems should be the higher members of the series. Indeed, evidence for double CpCo attachment was obtained in the form of the minor by-products **73** and **74** (Scheme 2.24) obtained during the

Scheme 2.24. Side Products in the Preparation of Linear [4]- and [5]Phenylene(CpCo)

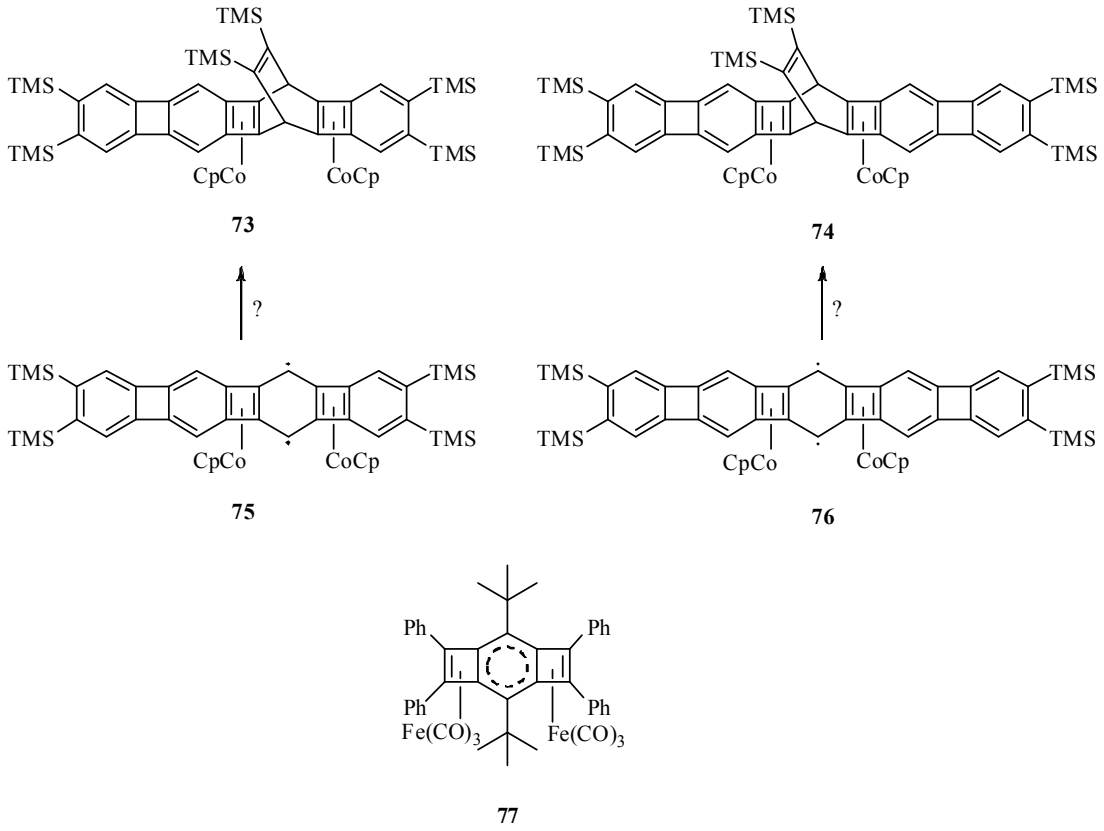

preparation of **20** and **21**, respectively (Scheme 1.3). These Diels-Alder type adducts of a third BTMSA molecule to the π-frame can be envisaged to be derived from **75** and **76**, respectively, in which the six-membered ring flanked by the two CpCo(cyclobutadiene) units would be expected to have an unusual (biradicaloid?) electronic structure. Evidence for the feasibility of such arrays rests on the unique black-red syn-bis(irontricarbonyl) compound **77**, whose structure was determined by X-ray analysis.[69]

With reasonable quantities of **19** in hand, the possibility of ligating a second CpCo unit to it was explored. This idea was further encouraged by the observation that crude samples of bis(trimethylsilyl) linear [3] phenylene(CpCo) complex **53** contained a very small (3 %) peak at *m/z* = 618, an exact match for the mass of a doubly metallated analog. Consequently, **19** was treated with one equivalent of $CpCo(C_2H_4)_2$ in benzene to afford a reddish black solid (Scheme 2.25). The mass spectrum data exhibited a

Scheme 2.25. Preparation of Complex **78** from Complex **19**

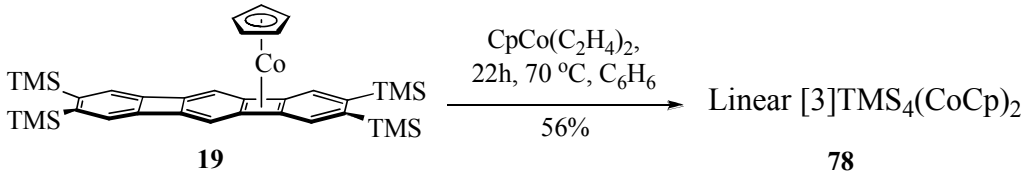

molecular ion peak at *m*/*z* 762, corresponding to **19**$(CpCo)_2$. The ^{1}H-NMR spectrum (acetone-d_6) revealed four sharp singlets integrating in the ratio 4:10:2:36, indicative of a highly symmetrical structure. The chemical shift of the benzene termini (7.36 ppm) suggested that these rings have significant aromatic character and is similar to the value of 7.45 ppm seen for the hydrogen positioned farthest away from the CpCo in **19** (Figure 2.7). Similarly, the ^{13}C signals of the terminal rings in **78** (150.5, 145.4, and 125.8 ppm) are analogous to those from the corresponding terminal ring in **19** (148.4, 143.3, and 125.6 ppm; Figure 2.8).

Detailed analysis of **78** with two-dimensional NMR techniques (HSQC and HMBC) allowed for a complete assignment of all peaks in the ^{1}H and ^{13}C spectra (Figure 2.29). The strongly shielded (relative to the free ligand) proton (4.81 ppm) and carbon (53.7 and 57.1 ppm) resonances assigned to the central benzene ring clearly showed that both cobalt fragments are coordinated to the phenylene ligand at this position. Interestingly, these data bear a very close resemblance to those of the corresponding diiron complex **31** (Scheme 1.5) and are compared in Figure 2.29. Its central ^{13}C resonances (68.8 and 58.2 ppm) are shifted upfield in a manner akin to **78**, although not quite as much, reflecting the increased electron withdrawing ability of the $Fe(CO)_3$ group relative to CpCo.[70] Complex **31**, like **78**, exhibits aromatized terminal benzene rings, as indicated by its ^{1}H (7.50 ppm) and ^{13}C (148.4, 144.6, and 125.8 ppm) chemical shifts.

These spectral similarities make it likely that **78** and **31** are isostructural. The only structural ambiguity pertains to the orientation of the two metal fragments with respect to the π ligand, a problem that had been left undecided in the assignment of structure **31**, i.e. **31a** (syn) versus **b** (anti; Scheme 1.5).[27] These options for **78** are

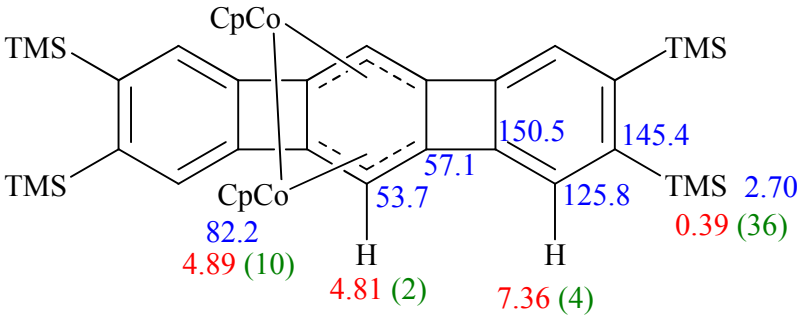

78

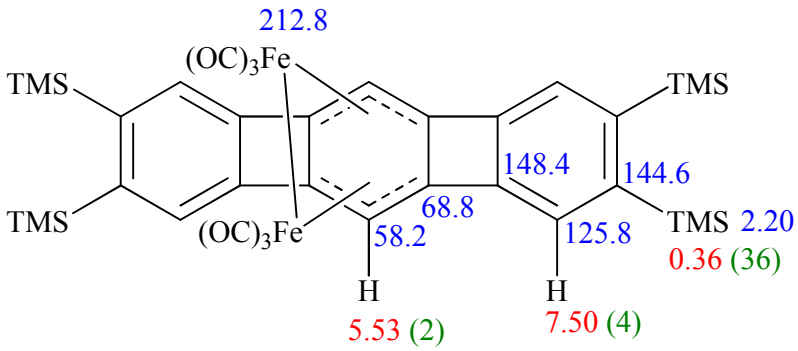

31a

Figure 2.29. Comparison of ^{1}H- and ^{13}C-NMR assignments (ppm) for molecules **78** (acetone-d_6), and **31** (^{1}H: acetone-d_6, ^{13}C: $CDCl_3$). Proton chemical shifts are in red and carbon in blue. Integrations for the proton resonances are in green. HSQC for **78**: δ = 0.39 ppm correlates with δ = 2.70 ppm, δ = 4.81 ppm correlates with δ = 53.7 ppm, δ = 4.89 ppm correlates with δ = 82.2, δ = 7.36 ppm correlates with δ = 125.8 ppm. HMBC for **78**: δ = 0.36 ppm correlates with δ = 145.4 ppm, δ = 4.81 ppm correlates with δ = 57.1 and 150.5 ppm, δ = 7.36 ppm correlates with δ = 57.1, 145.4, and 150.5 ppm. The placement of the cobalt atoms in **78** is tentative (see Figure 2.29).

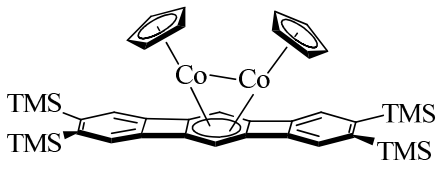

78a

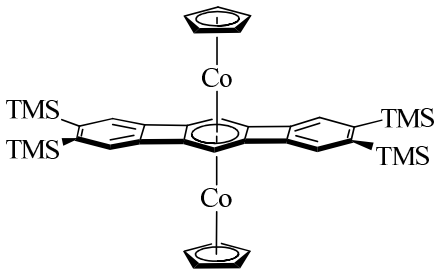

78b

Figure 2.30. Possible structures for 2,3,7,8-tetrakis(trimethylsilyl) linear [3]phenylene$(CpCo)_2$ **78**.

shown in Figure 2.30). Both equally exotic options are precedented in the literature and corroborated by X-ray structural analyses (Figure 2.31).[71]

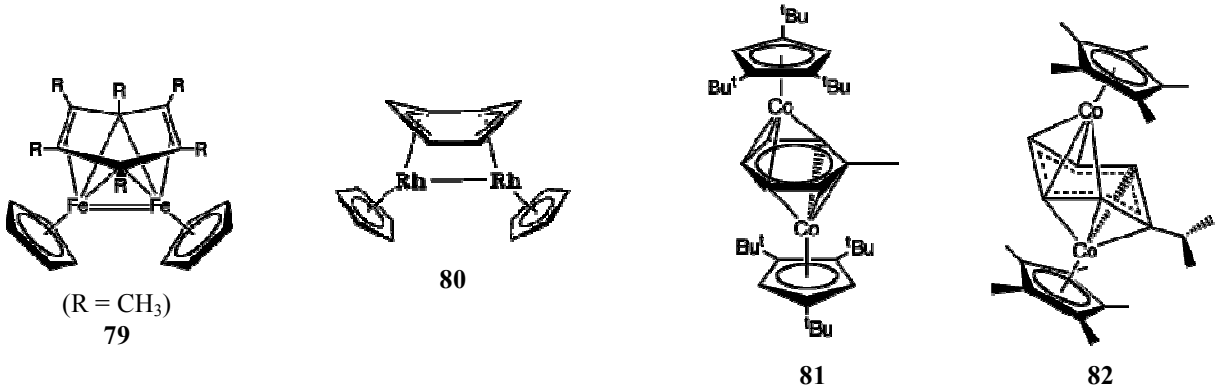

(R = CH_3)
79

80

81

82

Figure 2.31. Illustrative examples of complexes with two metal fragments coordinated to the same benzene ring.

Bis(CpFe) complex **79**[72] and its rhodium analog **80**[73] contain [{M_2}(*syn*-*μ*-arene)] units, in which the metals are linked.[58] Molecule **79** consists of two CpFe units coordinated η^4 to the boat-shaped benzene ring, sharing ligating carbon atoms. In contrast, the CpRh fragments in **80** are bound in an allyl η^3 manner and the arene also adopts a boat conformation. On the other hand, bis[tris(*tert*-butyl)]toluene(CpCo) complex **81**,[74] and the related system **82**,[75] both exhibit [{M_2}(*anti*-*μ*-arene)] units, in which η^4 coordination between the benzene ring and each of the metal fragments takes place. Here, the metals share carbon atoms, but now involving a sandwiched ligand. The arene in **81** retains a planar aromatic geometry, while the benzene moiety in **82** is bent into a highly distorted chair conformation.

Unfortunately, model structures **79**–**82** do not exhibit diagnostic NMR properties that would provide a clear distinction between *syn*/*anti* and planar/non-planar topologies. For example, the ^{1}H-NMR peaks for the toluene ligand in *anti*-complex **81** range from 4.00–3.80 ppm[74] whereas the signals for the benzene moiety in *syn*-bis(CpRh) **80** appear at 4.00–3.30 ppm.[73] The ^{13}C data are similarly inconclusive, as illustrated by comparison of **78** (56.2–53.1 ppm for the benzene ring) with **79** (64.8–52.5 ppm).[72b]

An interesting property of these bis(metal) arene complexes is fluxionality of the metal fragments by haptotropic shifts along the periphery of the aromatic ring, as depicted in Scheme 2.26. In complex **79**, the hexamethylbenzene ligand (bound η^4:η^4 in the solid state) displays a single arene resonance at 58.8 ppm in its room temperature carbon NMR spectrum. Cooling to –90 °C, however, produces two distinct arene peaks at 52.5 and 64.8 ppm (for the shared and single-metal-bound carbons, respectively, as shown in **79a** in Scheme 2.27). Fluxionality was postulated to proceed through an η^3:η^3 intermediate (**79b**) that is structurally similar to Rh complex **80**, which is itself a fluxional species.

Scheme 2.26. Examples of Fluxional Processes in Dinuclear Arene Complexes **79** and **80**

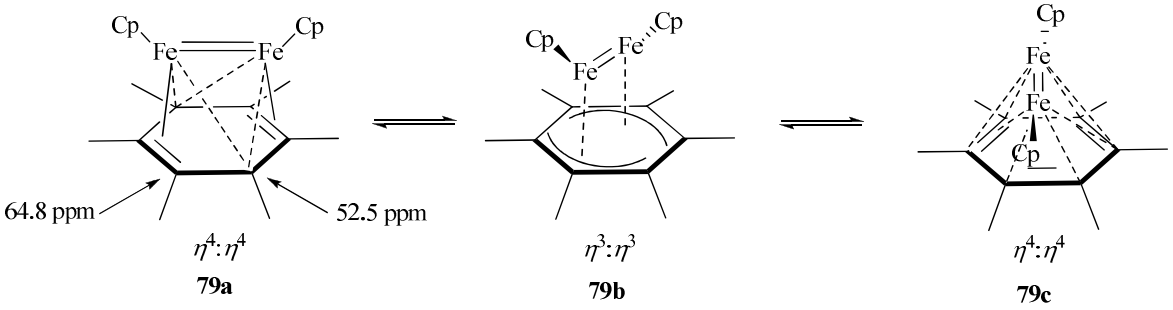

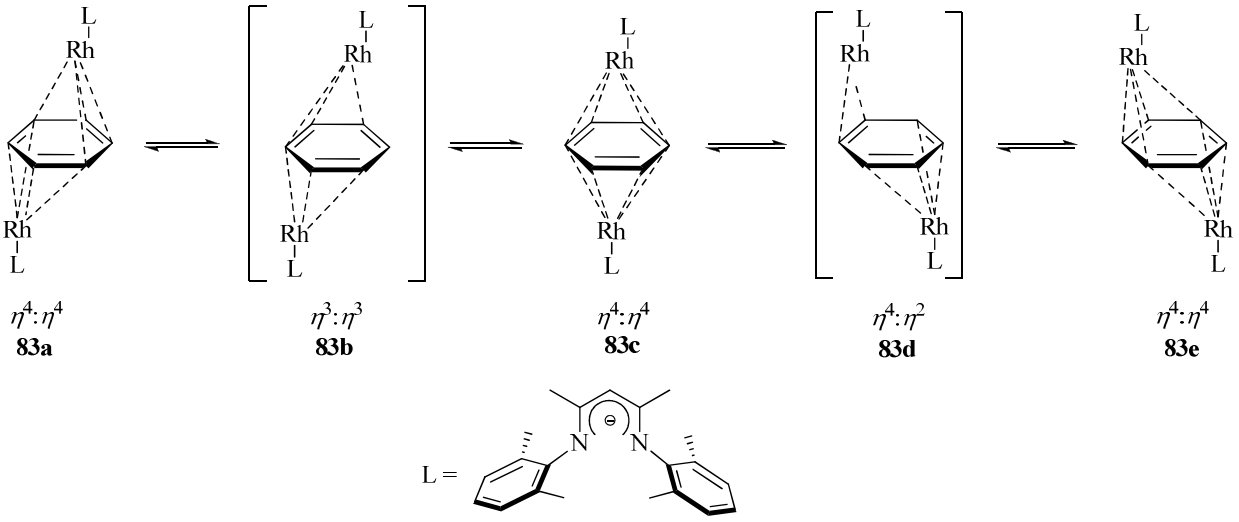

A*nti*-bis(*β*-diiminate)Rh complex **83** shows similar mobility (Scheme 2.26).[76] A mechanism for η^4:η^4 migration of the *anti*-metal fragments was proposed using the lowest energy species found by DFT calculations. In these compounds, the *anti*-metal fragments convert between η^4:η^4 (**83a**, **83c**, **83e**) structures by passing through η^3:η^3 (**83b**) and η^4:η^2 (**83d**) transition states. The energy barrier for η^4:η^4 migration in **83** was experimentally determined to be 6 kcal/mol. This value is in line with other experimentally measured *syn* and *anti* dinuclear ring slippage processes, which are typically ≤ ~10 kcal/mol.[71-75]

The possibility of fluxionality in **78** might be observable if asymmetric configurations, such as **78c** and **78d** (Figure 2.31), represent the lowest energy forms, since they entail NMR observable desymmmetrization of the ligand. Unfortunately, cooling **78** in the NMR probe to temperatures as low as –80 °C in toluene-d_8 did not reveal any signs of signal decoalescence.

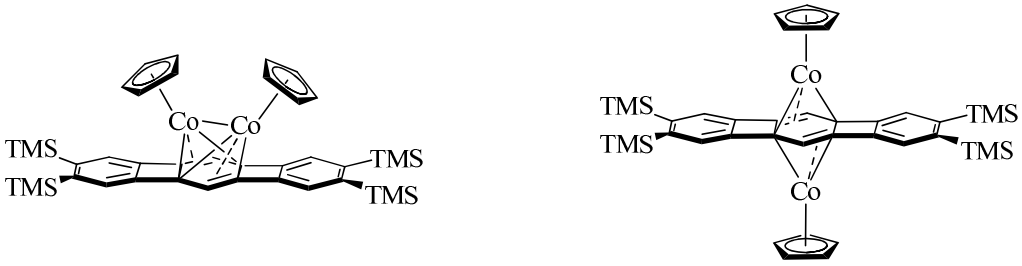

78c **78d**

Figure 2.32. Possible lowest energy forms of complex **78**.

Hoping that further light could be shed on the disposition of the CpCo moieties in **78** by chemical transformations, a brief investigation of its reactivity was undertaken. For example, bis(metal) arene complexes have been shown to readily undergo arene exchange reactions.[71] In complex **81**, for example, the toluene ligand is displaced by benzene at room temperature.[74] However, heating a sample of **78** to 120 °C in toluene-d_8 did not lead to any changes in the NMR spectra.

Turning to potential photochemical activation, **78** was irradiated at various wavelengths (300–365 nm). These conditions, as well as ambient sunlight, did not cause any changes in its ^{1}H-NMR spectrum, further documenting **78** as a rather inert species. X-ray crystallographic analysis would appear to be the only method of resolving the identity of complex **78**. Producing suitable crystals of this molecule, however, has proven extremely difficult and will be the subject of future investigations.

2.7 Summary and Outlook

The work presented in this chapter, published as a communication,[77] has detailed the first examples of η^4:η^4 intercyclobutadiene migration and detailed mechanistic studies of this unprecedented reaction. The haptotropic shift was found to be an intramolecular process, with the CpCo fragment undergoing various changes in hapticity for the thermal isomerization. Low temperature photolytic studies have revealed the existence of a thermally unstable intermediate species, the exact structure of which is uncertain. These results point to what appear to be significant differences between the photo- and thermal haptotropic pathways. Further work, both experimental and computational, will be required to elucidate the details of the photochemical reaction.

In addition to the studies of linear phenylene(CpCo) haptotropism, a hitherto unknown complex containing two CpCo fragments bound to linear [3]phenylene was prepared and scrutinized in preliminary form. Despite extensive characterization, the structure of this complex with respect to the position of the metal centers remains elusive. Future work will focus on the acquisition of a crystal structure.

Chapter 3

Nickel-Catalyzed Insertion Reactions for the Preparation of [N]Phenacene Derivatives

3.1 Introduction

Transformations involving metal insertion into the four-membered ring of the [*N*]phenylenes, as discussed in Section 1.2, represent a significant mode of reactivity with a high potential for practical synthetic utility. One specific application of this chemistry is the synthesis of the phenanthrene moiety via tandem metal insertion and alkyne cycloaddition to the four-membered ring (Scheme 3.1). Such a methodology

Scheme 3.1. Potential Preparation of the Phenanthrene Group from the Alkyne Cycloaddition with Biphenylene

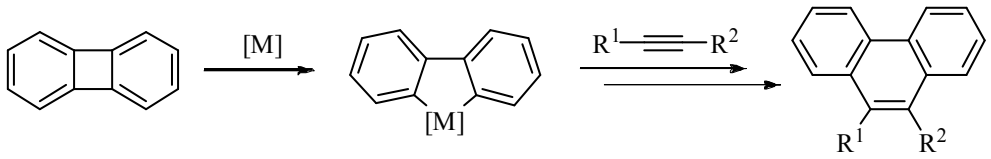

would be valuable for the preparation of PAHs possessing phenanthrene subunits but has remained fairly unexplored. Only a few examples demonstrating this transformation have been detailed previously for biphenylene (**7**) (Scheme 3.2).

Scheme 3.2. Metal Catalyzed Alkyne Cycloaddition Reactions with Biphenylene

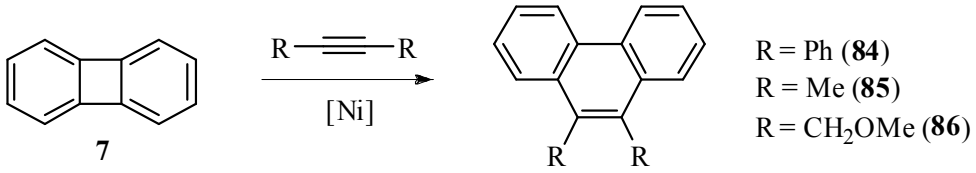

The first report of this process is by Eisch in 1985,[33a] who treated biphenylene with $Ni(PEt_3)_4$ and diphenylacetylene to produce 9,10-diphenylphenanthrene **84**. Since then a number of metals have been shown to mediate this process,[19] Ni systems being most relevant to this chapter. Thus, for example **84** can also be made using an *N*-heterocyclic carbene-based Ni(0) catalyst.[78] Bis(diisopropylphosphino)ethane Ni(alkyne) species enable similar cycloadditions of fairly hindered (trimethylsilyl)alkynes, sometimes involving more complex processes of silyl group migration,[79] while less hindered substrates lead to **84–86**.[80a] A mixed phosphinoaminoethane-chelated Ni species proved more reactive, enabling cycloaddition of even the encumbered *tert*-butyl(phenyl)acetylene to furnish the corresponding phenanthrene.[80b] With this background in mind, our attention turned to applying this reaction to larger phenylene systems.

Of the various topologies of phenylenes at our disposal, the angular version was

particularly intriguing as it offered two extreme modes of alkyne addition (Scheme 3.3). In the first scenario, exclusive attack at the outer periphery of the four-membered rings would produce the helical shaped PAHs known as helicenes (Scheme 3.3a).[81]

Scheme 3.3. Alkyne Cycloaddition with Angular Phenylenes to Produce (a) Helicenes or (b) Phenacenes

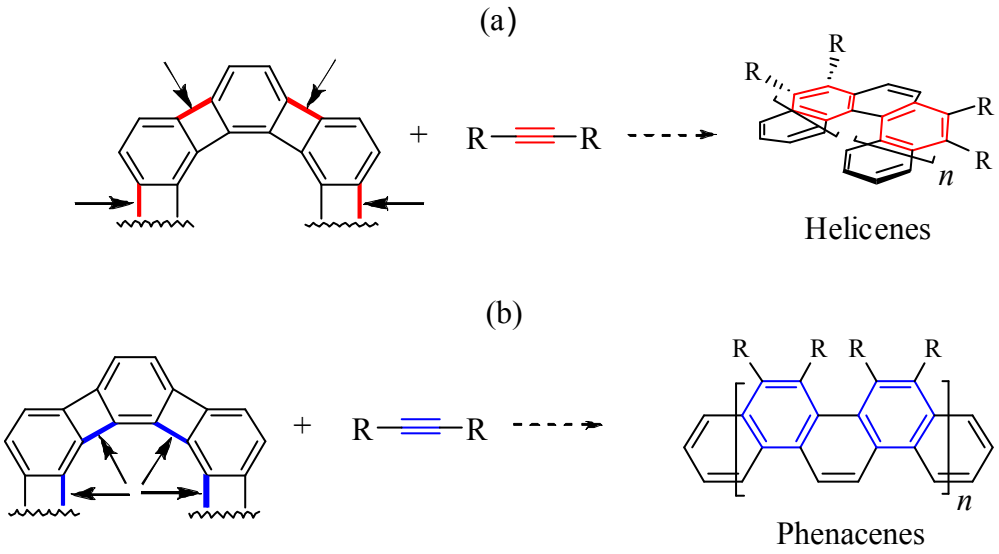

Reactions occurring only at the interior, or "bay" region (Scheme 3.3b), however, would afford a class of compounds exhibiting a linear polyphenanthrene motif that are known as [N]phenacenes.[82] Unselective additions would result in mixed topologies. Helicenes and their various derivatives constitute a well studied[83] family of molecules and continue to be a popular area of research. Phenacenes, in contrast, have been scrutinized much less, in part because only four members of the parent series are known and because, for N = 5 and 6, they are extremely insoluble.[84]

Phenacene-based applications have been slow to develop, but the first reports of the utilization of these molecules as functional organic materials suggest the beginning of a rich and promising field.[85] Thus, in 2008, [5]phenacene (picene) was demonstrated to behave as stable, high performance, organic field effect transistor (FET).[85b] Currently, the most common organic polycyclic benzenoid hydrocarbon-based FETs employ acenes, which have a polyanthracene structure (Figure 3.1). The sensitivity

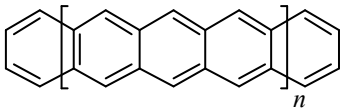

Figure 3.1. Linearly fused benzene topology of the acenes.

of these systems to air, however, has obstructed progress in this area.[86] For example, pentacene, a commonly used acene in FETs, reacts readily with oxygen to form

pentacenequinone, a process that severely reduces device efficiency (Scheme 3.4).

Scheme 3.4. Degradation of Pentacene to Pentacenequinone Under Aerobic Conditions

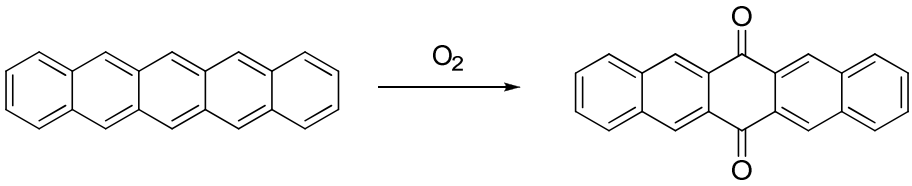

Phenacenes, on the other hand, are much less prone to such decomposition pathways due to their higher HOMO-LUMO gap, thus rendering them less reactive.[85b,86a] Their enhanced stability relative to acenes[87] makes them better candidates for molecular electronic applications. In a second seminal breakthrough, [5]phenacene was very recently also found to behave as a superconductor at low temperature, when doped with potassium.[85a] This work paves the way for a new class of PAH-based superconducting materials in which phenacenes may play a key role.

As this chemistry advances, new synthetic methods for preparing derivatives of these molecules will be required, in particular those bearing solubilizing and/or otherwise functionally useful substituents. The most general procedure for synthesizing phenacenes, as developed by Mallory,[88] makes use of oxidative stilbene photocyclizations (Scheme 3.5).[83,88] In this transformation, irradiation of the stilbene

Scheme 3.5. Generic Oxidative Stilbene Photocyclization Used to Prepare Phenacenes, as Illustrated for Phenanthrene

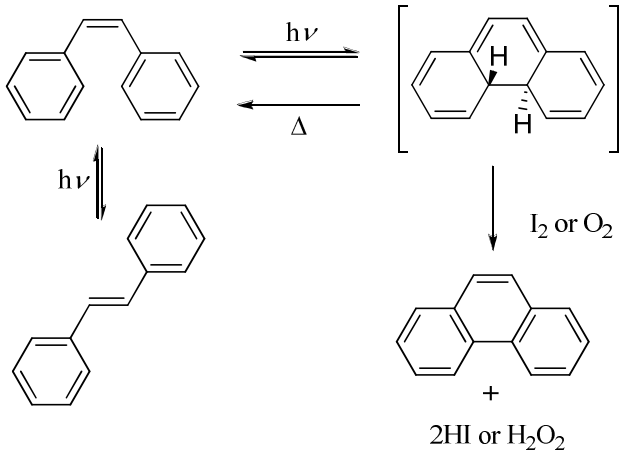

moiety leads to conrotatory electrocyclic ring closure. Trapping of the resulting intermediate with oxidizing reagents, such as iodine or oxygen, yields the desired phenanthrene subunit. The requisite stilbenes are most generally accessible via the Wittig reaction, as illustrated in the synthesis of [7]phenacene derivative **87** (Scheme 3.6). Although the yields for the photocyclization are typically reasonable (60–90 %),[85a] the major drawback of this methodology is the numerous steps associated with preparing the functional groups required for the prerequisite Wittig reaction. These

transformations serve to decrease the overall yield of the target molecule.

Scheme 3.6. Synthesis of [7]Phenacene **87**

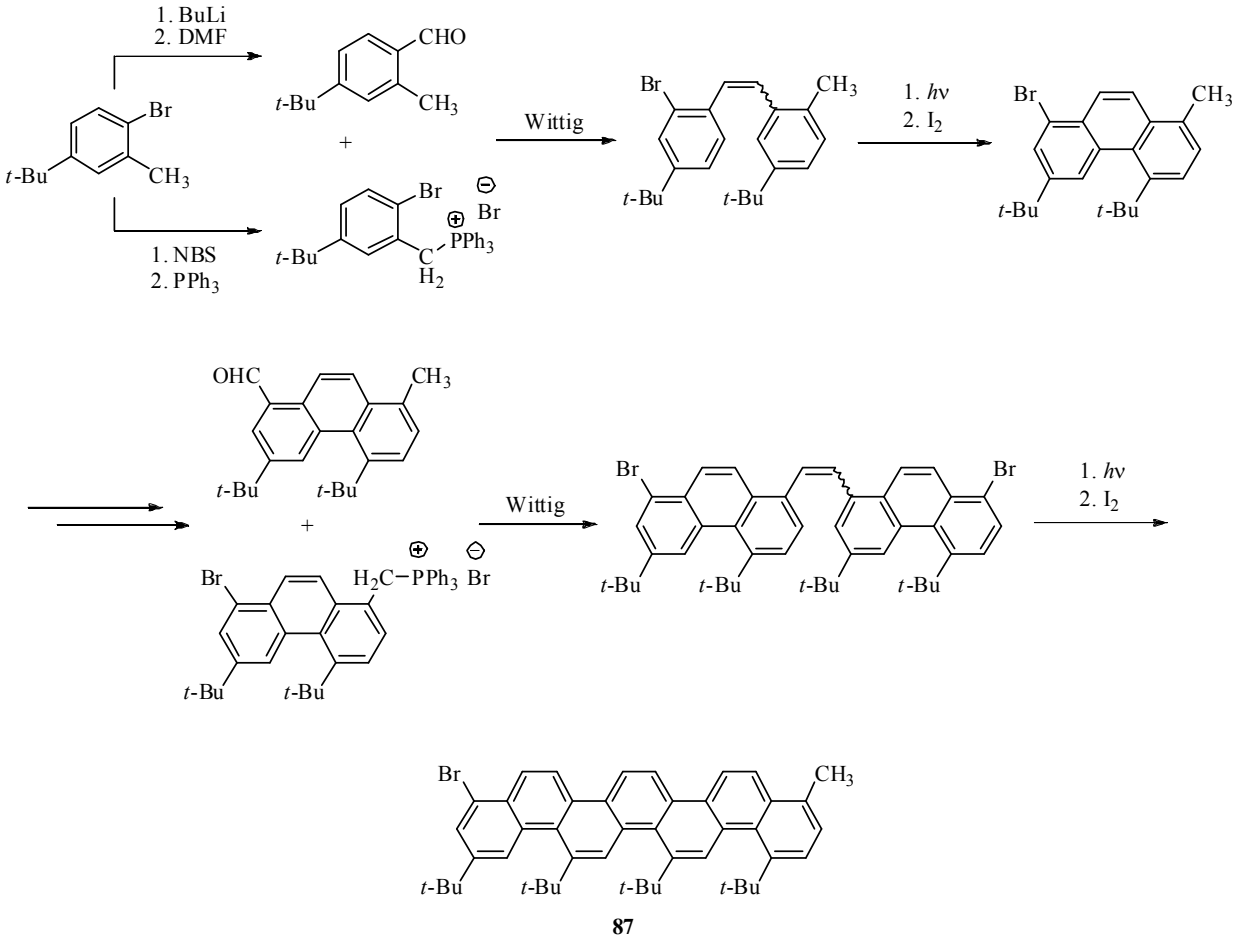

87

While laborious, Mallory's method addresses successfully the problem of solubility. As alluded to in Section 2.1, large PAHs become insoluble due to the increased π-π stacking forces that are experienced between aromatic rings. The best solubilizing groups for the phenacenes were found to be sterically bulky groups located in the bay regions.[85a] These modifications distort the phenacene framework from planarity, thereby disrupting π-stacking and increasing solubility, as demonstrated by the *tert*-butyl [7]phenacene **87** (Figure 3.2). This approach was applied to systems as large as [11]phenacene, the current record in the series.[85a]

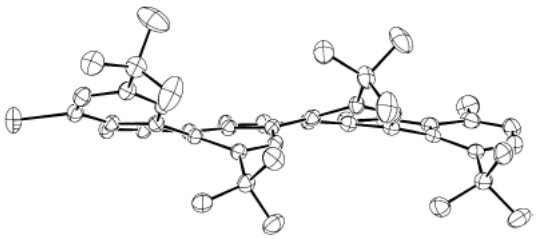

Figure 3.2. Crystal structure of tetrakis(*tert*-butyl) [7]phenacene **87**. Hydrogens are omitted for clarity.

To test the viability of angular phenylenes as substrates in Ni catalyzed alkyne cycloadditions, the simplest member, **22**, was chosen, raising a number of questions. First, how many and what kind of products will be formed (**A**–**E** in Scheme 3.7)? Will there be inherent selectivity toward helicene **C** or phenacene **E** formation, respectively? If not, can the reaction conditions be modified so as to induce such? What will be the limitations with respect to the size of substituents, especially in view of the crowded fjord and bay regions of **D** and **E**, respectively? The work presented in this chapter, carried out in collaboration with Dr. Zhenhua Gu,[89] explores these questions.

Scheme 3.7. Possible Cycloaddition Products of Angular [3]Phenylene **22**

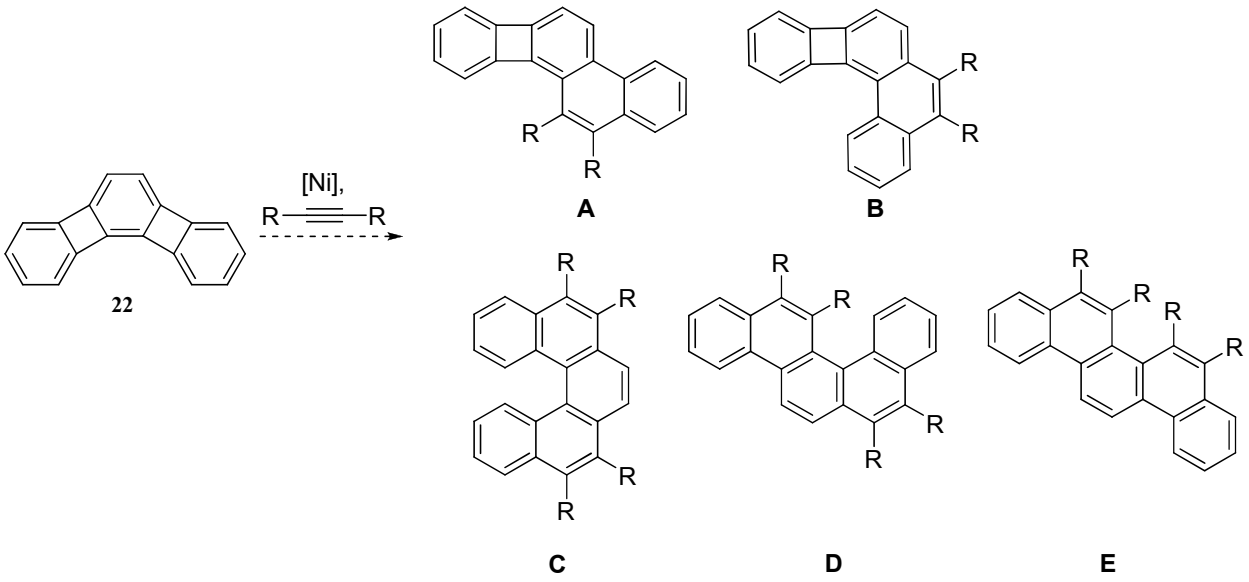

3.2 Experimental Mechanistic Studies of Nickel Catalyzed Insertion-Alkyne Cycloaddition Reactions with Angular [3]Phenylene

Before embarking on the proposed chemistry, the reactivity of **22** in the presence of nickel, in the form of $Ni(COD)(PMe_3)_2$, in the absence of alkynes was queried. Only starting material was recovered and there was no sign of dimerization (or oligomerization) to products of the type shown in Scheme 3.8, a mode of reactivity

readily attained by biphenylene and substituted derivatives.[33b]

Scheme 3.8. Attempted Dimerization of Angular [3]Phenylene **22**

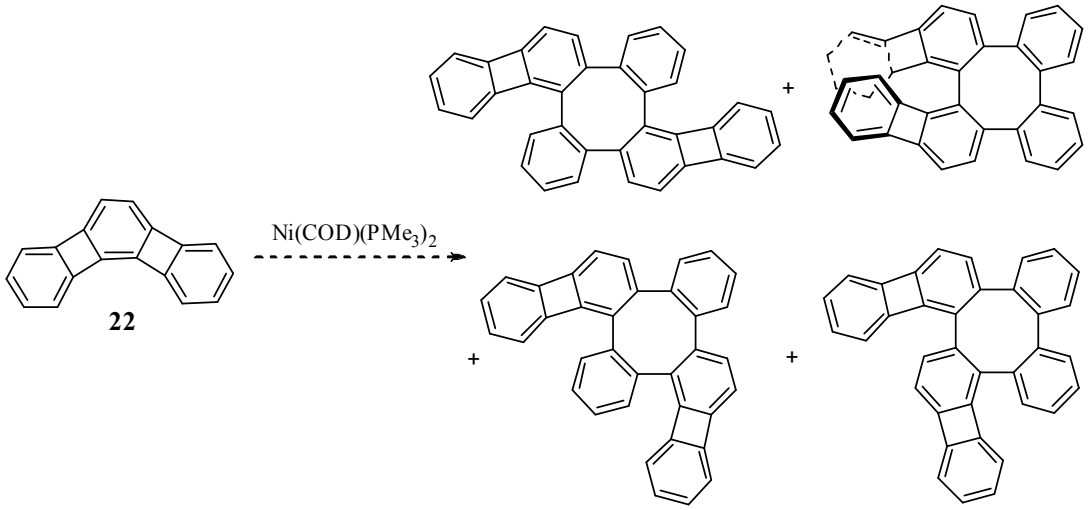

In contrast, exposing diphenylacetylene **88** to $Ni(COD)(PMe_3)_2$ and a small excess (1.09 equivalents) of angular phenylene **22** generated two products in the absence of any other (Figure 3.9). The first, molecule **89**, was the result of the cycloaddition of one diphenylacetylene at the bay region and the minor component. The major product constituted tetraphenyl [5]phenacene **90**, derived from **22** by double bay region attack. The structures of both compounds were confirmed by X-ray analysis, revealing highly distorted frames.[89]

Scheme 3.9. Nickel Catalyzed Cycloaddition of Angular [3]Phenylene **22** to Diphenylacetylene. Yields Based on Diphenylacetylene

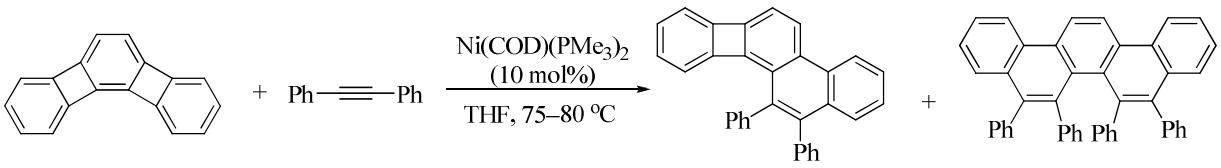

22 **88** **89** 20% **90** 59%

The outcome of this transformation was gratifying in its seeming simplicity and selectivity. Thus, it appeared that metal insertion occurred exclusively to bay region bonds, heralding the discovery of a new phenacene synthesis. The observation of relatively large amounts of **90** could be ascribed to increased reactivity of **89** relative to **22**, possibly due to steric activation by the newly introduced bay region phenyl group. To test this hypothesis, **89** was subjected to the cycloaddition reaction conditions (Scheme 3.10). Surprisingly, not only was this reaction slower than that of **22**, but the expected phenacene **90** was only a minor product (6 %). Instead, tetraphenylbenzo[*c*]chrysene **91**, a regioisomer of **90**, as confirmed by X-ray analysis,[89]

was isolated in 74 % yield, the result of non-bay alkyne cycloaddition to **89**. Therefore, **89** is not the precursor of **90**. Rather, there must be separate reaction pathways leading to each respective product.

Scheme 3.10. Cycloaddition Reaction of **89** with Diphenylacetylene **88**

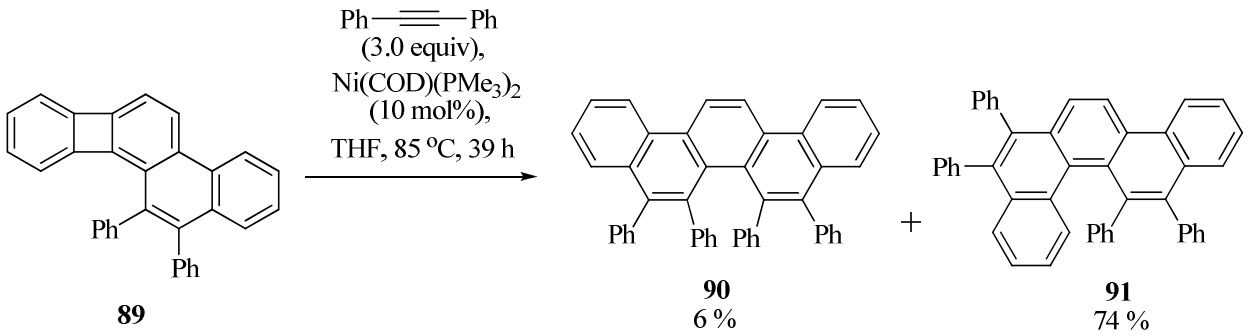

89 **90** 6 % **91** 74 %

A series of semi-quantitative experiments, monitored by ^{1}H-NMR spectroscopy, was carried out to shed some light on this mechanistic problem. First, the reaction of angular [3]phenylene **22** with diphenylacetylene **88** in Scheme 3.9 was addressed. Because dinuclear metallic activation of the strained C-C bond in biphenylenes has been implicated in a number of studies,[19] it was possible that the above mechanistic duality was caused by the presence of catalytic Ni_2 species, in addition to the "regular" mononuclear alternatives. Alternatively, double Ni insertion before cycloaddition might be responsible for one product, whereas sequential "normal" activation might be the origin of the other. Therefore, the amount of initial $Ni(COD)(PMe_3)_2$ was gradually increased and the effect of this incremental change on rate and product ratios recorded. As shown in Table 3.1, the speed with which **89** and **90** formed, was roughly proportional to the amount of metal present, while the product ratio stayed unchanged.

Table 3.1. Variation of Catalyst Loading in the Reaction of Phenylene **22** with Diphenylacetylene **88**. Reactions Were Carried Out with Equimolar Amounts of **22** and **88** in THF-d_8 at 40 °C

Run	$Ni(COD)(PMe_3)_2$ (mol%)	Rate of formation of **89** (mol/ L·h)	Rate of formation of **90** (mol/ L·h)	Ratio of **89**:**90**
1	50	3.2×10^{-4}	0.31×10^{-4}	10.3
2	35	2.0×10^{-4}	0.22×10^{-4}	9.1
3	7	0.64×10^{-4}	0.064×10^{-4}	10.0

Next, the amount of diphenylacetylene **88** was gradually increased from 1 to 4 equivalents (Table 3.2). The outcome of this series of experiments was counterintuitive, as it led to a larger preference for the production of monoadduct **89**, suggesting a mechanistic bifurcation in which whatever Ni species is responsible for the eventual formation of **90** is sequestered by external ligand (in this case **88**).

Table 3.2. Variation of Alkyne Equivalents in the Reaction of **22** (1 equiv) with Diphenylacetylene **88** in the Presence of 50 mol% of $Ni(COD)(PMe_3)_2$. Experiments Were Run in THF-d_8 at 40 °C

Run	**88** (equiv.)	Rate of formation of **89** (mol/ L·h)	Rate of formation of **90** (mol/ L·h)	**89**:**90**
1	1.0	3.20×10^{-4}	0.31×10^{-4}	10.3
2	2.0	2.20×10^{-4}	0.18×10^{-4}	12.2
3	4.0	2.20×10^{-4}	0.11×10^{-4}	20.0

Following the reaction progress by NMR spectroscopy afforded additional insights. Thus, mixing the ingredients at room temperature left the phenylene component untouched. Instead, there was a near instantaneous displacement of COD by diphenylacetylene to produce $Ni(PhC{\equiv}CPh)(PMe_3)_2$ (**92**) and free COD, in addition to the generation of $Ni(PMe_3)_4$.[90] The speed with which this complex was formed implied that it might be the active catalyst precursor. Consistent with this notion, higher reaction rates were observed when the reaction in Scheme 3.8 was carried out with pure **92**[91] as the catalyst (50 mol%) and 0.5 equivalent of **88** (Table 3.3, Run 2). In consonance with Table 3.2, the lesser concentration of available free alkyne increased the relative amount of **90** formed. Conversely (Run 3), using $Ni(COD)(PMe_3)_2$ with an extra equivalent of PMe_3 decreased the rates of formation of **89** and **90** and increased the ratio of **89**:**90**, consistent with ligand inhibition of the activation of **92** and the external ligand effect noted in Table 3.2.

Table 3.3. Variation of Catalyst in the Reaction of **22** with Diphenylacetylene **88** and its Effect on Reaction Rate. Experiments Were Run in THF-d_8 at 40 °C with 1 Equivalent of **22**

Run	Catalyst	**88** (equiv.)	Rate of formation of **89** (mol/ L·h)	Rate of formation of **90** (mol/ L·h)	**89**:**90**
1	$Ni(COD)(PMe_3)_2$	1.0	3.20×10^{-4}	0.31×10^{-4}	10.3
2	$Ni(PhC{\equiv}CPh)(PMe_3)_2$ (**92**) (0.5 equivalent)	0.5	12.70×10^{-4}	2.10×10^{-4}	6.0
3	$Ni(COD)(PMe_3)_2$ (0.5 equivalent) + PMe_3 (1.0 equiv)	1.0	0.88×10^{-4}	0.05×10^{-4}	16.3

Attention was then shifted to the reaction of monoadduct **89** with **88** as in Scheme 3.10 (Table 3.4). Here, increasing the amount of alkyne and catalyst favors the formation of **91**, consistent with an independent pathway. At low concentration of alkyne, it appears that **89** reenters the manifold of its generation and proceeds on to **90**. Indeed, following the change in the ratio of **91**:**90** in Run 1 (Table 3.4) with time reveals a decrease from 4.7 to the eventual 2.2, as **88** is depleted.

Table 3.4. Variation of Catalyst Loading and Alkyne Concentration in the Reaction of **90** with Diphenylacetylene **88**. Reactions Were Run in THF-d_8 at 40 °C

Run	**88** (equiv.)	$Ni(COD)(PMe_3)_2$ (mol%)	**91**:**90**
1	1.0	50	2
2	3.0	50	15
3	3.0	10	25

The information obtained from these experiments allowed a narrowing of mechanistic possibilities. For example, dinuclear Ni activation, only one possibility of which is shown in Scheme 3.11, was rendered unlikely by the absence of any observable changes in product distribution of the reaction in Scheme 3.9.

Scheme 3.11. Generic Example of a Dual Mechanism Based on Mono- and Dimetallic Phenylene Activation

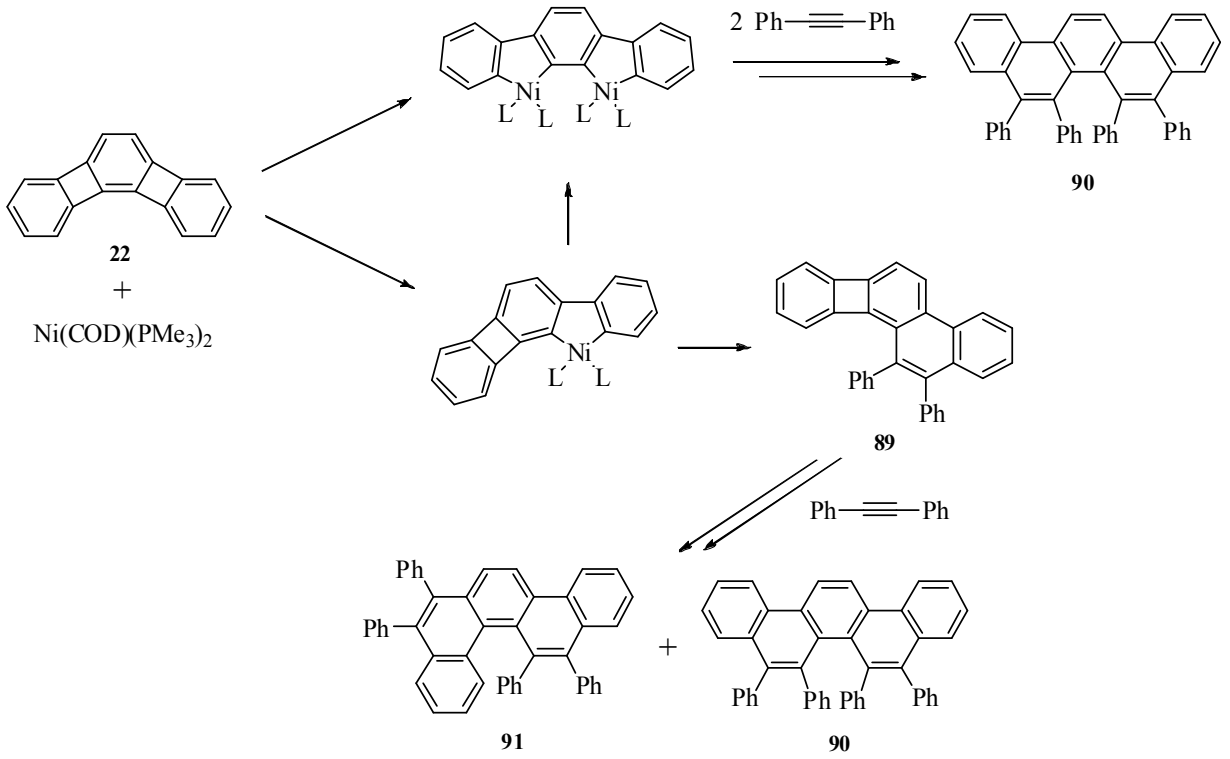

An alternative mechanism, shown in Scheme 3.12, was in much better agreement with the results of the various control experiments. The first step would be displacement of a phosphine in the initially dominant Ni-containing species **92** by angular [3]phenylene **22**, inhibited by added PMe_3. From **93**, oxidative addition can take place to afford metallacycle **94**. Why should bay region insertion be favored? Arguably, the regioselectivity of this step is controlled by the lesser steric hindrance in the resulting arene fragment or relative stabilization of the polarized Ni-C(α-

biphenylene) bond in **94** by the electron withdrawing nature of the neighboring cyclobutadienoid ring. This phenomenon in biphenylene is due to the rehybridization of the four-membered ring carbons to adopt relatively larger *p* character in the strained linkages, hence larger *s* character (i.e., electron withdrawing) in the remaining bond, and manifests itself most clearly in the relative acidity of the α-hydrogens.[7a] This step is followed by migratory insertion and reductive elimination to produce molecule **96**, the mechanistic bifurcation point. One branch proceeds through presumably ligand-assisted metal dissociation to generate the relatively unreactive free **89**. The second entails Ni migration[92] and insertion into the bay region of the remaining four-membered ring (**97**) before the second cycloaddition occurs, generating phenacene **90**.

Scheme 3.12. Possible Mechanism for the Alkyne Cycloaddition Reaction of Angular [3]Phenylene **22**

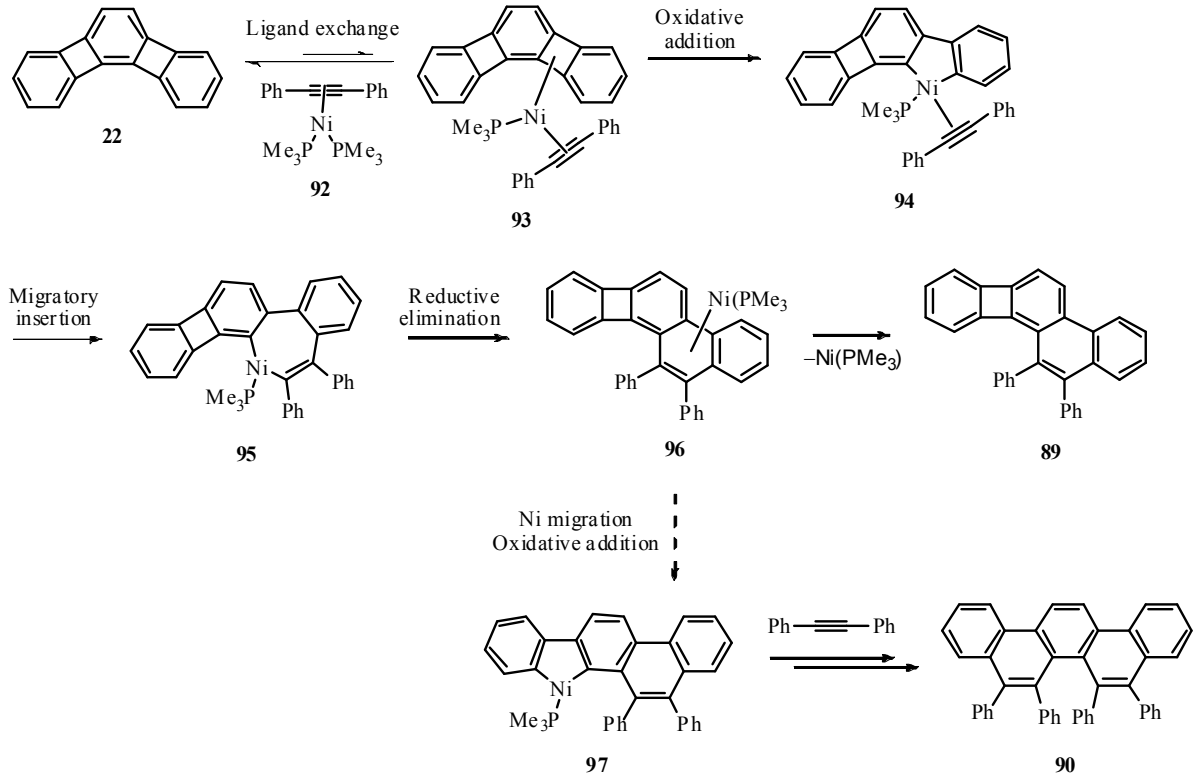

The regioselective formation of **97** may again be sterically dictated or may involve anchimeric assistance by the bay-region phenyl group as sketched in Scheme 3.13, specifically **99**.

Scheme 3.13. Anchimeric Assistance on Route to [5]Phenacene **90**

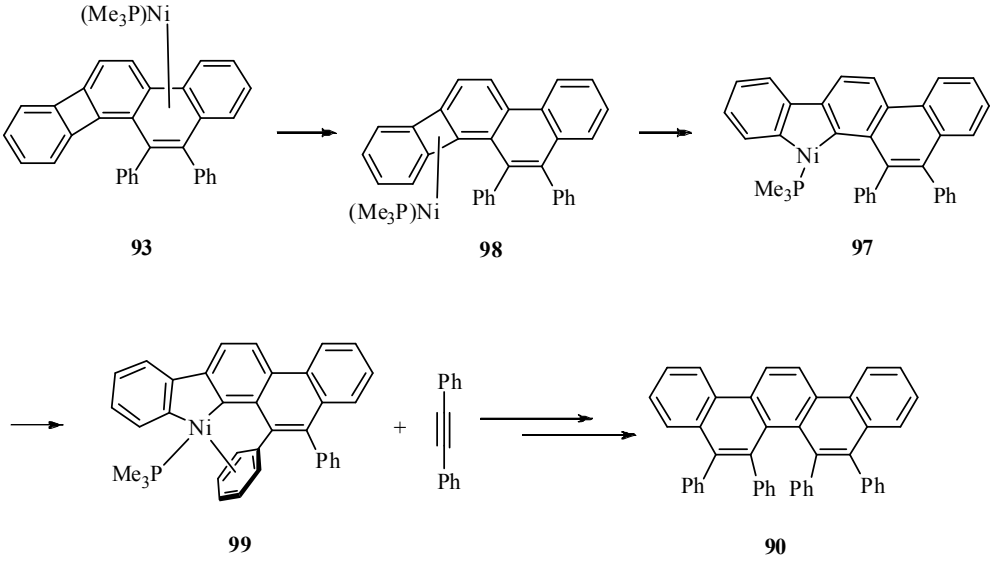

This type of metal coordination to the double bond of a proximal arene ligand is common, and two examples are provided based on ruthenium[94] and molybdenum[95] (Figure 3.3).

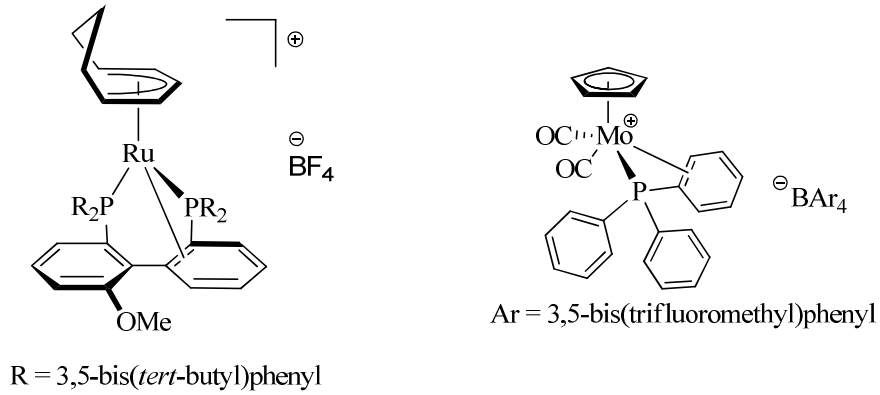

Figure 3.3. Examples of complexes with phenyl groups coordinating to a nearby metal center.

Turning to the largely selective conversion of **89** to **91** (Scheme 3.10) requires the postulate of preferential insertion of the metal at the non-bay region and hence a different Ni species from that in **96**, possibly a Ni(PMe_3)(alkyne) moiety akin to that in **93**, i.e. **100** (Scheme 3.14). Bay insertion would lead to metallacycle **101** and ultimately molecule **90**. The expected large degree of steric repulsion between the phenyl groups in **101** should disfavor this reaction pathway. On the other hand, non-bay insertion, to produce **102** should be relatively less impeded and would furnish **91**. Another option for the generation of **90** from **89** would be reentering the pathway described in Scheme 3.12, facilitated at low concentrations of alkyne, consistent with the data in Table 3.4.

Scheme 3.14. Proposed Mechanism for the Alkyne Cycloaddition Reaction of **89**

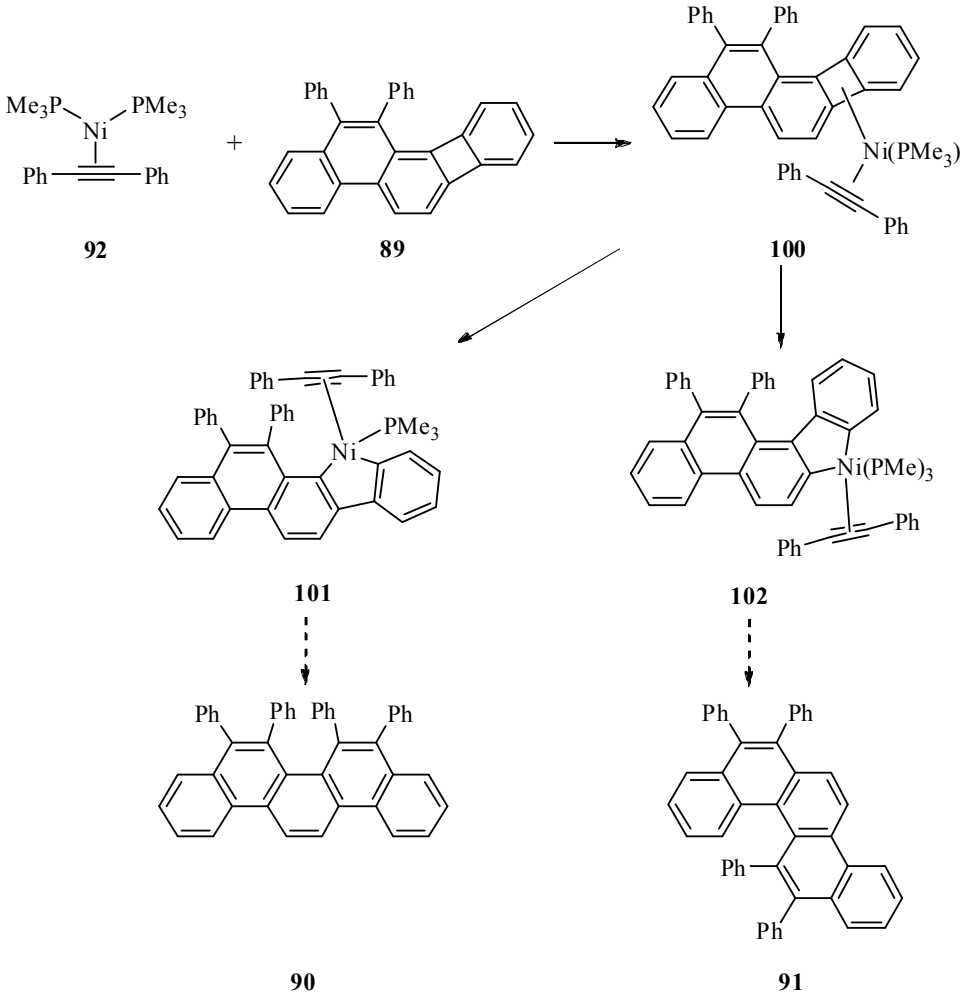

While the above mechanistic perambulations appear plausible, it should be stressed that they are speculative and may be restricted to diphenylacetylene **88** as the substrate. Thus, both 3-hexyne **103** and 1,4-dimethoxy-2-butyne **106** added to **22** less selectively than **88** to provide **only** the bay and non-bay monoadducts **104** and **105**, and **107** and **108**, respectively (Scheme 3.15).

Scheme 3.15. Reaction of Angular [3]Phenylene **22** with Other Alkynes

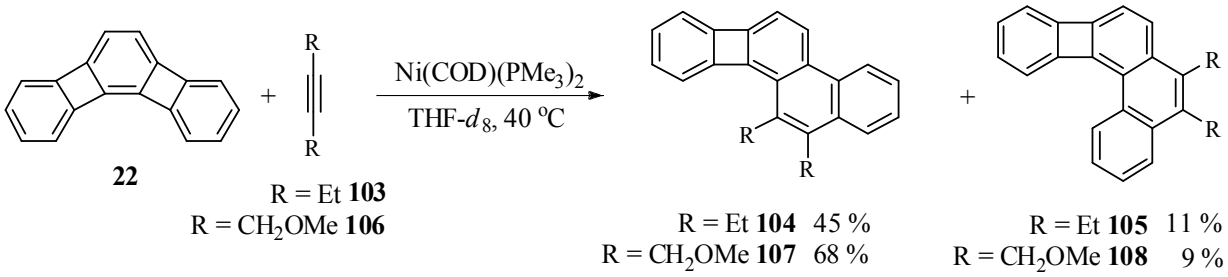

In view of these uncertainties, recourse was taken to DFT computations, delineated in the next section.

3.3 Computational Mechanistic Studies of the Nickel Catalyzed Cycloadditions of Diphenylacetylene to Angular [3]Phenylene

DFT studies were carried out in collaboration with Prof. Vincent Gandon of the Université Paris-Sud 11. The B3LYP 6-31G(d) basis set was used for hydrogen and carbon atoms, while LANL2DZ was used for nickel.

Before attempting to model the more complex alkyne cycloaddition reactions in Schemes 3.8 and 3.9, the basic Ni-catalyzed addition of the parent acetylene to biphenylene in the presence of PMe_3 was studied (Scheme 3.16). The free energies

Scheme 3.16. Computational Modeling of Ni-catalyzed Addition of Acetylene to Biphenylene. Free Energies (ΔG, Kcal/Mol) are Relative to **109**. Transition State Energies are Absolute Values for This Step

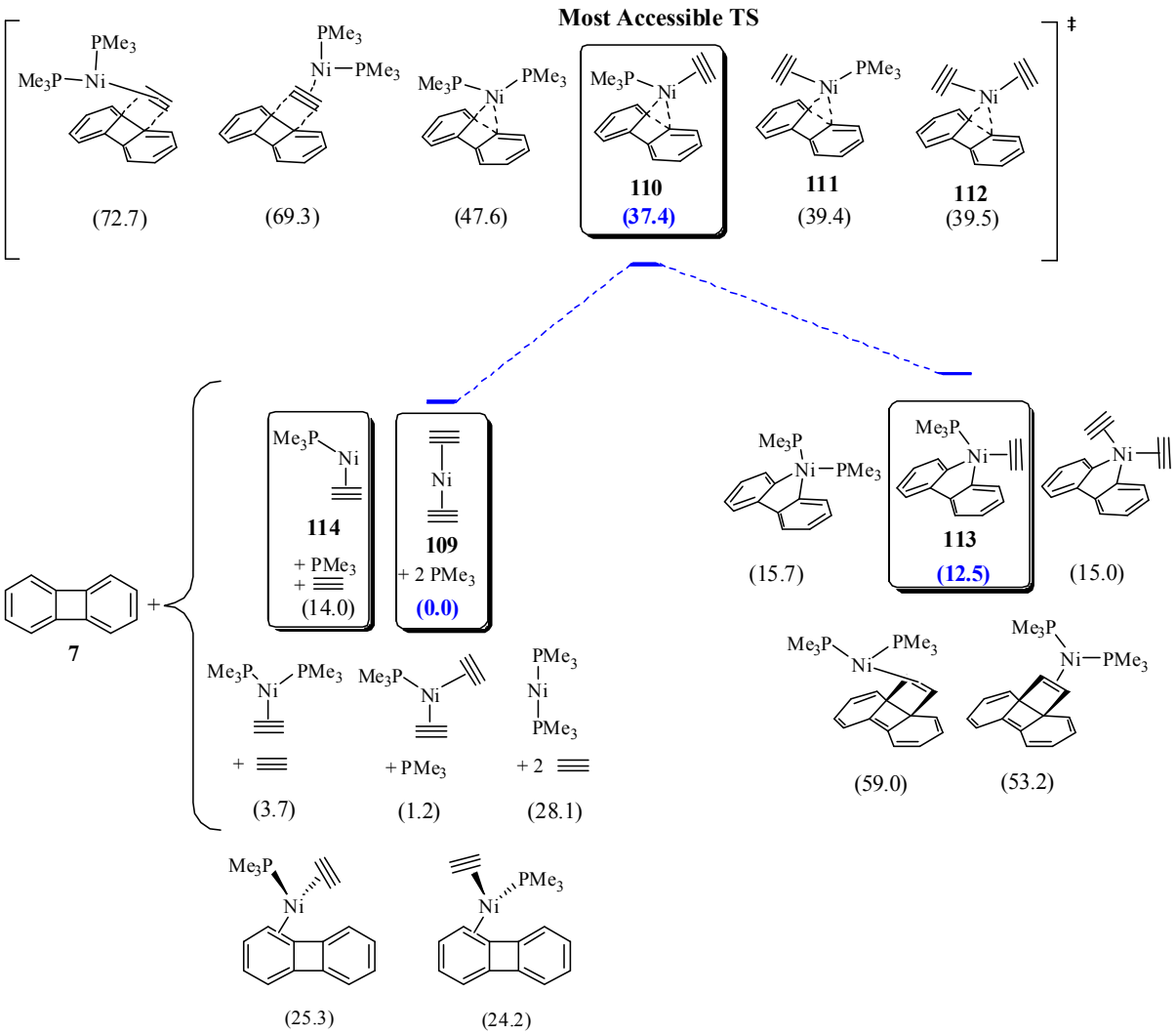

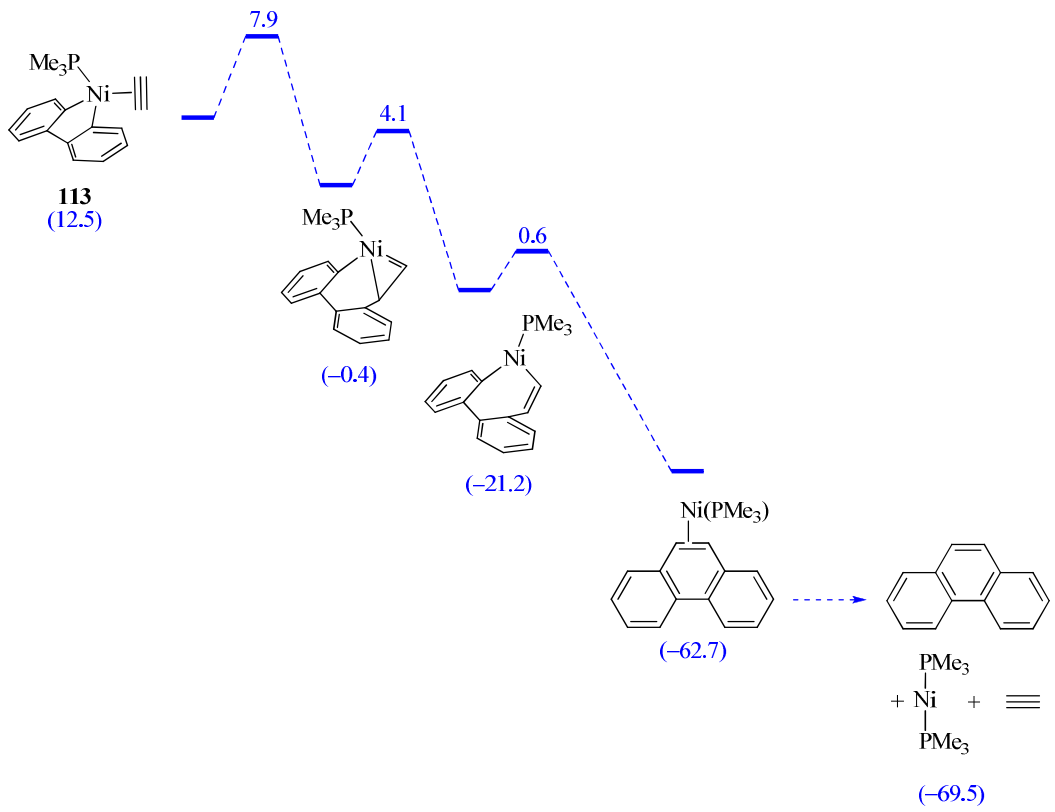

(Δ*G*) of various possible catalyst structures, consisting of an assortment of combinations of nickel, PMe_3, and acetylene, as well as those of several possible transition states and the resulting products were calculated. As is evident on inspection of the values in the first part of Scheme 3.16, a number of species were found to be very close in energy, making it difficult to pinpoint a specific structure for the initial insertion step. Bis(ethyne) nickel complex **109** was established as the lowest energy nickel species and was thus assigned a relative value of 0 kcal/mol. The most accessible transition state, **110**, features the oxidative addition of the $Ni(PMe_3)(C_2H_2)$ fragment **114** (+ 14 kcal/mol), in which the alkyne is held *exo* to biphenylene. The corresponding *endo* structure **111** was found to be just slightly higher in energy by 2.0 kcal/mol, as was the bisalkyne transition state **112**. It is likely that biphenylene-NiL_2 complexes (two of which were calculated at relative energies 24.2 and 25.3 kcal/mol) lie on the way to these maxima.[93] Metallacycle **113**, the structure ensuing from transition state **110**, constituted the lowest energy product, uphill from the starting **109** by 12.5 kcal/mol, but other alternatives are nearly isoenergetic. Clearly, however, attack by $Ni(PMe_3)_2$ or Diels-Alder type cycloadditions are not likely. From **113**, the species proceeds smoothly by alkyne insertion-reductive elimination to the phenanthrene product, a cascade associated with a large exergonic driving force.

Undaunted by the relatively complicated picture that emerged with biphenylene, attention was turned to the original object of scrutiny: the cycloaddition reaction between angular [3]phenylene **22** and diphenylacetylene **88** to produce [5]phenacene derivative **90**.

Modeled in the same manner as described above, the metal insertion into the four-membered ring of **22** is shown in Scheme 3.17. The lowest energy nickel species

was found to be diphenylacetylene complex **92**, gratifyingly corresponding to experiment, and was set to a reference value of 0.0 kcal/mol. One notes again, however, an array of at least 10 species, all of which must be in equilibrium in the initial reaction mixture. Notably, the Ni-π complexes to **22** are all more than 20 kcal/mol higher in energy than **92**, providing a computational rationale for the failure to observe such species by NMR. The first step in the optimal reaction pathway is the coordination of Ni(PMe_3) to the cyclobutadiene ring of **22**, which results in formation of η^2-like complex **114**. Again, in gratifying agreement with experiment, bay region insertion through transition state **115** to give **116** is favored, albeit by a bare 0.7 kcal/mol relative to its non-bay region counterpart **117**. Moreover, there are at least six other structures that are energetically viable in silico, although insertions of Ni(PhC≡CPh)(PMe_3) appear less so, possibly due to steric hindrance. The same observation is made for the products of insertion, although **116** emerges as the thermodynamically most stable possibility.

Scheme 3.17. Calculated Structures and Reaction Pathway for the Insertion of Nickel into the Four-Membered Ring of Angular [3]Phenylene **22**. Free Energies, Δ*G*, are in Kcal/Mol Relative to **92**

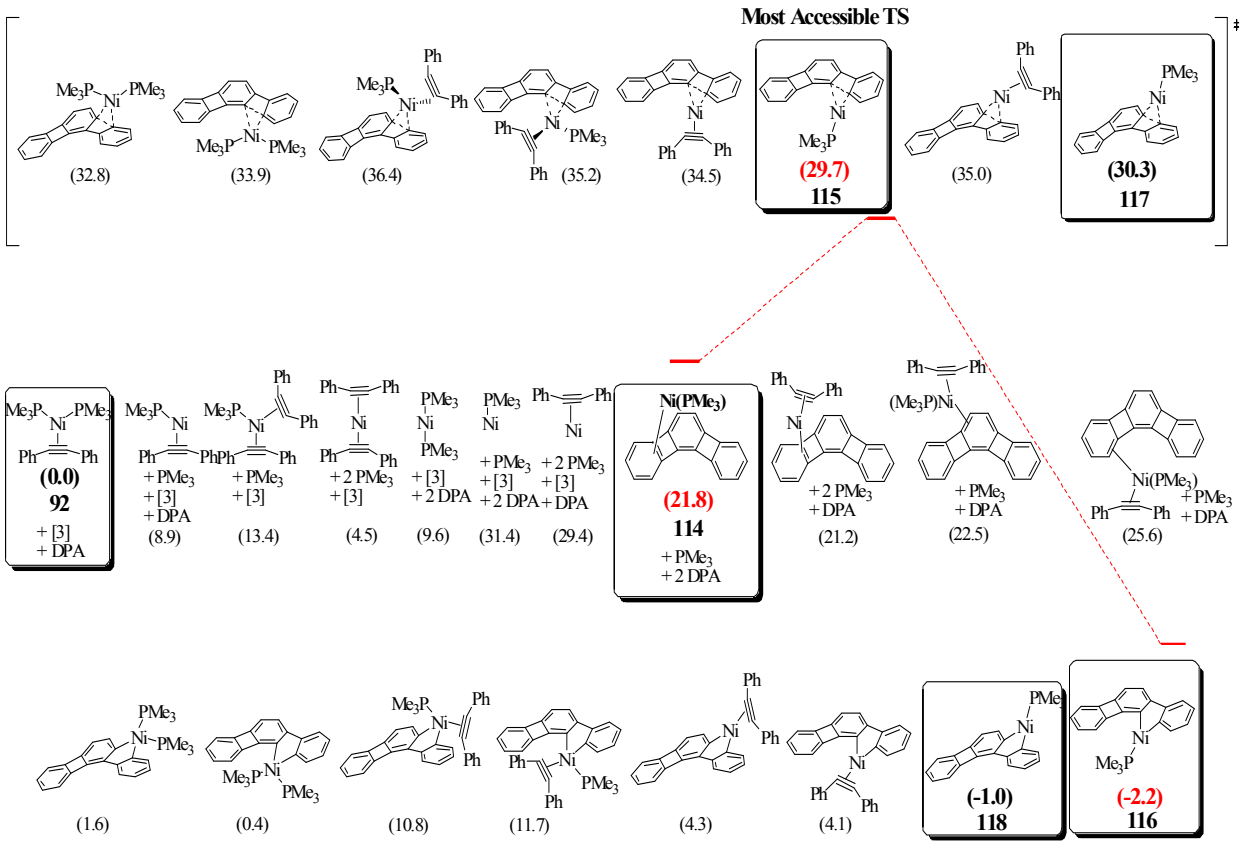

The next step was to map out the first alkyne cycloaddition (Scheme 3.18). Coordination of diphenylacetylene to **116** is endothermic by 13.9 kcal/mol and after migratory insertion, produces **119**. Interestingly, a transition state to regioisomer **95**

written (arbitrarily) in Scheme 3.12, could not be located.

Scheme 3.18. Calculated Reaction Pathway for the Coordination of Diphenylacetylene, Migratory Insertion, and Nickel Migration. Free Energies, ΔG, are in Kcal/Mol. Transition State Energies are Absolute Values for This Step

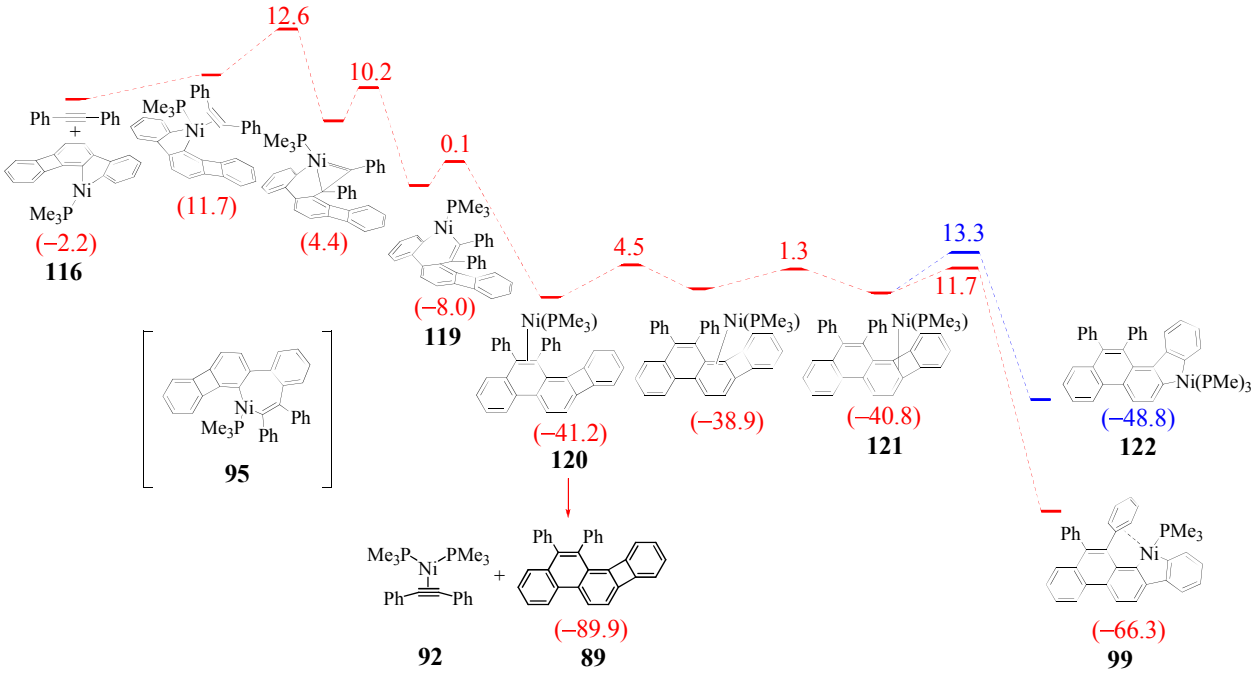

Subsequent reductive elimination from **119** occurs to produce nickel coordinated arene species **120**. From it, free **89** is presumably readily obtained by demetallation in the presence of external ligands, shown only for the formation of **92**, in a very favorable process (–48.7 kcal/mol). This step is sufficiently exothermic to tolerate the emergence of all the calculated species in the starting line up of Scheme 3.17 and is presumably the source of **89** in Scheme 3.9. However, if not removed, the Ni moiety in **120** can migrate along a shallow manifold across the π frame, choosing the phenyl functionalized edge of the molecule (cf. Section 2.4), until the remaining four-membered ring is reached (**121**). At this point, two separate reaction pathways become possible. Nickel insertion on the side proximal or opposite of the phenyl groups generates **99** or **122**, respectively. The barriers for these transformations are similar, but show a noticeable preference for the formation of **99**. In addition, there is a significant energy difference (17.5 kcal/mol) between **122** and **99** in favor of the bay region metallacycle. The reason is the coordination of the neighboring phenyl ring to the nickel, which serves to stabilize **103**, vindicating the proposal made in Scheme 3.13 and providing a rationale for the exclusive observation of **90** in Scheme 3.9.

From **99**, as shown in Scheme 3.19, coordination of diphenylacetylene (**123**) is followed by migratory insertion to produce **124**. Insertion occurs away from the bay region, so as to reduce steric repulsion due to the phenyl group in the phenanthrene part of the molecule. Finally, reductive elimination ensues, providing phenacene-Ni

complex **125**. At this point, the stage is set for exergonic nickel dissociation to **90** and catalyst turnover.

Scheme 3.19. Calculated Reaction Pathway for the Second Diphenylacetylene Insertion. All Relative Energies (in red) are in Kcal/Mol. Transition State Energies are Absolute Values for This Step

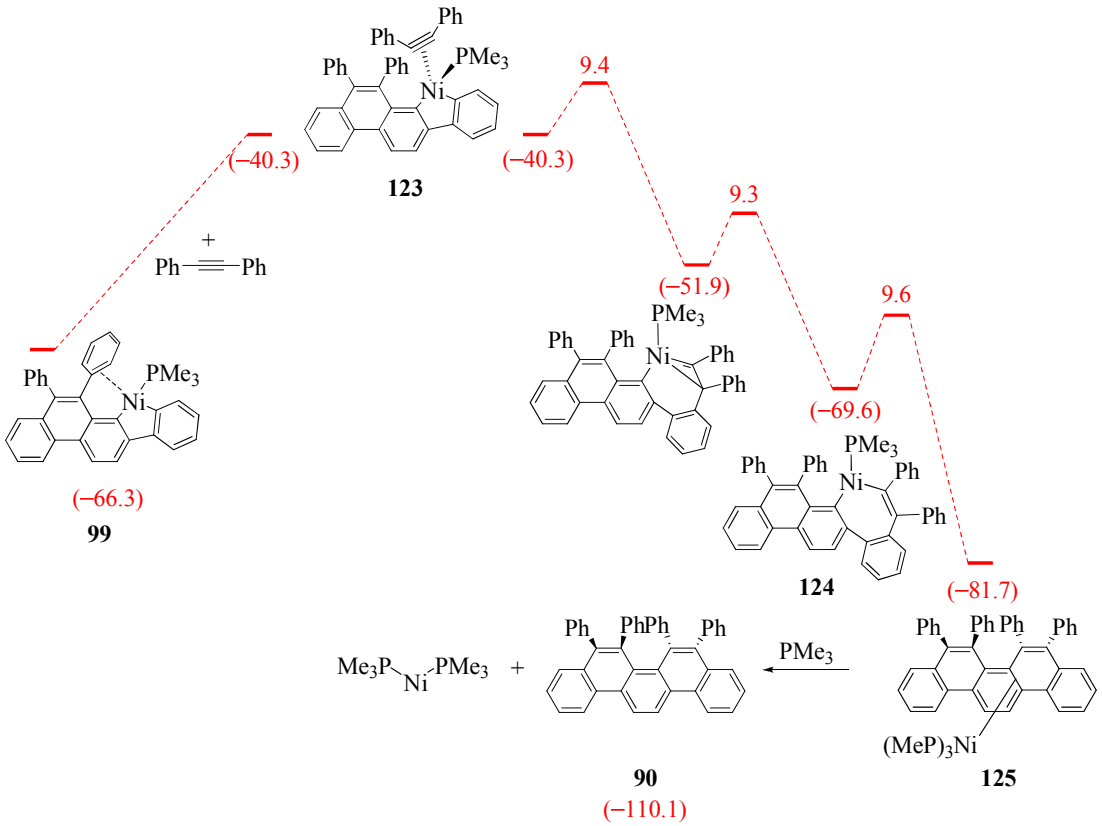

In conclusion of this discussion, the consideration of the combined computational and experimental data affords a mechanistic picture of the cycloaddition reaction of diphenylacetylene **88** to angular [3]phenylene **22** (Scheme 3.9), the essential features of which are summarized in Scheme 3.20. The crucial point is a mechanistic bifurcation in which **89** is either released early and (nearly?) irreversibly from the metal, or the metal stays attached so as to effect a second cycloaddition to give **90**. This mechanism implies that **91** is formed by a different mechanism involving a different Ni species.

Scheme 3.20. Essential Mechanistic Features of the Formation of **89** and **90** in the Nickel Catalyzed Cycloaddition Reaction Between Diphenylacetylene **88** and Angular [3]Phenylene **22**

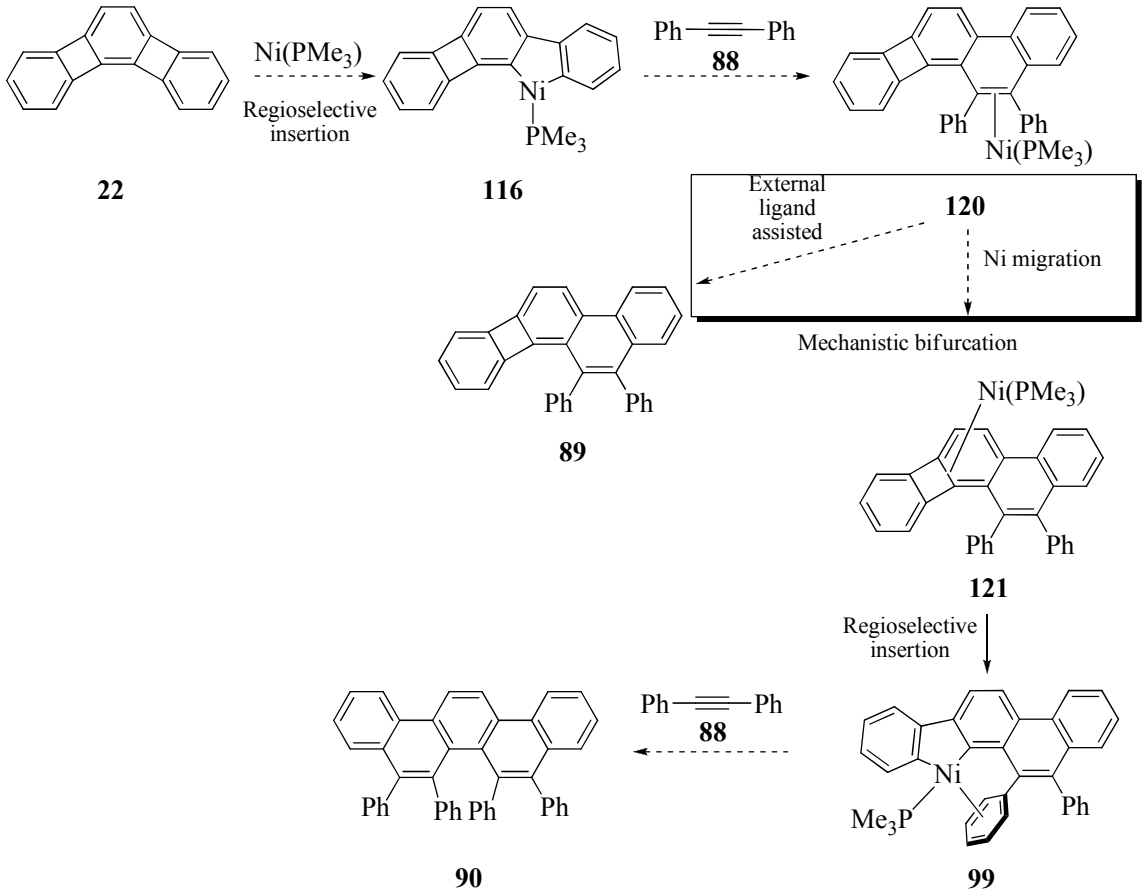

Consequently, the reaction of **89** with diphenylacetylene to give **91** (Scheme 3.10) was also modeled by DFT. Of the various options probed, that shown in Scheme 3.21 proved to be most plausible. The reaction pathway entails coordination of alkyne-Ni phosphine **126** to molecule **89**, which generates complex **127** in a process that is found to require 22.8 kcal/mol of energy. Insertion into the non-bay region of the four-membered ring has a barrier of 16 kcal/mol and provides metallacycle **128**. After the second cycloaddition event, benzo[*c*]chrysene **91** is formed. Interestingly, the transition state leading to insertion of nickel complex **126** into the bay region of **89**, structure **129**, was found to be so high in energy relative to **128** that it could not be modeled. This is not unexpected as the phenyl group closest to bay region effectively blocks the approach of any catalyst species. This result is consistent with the high ratio of **91** to **90** formed in Scheme 3.10, and the increase in this ratio at higher initial diphenylacetylene concentration. Why is any **90** formed and why does its relative proportion increase at lower diphenylacetylene concentration? A possible explanation is that under these conditions the concentrations of **92** and **126** are sufficiently small that **89** reenters Scheme 3.18 competitively.

Scheme 3.21. Calculated Reaction Mechanism for the Nickel Catalyzed Cycloaddition Reaction Between Diphenylacetylene and Compound **90**. Relative Energies are in Kcal/Mol. Transition State Energies are Absolute Values for This Step

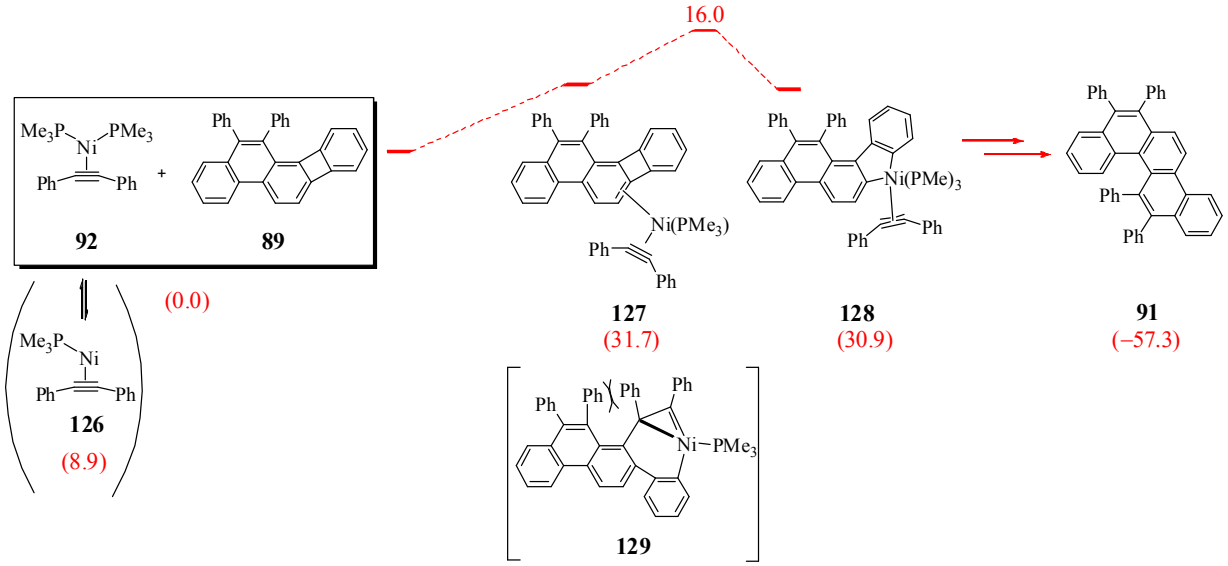

Consideration of Scheme 3.20 suggests that phenacene formation might be maximized by keeping the concentration of external ligand low during the course of the reaction. Experiments aimed at verifying this conjecture are the subject of Section 3.4, in addition to presenting extensions of the methodology to higher angular phenylenes.

3.4 Optimization and Application of Nickel Catalyzed Alkyne Cycloaddition Reactions

The experimental and computational studies described in Section 3.3 suggested that the decisive factor for selective formation of phenacene **90** is suppression of metal dissociation in Ni complex **120**. This scenario would be achievable by maintaining a low concentration of diphenylacetylene **88** (vide supra).

Previously, the alkyne cycloaddition was performed with all reagents mixed together at the start of the reaction, invariably resulting in a high initial concentration of **88**. To obviate this occurrence, an alternative procedure was devised. In this new arrangement, the required stoichiometric amount (in this case two equivalents) of alkyne **88** was slowly introduced to a mixture of **22** and Ni(COD)$(PMe_3)_2$ by means of a syringe pump (Scheme 3.22). The results of varying addition and reaction times are shown in Table 3.5.

Scheme 3.22. Modified Reaction Alkyne Cycloaddition Reaction Between **22** and **89**

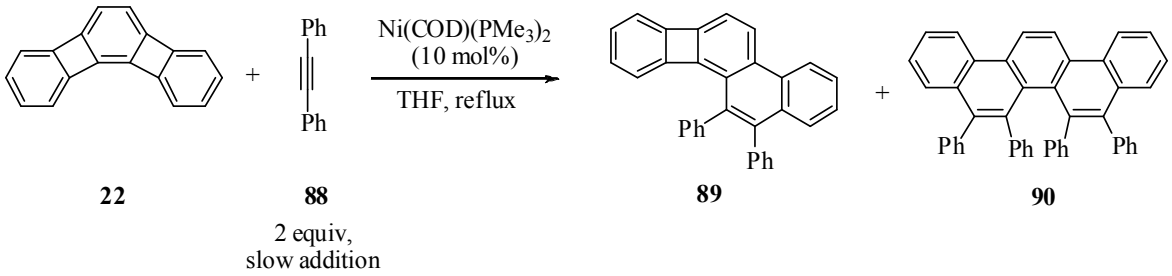

Table 3.5. Variation of Alkyne Addition and Total Reaction Time in the Scheme 3.22

Run	Addition time of **88** (h)	Total run time (h)	Yield of **89** (%)	Yield of **90** (%)
1	4	16	44	55
2	6	22	23	77
3	5	41	24	76
4	12	69	17	73
5	13	19	13	87

The most immediate result of the modified protocol was the quantitative conversion of **22** to cycloadduct products **89** and **90**. Turning to the product ratios, a four hour addition time led to a slight preference for **90**. Increasing the time to six hours dramatically influenced the product distribution, and **90** was isolated in 77 % yield, as compared to the 23 % for **89**. In the optimal Run 5, 87 % of **90** was generated vs. 13 % of **90**. Extending the run time after the addition of diphenylacetylene had a negligible effect. The successful enhancement in phenacene selectivity under these conditions makes the reaction a practical method for synthesizing compound **90** and also provides further experimental support for the proposed mechanism shown in Scheme 3.20.

Having reached a reasonable level of understanding both the mechanistic and experimental aspects of the reaction of angular [3]phenylene **22** with diphenylacetylene, attention was shifted to a larger and more challenging substrate: angular [4]phenylene (**17**). This system could conceivably afford 17 possible adducts, one of which is hexaphenyl[7]phenacene **130** (Scheme 3.24). Would the mechanistic features of this triple cycloaddition be sufficiently similar to those of **22** to apply the same principles and enable selectivity toward **130**?

Scheme 3.24. The Possible Cycloadducts of Diphenylacetylene **88** to Angular [4]Phenylene **17**

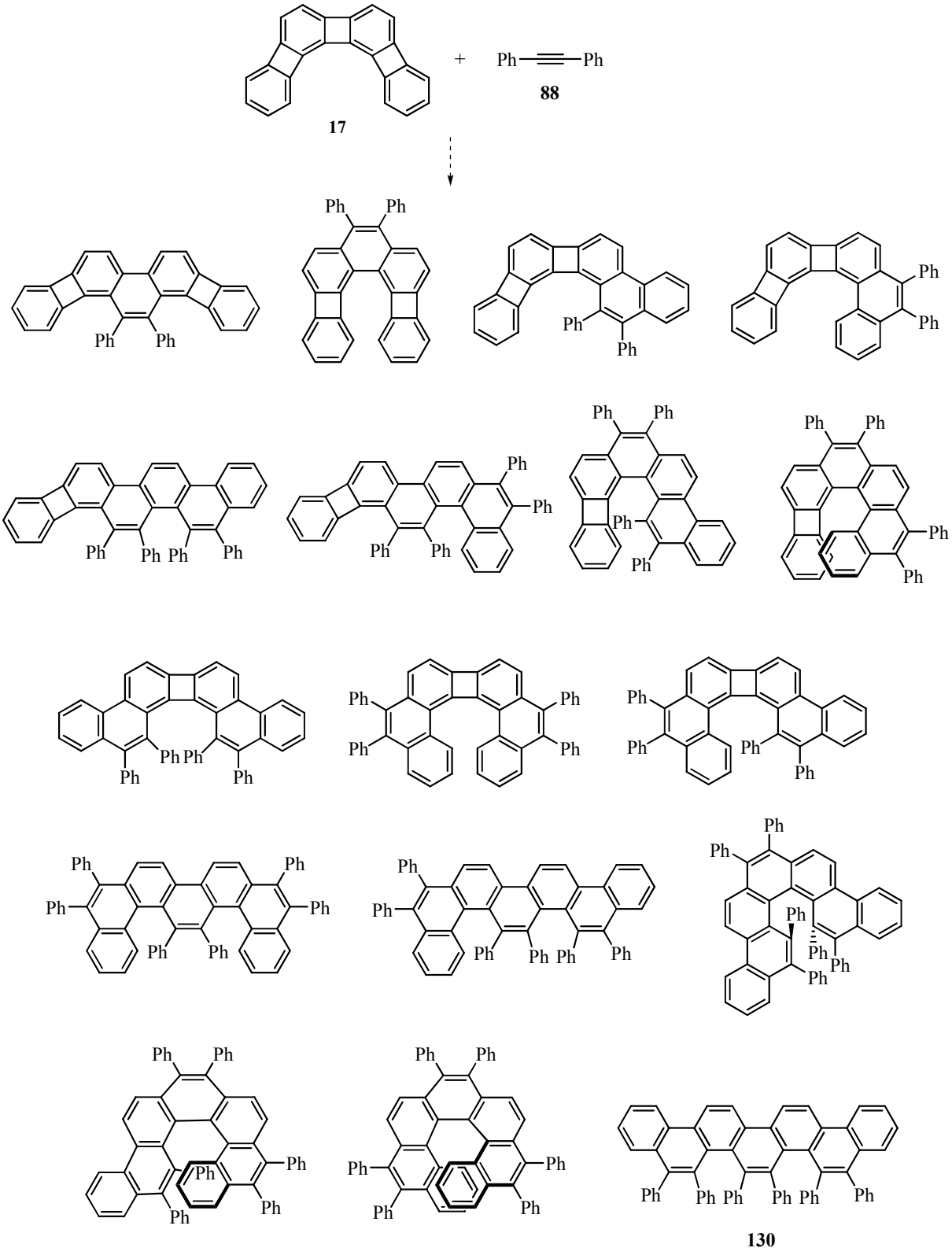

Encouragingly, a first experiment under conditions comparable to those in Scheme 3.9 for **22**, namely reaction of angular [4]phenylene (**17**) with one equivalent of diphenylacetylene in the absence of high dilution, indeed engendered only five products, two of which, monoadducts **131** and **132**, were minor (Scheme 3.25). The major components of the mixture were molecules **133**, **134**, and, most significantly **130**.

Scheme 3.25. Nickel Catalyzed Alkyne Cycloaddition with **17** and **88**

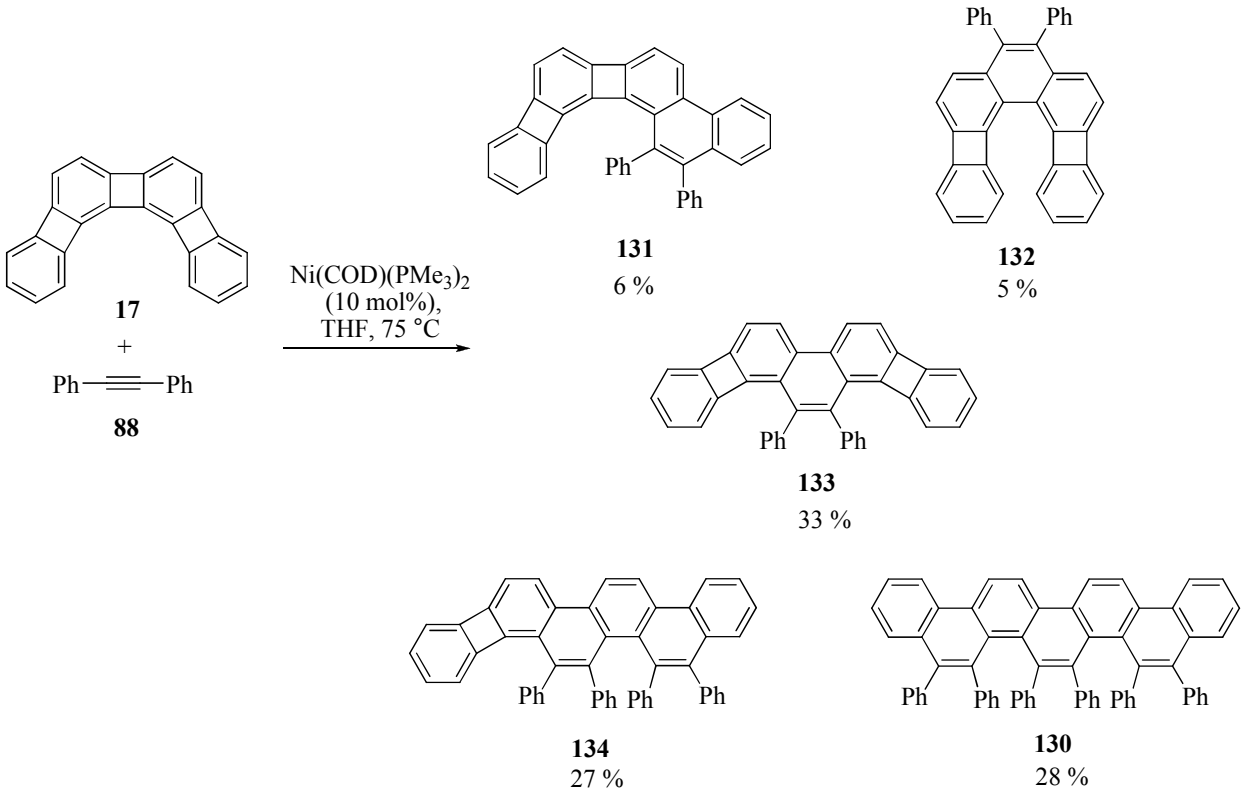

Monitoring the course of the transformation by NMR revealed that **133** is the sole initial new compound, followed by gradual appearance of the others. Extrapolation of the insights gained with **22**, it is tempting to propose that migration of the metal in Ni-complexed **133** is the source of **134** and ultimately **130**. If true, [7]phenacene **130** might be made selectively by application of the slow alkyne addition procedure of Scheme 3.22. Scheme 3.26 illustrates the proposed scenario. It starts with doubly regioselective Ni insertion into the central ring and from the bay region to give **135**. On the basis of the electron withdrawing effect of the adjacent cyclobutadienoid rings invoked earlier in the selective formation of **94** (Scheme 3.12), this metallacycle would seem the most stable. Again this conjecture is tentative, as the appearance of the minor products **131** and **132** would indicate. Metallacycle **135** would then give rise to **136** (and hence **133** by demetallation), which would connect by Ni migration and insertion to **137**. Alkyne cycloaddition would result in **138** (and hence **134** by demetallation), which would connect by Ni migration and insertion to **139**. Alkyne cycloaddition would result in **140** (and hence **130** by demetallation).

Scheme 3.26. Proposed Reaction Pathway to Phenacene **130** from Angular [4]Phenylene **17** via Ni Migration

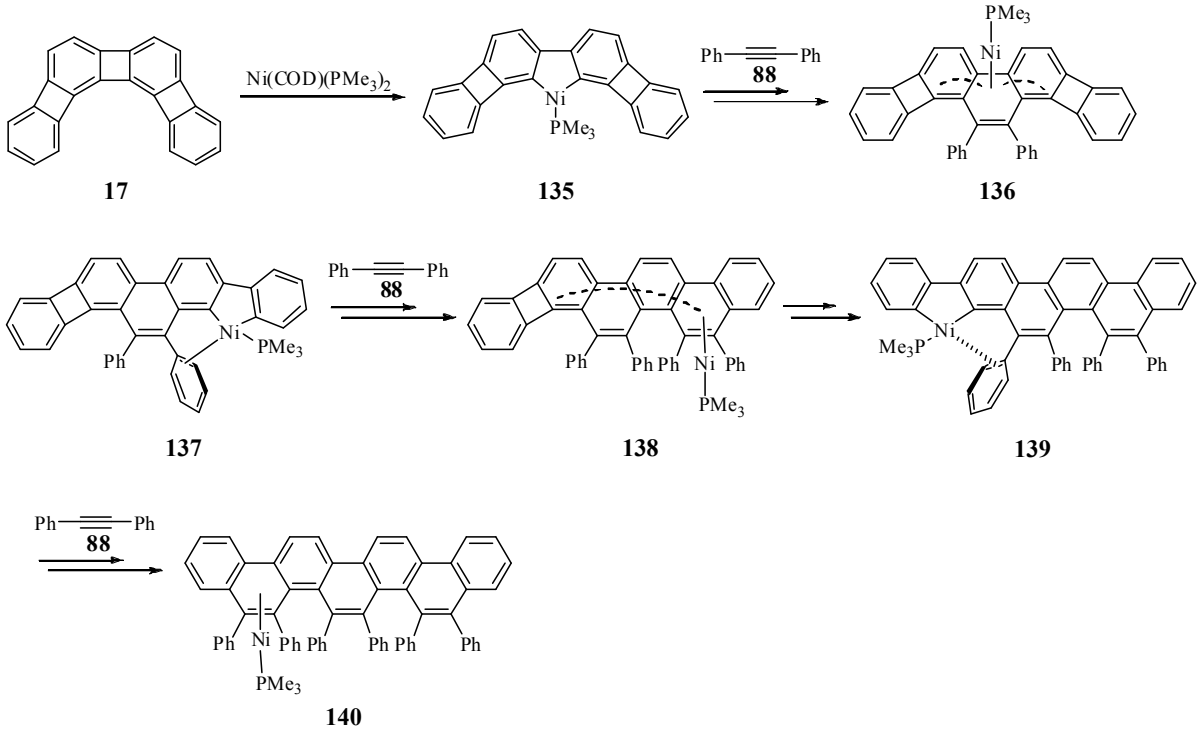

The successful preparation of [5]- and [7]phenacene from angular [3]- and [4]phenylene, respectively, prompted an attempt to prepare [13]phenacene derivative **141** from helical [7]phenylene **142**[10] (Scheme 3.27). This transformation would make use of six alkyne cycloadditions to produce the target molecule. In addition to the possibility of preparing the largest known phenacene, this reaction would also serve as an interesting test of the alkyne cycloaddition methodology.

Scheme 3.27. Proposed Synthesis of Dodecaphenyl [13]Phenacene **141** From Helical [7]Phenylene **142**

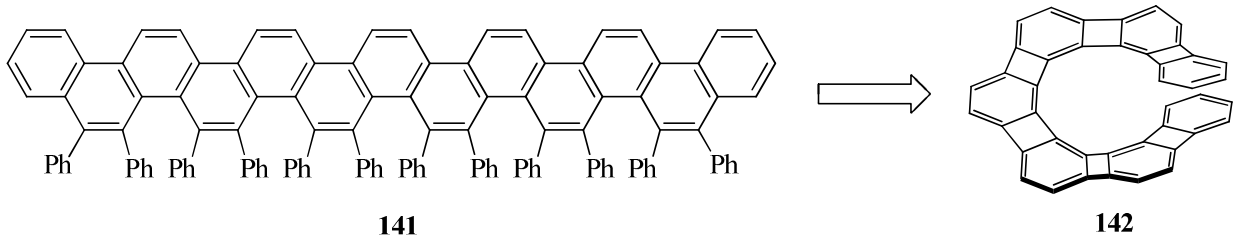

Using the slow addition procedure, phenylene **142** was subjected to the alkyne cycloaddition conditions (Scheme 3.29). All of the starting material was consumed but the reaction ultimately resulted in an intractable mixture of products. Unfortunately, no conclusive structural identifications for any of the ensuing compounds could be made from the ^{1}H-NMR data. A large assortment of peaks was seen in the region of 6–7

ppm, suggesting the presence of phenylene subunits. More informative was the absence of the highly diagnostic phenacene bay region proton signals that are typically found at ~8–9 ppm,[84] signaling the absence of any phenacene product(s).

Scheme 3.28. Attempted Synthesis of Dodecaphenyl [13]Phenacene **141** From Helical [7]Phenylene **142**

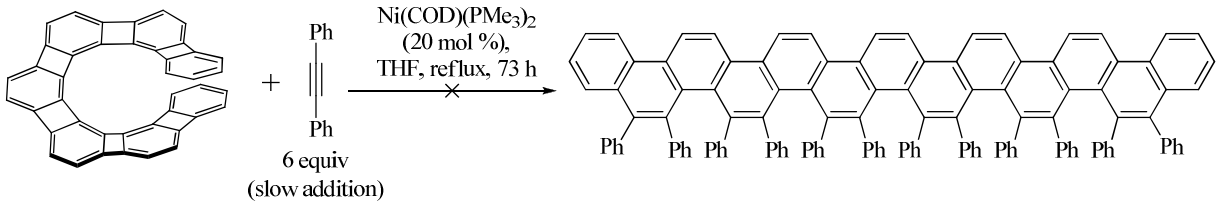

142 **141**

Nevertheless, mass spectral analysis clearly indicated that multiple alkyne cycloaddition had occurred (Table 3.6). Peaks were observed at *m/z* = 700, 1056, 1234, and 1412, which correspond to the presence of single, triple, quadruple, and quintuple alkyne adducts in the reaction mixture. No signal corresponding to the mass of **141** (*m/z* = 1590) was detected, however. Although the structures of the resulting products remain to be established by follow-up experiments on a larger scale, the fact that five cycloadditions occurred is encouraging in the basic scientific quest for large novel polycyclic aromatic hydrocarbons.

Table 3.6. Mass Spectral Data (FAB) of the Product Mixture of the Cycloaddition Reaction of Phenylene **142** to Diphenylacetylene **88**

m/z	Percentage	Cycloaddition count
700	13	1
1056	11	3
1234	8	4
1412	7	5

Our disappointment in the apparent failure to generate **141** in this reaction may be the result of overambitious expectations on our part. Thus, we assumed, in analogy to the reactivity of angular systems **17** and **22**, that bay region cycloaddition to one of the inner cyclobutadiene rings would be preferred, ideally producing an initial structure such as **143** (Figure 3.8). The corresponding non-bay adduct is illustrated by **144**. It is evident on comparison that such bay region reactivity would lead to constructs devoid of the helical strain present in the starting material,[96] as well as non-bay structures like **144**. The subsequent course of the reaction, however, may be marred by relatively non-selective cycloadditions, as already indicated for **17** (Scheme 3.25). Therefore, it will be prudent for future investigators to return to the latter, optimize its outcome, and then proceed along the series in the quest for large phenacene (or other) structures.

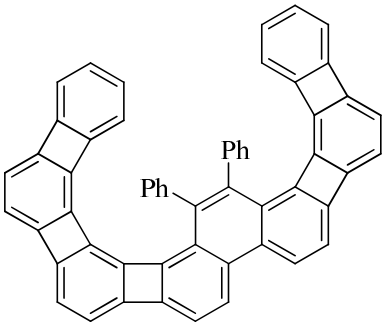

143

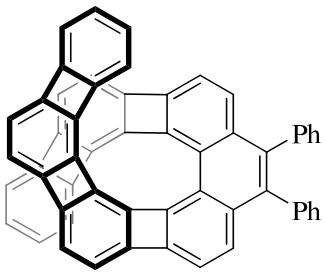

144

Figure 3.8. Proposed, representative initial bay (**143**) and non-bay (**144**) alkyne cycloaddition products of the reaction of [7]heliphene **141** with diphenylacetylene **88**.

3.5 Summary and Outlook

The first alkyne cycloaddition studies were carried with angular phenylene systems. Angular [3]phenylene **22** was successfully used as a precursor to a novel phenyl substituted [5]phenacene derivative **90**. Similarly, hexaphenyl [7]phenacene **131** was prepared from angular [4]phenylene **17**. Extensive experiment and computational mechanistic studies suggested that the optimal conditions for preparing phenacene **90** from phenylene **22** were the maintenance of a low concentration of alkyne in the reaction mixture. Future work will focus on applying these conditions to the synthesis of [7]phenacene **130** from angular [4]phenylene **17**. An attempt to prepare a [13]phenacene **142** from helical [7]phenylene **141** proved unsuccessful for reasons that are not well understood. Nevertheless, cycloaddition was found to have occurred up to five times. This observation is promising with respect to the further application of the methodology described in this chapter.

The development of an alkyne cycloaddition-based approach to synthesizing phenacenes should greatly facilitate the study of this emerging class of molecules. Future work will focus on expanding the substrate scope of the reaction by examining various functionalized alkynes, the application of metal systems that may allow the isolation of crucial intermediates, and the expansion of the substrate scope to the higher angular phenylenes, as well as other topologies.

Chapter Four: Experimental and Computational Details

4.1 General Considerations

All glassware was oven-dried (180 °C) prior to use. Reagents were used as received from suppliers unless otherwise noted. Flash chromatography[97] was performed with Merck 60 230–400 mesh silica gel. MP EcoChrom neutral alumina was deactivated to activity III by adding 6 % water by mass, followed by thorough mixing.[98] Air sensitive compounds were handled under argon with standard Schlenk techniques and/or in a nitrogen atmosphere glovebox (Vacuum Atmospheres Model Nexus).

Irradiation in $CpCo(CO)_2$ reactions was carried out with a 120V, 300W slide projection lamp (ELH) positioned 5 cm away from the reaction vessel. UV-irradiation experiments were conducted in a Rayonet Photochemical Reactor (RPR-100). Bis(trimethylsilyl)- and trimethylsilylacetylene (BTMSA and TMSA, respectively) were distilled from molecular sieves (4 Å) prior to use. TMSA was degassed with four, freeze-pump-thaw cycles while BTMSA was degassed using a 20 min Ar purge. BTMSA was recycled using from all $CpCo(CO)_2$ reactions using the following procedure. The BTMSA was first removed by vacuum transfer. Residual cobalt was removed by dissolving the BTMSA in pentane and washing the pentane/BMTSA layer mixture with a dilute solution of ceric ammonium nitrate in acetonitrile in a separatory funnel. The denser acetonitrile layer was drained off and the pentane removed by distillation at atmospheric pressure. Vacuum distillation of the BTMSA from molecular sieves afforded a product pure enough for future use. All solvents were distilled under N_2 immediately before use from the appropriate drying agent: triethylamine (KOH pellets), benzene, toluene, CH_2Cl_2 (CaH_2), THF and diethylether (Na/benzophenone), acetonitrile (CaH_2). Deoxygenation of solvents and/or reaction mixtures was carried out by a 20 min Ar purge or four free-pump-thaw cycles for volatile (b.p. < 70 °C) mixtures/solvents. $Ni(COD)_2$ (Strem) was stored and manipulated in the glovebox.

^1H and proton decoupled ^{13}C spectra were measured at 500 MHz and 125 MHz respectively unless otherwise noted. ^1H-NMR chemical shifts are reported in ppm units, relative to the signal of the solvent: ($CDCl_3$–7.26 ppm; C_6D_6–7.15 ppm; acetone-d_6–2.05 ppm, CD_2Cl_2–5.32 ppm, toluene-d_8–2.09 ppm (for $-CD_3$). Except where noted, two-dimensional NMR experiments were run under temperature control at 300 K. All spectral data were processed with Bruker TopSpin 2.1 software.

Melting points were recorded in open capillary tubes using a Thomas Hoover Unimelt apparatus and are uncorrected. Melting points for air-sensitive samples were carried out in flame sealed capillary tubes. Mass spectral measurements (Electron Impact, Fast Atom Bombardment) and elemental analyses were supplied by the Micro-Mass Facility of the College of Chemistry, University of California Berkeley. UV-Vis spectra were recorded on Agilent 8453 and Perkin-Elmer Lambda 35 spectrophotometers with absorbance data reported in nm (log ε). IR spectra were taken on a Perkin-Elmer Spectrum 100. Where appropriate, analysis by GC/MS was done with an Agilent 5973 instrument.

4.2 Experimental Section for Chapter Two

2,3,7,8-Tetrakis(trimethylsilyl) linear [3]phenylene(CpCo) **19**:

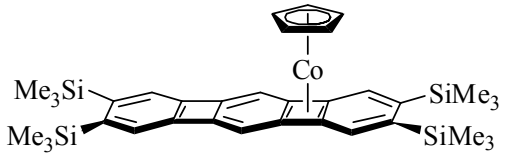

A mixture of KF·2 H_2O (700 mg, 7.44 mmol), [18]crown-6 (100 mg, 0.378 mmol), and 2,3,7,8-tetrakis[(triisopropylsilyl)ethynyl] linear [3]phenylene[26] (370 mg, 0.800 mmol) in degassed THF (25 mL) was stirred for 70 min at RT. The orange solution was filtered through a plug of silica gel (1 x 3 cm), eluting with degassed THF (15 mL), providing a light-yellow solution. After adding $CpCo(CO)_2$ (260 mg, 1.44 mmol), the solution was protected from light and added via syringe pump over a period of 6 h to a boiling mixture of degassed BTMSA (50 mL) and THF (200 mL), which was irradiated with a projector lamp under nitrogen. After additional heating and irradiation for 15 h, the solvents were removed by vacuum transfer and the black residue filtered through a plug of neutral alumina, activity III, eluting with hexane/THF (50:1). The volatiles were removed and the dark brown residue crystallized from degassed acetone yielding **19** (330 mg, 65 %) as black needles, m.p. 192–195 °C (decomp); ^{1}H-NMR (400 MHz, C_6D_6): δ = 7.94 (s, 2 H), 7.44 (s, 2 H), 6.90 (s, 2 H), 4.41 (s, 5 H), 0.35 (s, 18 H), 0.31 (s, 18 H) ppm; ^{13}C-NMR (100 MHz, C_6D_6): δ = 149.4, 148.4, 143.3, 139.4, 136.0, 125.6, 115.5, 80.2, 78.1, 73.9, 2.69, 2.61 ppm; IR (neat) $\tilde{\nu}$ = 2951, 2898, 1259, 1248, 1073, 830, 799, 752 cm^{-1}; UV-VIS (ethanol): λ_{max} (log ε) = 288 (4.86), 299 (5.00), 352 (4.45), 410 (4.39), 4.38 (4.49), end absorption to 550 nm; MS (70 eV): *m*/*z* (%): 638 (9) [M^+], 514 (100), 499 (3), 387 (2), 73 (24); HRMS (FAB): calcd for $C_{35}H_{47}CoSi_4$: 638.2087; found: 638.2095. Elemental analysis calcd for $C_{35}H_{47}CoSi_4$: C 65.78, H 7.41; found: 65.82, 7.21.

Crystallographic information for **19** (H atoms omitted):

Table 4.1 Crystal Data and Structure Refinement For **19**

Empirical formula	$C_{35}H_{47}CoSi_4$
Formula weight	639.02
cryst size (mm)	0.25 x 0.20 x 0.05
cryst syst	Triclinic
# refl used for unit cell determination	6958
2 θ range (deg)	2.45–29.00
a (Å)	9.497(3)
b (Å)	12.321(4)
c (Å)	16.469(5)
α (deg)	74.058(5)
β (deg)	82.154(5)

γ (deg)	72.276(5)
V (Å^3)	1762.0(10)
space group	P–1
Z	2
D_{calc}, g/cm^3	1.762
F_{000}	680
μ, cm^{-1}	6.45
temp, ºC	–173
T_{max}, T_{min}	0.858, 0.972
no. of total rflns	24355
no. of unique rflns	6958
no. of obsd. rflns	9209
no. of variables	361
Reflection to Parameter Ratio	25.5
R	0.0503
R_w	0.1426
R_{all}	0.0734
GOF	1.006
Max. Peak in Final Diff. Map (e–/ Å^3)	0.867
Min. Peak in Final Diff. Map (e–/ Å^3)	–0.755

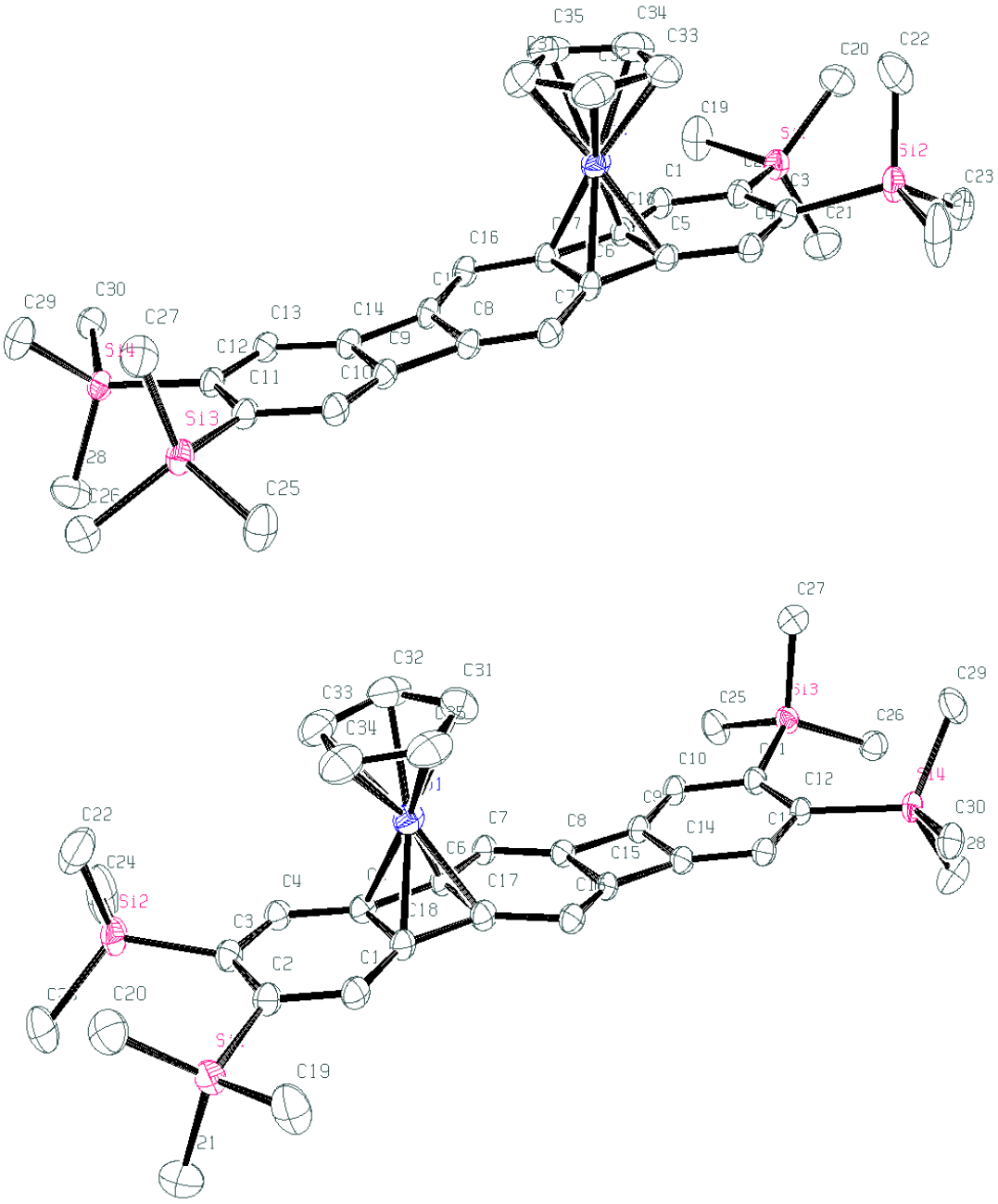

Figure 4.1. ORTEP representation of **19**.

Table 4.2. Atomic Coordinates and Equivalent Isotropic Displacement Parameters for **19**. U(eq) is Defined as One Third of the Trace of the Orthogonalized Uij Tensor

Atom	**x**	**y**	**Z**	**U (eq)**
Co1	0.73881(4)	–0.00927(3)	0.60643(2)	0.02551(10)
Si1	0.77416(8)	–0.19090(6)	0.94343(4)	0.02594(16)
Si2	1.13437(8)	–0.16706(7)	0.82404(5)	0.03023(17)
Si3	0.40491(7)	0.62139(6)	0.20406(4)	0.02291(15)
Si4	0.05088(7)	0.56545(6)	0.30946(4)	0.02144(14)
C1	0.6709(3)	–0.0385(2)	0.79440(16)	0.0239(5)
C2	0.8019(3)	–0.0967(2)	0.83428(16)	0.0241(5)
C3	0.9418(3)	–0.0743(2)	0.79331(16)	0.0233(5)
C4	0.9428(3)	0.0098(2)	0.71779(15)	0.0225(5)
C5	0.8094(2)	0.0691(2)	0.67735(15)	0.0207(4)
C6	0.7282(2)	0.1574(2)	0.60605(15)	0.0207(4)
C7	0.7303(2)	0.2531(2)	0.53306(15)	0.0211(4)
C8	0.5938(2)	0.3094(2)	0.50431(15)	0.0205(4)
C9	0.5057(2)	0.3981(2)	0.43438(15)	0.0207(4)
C10	0.5076(2)	0.4760(2)	0.35695(15)	0.0227(5)
C11	0.3734(2)	0.5293(2)	0.31459(15)	0.0215(4)
C12	0.2408(2)	0.5011(2)	0.35315(15)	0.0205(4)
C13	0.2432(2)	0.4196(2)	0.43269(15)	0.0215(4)
C14	0.3751(2)	0.3698(2)	0.47171(15)	0.0208(4)
C15	0.4564(2)	0.2794(2)	0.54277(15)	0.0211(4)
C16	0.4487(2)	0.1908(2)	0.61161(15)	0.0224(5)
C17	0.5916(3)	0.1278(2)	0.64393(15)	0.0221(5)
C18	0.6734(2)	0.0417(2)	0.71473(15)	0.0215(5)
C19	0.5795(3)	–0.2027(3)	0.9572(2)	0.0446(8)
C20	0.8892(4)	–0.3470(2)	0.9642(2)	0.0387(7)
C21	0.7986(4)	–0.1192(3)	1.0246(2)	0.0419(7)
C22	1.1685(4)	–0.3077(3)	0.7914(3)	0.0584(10)
C23	1.1726(3)	–0.1969(3)	0.9372(2)	0.0426(7)
C24	1.2742(4)	–0.0933(4)	0.7624(3)	0.0640(12)
C25	0.5777(3)	0.6657(3)	0.20261(18)	0.0348(6)
C26	0.2610(3)	0.7629(2)	0.16564(17)	0.0292(5)
C27	0.4355(3)	0.5272(3)	0.12760(18)	0.0347(6)
C28	–0.0272(3)	0.7195(2)	0.3194(2)	0.0360(6)
C29	0.0487(3)	0.5542(3)	0.19882(18)	0.0344(6)
C30	–0.0786(3)	0.4816(2)	0.37272(18)	0.0278(5)
C31	0.6994(4)	–0.0612(3)	0.5062(2)	0.0432(7)
C32	0.8520(4)	–0.0698(3)	0.5033(2)	0.0407(7)
C33	0.9085(3)	–0.1473(3)	0.5788(2)	0.0407(7)
C34	0.7922(4)	–0.1879(3)	0.6277(2)	0.0424(7)
C35	0.6647(4)	–0.1370(3)	0.5833(2)	0.0403(7)

Table 4.3. Bond Lengths (Å) for Complex **19**

Atom1	**Atom2**	**Length**
Co1	C5	1.993(3)
Co1	C6	2.023(3)
Co1	C17	2.022(2)
Co1	C18	2.009(3)
Co1	C31	2.042(4)
Co1	C32	2.075(3)
Co1	C33	2.062(3)
Co1	C34	2.042(4)
Co1	C35	2.048(4)
Si1	C2	1.886(2)
Si1	C19	1.877(3)
Si1	C20	1.863(2)
Si1	C21	1.865(4)
Si2	C3	1.889(3)
Si2	C22	1.876(5)
Si2	C23	1.862(3)
Si2	C24	1.865(4)
Si3	C11	1.901(2)
Si3	C25	1.876(4)
Si3	C26	1.867(2)
Si3	C27	1.875(4)
Si4	C12	1.889(2)
Si4	C28	1.860(3)
Si4	C29	1.868(3)
Si4	C30	1.870(3)
C1	C2	1.384(4)
C1	C18	1.411(3)
C2	C3	1.474(4)
C3	C4	1.384(3)
C4	C5	1.408(3)
C5	C6	1.480(3)
C5	C18	1.448(3)
C6	C7	1.437(3)
C6	C17	1.465(4)
C7	C8	1.351(3)
C8	C9	1.495(3)
C8	C15	1.476(3)
C9	C10	1.371(3)
C9	C14	1.405(3)
C10	C11	1.423(3)
C11	C12	1.427(3)
C12	C13	1.413(3)
C13	C14	1.376(3)

C14	C15	1.488(3)
C15	C16	1.352(3)
C16	C17	1.434(3)
C17	C18	1.468(3)
C31	C32	1.416(6)
C31	C35	1.419(4)
C32	C33	1.401(4)
C33	C34	1.411(5)
C34	C35	1.386(5)

Table 4.4. Bond Angles (°) for Complex **19**

Atom1	**Atom2**	**Atom3**	**Angle**
C5	Co1	C6	43.25(9)
C5	Co1	C17	62.1(1)
C5	Co1	C18	42.40(9)
C5	Co1	C31	162.9(1)
C5	Co1	C32	127.1(1)
C5	Co1	C33	110.2(1)
C5	Co1	C34	122.3(1)
C5	Co1	C35	155.6(1)
C6	Co1	C17	42.5(1)
C6	Co1	C18	61.91(9)
C6	Co1	C31	125.3(1)
C6	Co1	C32	116.4(1)
C6	Co1	C33	132.9(1)
C6	Co1	C34	165.1(1)
C6	Co1	C35	155.0(1)
C17	Co1	C18	42.7(1)
C17	Co1	C31	120.4(1)
C17	Co1	C32	145.1(1)
C17	Co1	C33	172.2(1)
C17	Co1	C34	141.9(1)
C17	Co1	C35	119.4(1)
C18	Co1	C31	151.7(1)
C18	Co1	C32	167.6(1)
C18	Co1	C33	131.2(1)
C18	Co1	C34	111.2(1)
C18	Co1	C35	119.8(1)
C31	Co1	C32	40.2(1)
C31	Co1	C33	67.3(1)
C31	Co1	C34	67.5(1)
C31	Co1	C35	40.6(1)
C32	Co1	C33	39.6(1)
C32	Co1	C34	67.2(1)

C32	Co1	C35	67.5(1)
C33	Co1	C34	40.2(1)
C33	Co1	C35	67.1(1)
C34	Co1	C35	39.6(1)
C2	Si1	C19	108.5(1)
C2	Si1	C20	115.7(1)
C2	Si1	C21	109.6(1)
C19	Si1	C20	103.5(1)
C19	Si1	C21	108.1(2)
C20	Si1	C21	111.0(2)
C3	Si2	C22	107.1(2)
C3	Si2	C23	116.2(1)
C3	Si2	C24	110.0(2)
C22	Si2	C23	111.0(2)
C22	Si2	C24	106.7(2)
C23	Si2	C24	105.6(2)
C11	Si3	C25	107.7(1)
C11	Si3	C26	117.7(1)
C11	Si3	C27	108.3(1)
C25	Si3	C26	104.5(1)
C25	Si3	C27	108.6(1)
C26	Si3	C27	109.7(1)
C12	Si4	C28	109.9(1)
C12	Si4	C29	113.2(1)
C12	Si4	C30	110.1(1)
C28	Si4	C29	111.9(1)
C28	Si4	C30	106.6(1)
C29	Si4	C30	104.8(1)
C2	C1	C18	119.3(2)
Si1	C2	C1	113.0(2)
Si1	C2	C3	127.0(2)
C1	C2	C3	119.8(2)
Si2	C3	C2	126.0(2)
Si2	C3	C4	112.4(2)
C2	C3	C4	120.8(2)
C3	C4	C5	119.2(2)
Co1	C5	C4	118.8(2)
Co1	C5	C6	69.5(1)
Co1	C5	C18	69.4(1)
C4	C5	C6	149.8(2)
C4	C5	C18	120.0(2)
C6	C5	C18	90.2(2)
Co1	C6	C5	67.3(1)
Co1	C6	C7	126.7(2)
Co1	C6	C17	68.7(1)
C5	C6	C7	147.4(2)

C5	C6	C17	89.3(2)
C7	C6	C17	122.7(2)
C6	C7	C8	112.1(2)
C7	C8	C9	146.1(2)
C7	C8	C15	125.1(2)
C9	C8	C15	88.5(2)
C8	C9	C10	147.1(2)
C8	C9	C14	91.2(2)
C10	C9	C14	121.4(2)
C9	C10	C11	118.6(2)
Si3	C11	C10	111.6(2)
Si3	C11	C12	128.3(2)
C10	C11	C12	119.7(2)
Si4	C12	C11	126.4(2)
Si4	C12	C13	113.5(2)
C11	C12	C13	120.1(2)
C12	C13	C14	118.5(2)
C9	C14	C13	121.6(2)
C9	C14	C15	91.5(2)
C13	C14	C15	146.5(2)
C8	C15	C14	88.8(2)
C8	C15	C16	125.0(2)
C14	C15	C16	145.8(2)
C15	C16	C17	111.8(2)
Co1	C17	C6	68.8(1)
Co1	C17	C16	126.5(2)
Co1	C17	C18	68.2(1)
C6	C17	C16	123.3(2)
C6	C17	C18	90.0(2)
C16	C17	C18	146.0(2)
Co1	C18	C1	122.9(2)
Co1	C18	C5	68.2(1)
Co1	C18	C17	69.1(1)
C1	C18	C5	120.6(2)
C1	C18	C17	148.7(2)
C5	C18	C17	90.5(2)
Co1	C31	C32	71.2(2)
Co1	C31	C35	69.9(2)
C32	C31	C35	107.7(3)
Co1	C32	C31	68.6(2)
Co1	C32	C33	69.7(2)
C31	C32	C33	107.6(3)
Co1	C33	C32	70.7(2)
Co1	C33	C34	69.1(2)
C32	C33	C34	108.1(3)
Co1	C34	C33	70.7(2)

Co1	C34	C35	70.4(2)
C33	C34	C35	108.6(3)
Co1	C35	C31	69.5(2)
Co1	C35	C34	70.0(2)
C31	C35	C34	107.9(3)

Table 4.4. Torsion Angles (°) for Complex **19**

Atom1	**Atom2**	**Atom3**	**Atom4**	**Torsion**
C6	Co1	C5	C4	–147.9(3)
C6	Co1	C5	C18	98.3(2)
C17	Co1	C5	C4	163.0(2)
C17	Co1	C5	C6	–49.1(1)
C17	Co1	C5	C18	49.2(1)
C18	Co1	C5	C4	113.8(2)
C18	Co1	C5	C6	–98.3(2)
C31	Co1	C5	C4	–94.1(4)
C31	Co1	C5	C6	53.8(4)
C31	Co1	C5	C18	152.2(4)
C32	Co1	C5	C4	–57.3(2)
C32	Co1	C5	C6	90.6(2)
C32	Co1	C5	C18	–171.0(2)
C33	Co1	C5	C4	–16.0(2)
C33	Co1	C5	C6	131.9(1)
C33	Co1	C5	C18	–129.7(2)
C34	Co1	C5	C4	27.1(2)
C34	Co1	C5	C6	175.0(2)
C34	Co1	C5	C18	–86.6(2)
C35	Co1	C5	C4	62.9(4)
C35	Co1	C5	C6	–149.2(3)
C35	Co1	C5	C18	–50.9(3)
C5	Co1	C6	C7	145.8(3)
C5	Co1	C6	C17	–98.6(2)
C17	Co1	C6	C5	98.6(2)
C17	Co1	C6	C7	–115.6(3)
C18	Co1	C6	C5	49.1(1)
C18	Co1	C6	C7	–165.0(2)
C18	Co1	C6	C17	–49.4(1)
C31	Co1	C6	C5	–163.1(2)
C31	Co1	C6	C7	–17.3(3)
C31	Co1	C6	C17	98.3(2)
C32	Co1	C6	C5	–117.0(2)
C32	Co1	C6	C7	28.8(2)
C32	Co1	C6	C17	144.4(2)
C33	Co1	C6	C5	–72.5(2)

C33	Co1	C6	C7	73.4(3)
C33	Co1	C6	C17	–171.0(2)
C34	Co1	C6	C5	–16.6(5)
C34	Co1	C6	C7	129.3(5)
C34	Co1	C6	C17	–115.1(5)
C35	Co1	C6	C5	149.9(3)
C35	Co1	C6	C7	–64.2(4)
C35	Co1	C6	C17	51.4(3)
C5	Co1	C17	C6	50.1(1)
C5	Co1	C17	C16	166.6(3)
C5	Co1	C17	C18	–48.9(1)
C6	Co1	C17	C16	116.5(3)
C6	Co1	C17	C18	–98.9(2)
C18	Co1	C17	C6	98.9(2)
C18	Co1	C17	C16	–144.6(3)
C31	Co1	C17	C6	–110.6(2)
C31	Co1	C17	C16	5.9(3)
C31	Co1	C17	C18	150.5(2)
C32	Co1	C17	C6	–65.6(3)
C32	Co1	C17	C16	51.0(3)
C32	Co1	C17	C18	–164.5(2)
C33	Co1	C17	C6	57.1(9)
C33	Co1	C17	C16	173.6(8)
C33	Co1	C17	C18	–41.8(9)
C34	Co1	C17	C6	157.8(2)
C34	Co1	C17	C16	–85.7(3)
C34	Co1	C17	C18	58.9(2)
C35	Co1	C17	C6	–157.8(2)
C35	Co1	C17	C16	–41.3(3)
C35	Co1	C17	C18	103.3(2)
C5	Co1	C18	C1	–113.3(3)
C5	Co1	C18	C17	99.3(2)
C6	Co1	C18	C1	–163.5(2)
C6	Co1	C18	C5	–50.2(1)
C6	Co1	C18	C17	49.1(1)
C17	Co1	C18	C1	147.4(3)
C17	Co1	C18	C5	–99.3(2)
C31	Co1	C18	C1	83.6(3)
C31	Co1	C18	C5	–163.2(2)
C31	Co1	C18	C17	–63.8(3)
C32	Co1	C18	C1	–77.9(6)
C32	Co1	C18	C5	35.3(6)
C32	Co1	C18	C17	134.6(5)
C33	Co1	C18	C1	–39.5(3)
C33	Co1	C18	C5	73.7(2)
C33	Co1	C18	C17	173.1(2)

C34	Co1	C18	C1	2.0(2)
C34	Co1	C18	C5	115.2(2)
C34	Co1	C18	C17	–145.5(2)
C35	Co1	C18	C1	45.1(3)
C35	Co1	C18	C5	158.3(2)
C35	Co1	C18	C17	–102.3(2)
C5	Co1	C31	C32	47.8(5)
C5	Co1	C31	C35	165.6(4)
C6	Co1	C31	C32	90.4(2)
C6	Co1	C31	C35	–151.7(2)
C17	Co1	C31	C32	141.2(2)
C17	Co1	C31	C35	–101.0(2)
C18	Co1	C31	C32	–173.9(2)
C18	Co1	C31	C35	–56.1(3)
C32	Co1	C31	C35	117.9(3)
C33	Co1	C31	C32	–37.0(2)
C33	Co1	C31	C35	80.8(2)
C34	Co1	C31	C32	–80.8(2)
C34	Co1	C31	C35	37.1(2)
C35	Co1	C31	C32	–117.9(3)
C5	Co1	C32	C31	–164.2(2)
C5	Co1	C32	C33	76.4(2)
C6	Co1	C32	C31	–114.3(2)
C6	Co1	C32	C33	126.3(2)
C17	Co1	C32	C31	–71.0(3)
C17	Co1	C32	C33	169.7(2)
C18	Co1	C32	C31	166.6(5)
C18	Co1	C32	C33	47.2(6)
C31	Co1	C32	C33	–119.4(3)
C33	Co1	C32	C31	119.4(3)
C34	Co1	C32	C31	81.6(2)
C34	Co1	C32	C33	–37.7(2)
C35	Co1	C32	C31	38.5(2)
C35	Co1	C32	C33	–80.8(2)
C5	Co1	C33	C32	–124.3(2)
C5	Co1	C33	C34	116.6(2)
C6	Co1	C33	C32	–80.2(2)
C6	Co1	C33	C34	160.7(2)
C17	Co1	C33	C32	–130.9(8)
C17	Co1	C33	C34	110.0(9)
C18	Co1	C33	C32	–167.9(2)
C18	Co1	C33	C34	73.0(2)
C31	Co1	C33	C32	37.6(2)
C31	Co1	C33	C34	–81.5(2)
C32	Co1	C33	C34	–119.1(3)
C34	Co1	C33	C32	119.1(3)

C35	Co1	C33	C32	81.8(2)
C35	Co1	C33	C34	–37.3(2)
C5	Co1	C34	C33	–83.3(2)
C5	Co1	C34	C35	157.7(2)
C6	Co1	C34	C33	–70.0(5)
C6	Co1	C34	C35	171.1(4)
C17	Co1	C34	C33	–168.1(2)
C17	Co1	C34	C35	73.0(3)
C18	Co1	C34	C33	–129.5(2)
C18	Co1	C34	C35	111.5(2)
C31	Co1	C34	C33	80.9(2)
C31	Co1	C34	C35	–38.0(2)
C32	Co1	C34	C33	37.2(2)
C32	Co1	C34	C35	–81.8(2)
C33	Co1	C34	C35	–118.9(3)
C35	Co1	C34	C33	118.9(3)
C5	Co1	C35	C31	–169.9(3)
C5	Co1	C35	C34	–50.8(4)
C6	Co1	C35	C31	66.3(4)
C6	Co1	C35	C34	–174.6(2)
C17	Co1	C35	C31	103.6(2)
C17	Co1	C35	C34	–137.3(2)
C18	Co1	C35	C31	153.1(2)
C18	Co1	C35	C34	–87.8(2)
C31	Co1	C35	C34	119.1(3)
C32	Co1	C35	C31	–38.2(2)
C32	Co1	C35	C34	80.9(2)
C33	Co1	C35	C31	–81.2(2)
C33	Co1	C35	C34	37.8(2)
C34	Co1	C35	C31	–119.1(3)
C19	Si1	C2	C1	11.8(2)
C19	Si1	C2	C3	–173.1(2)
C20	Si1	C2	C1	127.5(2)
C20	Si1	C2	C3	–57.4(3)
C21	Si1	C2	C1	–106.1(2)
C21	Si1	C2	C3	69.0(3)
C22	Si2	C3	C2	71.4(3)
C22	Si2	C3	C4	–98.8(2)
C23	Si2	C3	C2	–53.2(3)
C23	Si2	C3	C4	136.5(2)
C24	Si2	C3	C2	–173.1(3)
C24	Si2	C3	C4	16.7(3)
C25	Si3	C11	C10	–24.1(2)
C25	Si3	C11	C12	162.4(2)
C26	Si3	C11	C10	–141.7(2)
C26	Si3	C11	C12	44.7(3)

C27	Si3	C11	C10	93.2(2)
C27	Si3	C11	C12	–80.4(2)
C28	Si4	C12	C11	–73.1(2)
C28	Si4	C12	C13	105.5(2)
C29	Si4	C12	C11	52.9(2)
C29	Si4	C12	C13	–128.5(2)
C30	Si4	C12	C11	169.8(2)
C30	Si4	C12	C13	–11.6(2)
C18	C1	C2	Si1	175.5(2)
C18	C1	C2	C3	0.0(4)
C2	C1	C18	Co1	78.4(3)
C2	C1	C18	C5	–4.1(4)
C2	C1	C18	C17	–177.2(4)
Si1	C2	C3	Si2	19.8(4)
Si1	C2	C3	C4	–170.7(2)
C1	C2	C3	Si2	–165.4(2)
C1	C2	C3	C4	4.1(4)
Si2	C3	C4	C5	166.8(2)
C2	C3	C4	C5	–4.0(4)
C3	C4	C5	Co1	–81.6(3)
C3	C4	C5	C6	179.9(4)
C3	C4	C5	C18	–0.1(4)
Co1	C5	C6	C7	–123.3(4)
Co1	C5	C6	C17	67.1(1)
C4	C5	C6	Co1	112.2(4)
C4	C5	C6	C7	–11.2(7)
C4	C5	C6	C17	179.3(4)
C18	C5	C6	Co1	–67.8(1)
C18	C5	C6	C7	168.8(4)
C18	C5	C6	C17	–0.7(2)
Co1	C5	C18	C1	116.4(2)
Co1	C5	C18	C17	–67.2(1)
C4	C5	C18	Co1	–112.1(2)
C4	C5	C18	C1	4.2(3)
C4	C5	C18	C17	–179.3(2)
C6	C5	C18	Co1	67.9(1)
C6	C5	C18	C1	–175.7(2)
C6	C5	C18	C17	0.7(2)
Co1	C6	C7	C8	85.8(2)
C5	C6	C7	C8	–168.3(3)
C17	C6	C7	C8	–0.8(3)
Co1	C6	C17	C16	–120.5(2)
Co1	C6	C17	C18	66.5(1)
C5	C6	C17	Co1	–65.8(1)
C5	C6	C17	C16	173.6(2)
C5	C6	C17	C18	0.7(2)

C7	C6	C17	Co1	120.9(2)
C7	C6	C17	C16	0.3(4)
C7	C6	C17	C18	–172.6(2)
C6	C7	C8	C9	–169.7(3)
C6	C7	C8	C15	0.9(3)
C7	C8	C9	C10	0.5(7)
C7	C8	C9	C14	172.8(4)
C15	C8	C9	C10	–171.8(4)
C15	C8	C9	C14	0.5(2)
C7	C8	C15	C14	–175.2(2)
C7	C8	C15	C16	–0.6(4)
C9	C8	C15	C14	–0.4(2)
C9	C8	C15	C16	174.2(2)
C8	C9	C10	C11	171.4(3)
C14	C9	C10	C11	0.5(3)
C8	C9	C14	C13	–175.6(2)
C8	C9	C14	C15	–0.5(2)
C10	C9	C14	C13	–0.6(4)
C10	C9	C14	C15	174.6(2)
C9	C10	C11	Si3	–174.1(2)
C9	C10	C11	C12	0.1(3)
Si3	C11	C12	Si4	–9.0(3)
Si3	C11	C12	C13	172.5(2)
C10	C11	C12	Si4	177.9(2)
C10	C11	C12	C13	–0.7(3)
Si4	C12	C13	C14	–178.1(2)
C11	C12	C13	C14	0.6(3)
C12	C13	C14	C9	–0.0(3)
C12	C13	C14	C15	–171.3(3)
C9	C14	C15	C8	0.5(2)
C9	C14	C15	C16	–171.7(4)
C13	C14	C15	C8	173.0(4)
C13	C14	C15	C16	0.9(7)
C8	C15	C16	C17	0.0(3)
C14	C15	C16	C17	170.4(3)
C15	C16	C17	Co1	–87.0(3)
C15	C16	C17	C6	0.1(3)
C15	C16	C17	C18	167.4(4)
Co1	C17	C18	C1	–119.5(4)
Co1	C17	C18	C5	66.4(1)
C6	C17	C18	Co1	–67.1(1)
C6	C17	C18	C1	173.4(4)
C6	C17	C18	C5	–0.7(2)
C16	C17	C18	Co1	123.5(4)
C16	C17	C18	C1	4.0(7)
C16	C17	C18	C5	–170.1(4)

Co1	C31	C32	C33	59.0(2)
C35	C31	C32	Co1	–60.7(2)
C35	C31	C32	C33	–1.6(4)
Co1	C31	C35	C34	–59.6(3)
C32	C31	C35	Co1	61.5(3)
C32	C31	C35	C34	1.8(4)
Co1	C32	C33	C34	59.2(2)
C31	C32	C33	Co1	–58.3(2)
C31	C32	C33	C34	0.9(4)
Co1	C33	C34	C35	60.5(3)
C32	C33	C34	Co1	–60.2(2)
C32	C33	C34	C35	0.3(4)
Co1	C34	C35	C31	59.3(3)
C33	C34	C35	Co1	–60.6(2)
C33	C34	C35	C31	–1.3(4)

2,3-Bis(trimethylsilyl) linear [3]phenylene(CpCo) **52**:

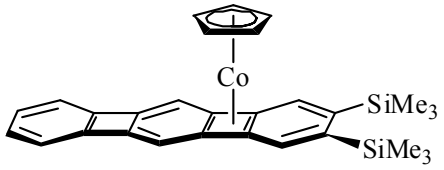

To a Schlenk flask containing a solution of 2,3-bis(trimethylsilylethynyl)biphenylene **51** (0.29 g, 0.85 mmol)[27] in ether (20 mL) and CH_3OH (10 mL) was added K_2CO_3 (0.14 g, 1.01 mmol). The mixture was stirred for 1.5 h and monitored via TLC, eluting with hexane/CH_2Cl_2 (5:1). After the starting material had been consumed, the solvents were removed and the yellow residue dissolved in ether (30 mL). Aqueous workup with sat. NaCl (2 x 20 mL), followed by drying over $MgSO_4$ and concentration in vacuo provided a yellow solid. This material was redissolved in THF (15 mL), degassed (Ar), and $CpCo(CO)_2$ (0.140 g, 0.78 mmol) added. The resulting solution (protected from light with foil) was injected (syringe pump) over 8 h into a boiling mixture of THF (200 mL) and BTMSA (50 mL), while irradiating with a slide projection lamp. Once addition was complete, heating and irradiation were continued for another 14 h. The volatiles were removed via vacuum transfer and the remaining black residue filtered through a plug of neutral alumina, activity III (4 x 4 cm), eluting with a degassed mixture of hexane/THF (10:1). The solvents were removed in vacuo and the residue crystallized from acetone yielding **52** (0.24 g, 57 %) as dark red crystals, m.p. 198–202 °C (decomp); ^{1}H-NMR (500 MHz, C_6D_6): δ = 7.96 (s, 2 H), 6.78 (AA'm, 2 H), 6.75 (s, 2 H), 6.74 (BB'm, 2 H), 4.36 (s, 5 H), 0.37 (s, 18 H) ppm; ^{13}C-NMR (125 MHz, C_6D_6): δ = 150.2, 142.6, 139.3, 136.0, 129.4, 119.4, 114.9, 80.2, 77.9, 73.8, 2.68 ppm; IR (neat) $\tilde{\nu}$ = 2960, 2923, 2853, 1461, 1455, 1378, 1260, 1093, 1019, 800 cm^{-1}; UV-VIS (hexane): λ_{max} (log ε) = 255 (3.93), 282 (3.76), 293 (sh, 3.78), 308 (3.89), 348 (3.90), 397 (sh, 3.35), 436 (3.01), 511

(2.62); MS (70 eV): *m*/*z* (%): 494 (100) [M^+], 370 (14); HRMS (FAB) calcd for $C_{29}H_{31}CoSi_2$: 494.1296; found: 494.1292. Elemental analysis calcd for $C_{29}H_{31}CoSi_2$: C 70.41, H 6.32; found: 70.48, 6.28.

Crystallographic information for **52** (H atoms omitted):

Table 4.5. Crystal Data and Structure Refinement For **52**

Empirical formula	$C_{29}H_{31}CoSi_2$
Formula weight	494.65
cryst size (mm)	0.30 x 0.20 x 0.05
cryst syst	Monoclinic
# refl used for unit cell determination	2640
2 θ range (deg)	2.42–25.03
a (Å)	43.91(3)
b (Å)	7.472(4)
c (Å)	16.869(11)
α (deg)	
β (deg)	111.522(11)
γ (deg)	
V (Å^3)	5149(6)
space group	C2/c
Z	8
D_{calc}, g/cm^3	1.276
F_{000}	2080
μ, cm^{-1}	7.74
temp, ºC	–153
T_{max}, T_{min}	0.963, 0.800
no. of total rflns	18401
no. of unique rflns	2640
no. of obsd. rflns	4266
no. of variables	271
Reflection to Parameter Ratio	9.74
R	0.0892
R_w	0.2042
R_{all}	0.1248
GOF	1.008
Max. Peak in Final Diff. Map (e–/ Å^3)	1.051
Min. Peak in Final Diff. Map (e–/ Å^3)	–0.707

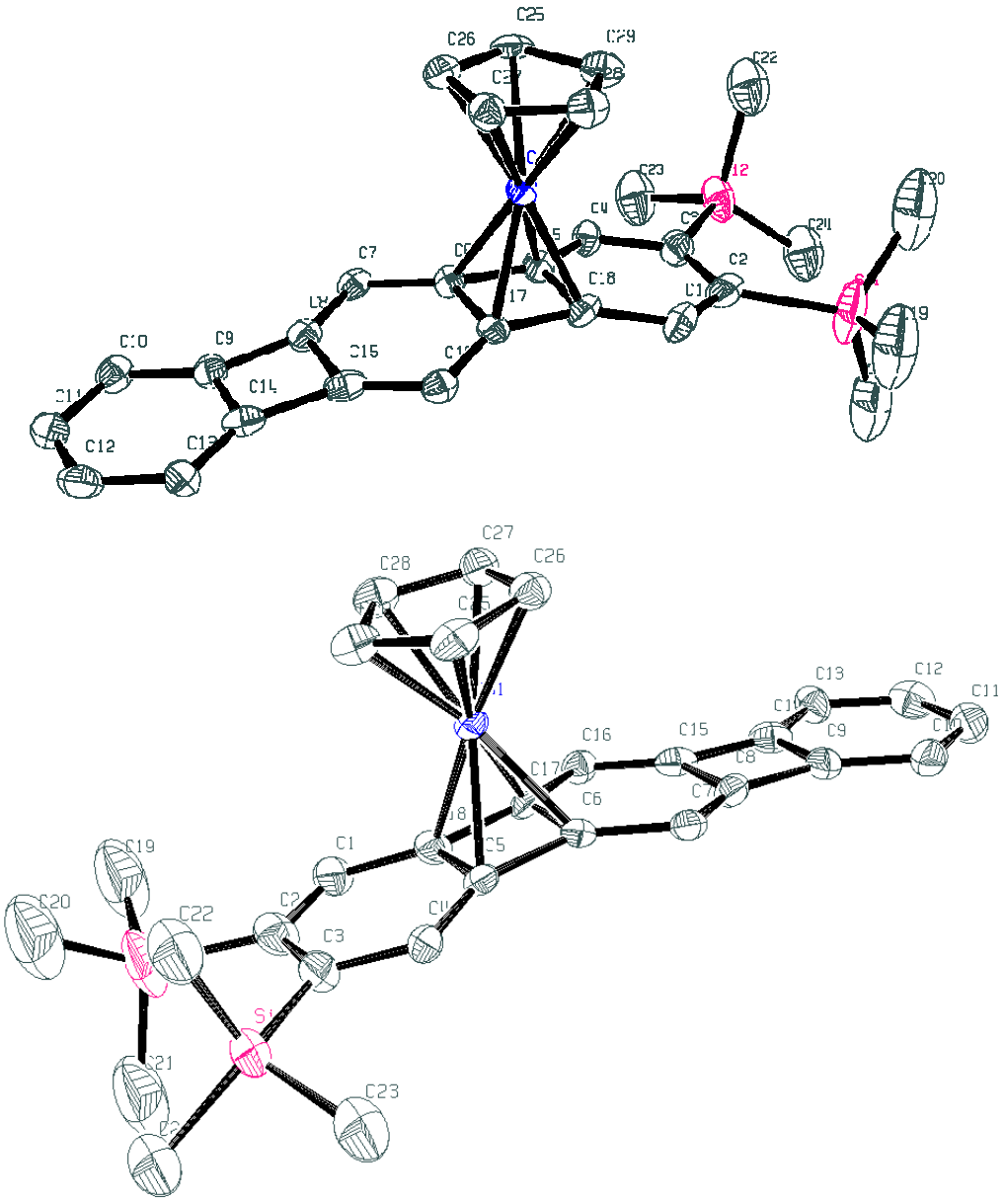

Figure 4.2. ORTEP representation of **52**.

Table 4.6. Atomic Coordinates and Equivalent Isotropic Displacement Parameters for **52**. U(eq) is Defined as One Third of the Trace of the Orthogonalized Uij Tensor

Atom	**x**	**y**	**z**	**U(eq)**
Co1	0.06961(2)	0.87577(12)	0.38136(6)	0.0200(3)
Si1	0.18827(6)	0.8761(5)	0.63753(18)	0.0627(9)
Si2	0.18540(5)	0.5425(3)	0.46900(16)	0.0410(6)
C1	0.12151(19)	0.8410(10)	0.5589(5)	0.0310(17)
C2	0.15018(13)	0.7767(11)	0.5552(4)	0.0343(18)
C3	0.15002(14)	0.6417(10)	0.4926(5)	0.0324(17)
C4	0.11985(17)	0.5770(9)	0.4357(4)	0.0247(16)
C5	0.09030(17)	0.6465(9)	0.4383(4)	0.0220(14)
C6	0.05450(16)	0.6378(9)	0.4077(4)	0.0216(14)
C7	0.02537(17)	0.5420(9)	0.3591(4)	0.0224(15)
C8	–0.00060(18)	0.5847(9)	0.3798(4)	0.0246(15)
C9	–0.03560(17)	0.5555(10)	0.3644(4)	0.0256(16)
C10	–0.06399(18)	0.4581(10)	0.3174(4)	0.0284(17)
C11	–0.09208(19)	0.5019(12)	0.3360(5)	0.0344(18)
C12	–0.09130(19)	0.6274(12)	0.3957(5)	0.0340(18)
C13	–0.06300(17)	0.7256(11)	0.4422(5)	0.0294(17)
C14	–0.03558(19)	0.6826(10)	0.4247(4)	0.0274(16)
C15	0.00008(18)	0.7212(10)	0.4449(4)	0.0251(16)
C16	0.02653(17)	0.8159(10)	0.4925(4)	0.0234(15)
C17	0.05500(17)	0.7741(9)	0.4722(4)	0.0231(15)
C18	0.09090(17)	0.7798(10)	0.5007(4)	0.0247(15)
C19	0.1766(3)	1.0793(15)	0.6845(9)	0.098(3)
C20	0.2181(3)	0.957(2)	0.5901(7)	0.098(3)
C21	0.2076(3)	0.7068(14)	0.7228(7)	0.098(3)
C22	0.1946(2)	0.6941(13)	0.3925(6)	0.0631(17)
C23	0.1724(2)	0.3224(9)	0.4142(7)	0.0631(17)
C24	0.22363(17)	0.4883(16)	0.5614(5)	0.0631(17)
C25	0.07501(19)	0.9264(10)	0.2652(4)	0.0281(17)
C26	0.04279(18)	0.9614(10)	0.2593(4)	0.0264(16)
C27	0.04343(18)	1.0945(10)	0.3211(4)	0.0271(16)
C28	0.07584(19)	1.1429(10)	0.3645(5)	0.0296(17)
C29	0.0960(2)	1.0392(11)	0.3322(5)	0.0321(17)

Table 4.7. Bond Lengths (Å) for Complex **52**

Atom1	**Atom2**	**Length**
Co1	C5	2.011(7)
Co1	C6	2.004(7)
Co1	C17	2.014(8)
Co1	C18	2.015(6)
Co1	C25	2.093(8)

Co1	C26	2.063(6)
Co1	C27	2.042(7)
Co1	C28	2.049(8)
Co1	C29	2.06(1)
Si1	C2	1.890(6)
Si1	C19	1.87(1)
Si1	C20	1.87(2)
Si1	C21	1.87(1)
Si2	C3	1.891(8)
Si2	C22	1.87(1)
Si2	C23	1.870(8)
Si2	C24	1.869(7)
C1	C2	1.37(1)
C1	C18	1.418(9)
C2	C3	1.46(1)
C3	C4	1.406(8)
C4	C5	1.41(1)
C5	C6	1.47(1)
C5	C18	1.44(1)
C6	C7	1.432(9)
C6	C17	1.48(1)
C7	C8	1.35(1)
C8	C9	1.48(1)
C8	C15	1.49(1)
C9	C10	1.410(9)
C9	C14	1.39(1)
C10	C11	1.42(1)
C11	C12	1.37(1)
C12	C13	1.41(1)
C13	C14	1.38(1)
C14	C15	1.50(1)
C15	C16	1.345(9)
C16	C17	1.45(1)
C17	C18	1.47(1)
C25	C26	1.41(1)
C25	C29	1.44(1)
C26	C27	1.43(1)
C27	C28	1.39(1)
C28	C29	1.43(1)

Table 4.8. Bond Angles (°) for Complex **52**

Atom1	**Atom2**	**Atom3**	**Angle**
C5	Co1	C6	42.8(3)
C5	Co1	C17	61.9(3)

C5	Co1	C18	42.0(3)
C5	Co1	C25	114.5(3)
C5	Co1	C26	137.2(3)
C5	Co1	C27	173.3(3)
C5	Co1	C28	146.8(3)
C5	Co1	C29	118.4(3)
C6	Co1	C17	43.4(3)
C6	Co1	C18	62.1(3)
C6	Co1	C25	121.9(3)
C6	Co1	C26	112.5(3)
C6	Co1	C27	130.5(3)
C6	Co1	C28	165.3(3)
C6	Co1	C29	153.9(3)
C17	Co1	C18	42.8(3)
C17	Co1	C25	163.2(3)
C17	Co1	C26	130.7(3)
C17	Co1	C27	113.7(3)
C17	Co1	C28	124.7(3)
C17	Co1	C29	156.2(3)
C18	Co1	C25	146.0(3)
C18	Co1	C26	173.3(3)
C18	Co1	C27	138.8(3)
C18	Co1	C28	116.7(3)
C18	Co1	C29	119.4(3)
C25	Co1	C26	39.5(3)
C25	Co1	C27	68.0(3)
C25	Co1	C28	68.1(3)
C25	Co1	C29	40.6(3)
C26	Co1	C27	40.9(3)
C26	Co1	C28	67.4(3)
C26	Co1	C29	67.2(3)
C27	Co1	C28	39.7(3)
C27	Co1	C29	67.8(3)
C28	Co1	C29	40.7(3)
C2	Si1	C19	108.9(5)
C2	Si1	C20	112.5(5)
C2	Si1	C21	109.2(4)
C19	Si1	C20	105.3(6)
C19	Si1	C21	110.0(6)
C20	Si1	C21	110.9(6)
C3	Si2	C22	108.1(4)
C3	Si2	C23	108.9(4)
C3	Si2	C24	117.7(4)
C22	Si2	C23	107.2(4)
C22	Si2	C24	110.6(4)
C23	Si2	C24	103.9(4)

C2	C1	C18	120.6(7)
Si1	C2	C1	114.1(5)
Si1	C2	C3	124.9(5)
C1	C2	C3	121.0(7)
Si2	C3	C2	129.6(5)
Si2	C3	C4	111.3(5)
C2	C3	C4	119.0(6)
C3	C4	C5	119.9(6)
Co1	C5	C4	123.9(5)
Co1	C5	C6	68.4(4)
Co1	C5	C18	69.2(4)
C4	C5	C6	148.4(7)
C4	C5	C18	120.3(6)
C6	C5	C18	91.0(6)
Co1	C6	C5	68.8(4)
Co1	C6	C7	128.0(5)
Co1	C6	C17	68.7(4)
C5	C6	C7	147.3(6)
C5	C6	C17	89.2(5)
C7	C6	C17	122.2(6)
C6	C7	C8	113.3(6)
C7	C8	C9	147.5(7)
C7	C8	C15	124.2(7)
C9	C8	C15	88.2(6)
C8	C9	C10	145.4(7)
C8	C9	C14	92.8(6)
C10	C9	C14	121.8(7)
C9	C10	C11	114.7(7)
C10	C11	C12	122.2(8)
C11	C12	C13	123.1(8)
C12	C13	C14	114.9(7)
C9	C14	C13	123.3(7)
C9	C14	C15	91.0(6)
C13	C14	C15	145.7(7)
C8	C15	C14	87.9(6)
C8	C15	C16	125.4(7)
C14	C15	C16	146.7(7)
C15	C16	C17	112.1(6)
Co1	C17	C6	67.9(4)
Co1	C17	C16	130.0(5)
Co1	C17	C18	68.6(4)
C6	C17	C16	122.7(6)
C6	C17	C18	89.2(5)
C16	C17	C18	146.4(7)
Co1	C18	C1	123.5(5)
Co1	C18	C5	68.8(4)

Co1	C18	C17	68.6(4)
C1	C18	C5	119.1(7)
C1	C18	C17	150.0(7)
C5	C18	C17	90.6(6)
Co1	C25	C26	69.1(4)
Co1	C25	C29	68.3(4)
C26	C25	C29	106.5(7)
Co1	C26	C25	71.4(4)
Co1	C26	C27	68.8(4)
C25	C26	C27	109.1(6)
Co1	C27	C26	70.4(4)
Co1	C27	C28	70.4(5)
C26	C27	C28	107.9(7)
Co1	C28	C27	69.9(5)
Co1	C28	C29	69.9(5)
C27	C28	C29	108.5(7)
Co1	C29	C25	71.1(5)
Co1	C29	C28	69.4(5)
C25	C29	C28	108.0(7)

Table 4.9. Torsion Angles (°) for Complex **52**

Atom1	**Atom2**	**Atom3**	**Atom4**	**Torsion**
C6	Co1	C5	C4	146.8(8)
C6	Co1	C5	C18	–99.9(5)
C17	Co1	C5	C4	–162.7(7)
C17	Co1	C5	C6	50.4(4)
C17	Co1	C5	C18	–49.4(4)
C18	Co1	C5	C4	–113.3(8)
C18	Co1	C5	C6	99.9(5)
C25	Co1	C5	C4	35.6(7)
C25	Co1	C5	C6	–111.3(4)
C25	Co1	C5	C18	148.9(4)
C26	Co1	C5	C4	76.5(7)
C26	Co1	C5	C6	–70.3(5)
C26	Co1	C5	C18	–170.2(4)
C27	Co1	C5	C4	146(2)
C27	Co1	C5	C6	–1(3)
C27	Co1	C5	C18	–101(2)
C28	Co1	C5	C4	–51.5(9)
C28	Co1	C5	C6	161.7(5)
C28	Co1	C5	C18	61.9(7)
C29	Co1	C5	C4	–9.8(7)
C29	Co1	C5	C6	–156.7(4)
C29	Co1	C5	C18	103.5(5)

C5	Co1	C6	C7	–147.4(8)
C5	Co1	C6	C17	97.7(5)
C17	Co1	C6	C5	–97.7(5)
C17	Co1	C6	C7	114.9(8)
C18	Co1	C6	C5	–48.2(4)
C18	Co1	C6	C7	164.4(7)
C18	Co1	C6	C17	49.5(4)
C25	Co1	C6	C5	92.7(5)
C25	Co1	C6	C7	–54.7(7)
C25	Co1	C6	C17	–169.6(4)
C26	Co1	C6	C5	136.2(4)
C26	Co1	C6	C7	–11.2(7)
C26	Co1	C6	C17	–126.1(4)
C27	Co1	C6	C5	179.9(4)
C27	Co1	C6	C7	32.5(8)
C27	Co1	C6	C17	–82.4(5)
C28	Co1	C6	C5	–137(1)
C28	Co1	C6	C7	75(1)
C28	Co1	C6	C17	–40(1)
C29	Co1	C6	C5	52.3(8)
C29	Co1	C6	C7	–95.1(9)
C29	Co1	C6	C17	150.1(7)
C5	Co1	C17	C6	–49.7(4)
C5	Co1	C17	C16	–164.6(8)
C5	Co1	C17	C18	48.4(4)
C6	Co1	C17	C16	–114.9(8)
C6	Co1	C17	C18	98.1(5)
C18	Co1	C17	C6	–98.1(5)
C18	Co1	C17	C16	147.0(9)
C25	Co1	C17	C6	32(1)
C25	Co1	C17	C16	–83(1)
C25	Co1	C17	C18	130(1)
C26	Co1	C17	C6	79.9(5)
C26	Co1	C17	C16	–35.0(8)
C26	Co1	C17	C18	178.0(4)
C27	Co1	C17	C6	124.5(4)
C27	Co1	C17	C16	9.7(8)
C27	Co1	C17	C18	–137.3(4)
C28	Co1	C17	C6	168.6(4)
C28	Co1	C17	C16	53.8(8)
C28	Co1	C17	C18	–93.2(5)
C29	Co1	C17	C6	–147.1(7)
C29	Co1	C17	C16	98(1)
C29	Co1	C17	C18	–48.9(9)
C5	Co1	C18	C1	111.7(8)
C5	Co1	C18	C17	–99.5(5)

C6	Co1	C18	C1	160.9(7)
C6	Co1	C18	C5	49.2(4)
C6	Co1	C18	C17	–50.2(4)
C17	Co1	C18	C1	–148.8(8)
C17	Co1	C18	C5	99.5(5)
C25	Co1	C18	C1	54.4(9)
C25	Co1	C18	C5	–57.3(7)
C25	Co1	C18	C17	–156.8(5)
C26	Co1	C18	C1	–162(2)
C26	Co1	C18	C5	87(3)
C26	Co1	C18	C17	–13(3)
C27	Co1	C18	C1	–78.4(8)
C27	Co1	C18	C5	169.9(4)
C27	Co1	C18	C17	70.5(6)
C28	Co1	C18	C1	–35.6(7)
C28	Co1	C18	C5	–147.3(4)
C28	Co1	C18	C17	113.3(4)
C29	Co1	C18	C1	10.7(8)
C29	Co1	C18	C5	–101.0(5)
C29	Co1	C18	C17	159.5(4)
C5	Co1	C25	C26	135.6(4)
C5	Co1	C25	C29	–105.8(5)
C6	Co1	C25	C26	87.3(5)
C6	Co1	C25	C29	–154.0(5)
C17	Co1	C25	C26	62(1)
C17	Co1	C25	C29	–179.6(9)
C18	Co1	C25	C26	173.8(5)
C18	Co1	C25	C29	–67.5(7)
C26	Co1	C25	C29	118.7(6)
C27	Co1	C25	C26	–37.6(4)
C27	Co1	C25	C29	81.0(5)
C28	Co1	C25	C26	–80.6(5)
C28	Co1	C25	C29	38.1(5)
C29	Co1	C25	C26	–118.7(6)
C5	Co1	C26	C25	–69.6(6)
C5	Co1	C26	C27	170.3(4)
C6	Co1	C26	C25	–113.4(5)
C6	Co1	C26	C27	126.5(4)
C17	Co1	C26	C25	–160.4(4)
C17	Co1	C26	C27	79.5(5)
C18	Co1	C26	C25	–149(2)
C18	Co1	C26	C27	91(3)
C25	Co1	C26	C27	–120.1(6)
C27	Co1	C26	C25	120.1(6)
C28	Co1	C26	C25	82.5(5)
C28	Co1	C26	C27	–37.6(4)

C29	Co1	C26	C25	38.3(5)
C29	Co1	C26	C27	–81.8(5)
C5	Co1	C27	C26	–77(3)
C5	Co1	C27	C28	165(2)
C6	Co1	C27	C26	–77.4(5)
C6	Co1	C27	C28	164.4(5)
C17	Co1	C27	C26	–125.4(4)
C17	Co1	C27	C28	116.3(5)
C18	Co1	C27	C26	–169.8(5)
C18	Co1	C27	C28	72.0(6)
C25	Co1	C27	C26	36.4(4)
C25	Co1	C27	C28	–81.8(5)
C26	Co1	C27	C28	–118.2(6)
C28	Co1	C27	C26	118.2(6)
C29	Co1	C27	C26	80.4(5)
C29	Co1	C27	C28	–37.8(5)
C5	Co1	C28	C27	–176.8(5)
C5	Co1	C28	C29	63.7(7)
C6	Co1	C28	C27	–54(1)
C6	Co1	C28	C29	–173(1)
C17	Co1	C28	C27	–86.1(5)
C17	Co1	C28	C29	154.4(5)
C18	Co1	C28	C27	–135.5(5)
C18	Co1	C28	C29	105.0(5)
C25	Co1	C28	C27	81.5(5)
C25	Co1	C28	C29	–38.0(5)
C26	Co1	C28	C27	38.7(4)
C26	Co1	C28	C29	–80.9(5)
C27	Co1	C28	C29	–119.5(7)
C29	Co1	C28	C27	119.5(7)
C5	Co1	C29	C25	95.3(5)
C5	Co1	C29	C28	–146.1(5)
C6	Co1	C29	C25	57.6(9)
C6	Co1	C29	C28	176.2(6)
C17	Co1	C29	C25	179.7(7)
C17	Co1	C29	C28	–61.7(9)
C18	Co1	C29	C25	143.7(4)
C18	Co1	C29	C28	–97.7(5)
C25	Co1	C29	C28	118.6(7)
C26	Co1	C29	C25	–37.3(4)
C26	Co1	C29	C28	81.3(5)
C27	Co1	C29	C25	–81.7(5)
C27	Co1	C29	C28	36.9(5)
C28	Co1	C29	C25	–118.6(7)
C19	Si1	C2	C1	–14.4(8)
C19	Si1	C2	C3	166.3(7)

C20	Si1	C2	C1	–130.7(7)
C20	Si1	C2	C3	50.0(8)
C21	Si1	C2	C1	105.7(7)
C21	Si1	C2	C3	–73.6(7)
C22	Si2	C3	C2	–85.2(7)
C22	Si2	C3	C4	90.8(6)
C23	Si2	C3	C2	158.7(7)
C23	Si2	C3	C4	–25.3(7)
C24	Si2	C3	C2	41.0(8)
C24	Si2	C3	C4	–143.1(6)
C18	C1	C2	Si1	179.5(6)
C18	C1	C2	C3	–1(1)
C2	C1	C18	Co1	–81.7(9)
C2	C1	C18	C5	1(1)
C2	C1	C18	C17	173(1)
Si1	C2	C3	Si2	–5(1)
Si1	C2	C3	C4	179.0(5)
C1	C2	C3	Si2	175.5(6)
C1	C2	C3	C4	–0(1)
Si2	C3	C4	C5	–174.7(5)
C2	C3	C4	C5	2(1)
C3	C4	C5	Co1	82.2(8)
C3	C4	C5	C6	–174(1)
C3	C4	C5	C18	–2(1)
Co1	C5	C6	C7	128(1)
Co1	C5	C6	C17	–67.4(4)
C4	C5	C6	Co1	–120(1)
C4	C5	C6	C7	8(2)
C4	C5	C6	C17	173(1)
C18	C5	C6	Co1	67.1(4)
C18	C5	C6	C7	–165(1)
C18	C5	C6	C17	–0.3(6)
Co1	C5	C18	C1	–117.5(7)
Co1	C5	C18	C17	66.7(4)
C4	C5	C18	Co1	117.9(7)
C4	C5	C18	C1	0(1)
C4	C5	C18	C17	–175.4(7)
C6	C5	C18	Co1	–66.3(4)
C6	C5	C18	C1	176.2(7)
C6	C5	C18	C17	0.4(6)
Co1	C6	C7	C8	–88.7(8)
C5	C6	C7	C8	160(1)
C17	C6	C7	C8	–2(1)
Co1	C6	C17	C16	124.3(7)
Co1	C6	C17	C18	–67.2(4)
C5	C6	C17	Co1	67.5(4)

C5	C6	C17	C16	–168.1(7)
C5	C6	C17	C18	0.3(5)
C7	C6	C17	Co1	–122.3(7)
C7	C6	C17	C16	2(1)
C7	C6	C17	C18	170.5(7)
C6	C7	C8	C9	–180(1)
C6	C7	C8	C15	2(1)
C7	C8	C9	C10	2(2)
C7	C8	C9	C14	–179(1)
C15	C8	C9	C10	–179(1)
C15	C8	C9	C14	0.1(6)
C7	C8	C15	C14	179.1(7)
C7	C8	C15	C16	–2(1)
C9	C8	C15	C14	–0.1(5)
C9	C8	C15	C16	179.2(8)
C8	C9	C10	C11	–180(1)
C14	C9	C10	C11	1(1)
C8	C9	C14	C13	179.1(7)
C8	C9	C14	C15	–0.1(6)
C10	C9	C14	C13	–1(1)
C10	C9	C14	C15	179.6(7)
C9	C10	C11	C12	–1(1)
C10	C11	C12	C13	1(1)
C11	C12	C13	C14	–2(1)
C12	C13	C14	C9	2(1)
C12	C13	C14	C15	–180(1)
C9	C14	C15	C8	0.1(6)
C9	C14	C15	C16	–179(1)
C13	C14	C15	C8	–179(1)
C13	C14	C15	C16	2(2)
C8	C15	C16	C17	1(1)
C14	C15	C16	C17	–180(1)
C15	C16	C17	Co1	85.8(8)
C15	C16	C17	C6	–2(1)
C15	C16	C17	C18	–161(1)
Co1	C17	C18	C1	120(1)
Co1	C17	C18	C5	–66.9(4)
C6	C17	C18	Co1	66.6(4)
C6	C17	C18	C1	–173(1)
C6	C17	C18	C5	–0.3(5)
C16	C17	C18	Co1	–131(1)
C16	C17	C18	C1	–11(2)
C16	C17	C18	C5	162(1)
Co1	C25	C26	C27	58.6(5)
C29	C25	C26	Co1	–58.3(5)
C29	C25	C26	C27	0.3(9)

Co1	C25	C29	C28	–59.8(6)
C26	C25	C29	Co1	58.8(5)
C26	C25	C29	C28	–1.0(9)
Co1	C26	C27	C28	60.7(5)
C25	C26	C27	Co1	–60.2(5)
C25	C26	C27	C28	0.5(9)
Co1	C27	C28	C29	59.5(6)
C26	C27	C28	Co1	–60.7(5)
C26	C27	C28	C29	–1.2(9)
Co1	C28	C29	C25	60.9(6)
C27	C28	C29	Co1	–59.5(6)
C27	C28	C29	C25	1.4(9)

Photo-thermal cycle between **52** and **53**:

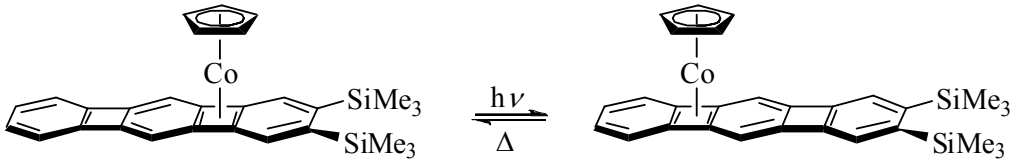

52 **53**

An NMR tube containing a solution of **52** was placed in a Rayonet photochemical reactor fitted with an equal number each of 350 and 300 nm lamps and irradiated up to 10 h to reach the photostationary state. **53**: ^{1}H-NMR (300 MHz, C_6D_6): δ = 7.47 (s, 2 H), 7.24 (AA'm, 2 H), 6.83 (s, 2 H), 6.62 (BB'm, 2 H), 4.44 (s, 5 H), 0.32 (s, 18 H) ppm; ^{13}C-NMR (100 MHz, C_6D_6): δ = 149.3, 148.2, 143.0, 127.6, 125.6, 124.1, 115.5, 80.3, 79.6, 72.5, 2.22 ppm. Thermal reversal could be conveniently followed by VT-NMR.

Kinetic studies of the thermal CoCp migration in **53**:

In the glovebox, 2,3-[bis(trimethylsilyl)] linear[3]phenylene(CpCo) **52**, dissolved in the solvent of choice (C_6D_6 or toluene-d_8), was passed through an HPLC filter and then transfered via syringe into a thick-walled NMR tube connected to a vacuum line adapter. The sample was then degassed by three freeze-pump-thaw cycles and flame-sealed under vacuum. Prior to the kinetic runs, the mixtures were irradiated for 10 h in a Rayonet Photochemical Reactor fitted with lamps emitting at 310 and 365 nm. After this treatment, care was taken to exclude ambient light, as it causes some isomerization. The irradiated samples were then placed in the NMR spectrometer at –65 °C (500 MHz), which was then warmed to the required temperature. In the case of the 60 °C runs, the magnet was prewarmed because of the fast reaction rate at this temperature. After five min, the spectra were recorded. The Cp signal of the photoisomer was integrated relative to the solvent peak of C_6D_6 or the CD_3 peak of toluene-d_8 and monitored as a function of time. The integral from the first scan was used as $[A]_o$. Since the equilibrium constant between the isomers was 50, the kinetic analysis treated the isomerization as a first-order, non-reversible process. Plotting the data accordingly

yielded the reaction rate constants, which were used in the Eyring plots to obtain the activation parameters.

Kinetic studies of the thermal haptotropic shift for complex **52**:

Kinetic runs were executed in C_6D_6 as the optimum solvent. A sample of **52** in degassed C_6D_6 or toluene-d_8 was subjected to UV light for 10 h, leading to maximum enrichment of **53**. The sample was kept at the specified temperature and the disappearance of **53** monitored by ^{1}H-NMR spectroscopy. The reaction proved to be first-order (eq 1) consistent with an intramolecular process.

$$\frac{d[A]}{dt} = -k[A] \qquad (1)$$

$$-\frac{d[A]}{[A]} = k\,dt \qquad (2)$$

$$-\ln\frac{[A]}{[A]_0} = k\,t \qquad (3)$$

The rate constant (k) at 30, 40, 50, and 60 °C was obtained from the slope of a plot of $-\ln([A]/[A]_0)$ versus time (t) following eq 2 and 3. The actual error in reproducibility was estimated by the calculation of one standard deviation (σ) for a triplicate run at 60 °C. The percentage error was applied for k at 30, 40 and 50 °C. The rate constants and their errors are given in Tables 4.11 and 4.14. The values for k and their standard deviations were used to calculate the activation enthalpy ($\Delta H^{\ddagger}$) and entropy ($\Delta S^{\ddagger}$) of the haptotropic shift. The basis for these calculations is the Eyring equation (eq 4). This expression (eq 4) was transformed to eq 5 and the activation enthalpy ($\Delta H^{\ddagger}$) obtained from the slope of a plot of $-\ln(k/T)$ versus 1/RT. The intercept (–C) provides the activation entropy ($\Delta S^{\ddagger}$) following eq 6 and 7.

$$-\ln\frac{k}{T} = \frac{\Delta H^{\neq}}{RT} - \left(\ln\frac{k_B}{h} + \frac{\Delta S^{\neq}}{R}\right)$$

$$= \frac{\Delta H^{\neq}}{RT} - C \qquad (4)$$

$$C = \ln\frac{k_B}{h} + \frac{\Delta S^{\neq}}{R} \qquad (5)$$

$$\Delta S^{\neq} = R\left(C - \ln\frac{k_B}{h}\right) \qquad (6)$$

The errors in $\Delta H^{\ddagger}$ and $\Delta S^{\ddagger}$ were calculated based on those in the rate constants, leading to two additional least square fits in the Eyring plot. These fits represent the two most extreme deviations from the original plot. This provides a conservative error estimate and finally the values of 20.4±1.4 kcal/mol for $\Delta H^{\ddagger}$ and 15.8±2.2 eu (cal/mol·K) for $\Delta S^{\ddagger}$ in C_6D_6. In order to probe for solvent effects, the kinetics were also repeated in toluene-d_8. The preparation of the sample followed the described procedure and the rate constants (k) were obtained at 30, 40, 50, and 60 °C. At 60 °C, three measurements were carried out to estimate the errors in reproducibility for k and the activation parameters. Error propagation was done as described for the kinetic experiments in C_6D_6. It is assumed that those rate constants (k) show the same relative error as the ones for the rearrangement of **53** to **52** in C_6D_6. The activation parameters in toluene-d_8 were found to be 23.1±0.7 kcal/mol and 6.0±1.3 eu.

Table 4.10. Kinetic Data for the Conversion of **53** to **52** in C_6D_6

303.15 K		
Time (s)	**Rel. Conc.**	**$-\ln[A/A_o]$**
0	1.0000	0.0000
3000	0.9657	0.0349
6000	0.9380	0.0640
9000	0.9038	0.1012
12000	0.8760	0.1324
15000	0.8418	0.1723
18000	0.8206	0.1978
21000	0.8010	0.2219

313.15 K		
Time (s)	**Rel. Conc.**	**$-\ln[A/A_o]$**
0	1.0000	0.0000
1000	0.9419	0.0599
2000	0.9018	0.1034
3000	0.8557	0.1558
4000	0.8176	0.2013
5000	0.7796	0.2490
6000	0.7555	0.2804
7000	0.7255	0.3210

	323.15 K	
Time (s)	**Rel. Conc.**	**$-\ln[A/A_o]$**
0	1.0000	0.0000
400	0.9541	0.0470
800	0.9197	0.0837
1200	0.8910	0.1154
1600	0.8489	0.1638
2000	0.8298	0.1865
2400	0.7954	0.2289
2800	0.7591	0.2756

	333.15 K (1)	
Time (s)	**Rel. Conc.**	**$-\ln[A/A_o]$**
0	1.0000	0.0000
30	0.9888	0.0113
60	0.9820	0.0181
90	0.9708	0.0296
120	0.9596	0.0413
150	0.9506	0.0507
180	0.9416	0.0602
210	0.9348	0.0674
240	0.9281	0.0746
270	0.9213	0.0819
300	0.9124	0.0917
330	0.9034	0.1016
360	0.8966	0.1091

	333.15 K (2)	
Time (s)	**Rel. Conc.**	**$-\ln[A/A_o]$**

	333.15 K (3)	
Time (s)	**Rel. Conc.**	**$-\ln[A/A_o]$**

0	1.0000	0.0000
30	0.9950	0.0050
60	0.9900	0.0101
90	0.9800	0.0202
120	0.9750	0.0253
150	0.9700	0.0305
180	0.9625	0.0382
210	0.9575	0.0434
240	0.9475	0.0539
270	0.9400	0.0619
300	0.9350	0.0672
330	0.9300	0.0726
360	0.9250	0.0780

0	1.0000	0.0000
30	0.9909	0.0092
60	0.9854	0.0147
90	0.9762	0.0241
120	0.9671	0.0335
150	0.9634	0.0372
180	0.9543	0.0468
210	0.9433	0.0583
240	0.9397	0.0622
270	0.9287	0.0740
300	0.9232	0.0799
330	0.9177	0.0858
360	0.9086	0.0959

Table 4.11. The Rate Constants (k) in C_6D_6 Calculated From the Data in Table 4.10 and Their Standard Deviations (σ)

Temp (K)	***k* (1/s)**	**σ of *k* (1/s)**	**R^2**	**–ln(*k*/T)**	**σ of –ln(*k*/T)**
303.15	1.0809E–05	7.4258E–07	0.9970	17.1494	0.0688
313.15	4.5615E–05	3.1338E–06	0.9948	15.7420	0.0688
323.15	9.5118E–05	6.5346E–06	0.9965	15.0385	0.0688
333.15 (1)	2.7425E–04		0.9965		
333.15 (2)	2.5714E–04		0.9964		
333.15 (3)	3.0051E–04		0.9990		
333.15 (avg.)	2.6511E–04	1.8841E–05		14.0101	0.0688

Table 4.12. Activation Parameters for the Kinetic Experiments in C_6D_6

	Positive Deviation		**Negative Deviation**
Slope of Eyring Plot	90990	85414	79291
Intercept	–17.89	–16.74	–15.59
R^2	0.9869	0.9869	0.9869
$\Delta H^{\ddagger}$ (J/mol)	90990	85414	79291
$\Delta H^{\ddagger}$ (kcal/mol)	21.7	20.4	19.0
$\Delta S^{\ddagger}$ (J/mol·K)	–56.9	–66.0	–75.1
$\Delta S^{\ddagger}$ (eu)	–13.6	–15.8	–18.0

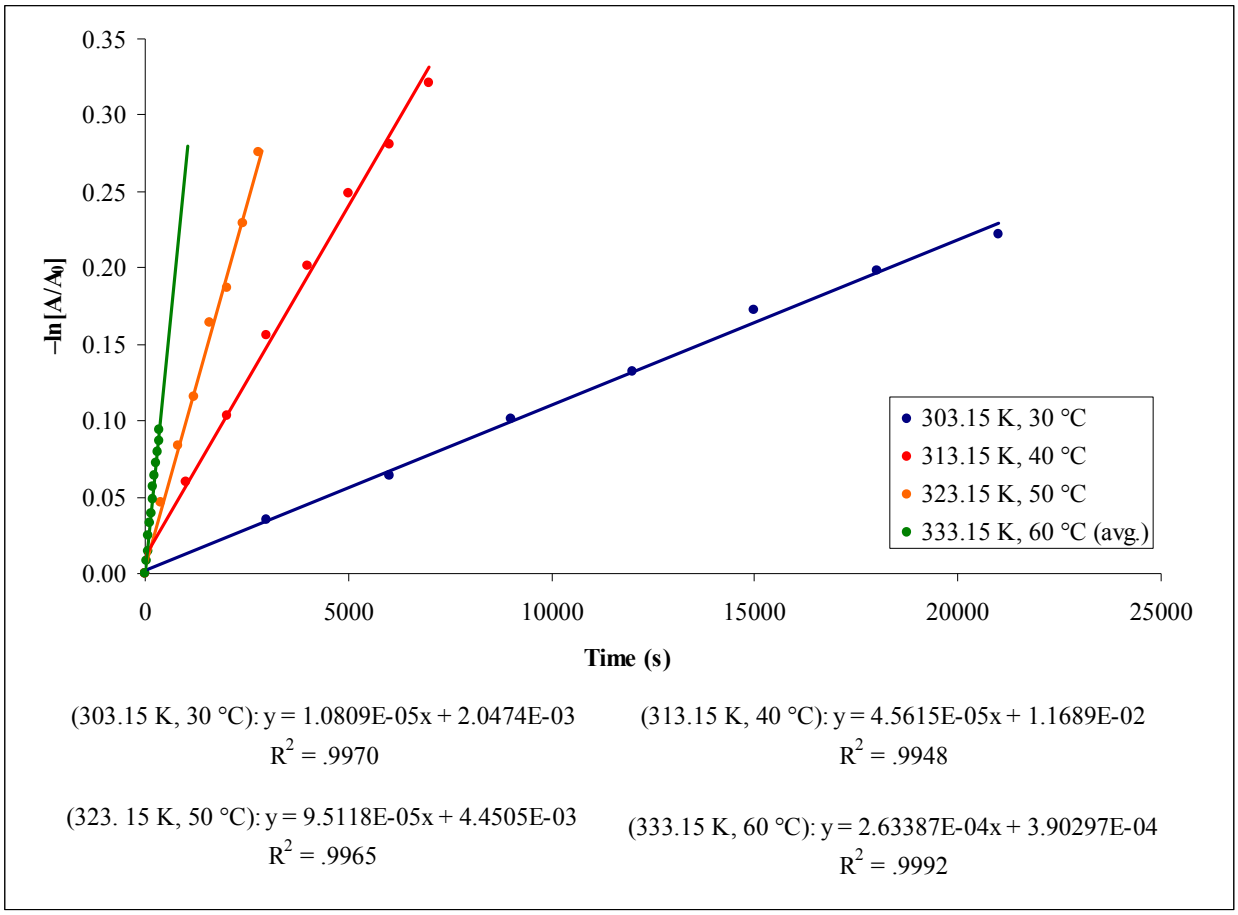

Figure 4.3. Kinetic plots for the conversion of **53** to **52** in C_6D_6.

Table 4.13. Kinetic Data for the Conversion of **53** to **52** in Toluene-d_8

303.15 K		
Time (s)	**Rel. Conc.**	**$-\ln[A/A_o]$**
0	1.0000	0.0000
3000	0.9556	0.0454
6000	0.9256	0.0773
9000	0.8956	0.1103
12000	0.8667	0.1430
15000	0.8343	0.1811
18000	0.8103	0.2103
21000	0.7863	0.2404

313.15 K		
Time (s)	**Rel. Conc.**	**$-\ln[A/A_o]$**
0	1.0000	0.0000
1000	0.9488	0.0526
2000	0.8931	0.1130
3000	0.8545	0.1572
4000	0.8143	0.2054
5000	0.7818	0.2461
6000	0.7559	0.2798
7000	0.7179	0.3314

	323.15 K	
Time (s)	**Rel. Conc.**	**$-\ln[A/A_o]$**
0.00	1.0000	0.0000
400.00	0.9470	0.0544
800.00	0.8934	0.1127
1200.00	0.8594	0.1515
1600.00	0.8175	0.2015
2000.00	0.7861	0.2406
2400.00	0.7502	0.2875
2800.00	0.6991	0.3579

	333.15 K (1)	
Time (s)	**Rel. Conc.**	**$-\ln[A/A_o]$**
0	1.0000	0.0000
30	0.9887	0.0113
60	0.9775	0.0228
90	0.9691	0.0314
120	0.9592	0.0416
150	0.9473	0.0542
180	0.9381	0.0639
210	0.9262	0.0767
240	0.9149	0.0889
270	0.9086	0.0959
300	0.8973	0.1083
330	0.8868	0.1202
360	0.8762	0.1321

	333.15 K (2)	
Time (s)	**Rel. Conc.**	**$-\ln[A/A_o]$**
0	1.0000	0.0000
30	0.9945	0.0055
60	0.9795	0.0207
90	0.9700	0.0304
120	0.9645	0.0361
150	0.9479	0.0535
180	0.9464	0.0551
210	0.9314	0.0711
240	0.9188	0.0847
270	0.9101	0.0942
300	0.8991	0.1064
330	0.8896	0.1170
360	0.8801	0.1277

	333.15 K (3)	
Time (s)	**Rel. Conc.**	**$-\ln[A/A_o]$**
0	1.0000	0.0000
30	0.9910	0.0090
60	0.9828	0.0173
90	0.9716	0.0288
120	0.9559	0.0451
150	0.9440	0.0576
180	0.9313	0.0712
210	0.9238	0.0792
240	0.9156	0.0882
270	0.8992	0.1063
300	0.8932	0.1129
330	0.8872	0.1197
360	0.8686	0.1409

Table 4.14. The Rate Constants (k) in Toluene-d_8 Calculated From the Data in Table 4.13 and Their Standard Deviations (σ)

Temp (K)	***k* (1/s)**	**σ of *k* (1/s)**	**R^2**	**–ln(*k*/T)**	**σ of –ln(*k*/T)**
303.15	1.1314E–05	3.7152E–07	0.9976	17.104	0.5610
313.15	4.6470E–05	1.5251E–06	0.9948	15.723	0.5157
323.15	1.2214E–04	4.01074E–06	0.9957	14.788	0.4851
333.15 (1)	3.6441E–04		0.9992		
333.15 (2)	3.6124E–04		0.9951		
333.15 (3)	3.8855E–04		0.9956		
333.15 (avg.)	3.7140E–04	1.4937E–05		13.707	0.4496

Table 4.15. Activation Parameters for the Kinetic Experiments in Toluene-d_8

	Positive Deviation		**Negative Deviation**
Slope of Eyring Plot	96590	93523	90455
Intercept	–20.73	–20.07	–19.41
R^2	0.9962	0.9962	0.9962
$\Delta H^{\ddagger}$ (J/mol)	96590	93523	90455
$\Delta H^{\ddagger}$ (kcal/mol)	23.09	22.35	21.62
$\Delta S^{\ddagger}$ (J/mol·K)	–25.21	–30.68	–36.15
$\Delta S^{\ddagger}$ (eu)	–6.02	–7.33	–8.64

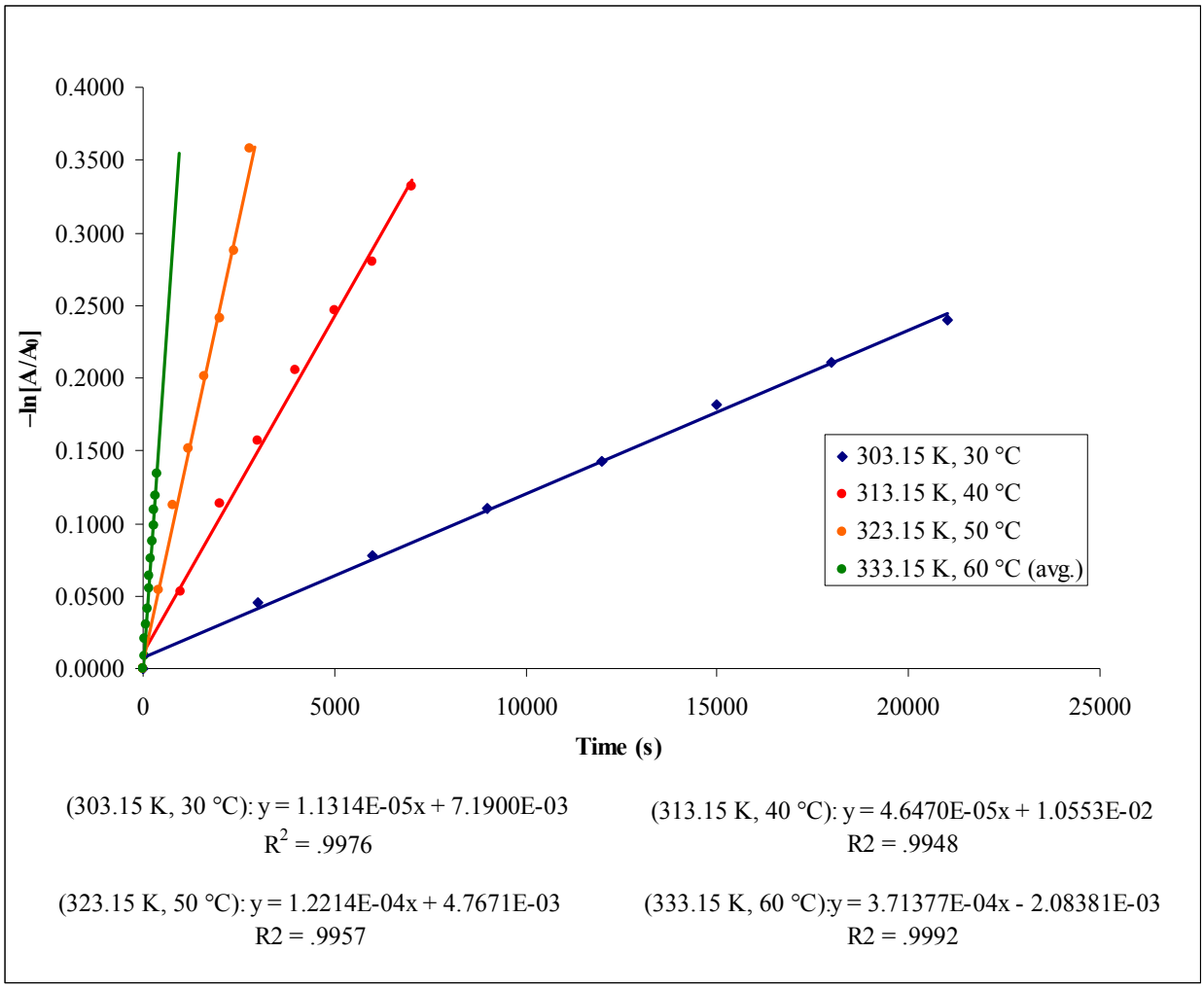

Figure 4.4. Kinetic plots for the conversion of **53** to **52** in toluene-d_8.

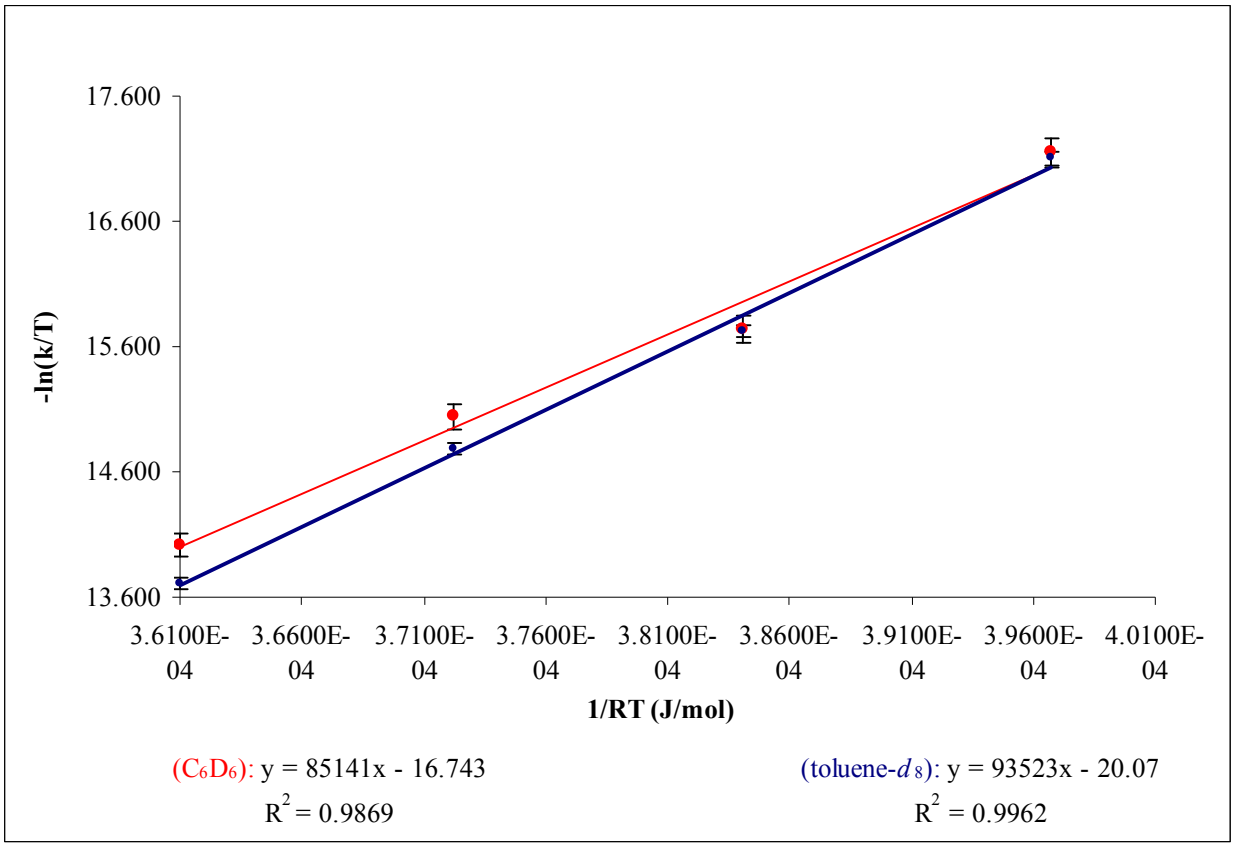

Figure 4.5. Eyring plots for conversion of **53** to **52**.

MeCpCo(CO)$_2$:

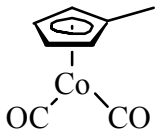

Adapted from the literature procedure.[50] $Co_2(CO)_8$ (8.09 g, 23.66 mmol) was added to a round bottom flask in the glovebox. The flask was capped with a septum and brought out of the glovebox. A reflux condenser connected to the high vacuum line was quickly exchanged with the septum under a heavy purge of argon. Degassed CH_2Cl_2 (30 mL) was added, followed by freshly cracked, deoxygenated methylcyclopentadiene (13.5 mL, 123 mmol). The mixture evolved gas upon addition of the methylcyclopentadiene, indicating CO liberation. The entire setup was protected from light with foil and heated to a gentle reflux using a heating mantle/variac heat source. After stirring at reflux for 26 h, the mixture, now dark crimson in color, was cooled to rt. The reflux condenser was quickly exchanged for a distillation head under an Ar purge and CH_2Cl_2 distilled off at atmospheric pressure under Ar. Vacuum distillation at 0.02 Torr was performed and the forerun discarded. The desired complex was obtained as a red liquid (7.296 g, 79%), b.p. = 31 °C (0.02 Torr), stored at –10 °C and shielded from light. Note: A small

amount of methylcyclopentadiene dimer (15 %), which could not be separated, was present in the isolated product. This was deemed harmless, however, and the obtained product was used in further experiments without further purification, 85% pure. ^{1}H-NMR data match those reported in the literature. ^{1}H-NMR (C_6D_6): δ = 1.45 (s, 3 H), 4.31 (br s, 2 H), 4.51 (br s, 2 H).

2,3-Bis(trimethylsilyl) linear [3]phenylene(MeCpCo) **54**:

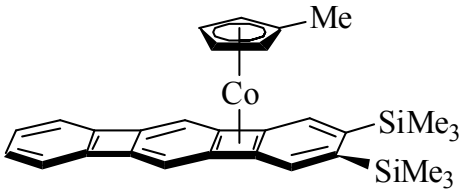

To a Schlenk flask containing a solution of 2,3-bis(trimethylsilylethynyl)biphenylene **51** (0.146 g, 0.424 mmol) in ether (20 mL) and CH_3OH (10 mL) was added K_2CO_3 (0.101 g, 0.731 mmol). The mixture was stirred for 100 min and monitored via TLC, eluting with hexane/CH_2Cl_2 (5:1). After the starting material had been consumed, the solvents were removed and the remaining yellow residue was dissolved in freshly distilled THF (15 mL). The green solution was separated from the solids via canula filtration and transferred into another Schlenk flask. After a 20 min Ar purge, $MeCpCo(CO)_2$ (0.092 g, 0.403 mmol) was added and the resulting solution (protected from light with foil) injected via syringe pump over 9 h into a boiling mixture of THF (100 mL) and BTMSA (25 mL), which was irradiated by a slide projection lamp. Heating and irradiation were continued for another 15 h. The solvents were removed by vacuum transfer and the remaining black residue filtered through a plug of neutral alumina, activity III (3.5 x 3.5 cm), eluting with a degassed mixture of hexane/THF (20:1). The volatiles were again removed under high vacuum line and the residue crystallized from acetone yielding **55** (0.125 g, 61 %) as black crystals, m.p. 163–165 °C; ^{1}H-NMR (500 MHz, C_6D_6): δ = 7.83 (s, 2 H), 6.76 (m, 4 H), 6.75 (s, 2 H), 4.42 (apparent t, J = 2.1 Hz, 2 H), 4.27 (apparent t, J = 2.1 Hz, 2 H), 1.34 (s, 3 H), 0.38 (s, 18 H) ppm; ^{13}C-NMR (125 MHz, C_6D_6): δ = 150.2, 142.3, 138.6, 135.4, 129.3, 119.3, 114.7, 89.9, 80.6, 79.8, 78.3, 73.9, 11.1, 2.79 ppm; IR (neat) $\tilde{\nu}$ = 2959, 2923, 2853, 1462, 1455, 1378, 1260, 1093, 1030, 802 cm^{-1}; UV-VIS (hexane): λ_{max} (log ε) = 256 (3.68), 281 (3.56), 293 (3.59), 310 (3.73), 350 (3.68), 386 (sh, 3.21), 437 (sh, 2.87), 499 (sh, 2.47), end absorption to 550 nm; MS (70 eV): m/z (%): 508 (100) [M^+], 370 (28); HRMS (FAB): calcd for $C_{30}H_{33}CoSi_2$: 508.1453; found: 508.1442.

Photo-thermal cycle between **54** and **56**:

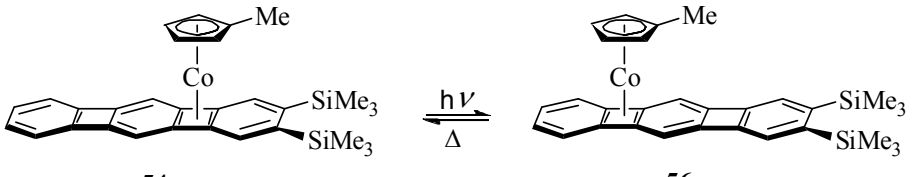

54 **56**

An NMR tube containing a solution of **54** was placed in a Rayonet photochemical reactor fitted with an equal number each of 350 and 300 nm lamps and irradiated up to 10 h to reach the photostationary state. **56**: ^{1}H-NMR (300 MHz, C_6D_6): δ = 7.47 (s, 2 H), 7.15 (AA'm, obscured by solvent peak), 6.80 (s, 2 H), 6.64 (AA'm, 2 H), 4.47 (apparent t, J = 2.1 Hz, 2 H), 4.28 (apparent t, J = 2.1 Hz, 2 H), 1.48 (s, 3 H), 0.32 (s, 18 H) ppm. Thermal reversal could be conveniently followed by VT-NMR.

1,4-Deuterio-2,3-bis(trimethylsilyl) linear [3]phenylene cyclopentadienylcobalt **55**:

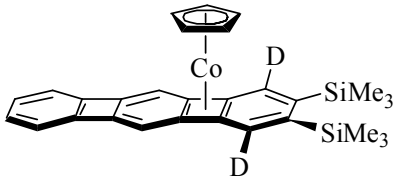

To 2,3-bis(trimethylsilylethynyl)biphenylene **52** (0.144 g, 0.418 mmol) in CH_3OD (10 mL) was added freshly distilled ether (20 mL) and K_2CO_3 (0.083 g, 0.600 mmol). The mixture was stirred for 100 min and monitored by TLC (hexane/CH_2Cl_2, 5:1). When the starting material had disappeared, the solvents were removed and the remaining yellow residue very quickly dissolved in freshly distilled THF (10 mL). The green solution was separated from the solids using a filter cannula and transferred to another Schlenk flask. After a 20 min Ar purge, $CpCo(CO)_2$ (0.072 g, 0.400 mmol) was added and the resulting solution (protected from light with foil) was injected via syringe pump over 7 h into a refluxing mixture of THF (100 mL) and BTMSA (25 mL), which was irradiated by a slide projection lamp. Heating and irradiation were continued for another 14 h. The solvents were removed by vacuum transfer and the remaining black residue filtered through a plug of neutral alumina, activity III (3.5 x 3.5 cm), eluting with a degassed mixture of hexane/THF (10:1). The solvents were removed on the high vacuum line and the residue recrystallized from acetone yielding **8** (0.085 g, 41 %) as dark red crystals; ^{1}H-NMR spectroscopy showed 63 % incorporation of deuterium, as indicated by the diminution of the peak intensity of the signal at δ = 7.96 (s, 0.74 H) ppm. MS (FAB): m/z (%): 496 (100), [M^+], 372 (19).

Crossover experiment with **54** and **55**:

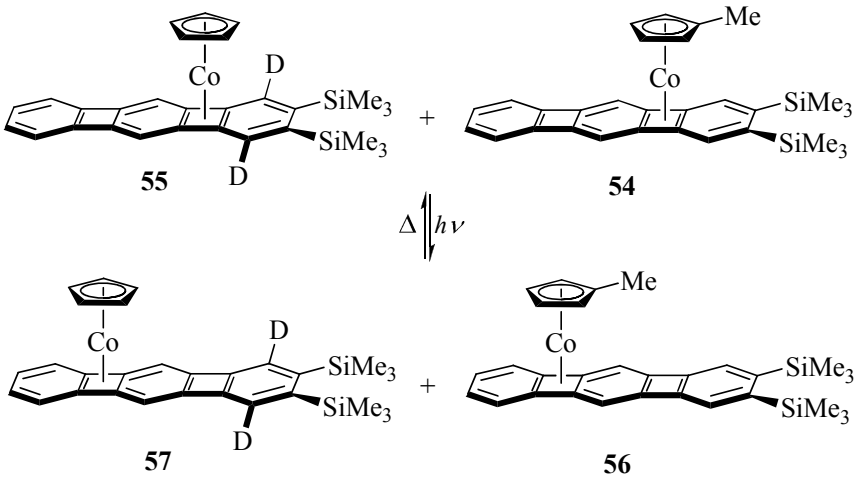

A solution of complex **55** (~2 mg) and **54** (~2 mg) in C_6D_6 (0.6 mL), rigorously protected from light, was analyzed by ^{1}H-NMR spectroscopy to reveal a 1.86:1 mixture of **55**:**54**. The peak for **55** at δ = 7.96 (s, 0.74 H) ppm exhibited the expected integration relative to the other hydrogens in this compound. A mass spectrum of an aliquot gave the appropriate composite of the two respective molecular ion patterns (Figure 4.6). The sample was then irradiated as described for above 13 h at RT. The ^{1}H-NMR spectrum of the irradiated mixture showed the presence of the respective photoisomers of **55** and **54**. There were no unidentifiable peaks, the signal at δ = 7.470 (s, 0.74 H) ppm exhibited the expected integration relative to the other hydrogens in this compound, and the clearly resolved peak for **56** at δ = 7.473 (s, 2 H) ppm revealed unattenuated intensity. An aliquot was submitted for mass spectral analysis, furnishing the same pattern as that depicted above. The sample was then placed in an oil bath preheated to 80 °C for 30 h, a treatment that regenerated the original NMR spectrum of the mixture of **55** and **54**, including the relative integration ratios. Similarly, mass spectral analysis resulted in the same pattern as that depicted in Figure 4.6.

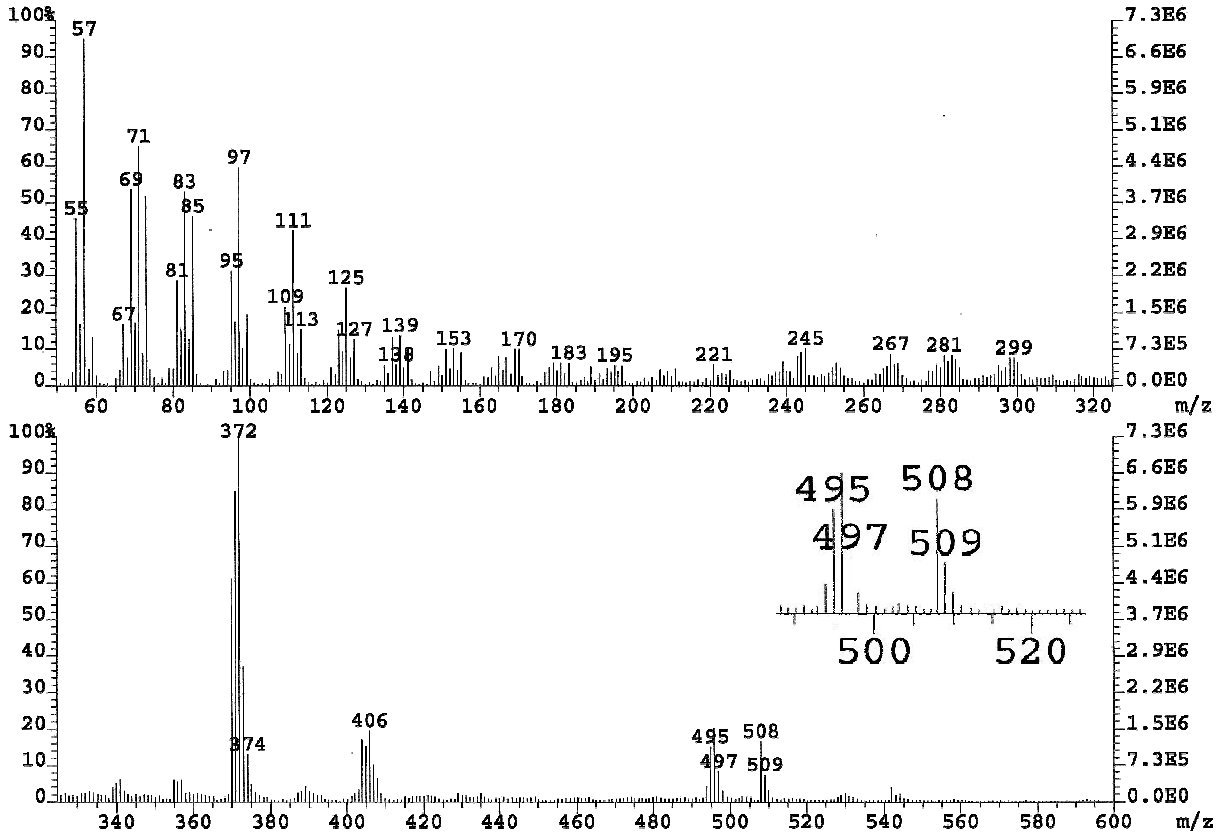

Figure 4.6. Mass spectrum from the crossover experiment between **55** and **56**.

Low temperature photolyses of **19** and **52**:

A small amount (~5 mg) of linear[3]phenylene(CpCo) **19** or **52**, dissolved in toluene-d_8, was added to a J-Young NMR tube in the glovebox. The sealed sample was then placed inside a Pyrex Dewar flask positioned in a Rayonet Photochemical Reactor outfitted with UV-lamps emitting at 310 and 350 nm (as shown in Figure 2.14). Cooling was achieved with the use of a Neslab Refrigerated Circulating bath employing isopropanol as the cooling medium. The cold isopropanol was pumped into and out of the Pyrex Dewar using securely fastened Tygon tubes, maintaining a temperature of –55 to –50 °C. Once the sample was chilled, irradiation was commenced. The total irradiation time varied from 2.5 to 4 h. When analysis was required, the sample was transported in another Dewar flask containing dry ice/isopropanol (–78 °C), while the NMR spectrometer was prepared for the low temperature experiment. The spectrometer was cooled (–80 to –30 °C, depending on the experiment), the sample wiped with a paper towel, placed inside the spinner, and *very quickly* lowered manually with a string into the cold magnet. After allowing time for the temperature to equilibrate (10 min), a spectrum was recorded. For VT experiments, the temperature was slowly

raised from –80 °C in 10 degree increments to 10 °C. Spectra were recorded at each interval. For all other experiments, spectra were recorded at –30 °C.

2,3,7,8-Tetrakis(trimethylsilyl) linear [3]phenylene$(CpCo)_2$ **78**:

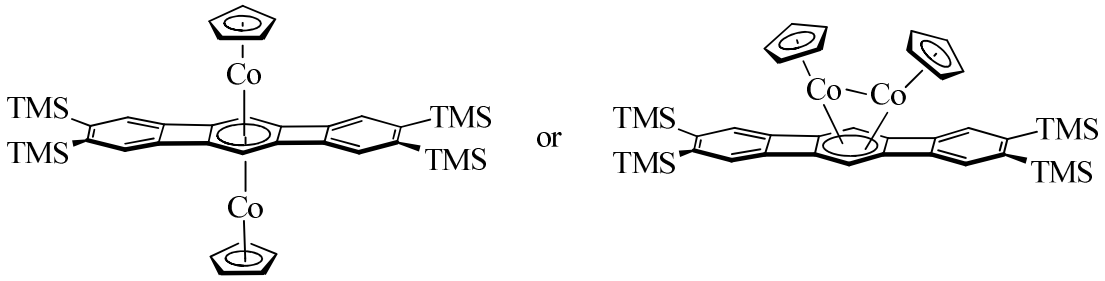

In the glovebox, 2,3,7,8-tetrakis(trimethylsilyl) linear [3]phenylene(CpCo) **19** (0.049 g 0.133 mmol) and $CpCo(C_2H_4)_2$ (0.025 g, 0.139 mmol)[99] were added to a Schlenk flask. The flask was sealed, brought out of the box, connected to a vacuum manifold, and freshly distilled, degassed benzene (15 mL) added. The mixture was heated to 70 °C on an oil bath for 23 h before being cooled to RT. The solvent was removed in vacuo, giving a black residue that was rapidly filtered through a plug of neutral alumina activity III (2.5 x 3.5 cm), eluting with a mixture of hexanes and THF (100:1) under nitrogen and into a Schlenk flask. The solvents were again removed in vacuo and the ensuing black residue recrystallized from acetone at –78 °C to give pure **78** (0.057 g, 56 %) as black crystals; ^{1}H-NMR (400 MHz, acetone-d_6): δ = 0.39 (s, 36H), 4.81 (s, 2H), 4.89 (m, 4H), 7.36 (s, 4H) ppm; ^{13}C-NMR (100 MHz, acetone-d_6): δ = 2.66, 53.72, 57.10, 82.84, 125.87, 145.42, 150.54 ppm; UV-VIS (hexane): λ_{max} (log ε) 197 (3.34), 221 (3.36, sh), 244 (3.44), 286 (3.63), 386 (2.79, sh), 439 (2.58); MS (FAB): 762 (M^+, 100); HRMS: calcd for: $C_{40}H_{52}Si_4Co_2$: 762.1810. found: 762.1791.

4.3 Computational Details for Chapter Two

All calculations were performed using the GAUSSIAN03[100] program. GaussView 3.0[101] and ChemCraft[102] were employed to input structures as well as view output results. Optimized geometries were obtained at the hybrid density functional theory (DFT) using Becke's three-parameter exchange-correlation functional[103] containing the non-local gradient correction of Lee, Yang, and Parr[104] (B3LYP). For optimization purposes, a standard basis 3-21G[105] was used for hydrogen and carbon atoms. For cobalt, the LANL2DZ[106] basis set was applied, with the outermost d function released, yielding a triple-zeta d basis, along with the effective core potentials (ECP) to describe the core electrons. For the single point energy calculations, the basis sets were increased to 6-31G[107] for hydrogen, 6-311G[108] for carbon, and the modified LANL2DZ basis as described above for cobalt with an added f-orbital coefficient.[109]

The potential energy surfaces were mapped through a scan calculation, a feature also available within the GAUSSIAN03 program. Transition state structures were obtained in three different steps: (i) determination of initial and final products or the minimum closest to a TS, (ii) a linear QST2[110] search for an initial guess of a TS; and

(iii) input of the results from (ii) into a QST3 search. Transition states and minima were confirmed by carrying out frequency calculations (using the same basis as that used for the optimizations).

Calculated structures for linear [3]phenylene(CpCo) (labels from Figures 2.9 and 2.10 in Section 2.4):

(a) Global minimum: η^4-cyclobutadiene (0.0 kcal/mol)

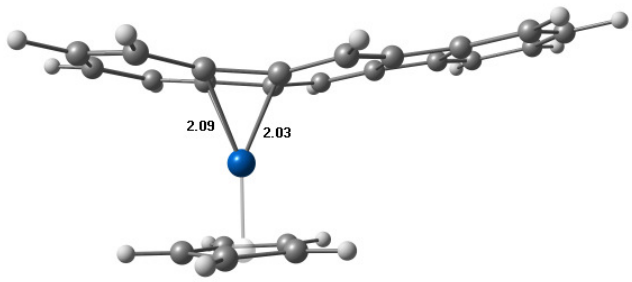

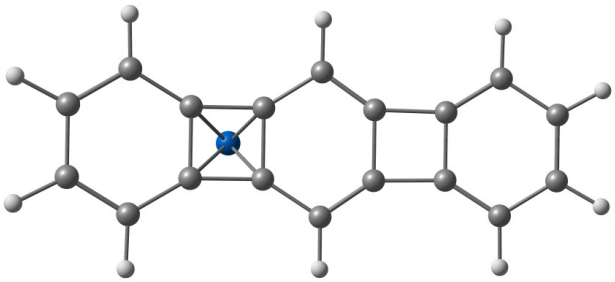

C	2.878616000	–1.675635000	–1.461246000
C	3.986441000	–2.043582000	–0.714088000
C	3.986471000	–2.043226000	0.714700000
C	2.878686000	–1.674908000	1.461732000
C	1.740663000	–1.265994000	0.736724000
C	1.740638000	–1.266353000	–0.736388000
H	2.884721000	–1.731772000	–2.551997000
H	2.884845000	–1.730511000	2.552509000
C	0.311237000	–0.833174000	0.748280000
C	0.311204000	–0.833522000	–0.748106000
C	–0.893980000	–0.698348000	–1.520584000
C	–0.893913000	–0.697588000	1.520749000
C	–1.996288000	–0.532216000	0.744771000
C	–1.996322000	–0.532586000	–0.744640000
C	–3.491040000	–0.328769000	–0.716524000
C	–3.490989000	–0.328300000	0.716632000
C	–4.645388000	–0.172650000	–1.448232000
C	–4.645276000	–0.171672000	1.448326000
C	–5.836534000	–0.014205000	–0.697760000

C	–5.836481000	–0.013731000	0.697841000
H	–0.905006000	–0.741217000	–2.609771000
H	–0.904887000	–0.739873000	2.609960000
H	–4.666353000	–0.168153000	–2.539086000
H	–6.785734000	0.111682000	–1.227959000
H	–6.785641000	0.112502000	1.228028000
H	–4.666162000	–0.166493000	2.539178000
Co	1.455829000	0.662094000	–0.000295000
C	0.672548000	2.613322000	0.000481000
C	1.502831000	2.459745000	1.168426000
C	2.819523000	2.140942000	0.722371000
C	2.818808000	2.141294000	–0.723848000
C	1.501651000	2.460224000	–1.168394000
H	–0.391329000	2.836892000	0.001070000
H	1.172930000	2.540112000	2.200200000
H	3.678957000	1.932268000	1.353707000
H	3.677612000	1.932967000	–1.356152000
H	1.170676000	2.541059000	–2.199789000
H	4.894703000	–2.369906000	1.230670000
H	4.894651000	–2.370516000	–1.229936000

(b) Transition state 1: η^2-cyclobutadiene (26.9 kcal/mol)

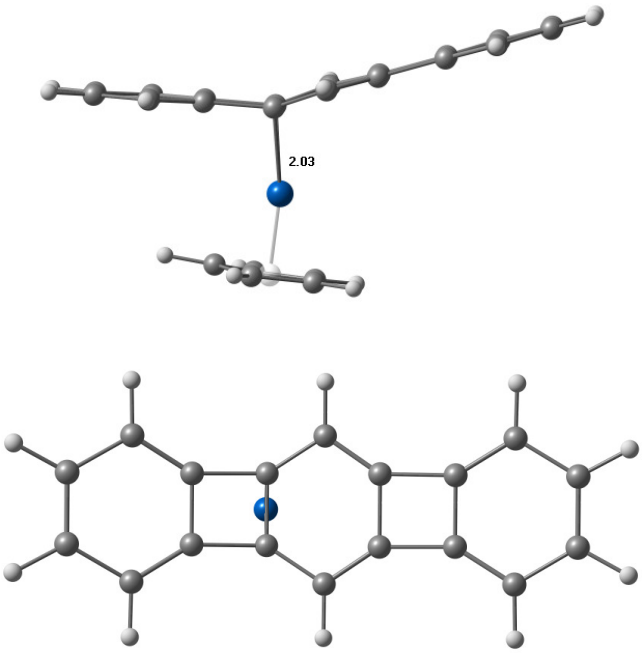

C	–3.991583000	–2.430244000	–0.695300000
C	–2.895249000	–1.923385000	–1.446977000
C	–1.838331000	–1.436925000	–0.718218000
C	–0.460541000	–0.772703000	–0.748934000

C	0.758545000	–0.733408000	–1.513161000
C	1.871918000	–0.586111000	–0.739684000
C	3.374782000	–0.432509000	–0.717168000
C	4.533131000	–0.322603000	–1.448209000
C	5.731498000	–0.208370000	–0.696796000
C	5.731438000	–0.207885000	0.696952000
C	4.533003000	–0.321597000	1.448333000
C	3.374722000	–0.432010000	0.717261000
C	1.871861000	–0.585642000	0.739747000
C	0.758457000	–0.732583000	1.513259000
C	–0.460578000	–0.772439000	0.748991000
C	–1.838348000	–1.436677000	0.718485000
C	–2.895298000	–1.922892000	1.447371000
C	–3.991613000	–2.429987000	0.695830000
H	–4.853881000	–2.841402000	–1.229010000
H	–2.909366000	–1.943431000	–2.538196000
H	0.770744000	–0.814782000	–2.600896000
H	4.554949000	–0.321315000	–2.539049000
H	6.684245000	–0.118682000	–1.227928000
H	6.684140000	–0.117859000	1.228104000
H	4.554722000	–0.319567000	2.539175000
H	0.770611000	–0.813312000	2.601042000
H	–2.909450000	–1.942588000	2.538596000
H	–4.853932000	–2.840954000	1.229654000
Co	–1.032604000	1.030206000	–0.000179000
C	–2.903591000	1.947430000	–0.000175000
C	–2.211742000	2.430689000	–1.177143000
C	–1.026232000	3.056089000	–0.732194000
C	–1.026229000	3.056139000	0.731719000
C	–2.211730000	2.430773000	1.176747000
H	–3.829247000	1.376180000	–0.000150000
H	–2.513347000	2.264399000	–2.207387000
H	–0.243163000	3.477094000	–1.358586000
H	–0.243137000	3.477190000	1.358051000
H	–2.513304000	2.264572000	2.207015000

(c) Local minimum 1: η^4-benzene (10.9 kcal/mol)

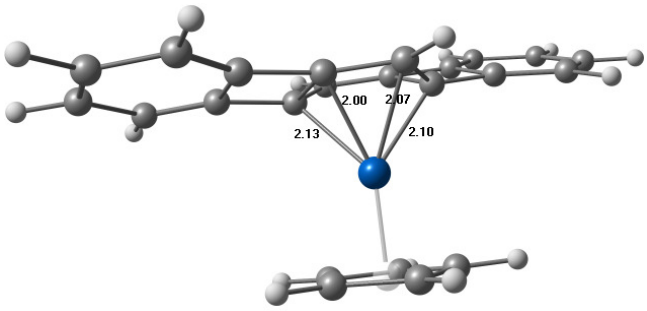

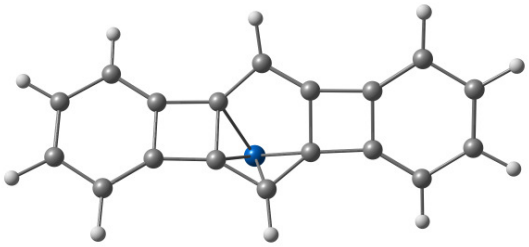

C	4.829664000	–1.220862000	0.883782000
C	3.649435000	–0.895915000	1.609183000
C	2.478533000	–0.900239000	0.886069000
C	0.985532000	–0.699413000	0.895282000
C	–0.207413000	–0.351140000	1.567281000
C	–1.295977000	–0.355264000	0.631690000
C	–2.799524000	–0.368596000	0.647705000
C	–3.950748000	0.104186000	1.252743000
C	–5.173877000	–0.370408000	0.725519000
C	–5.217559000	–1.270006000	–0.351644000
C	–4.043168000	–1.754445000	–0.967619000
C	–2.843350000	–1.293792000	–0.444950000
C	–1.365414000	–1.319830000	–0.538287000
C	–0.225558000	–1.662005000	–1.182029000
C	0.928168000	–1.009692000	–0.554559000
C	2.436156000	–1.209374000	–0.509824000
C	3.575395000	–1.530032000	–1.215144000
C	4.792344000	–1.526592000	–0.477473000
H	5.781080000	–1.237670000	1.406156000
H	3.693287000	–0.679862000	2.671420000
H	–0.279175000	–0.037747000	2.601166000
H	–3.939706000	0.801901000	2.083798000
H	–6.106757000	–0.031072000	1.165263000
H	–6.183419000	–1.601741000	–0.720200000
H	–4.097586000	–2.453276000	–1.795561000
H	–0.137803000	–2.306368000	–2.049380000
H	3.570207000	–1.781979000	–2.270507000
H	5.717527000	–1.774506000	–0.988963000
Co	0.235674000	0.924694000	–0.006080000
C	1.650242000	2.605908000	–0.261710000
C	0.606451000	3.071372000	0.583798000
C	–0.633939000	2.891762000	–0.112192000
C	–0.354070000	2.388098000	–1.431110000
C	1.060641000	2.182627000	–1.507942000
H	2.701380000	2.562827000	–0.018620000
H	0.717262000	3.431891000	1.595877000
H	–1.615358000	3.123686000	0.274491000
H	–1.077256000	2.190401000	–2.207047000

H	1.601331000	1.788686000	–2.355167000

(d) Transition State 2: η^3-benzene (24.9 kcal/mol)

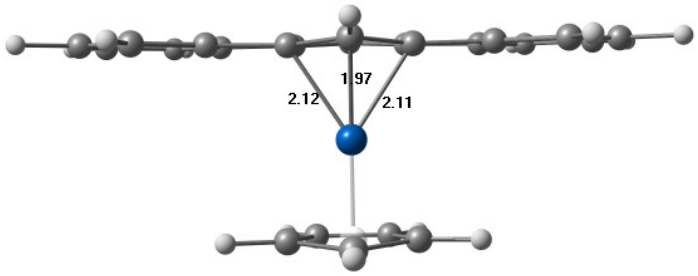

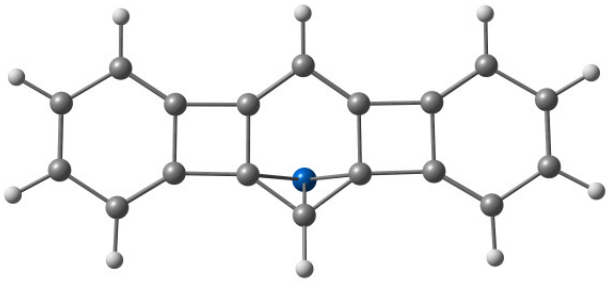

C	5.059641000	–0.675345000	0.741440000
C	3.868057000	–0.242461000	1.393542000
C	2.691208000	–0.611642000	0.796692000
C	1.164924000	–0.568451000	0.814993000
C	0.001006000	–0.193010000	1.575722000
C	–1.162903000	–0.569406000	0.815406000
C	–2.689168000	–0.613549000	0.797134000
C	–3.866228000	–0.245076000	1.394017000
C	–5.057560000	–0.678583000	0.741882000
C	–5.030442000	–1.430649000	–0.426732000
C	–3.802288000	–1.812828000	–1.038342000
C	–2.662603000	–1.392426000	–0.404590000
C	–1.143695000	–1.392940000	–0.383227000
C	0.001354000	–1.885575000	–1.010384000
C	1.146183000	–1.392203000	–0.383465000
C	2.665098000	–1.390792000	–0.404876000
C	3.805017000	–1.810598000	–1.038596000
C	5.032958000	–1.427555000	–0.427087000
H	6.017043000	–0.408623000	1.174840000
H	3.916675000	0.338622000	2.306082000
H	0.001106000	0.141040000	2.603832000
H	–3.915179000	0.335814000	2.306664000
H	–6.015116000	–0.412488000	1.175329000

H	–5.963925000	–1.737868000	–0.883265000
H	–3.794877000	–2.406462000	–1.944276000
H	0.001449000	–2.505619000	–1.894591000
H	3.797948000	–2.404400000	–1.944423000
H	5.966616000	–1.734262000	–0.883606000
Co	–0.000294000	1.006304000	0.016484000
C	1.144150000	2.811021000	–0.317903000
C	–0.001831000	3.236912000	0.413780000
C	–1.150105000	2.808519000	–0.312717000
C	–0.712506000	2.257800000	–1.588662000
C	0.702130000	2.259464000	–1.591918000
H	2.174046000	2.940434000	–0.021226000
H	–0.000096000	3.693787000	1.391408000
H	–2.178919000	2.935539000	–0.011312000
H	–1.360790000	1.903514000	–2.375388000
H	1.347563000	1.907002000	–2.381795000

Calculated structures for linear [5]phenylene CpCo (labels from Figures 2.11 and 2.12 in Section 2.4):

(a) Global minimum: η^4-cyclobutadiene (0.00 kcal/mol)

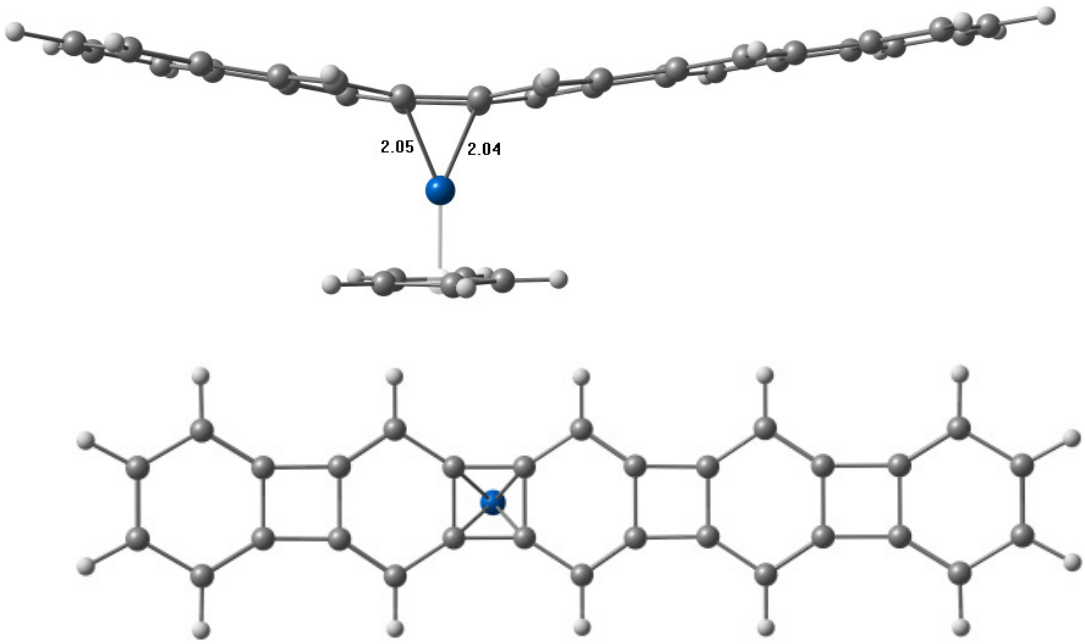

C	–2.147283000	–0.385762000	–0.741520000
C	–2.146881000	–0.382747000	0.740465000
C	–0.675330000	–0.218887000	0.741228000
C	–0.675503000	–0.222208000	–0.743565000
C	0.535474000	–0.309864000	–1.519364000

C	1.654024000	–0.363787000	–0.743565000
C	1.653968000	–0.359108000	0.742223000
C	0.535464000	–0.301263000	1.517648000
C	3.146303000	–0.437352000	0.715394000
C	3.146555000	–0.442081000	–0.715839000
H	0.537903000	–0.329735000	2.601810000
H	0.538062000	–0.344229000	–2.603354000
Co	–1.585768000	1.444604000	–0.004763000
C	–2.656365000	3.118646000	0.813641000
C	–1.264152000	3.247968000	1.115884000
C	–0.546296000	3.292610000	–0.128221000
C	–1.500173000	3.225060000	–1.199322000
C	–2.801883000	3.099872000	–0.616868000
H	–3.459184000	3.033020000	1.530368000
H	–0.824887000	3.279284000	2.101474000
H	0.525240000	3.366953000	–0.237713000
H	–1.272392000	3.239735000	–2.254384000
H	–3.732669000	2.998753000	–1.154572000
C	–3.315848000	–0.698077000	1.516941000
C	–3.316515000	–0.705270000	–1.515890000
C	–4.404590000	–0.970491000	0.742487000
C	–4.404888000	–0.974125000	–0.739677000
H	–3.311463000	–0.745189000	–2.599679000
H	–3.310191000	–0.733014000	2.600900000
C	–5.857232000	–1.346832000	–0.713671000
C	–5.856902000	–1.343302000	0.718959000
C	–6.992149000	–1.638138000	–1.445564000
C	–6.991464000	–1.630979000	1.452826000
C	4.314567000	–0.501395000	–1.493440000
C	4.313844000	–0.491124000	1.494022000
C	–8.157130000	–1.937355000	–0.695553000
C	–8.156796000	–1.933908000	0.704865000
H	–7.013569000	–1.630976000	2.537309000
H	–9.075842000	–2.169721000	1.232475000
H	–9.076411000	–2.175846000	–1.221548000
H	–7.014707000	–1.643790000	–2.530023000
C	5.464859000	–0.553191000	0.719930000
C	5.465218000	–0.558312000	–0.718328000
C	6.977989000	–0.635007000	–0.714777000
C	6.977565000	–0.629511000	0.717833000
H	4.313279000	–0.484164000	2.577745000
H	4.314609000	–0.502067000	–2.577185000
C	8.138196000	–0.684071000	1.451266000
C	8.139115000	–0.695400000	–1.446980000
C	9.348946000	–0.746919000	0.699256000
C	9.349380000	–0.752387000	–0.693700000

H	8.162380000	–0.700716000	–2.531270000
H	8.160717000	–0.680929000	2.535584000
H	10.294800000	–0.791917000	1.230058000
H	10.295576000	–0.801571000	–1.223516000

(b) Transition state 3: η^2-cyclobutadiene (37.0 kcal/mol)

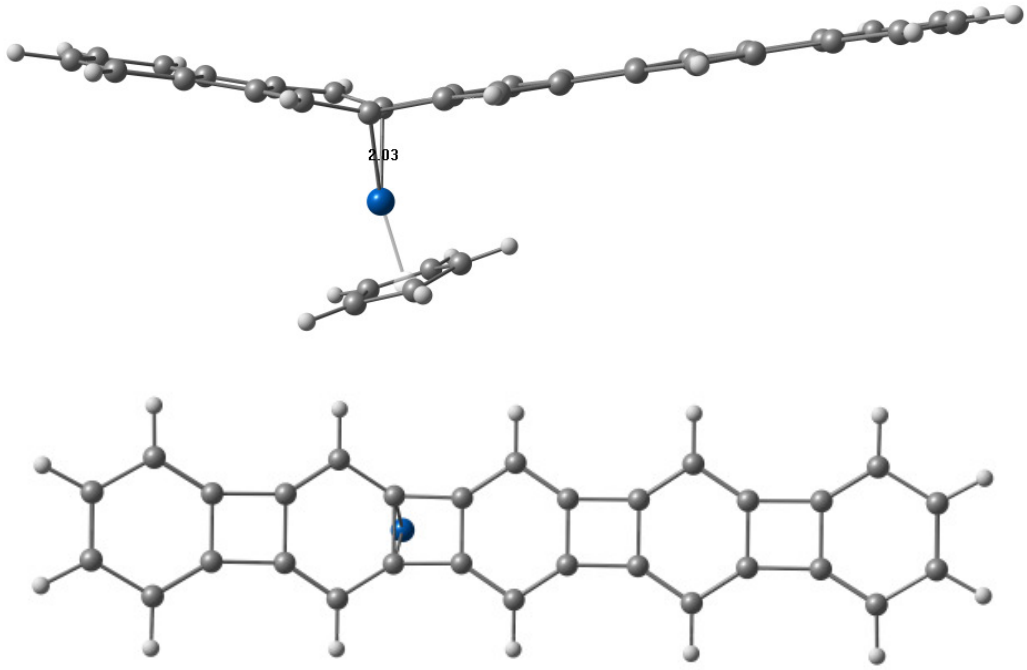

C	–8.026536000	–2.149127000	–0.697047000
C	–6.872771000	–1.801590000	–1.447012000
C	–5.755909000	–1.466198000	–0.717983000
C	–4.305789000	–1.041476000	–0.739357000
C	–3.218268000	–0.750848000	–1.510952000
C	–2.077793000	–0.315087000	–0.749237000
C	–0.550342000	–0.400850000	–0.716361000
C	0.616872000	–0.404801000	–1.489728000
C	1.770640000	–0.412395000	–0.716060000
C	3.300443000	–0.457807000	–0.715861000
C	4.454767000	–0.490291000	–1.489427000
C	5.616257000	–0.520747000	–0.712496000
C	5.616269000	–0.520699000	0.712492000
C	4.454793000	–0.490190000	1.489443000
C	3.300455000	–0.457762000	0.715895000
C	1.770651000	–0.412347000	0.716117000
C	0.616894000	–0.404700000	1.489800000
C	–0.550335000	–0.400796000	0.716454000
C	–2.077818000	–0.315060000	0.749341000
C	–3.218306000	–0.750915000	1.510996000

C	–4.305781000	–1.041534000	0.739359000
C	–5.755900000	–1.466256000	0.717962000
C	–6.872758000	–1.801708000	1.446971000
C	–8.026533000	–2.149171000	0.696987000
H	–6.893447000	–1.807486000	–2.529846000
H	–3.199702000	–0.827686000	–2.591829000
H	0.616147000	–0.415875000	–2.572166000
H	4.455855000	–0.492565000	–2.571217000
H	4.455901000	–0.492389000	2.571233000
H	0.616188000	–0.415693000	2.572238000
H	–3.199790000	–0.827916000	2.591862000
H	–6.893430000	–1.807681000	2.529804000
Co	–2.237895000	1.566525000	–0.000035000
C	–0.770702000	3.039808000	0.000091000
C	–1.582333000	3.276979000	1.176306000
C	–2.906316000	3.484053000	0.731575000
C	–2.906172000	3.484095000	–0.731735000
C	–1.582100000	3.277047000	–1.176233000
H	0.281094000	2.798829000	0.000215000
H	–1.247438000	3.209109000	2.198999000
H	–3.777291000	3.625124000	1.353071000
H	–3.777011000	3.625160000	–1.353424000
H	–1.246943000	3.209260000	–2.198847000
H	–8.933230000	–2.423019000	–1.224452000
H	–8.933222000	–2.423113000	1.224377000
C	7.146943000	–0.559737000	0.717588000
C	7.146931000	–0.559786000	–0.717614000
C	8.302361000	–0.588480000	1.447040000
C	8.302337000	–0.588576000	–1.447082000
C	9.516918000	–0.618789000	–0.692883000
C	9.516929000	–0.618742000	0.692823000
H	8.324450000	–0.589130000	2.529610000
H	10.461320000	–0.642422000	1.224406000
H	10.461300000	–0.642481000	–1.224480000
H	8.324409000	–0.589299000	–2.529653000

(c) Local minimum 2: η^4-benzene (20.3 kcal/mol)

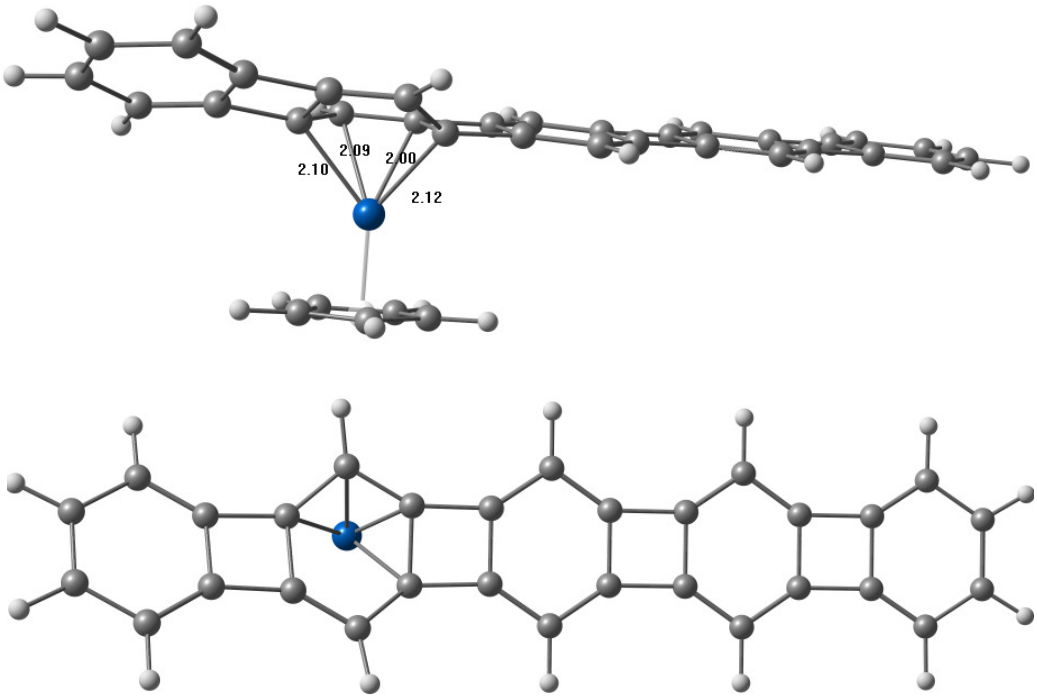

C	–7.810644000	–2.064896000	–0.088979000
C	–6.582065000	–2.396690000	–0.700394000
C	–5.469369000	–1.694626000	–0.259356000
C	–4.011414000	–1.478684000	–0.398743000
C	–2.839913000	–1.679834000	–1.045300000
C	–1.807973000	–0.777407000	–0.523048000
C	–0.288034000	–0.728447000	–0.497727000
C	0.877200000	–0.917515000	–1.257428000
C	2.033335000	–0.625143000	–0.541547000
C	3.550975000	–0.572504000	–0.566638000
C	4.702932000	–0.775398000	–1.323945000
C	5.869717000	–0.493099000	–0.604711000
C	5.877160000	–0.049178000	0.749672000
C	4.719648000	0.152978000	1.509600000
C	3.558389000	–0.127834000	0.791889000
C	2.041313000	–0.178303000	0.818968000
C	0.890228000	0.010834000	1.576182000
C	–0.275189000	–0.290874000	0.857465000
C	–1.777915000	–0.332627000	0.896504000
C	–3.000252000	–0.144927000	1.576583000
C	–4.087655000	–0.414543000	0.681649000
C	–5.565811000	–0.681071000	0.748878000
C	–6.769777000	–0.358061000	1.349731000
C	–7.902756000	–1.078577000	0.906205000
H	–6.531350000	–3.165530000	–1.463988000
H	–2.656944000	–2.379915000	–1.852763000

H	0.873498000	–1.259556000	–2.286041000
H	4.697058000	–1.113491000	–2.353481000
H	4.726794000	0.489146000	2.539724000
H	0.892018000	0.335667000	2.610226000
H	–3.107471000	0.242268000	2.582171000
H	–6.863567000	0.403771000	2.116786000
Co	–2.805901000	1.045228000	–0.126008000
C	–1.966955000	3.131745000	–0.137391000
C	–3.345106000	3.172285000	0.219040000
C	–4.105003000	2.591218000	–0.859559000
C	–3.194452000	2.177424000	–1.877135000
C	–1.861601000	2.475718000	–1.403791000
H	–1.139494000	3.467521000	0.469940000
H	–3.757304000	3.575577000	1.132204000
H	–5.178689000	2.478840000	–0.883920000
H	–3.449207000	1.717975000	–2.819531000
H	–0.944137000	2.267497000	–1.933863000
H	–8.711780000	–2.586977000	–0.395882000
H	–8.871888000	–0.864282000	1.346179000
C	7.394568000	0.005138000	0.727783000
C	7.387058000	–0.441388000	–0.634217000
C	8.557433000	0.273605000	1.404315000
C	8.542647000	–0.629395000	–1.349402000
C	9.760631000	–0.352464000	–0.653366000
C	9.767843000	0.080954000	0.667800000
H	8.586089000	0.612106000	2.434348000
H	10.716375000	0.279405000	1.157078000
H	10.703753000	–0.485281000	–1.174332000
H	8.560430000	–0.966385000	–2.380163000

(d) Transition state 4: η^3-benzene (36.7 kcal/mol)

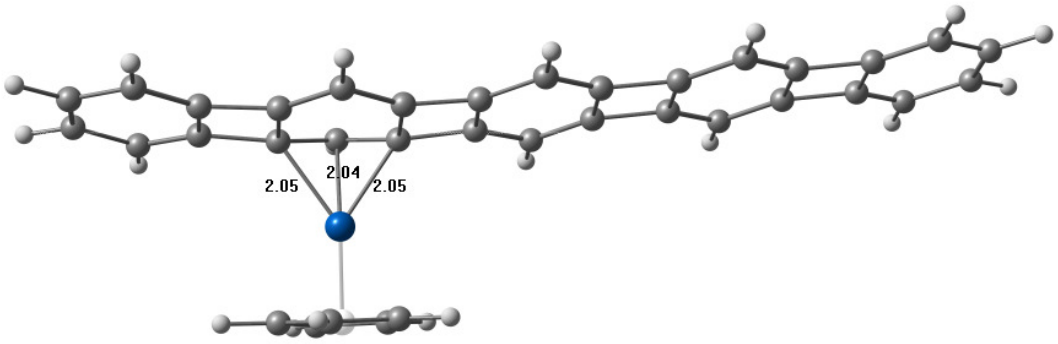

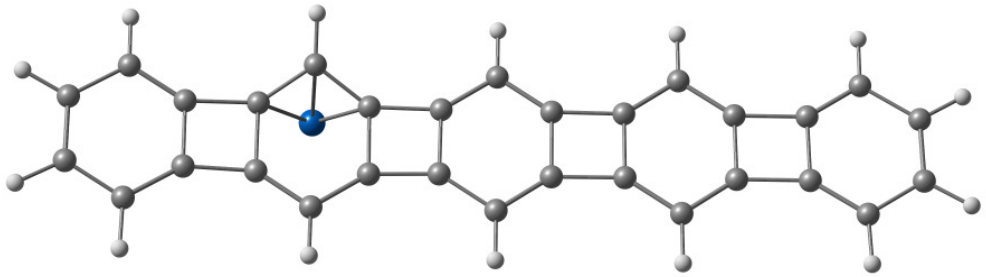

C	7.669717000	–2.174926000	–0.105923000
C	6.450462000	–2.458728000	0.544003000
C	5.349535000	–1.733337000	0.120322000
C	3.893688000	–1.505268000	0.269179000
C	2.708972000	–1.942858000	0.838638000
C	1.596115000	–1.239419000	0.370186000
C	0.149218000	–1.103313000	0.368184000
C	–1.061261000	–1.583264000	0.932639000
C	–2.167377000	–0.965378000	0.405284000
C	–3.686709000	–0.866795000	0.409630000
C	–4.872520000	–1.347856000	0.960688000
C	–5.997863000	–0.728310000	0.421450000
C	–5.941471000	0.288854000	–0.586107000
C	–4.758793000	0.770529000	–1.137452000
C	–3.629556000	0.150846000	–0.598044000
C	–2.119390000	0.068600000	–0.617626000
C	–0.945265000	0.548559000	–1.173832000
C	0.191709000	–0.072876000	–0.643629000
C	1.695402000	–0.118964000	–0.667389000
C	2.835200000	0.041396000	–1.507494000
C	3.981535000	–0.415532000	–0.796385000
C	5.449049000	–0.747489000	–0.920326000
C	6.638556000	–0.473422000	–1.556289000
C	7.762417000	–1.216205000	–1.122513000
H	6.396888000	–3.209338000	1.323030000
H	2.647172000	–2.772334000	1.532449000
H	–1.099468000	–2.356302000	1.688990000
H	–4.914534000	–2.116326000	1.720908000
H	–4.717626000	1.537921000	–1.898781000
H	–0.906852000	1.317204000	–1.935050000
H	2.849903000	0.560387000	–2.457942000
H	6.730568000	0.262385000	–2.346085000
Co	3.078365000	1.106450000	0.223118000
C	2.432920000	3.235925000	0.352954000
C	3.805628000	3.232135000	–0.000959000
C	4.525686000	2.519574000	1.027488000
C	3.591065000	2.151422000	2.051886000
C	2.287258000	2.550618000	1.620273000

H	1.625110000	3.662123000	–0.222202000
H	4.237852000	3.652387000	–0.895767000
H	5.588986000	2.336674000	1.044912000
H	3.828106000	1.629983000	2.966790000
H	1.363656000	2.417646000	2.161607000
H	8.562189000	–2.715853000	0.187384000
H	8.723754000	–1.039126000	–1.591154000
C	–7.467794000	0.379383000	–0.580257000
C	–7.522920000	–0.639213000	0.428535000
C	–8.594261000	0.964602000	–1.089561000
C	–8.706397000	–1.090617000	0.945872000
C	–9.887862000	–0.485330000	0.420145000
C	–9.834353000	0.499744000	–0.555359000
H	–8.574126000	1.734202000	–1.850912000
H	–10.757407000	0.931123000	–0.925119000
H	–10.851990000	–0.807405000	0.796463000
H	–8.770071000	–1.858056000	1.706995000

(e) Local minimum 3: η^4-benzene (19.0 kcal/mol)

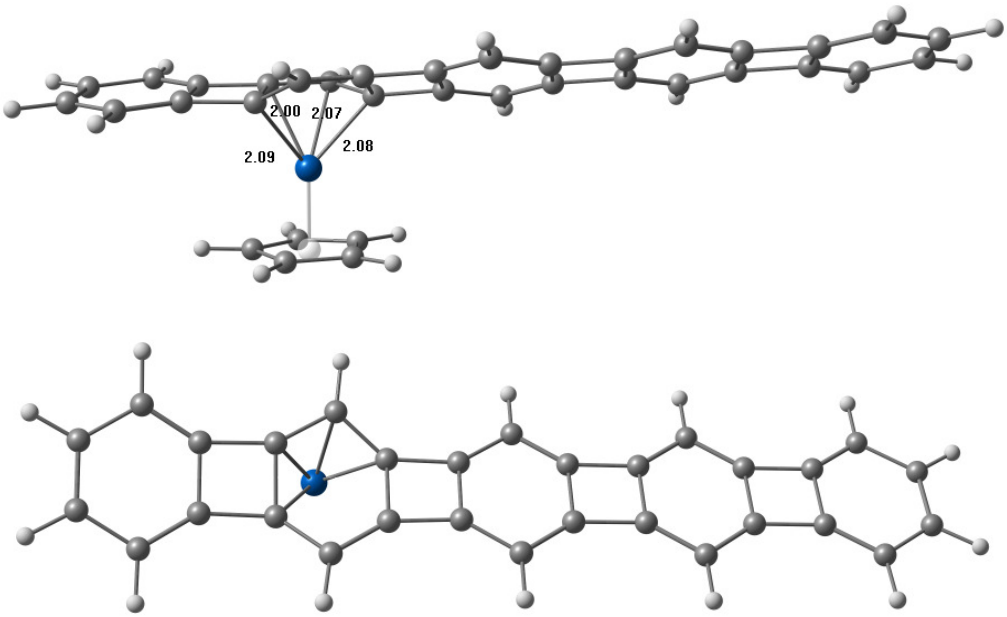

C	–7.704806000	–1.625445000	–0.076324000
C	–6.491455000	–1.789497000	–0.801300000
C	–5.352262000	–1.326936000	–0.190371000
C	–3.836374000	–1.127906000	–0.291559000
C	–2.669014000	–1.876939000	–0.775878000
C	–1.540408000	–1.361850000	–0.248671000
C	–0.067088000	–1.219487000	–0.231176000
C	1.147603000	–1.746746000	–0.723682000

C	2.245517000	–1.037457000	–0.289605000
C	3.767258000	–0.910575000	–0.313273000
C	4.961694000	–1.439625000	–0.795996000
C	6.075343000	–0.726547000	–0.354068000
C	5.999362000	0.418026000	0.498208000
C	4.804020000	0.947684000	0.980899000
C	3.691158000	0.235329000	0.538756000
C	2.171505000	0.121554000	0.570963000
C	0.990404000	0.649716000	1.051234000
C	–0.139369000	–0.066282000	0.613306000
C	–1.640889000	–0.139469000	0.665899000
C	–2.708579000	0.044357000	1.607074000
C	–3.890300000	–0.515482000	1.069631000
C	–5.389479000	–0.719093000	1.106627000
C	–6.553177000	–0.561696000	1.815459000
C	–7.736166000	–1.034716000	1.182797000
H	–6.489929000	–2.263627000	–1.775522000
H	–2.743316000	–2.692464000	–1.483904000
H	1.201969000	–2.617287000	–1.364047000
H	5.019196000	–2.306567000	–1.440440000
H	4.747029000	1.814065000	1.626168000
H	0.933710000	1.519855000	1.692796000
H	–2.640951000	0.605584000	2.529735000
H	–6.590996000	–0.122891000	2.805220000
Co	–3.231943000	0.870639000	–0.218177000
C	–2.631117000	2.925280000	–0.475333000
C	–4.019450000	2.955930000	–0.137499000
C	–4.720042000	2.167067000	–1.095287000
C	–3.768150000	1.717753000	–2.089396000
C	–2.477085000	2.188405000	–1.710046000
H	–1.832546000	3.399891000	0.073720000
H	–4.448788000	3.419647000	0.737399000
H	–5.777018000	1.951944000	–1.095854000
H	–3.999907000	1.119290000	–2.956393000
H	–1.549894000	2.013889000	–2.232360000
H	–8.630326000	–1.978241000	–0.517433000
H	–8.683428000	–0.939767000	1.701100000
C	7.524401000	0.541032000	0.473497000
C	7.600630000	–0.607844000	–0.382149000
C	8.637973000	1.216338000	0.890053000
C	8.792152000	–1.101412000	–0.836674000
C	9.961705000	–0.402146000	–0.407106000
C	9.887895000	0.708141000	0.420266000
H	8.602106000	2.084773000	1.535736000
H	10.801526000	1.207625000	0.721410000
H	10.931894000	–0.752974000	–0.739605000

H	8.871661000	–1.966753000	–1.482602000

(f) Transition state 5: η^2-cyclobutadiene (36.0 kcal/mol)

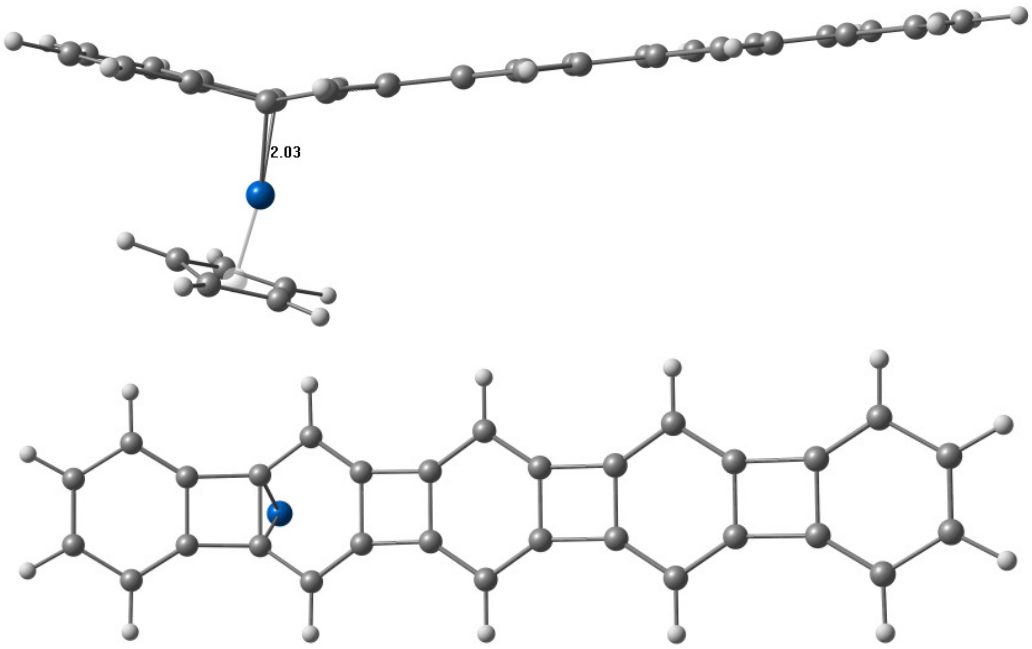

C	7.143264000	–2.348493000	0.699665000
C	6.037664000	–1.857298000	1.448523000
C	4.969251000	–1.391864000	0.720257000
C	3.582514000	–0.743198000	0.748195000
C	2.358402000	–0.737338000	1.512136000
C	1.240141000	–0.634711000	0.742222000
C	–0.262684000	–0.516912000	0.716494000
C	–1.428088000	–0.430968000	1.492584000
C	–2.574224000	–0.346717000	0.719319000
C	–4.098679000	–0.233199000	0.715866000
C	–5.251323000	–0.147278000	1.490294000
C	–6.408253000	–0.063372000	0.713741000
C	–7.934932000	0.047490000	0.717366000
C	–9.088044000	0.130556000	1.446914000
C	–10.299063000	0.217080000	0.692638000
C	–10.298939000	0.215301000	–0.693576000
C	–9.087782000	0.126841000	–1.447398000
C	–7.934811000	0.045602000	–0.717417000
C	–6.408180000	–0.065400000	–0.713264000
C	–5.251144000	–0.151514000	–1.489420000
C	–4.098619000	–0.235099000	–0.714599000
C	–2.574142000	–0.348081000	–0.717615000
C	–1.428022000	–0.433439000	–1.490677000

C	–0.262587000	–0.517946000	–0.714342000
C	1.239930000	–0.636111000	–0.739947000
C	2.357013000	–0.742891000	–1.511730000
C	3.581891000	–0.749703000	–0.749006000
C	4.968536000	–1.397444000	–0.717250000
C	6.036190000	–1.868351000	–1.443314000
C	7.142499000	–2.353756000	–0.691900000
H	8.003789000	–2.740125000	1.230531000
H	6.052031000	–1.874231000	2.531931000
H	2.350726000	–0.802237000	2.593967000
H	–1.427931000	–0.429806000	2.574521000
H	–5.251989000	–0.146640000	2.572026000
H	–9.110076000	0.132990000	2.529448000
H	–11.241535000	0.285430000	1.223689000
H	–11.241318000	0.282253000	–1.224971000
H	–9.109613000	0.126365000	–2.529940000
H	–5.251637000	–0.153720000	–2.571150000
H	–1.427824000	–0.434279000	–2.572612000
H	2.347832000	–0.810535000	–2.593375000
H	6.049185000	–1.893779000	–2.526553000
H	8.002469000	–2.749449000	–1.220666000
Co	4.148367000	1.055016000	–0.009106000
C	5.996101000	2.006266000	0.022069000
C	5.276853000	2.480887000	1.185002000
C	4.085420000	3.079352000	0.718350000
C	4.110596000	3.077077000	–0.745160000
C	5.316353000	2.474554000	–1.168669000
H	6.921324000	1.451094000	0.038659000
H	5.556549000	2.314709000	2.212960000
H	3.287274000	3.477873000	1.325692000
H	3.334253000	3.474398000	–1.380859000
H	5.631980000	2.304731000	–2.185537000

(g) Local minimum 4: η^4-cyclobutadiene (9.7 kcal/mol)

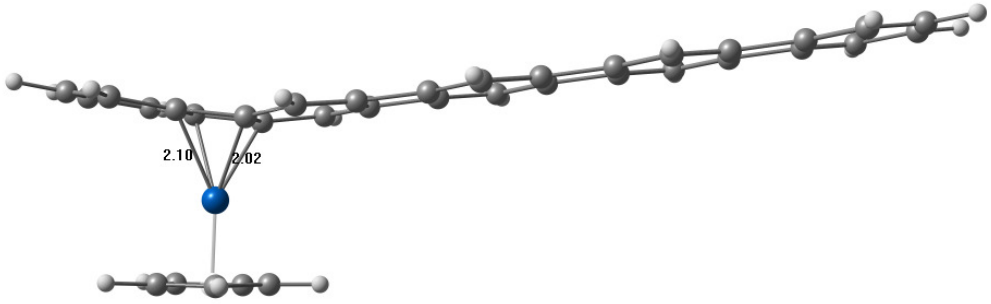

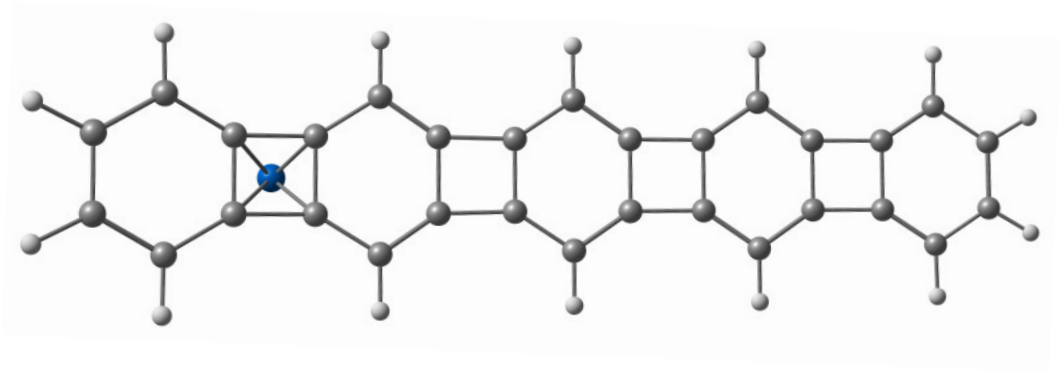

C	4.893664000	–1.209972000	0.735005000
C	4.893573000	–1.213475000	–0.730870000
C	3.475382000	–0.763132000	–0.743915000
C	3.475432000	–0.760320000	0.747049000
C	2.260316000	–0.690973000	1.520580000
C	1.145205000	–0.595973000	0.744946000
C	1.145156000	–0.599246000	–0.742744000
C	2.260358000	–0.697381000	–1.517904000
C	–0.343192000	–0.479177000	–0.713609000
C	–0.343168000	–0.476032000	0.715380000
H	2.252105000	–0.735285000	–2.601934000
H	2.251901000	–0.724154000	2.604763000
Co	4.601208000	0.736083000	–0.002055000
C	5.960130000	2.243618000	–0.721946000
C	4.640007000	2.540538000	–1.172530000
C	3.804522000	2.681992000	–0.008876000
C	4.632302000	2.544967000	1.160921000
C	5.955467000	2.247130000	0.721276000
H	6.816321000	2.038808000	–1.347044000
H	4.312673000	2.604006000	–2.199136000
H	2.745254000	2.890841000	–0.012873000
H	4.298236000	2.612143000	2.185222000
H	6.807361000	2.044890000	1.353015000
C	6.022290000	–1.649780000	1.464200000
C	6.022277000	–1.656609000	–1.457900000
C	7.122289000	–2.056771000	0.719324000
C	7.122311000	–2.060028000	–0.711126000
H	6.027301000	–1.702610000	2.548102000
H	8.011576000	–2.407816000	1.233935000
H	8.011528000	–2.413601000	–1.224115000
H	6.027432000	–1.714310000	–2.541551000
C	–1.512226000	–0.382902000	1.494684000
C	–1.512274000	–0.389473000	–1.493257000
C	–2.658093000	–0.297761000	0.720325000
C	–2.658103000	–0.300923000	–0.719236000
H	–1.511446000	–0.379165000	2.578406000

H	–1.511531000	–0.390614000	–2.576954000
C	–4.169046000	–0.190131000	–0.714237000
C	–4.169015000	–0.186849000	0.714915000
C	–5.325016000	–0.103295000	1.491764000
C	–5.325120000	–0.110177000	–1.491395000
C	–6.483203000	–0.023670000	0.713863000
C	–6.483258000	–0.027061000	–0.713749000
H	–5.325252000	–0.101647000	2.575308000
H	–5.325471000	–0.113799000	–2.574933000
C	–7.997403000	0.080746000	0.716440000
C	–7.997524000	0.076500000	–0.716680000
C	–9.155096000	0.160872000	1.448927000
C	–9.155379000	0.152083000	–1.449432000
C	–10.366775000	0.240123000	0.695134000
C	–10.366925000	0.235844000	–0.695874000
H	–9.178696000	0.150122000	–2.533721000
H	–11.311550000	0.297904000	–1.227155000
H	–11.311298000	0.305233000	1.226228000
H	–9.178228000	0.165001000	2.533216000

(h) Transition state 2: η^2-cyclobutadiene (35.7 kcal/mol)

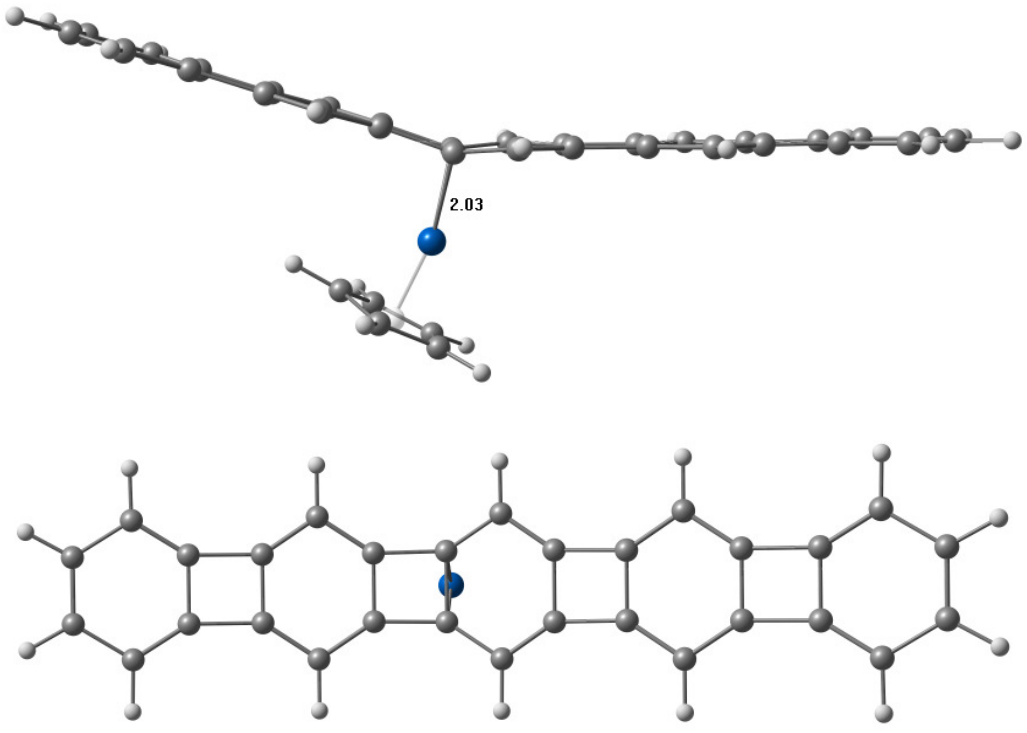

C	8.266704000	–2.005162000	0.692734000
C	7.088955000	–1.708719000	1.446000000
C	5.966603000	–1.428050000	0.716466000

C	4.483884000	–1.054830000	0.713802000
C	3.355736000	–0.795879000	1.487813000
C	2.219848000	–0.542568000	0.715155000
C	0.748349000	–0.122254000	0.743952000
C	–0.460068000	–0.300197000	1.509394000
C	–1.583463000	–0.354552000	0.739667000
C	–3.088504000	–0.455891000	0.716671000
C	–4.249167000	–0.553278000	1.491353000
C	–5.399475000	–0.634011000	0.717623000
C	–6.922525000	–0.754459000	0.717051000
C	–8.076029000	–0.852663000	1.446746000
C	–9.285359000	–0.940991000	0.693505000
C	–9.286426000	–0.927591000	–0.694047000
C	–8.078221000	–0.824629000	–1.447252000
C	–6.923651000	–0.740632000	–0.717519000
C	–5.400498000	–0.620402000	–0.717994000
C	–4.251528000	–0.525736000	–1.491803000
C	–3.089431000	–0.443610000	–0.717063000
C	–1.585243000	–0.344579000	–0.740307000
C	–0.463450000	–0.290395000	–1.513612000
C	0.748496000	–0.127629000	–0.751652000
C	2.219455000	–0.546002000	–0.721683000
C	3.355860000	–0.802470000	–1.493276000
C	4.483583000	–1.057975000	–0.718022000
C	5.966360000	–1.431783000	–0.719354000
C	7.088265000	–1.716549000	–1.447876000
C	8.266466000	–2.008718000	–0.693595000
H	9.183427000	–2.233531000	1.224348000
H	7.110060000	–1.714392000	2.528663000
H	3.353411000	–0.803478000	2.570367000
H	–0.456292000	–0.373454000	2.590614000
H	–4.248665000	–0.564171000	2.573279000
H	–8.096828000	–0.865292000	2.529266000
H	–10.227269000	–1.021159000	1.223954000
H	–10.229127000	–0.997490000	–1.224546000
H	–8.100648000	–0.816347000	–2.529785000
H	–4.252664000	–0.517117000	–2.573754000
H	–0.464650000	–0.354640000	–2.595436000
H	3.353541000	–0.815213000	–2.575752000
H	7.108905000	–1.727728000	–2.530504000
H	9.182976000	–2.239822000	–1.224379000
Co	1.060170000	1.739352000	–0.013647000
C	0.820599000	3.762931000	0.679296000
C	2.023158000	3.250849000	1.217023000
C	2.833506000	2.814255000	0.100512000
C	2.185795000	3.225276000	–1.129991000

C	0.924349000	3.753677000	–0.780133000
H	–0.033478000	4.112410000	1.239126000
H	2.257663000	3.114053000	2.260457000
H	3.791311000	2.322414000	0.171627000
H	2.565428000	3.065285000	–2.126458000
H	0.160713000	4.098445000	–1.460120000

(i) Local minimum 1: η^4-benzene (19.0 kcal/mol)

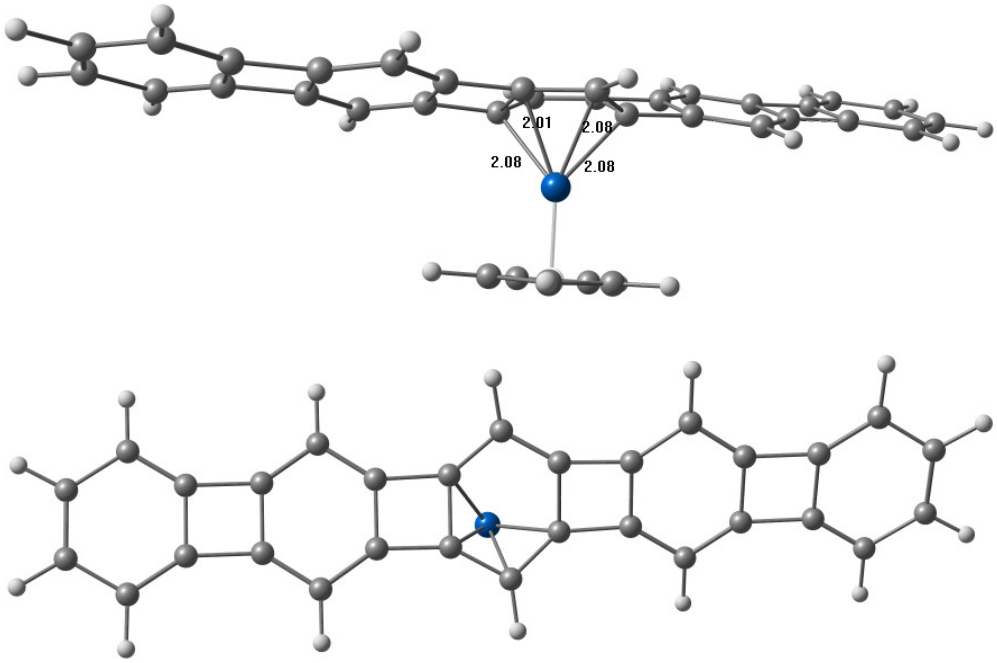

C	8.767525000	–0.664628000	0.869444000
C	7.569070000	–0.364489000	1.586360000
C	6.400497000	–0.535559000	0.896308000
C	4.872998000	–0.456407000	0.896648000
C	3.729258000	–0.166123000	1.633430000
C	2.558863000	–0.367557000	0.899969000
C	1.050529000	–0.274920000	0.917771000
C	–0.154687000	0.103769000	1.545183000
C	–1.231288000	–0.039565000	0.606842000
C	–2.736221000	–0.089835000	0.603708000
C	–3.901526000	0.467576000	1.153370000
C	–5.054648000	–0.104455000	0.647800000
C	–6.579036000	–0.120351000	0.673091000
C	–7.732820000	0.402806000	1.194768000
C	–8.948594000	–0.155119000	0.702959000
C	–8.958839000	–1.167887000	–0.247745000
C	–7.753788000	–1.707235000	–0.785423000
C	–6.589806000	–1.166201000	–0.307896000

C	–5.063448000	–1.158179000	–0.339650000
C	–3.923750000	–1.713712000	–0.884954000
C	–2.743411000	–1.141750000	–0.370168000
C	–1.264100000	–1.152263000	–0.442985000
C	–0.114410000	–1.509648000	–1.047872000
C	1.001557000	–0.717865000	–0.509678000
C	2.529242000	–0.815059000	–0.456630000
C	3.680301000	–1.106705000	–1.192448000
C	4.847485000	–0.909766000	–0.461159000
C	6.375435000	–0.989198000	–0.464503000
C	7.517684000	–1.280530000	–1.157992000
C	8.743181000	–1.104009000	–0.445669000
H	9.720775000	–0.544729000	1.371431000
H	7.610320000	–0.024462000	2.613574000
H	3.742883000	0.162901000	2.664422000
H	–0.241422000	0.534554000	2.534230000
H	–3.894210000	1.260341000	1.890621000
H	–7.746436000	1.191936000	1.936109000
H	–9.890199000	0.223840000	1.083439000
H	–9.908180000	–1.561665000	–0.592194000
H	–7.783148000	–2.497305000	–1.525270000
H	–3.929534000	–2.506814000	–1.621099000
H	0.005285000	–2.235278000	–1.842324000
H	3.664139000	–1.453900000	–2.217556000
H	7.520111000	–1.625509000	–2.184413000
H	9.677483000	–1.320445000	–0.950825000
Co	0.245526000	1.194775000	–0.183529000
C	–0.498660000	3.223481000	–0.207100000
C	0.902667000	3.310487000	0.056983000
C	1.591310000	2.661311000	–1.009417000
C	0.610054000	2.243094000	–1.989593000
C	–0.681576000	2.592200000	–1.494981000
H	–1.289524000	3.595536000	0.425619000
H	1.355880000	3.721411000	0.946130000
H	2.657726000	2.519341000	–1.088515000
H	0.823168000	1.743521000	–2.921425000
H	–1.626608000	2.403559000	–1.979282000

(j) Transition state 1: η^3-benzene (35.6 kcal/mol)

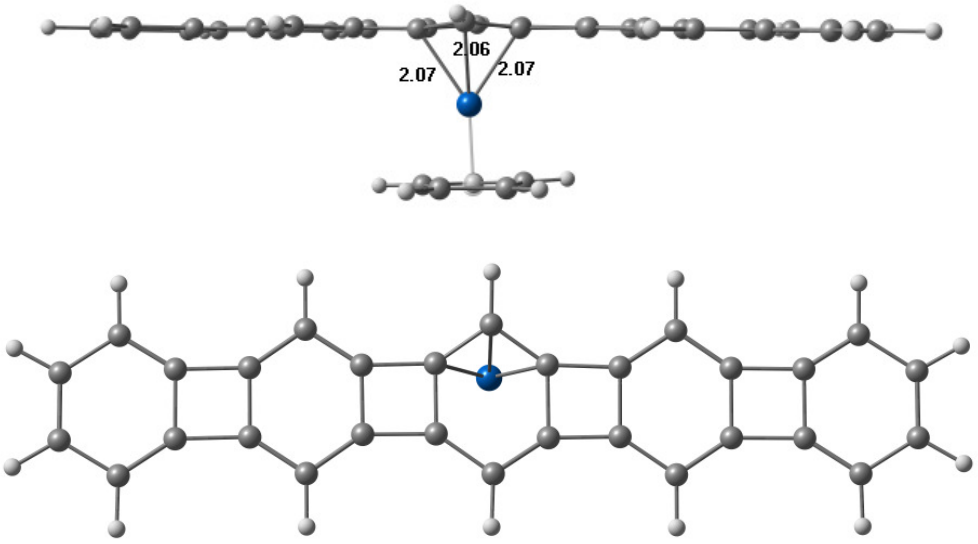

C	–8.901354000	–0.223681000	–0.743434000
C	–7.695103000	0.220198000	–1.360549000
C	–6.531343000	–0.208573000	–0.779115000
C	–5.007706000	–0.207407000	–0.796109000
C	–3.863247000	0.247302000	–1.433753000
C	–2.690760000	–0.206508000	–0.819013000
C	–1.184933000	–0.153490000	–0.843116000
C	–0.016095000	0.217826000	–1.588049000
C	1.142075000	–0.155798000	–0.877497000
C	2.665172000	–0.195830000	–0.859864000
C	3.835813000	0.283152000	–1.437197000
C	4.978920000	–0.204857000	–0.802474000
C	6.505676000	–0.216574000	–0.771205000
C	7.678527000	0.226433000	–1.319208000
C	8.875127000	–0.251684000	–0.703235000
C	8.845790000	–1.112691000	0.383544000
C	7.616005000	–1.570592000	0.948642000
C	6.475812000	–1.107284000	0.353147000
C	4.945633000	–1.092812000	0.320013000
C	3.774824000	–1.565295000	0.903163000
C	2.628495000	–1.080676000	0.265289000
C	1.119158000	–1.093642000	0.244670000
C	–0.052242000	–1.637616000	0.861793000
C	–1.193959000	–1.109215000	0.331010000
C	–2.676505000	–1.073633000	0.328062000
C	–3.841325000	–1.514463000	0.979035000
C	–4.995446000	–1.053912000	0.371366000
C	–6.522185000	–1.052982000	0.381089000
C	–7.676261000	–1.483950000	0.978498000
C	–8.892512000	–1.041633000	0.378747000

H	–9.850267000	0.087677000	–1.164894000
H	–7.723622000	0.856176000	–2.236504000
H	–3.873085000	0.886115000	–2.307512000
H	–0.031238000	0.768624000	–2.518870000
H	3.857949000	0.953892000	–2.286176000
H	7.723941000	0.897606000	–2.167700000
H	9.831384000	0.069893000	–1.099633000
H	9.779177000	–1.450269000	0.819087000
H	7.614291000	–2.243551000	1.796930000
H	3.751975000	–2.237828000	1.750478000
H	–0.016047000	–2.343040000	1.681308000
H	–3.832680000	–2.159963000	1.847727000
H	–7.691389000	–2.121828000	1.853393000
H	–9.834648000	–1.354566000	0.814012000
Co	–0.004249000	1.140918000	0.250383000
C	0.931445000	3.181201000	0.326993000
C	–0.487068000	3.279997000	0.223542000
C	–1.069741000	2.607436000	1.368652000
C	0.008159000	2.107122000	2.176577000
C	1.235098000	2.411215000	1.492603000
H	1.650004000	3.565479000	–0.380430000
H	–1.033454000	3.774248000	–0.564979000
H	–2.124544000	2.537255000	1.584462000
H	–0.094112000	1.572170000	3.107766000
H	2.227446000	2.134637000	1.815486000

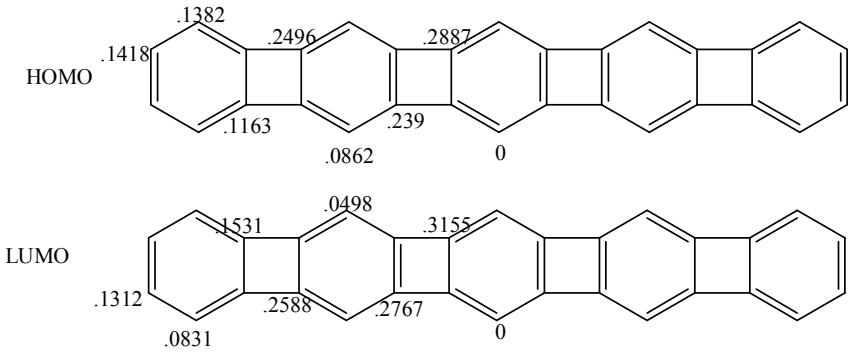

Figure 4.7. Orbital coefficients of linear [5]phenylene.

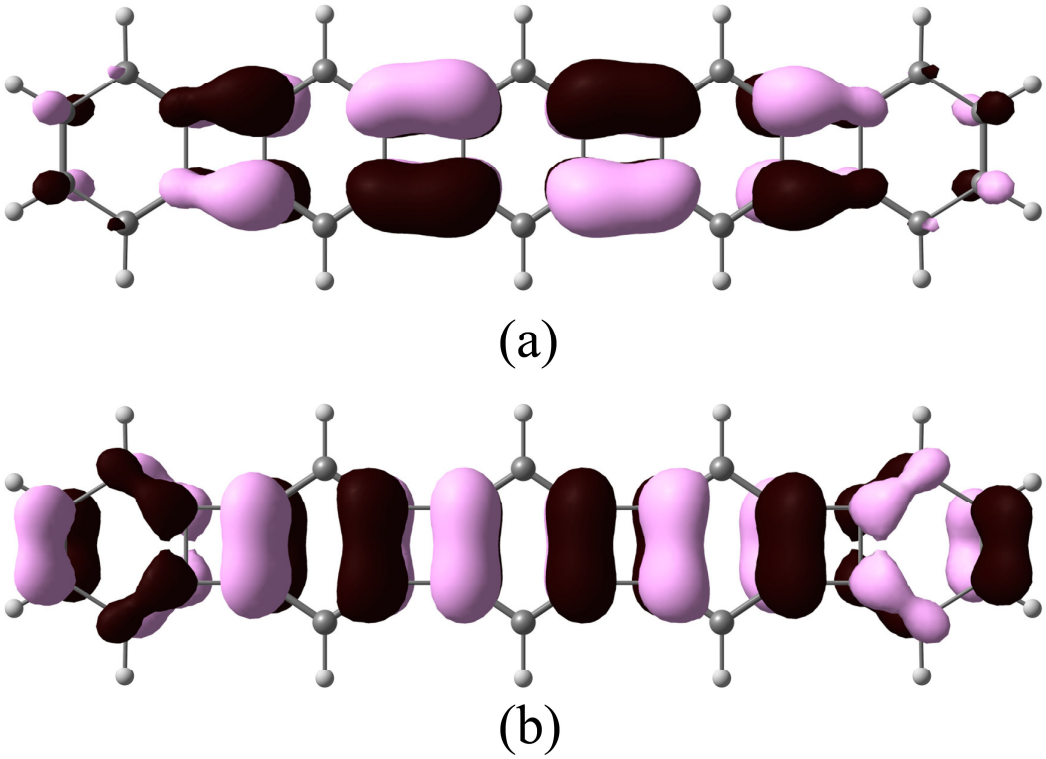

Figure 4.8. Top view of the contour plots of (a) the HOMO and (b) the LUMO of the [5]-phenylene ligand.

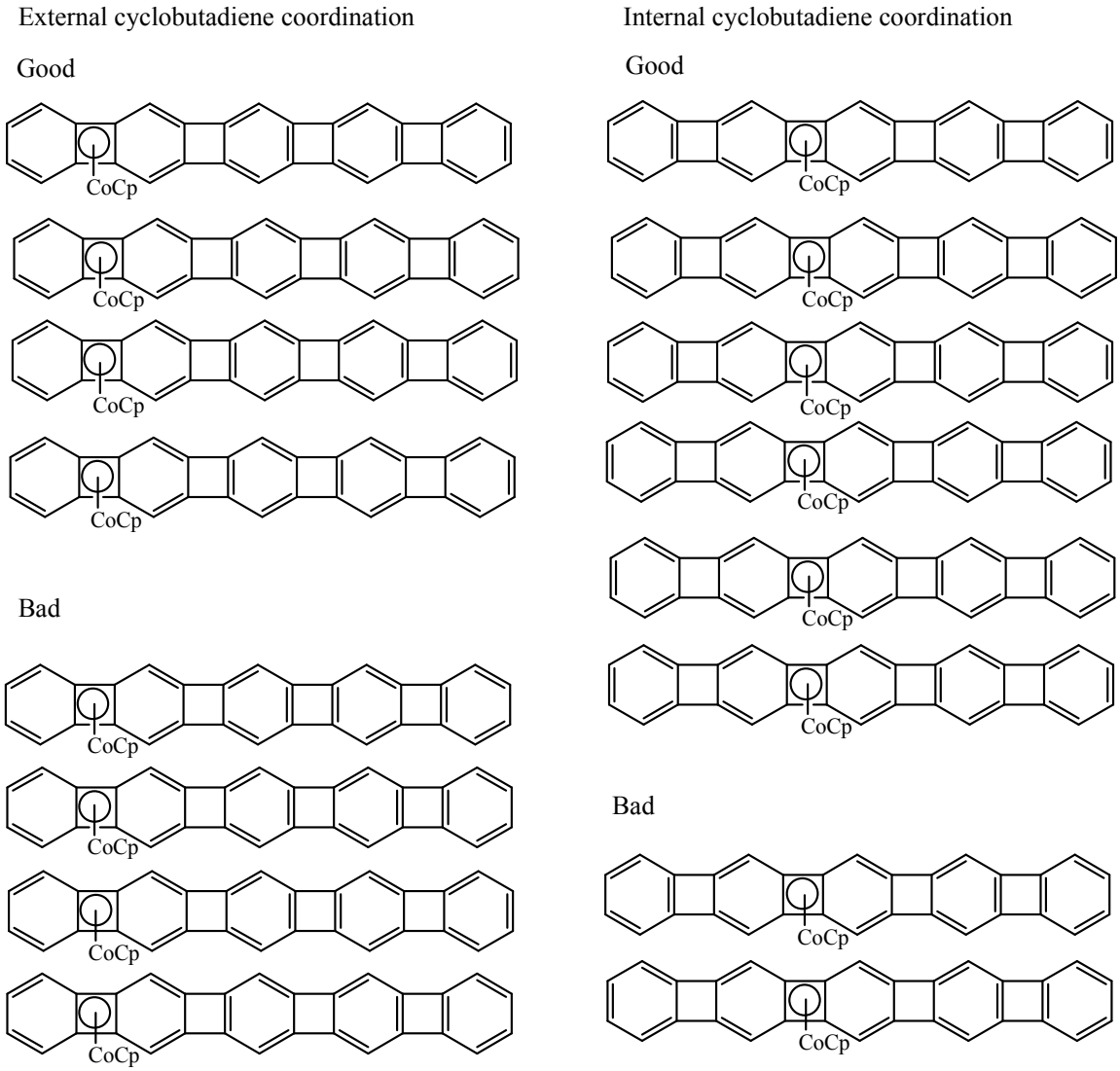

Figure 4.9. Resonance rationale for the increased stability of internal Co coordination in linear [5]phenylene.

4.4 NMR Data for Chapter Two

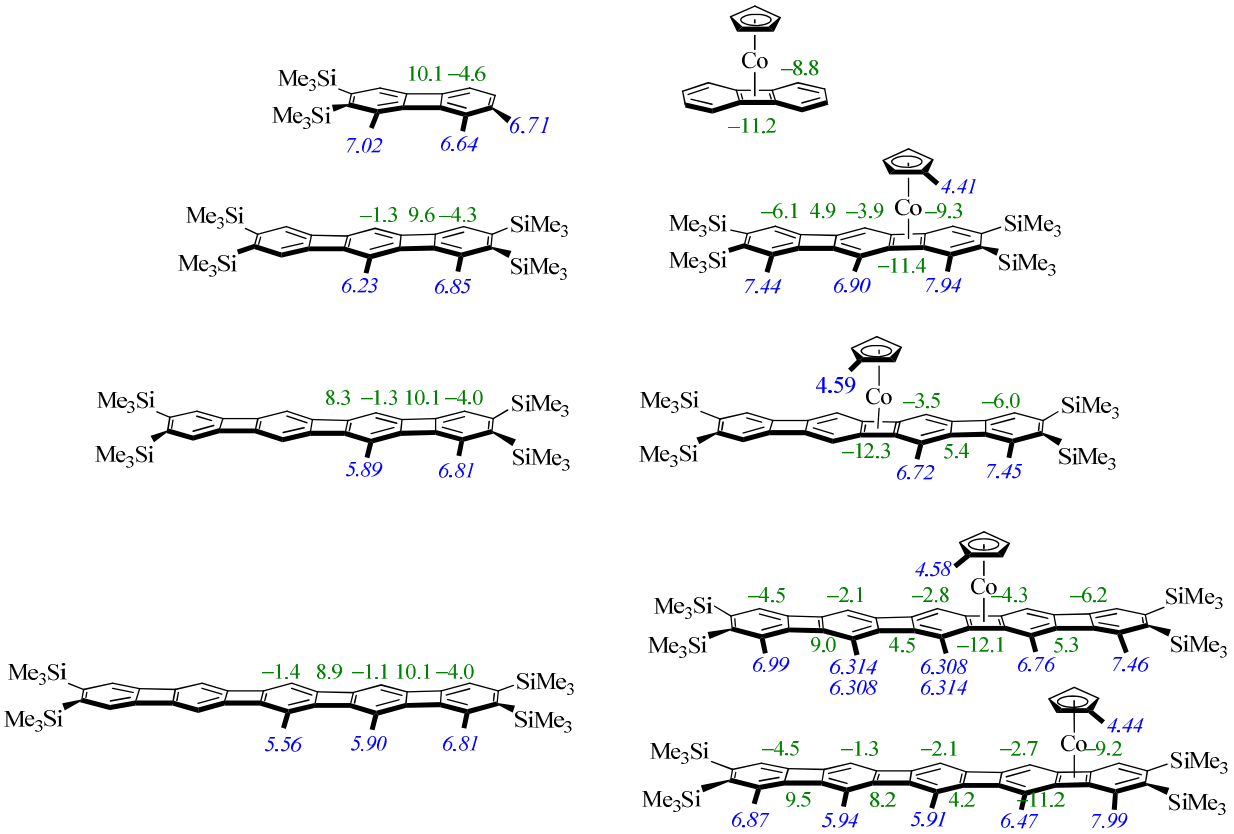

Figure 4.10. ^{1}H-NMR data for the respective parent phenylene frames: experimental (C_6D_6) and calculated [NICS (1), B3LYP/6-31+G*]. Assignments by NOESY, DEPT, HMBC, and HSQC, as applicable.

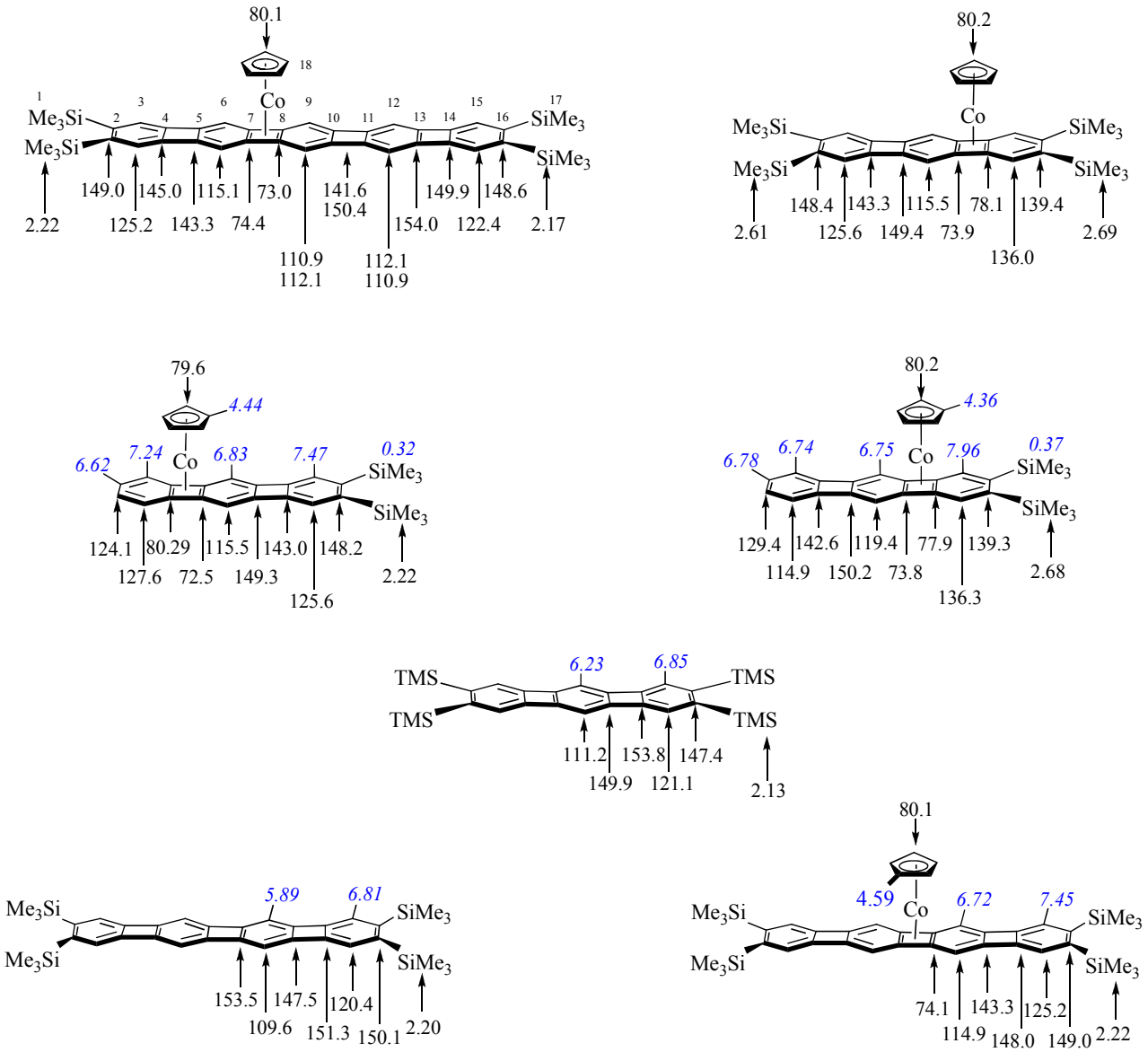

Figure 4.11. Comparison of ^{1}H-NMR (blue) and ^{13}C-NMR assignments (C_6D_6).

NICS-Scan calculations:

Methods: The free ligands were optimized at the B3LYP/6-31G* and the CpCo complexes at the B3LYP/LANL2DZ computational levels. Analytical frequency calculations were executed to ensure real minima (*N*imag = 0). GIAO-B3LYP/6-31+G* was used to calculate NICS values. The NICS-scan procedure is indicative of para- and diamagnetic ring currents in carbocycles and consists of (a) dissection of NICS values into in-plane (ipc or NICSXY) and out-of-plane components (oopc or NICSZZ), in which the latter is the π ring current diagnostic, and (b) composition of graphical plots of the values of the NICS components versus distance r (from the ring centroid under scrutiny) and their interpretation.

Since there are no published NICS-scan studies of transition metal complexed cyclic polyenes, we benchmark the method with $(C_6H_6)Cr(CO)_3$.[53]

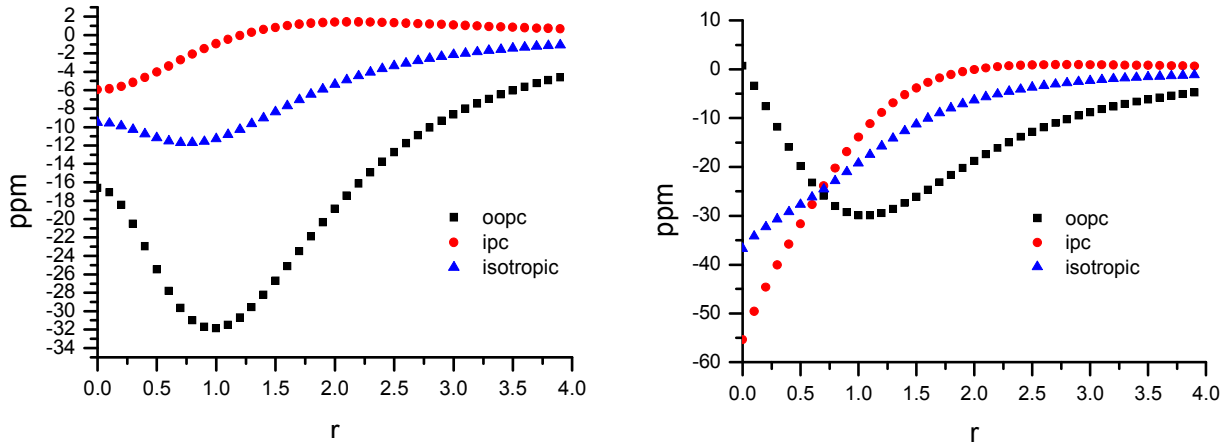

Figure 4.12. NICS-scan of benzene (left) and (benzene)$Cr(CO)_3$ (right).

The shape of the oopc curve suggests that the diamagnetic ring current in the ligand is diminished on complexation, although still prevalent. Thus, at r = 0 Å (i.e., at the benzene plane) the oopc value [NICSZZ(0)] of the complex is less negative than that of benzene, and the minimum of the curve is less negative and occurs at a larger distance (–29.9@1.1 vs. –31.9@1.0). A larger change is observed in the ipc (which is governed by the σ electrons), which shows far more negative values in the complex relative to benzene itself (e.g., –55.4@0.0 vs. –5.9@0.0 and –13.9@1.0 vs. –0.9@1.0). Therefore, isotropic NICS values are misleading with respect to the diatropism in the complex, because they originate largely from the diamagnetic effect of the σ framework. NICS-scans for the four-membered ring B in linear [3]phenylene and its CpCo complex are shown below.

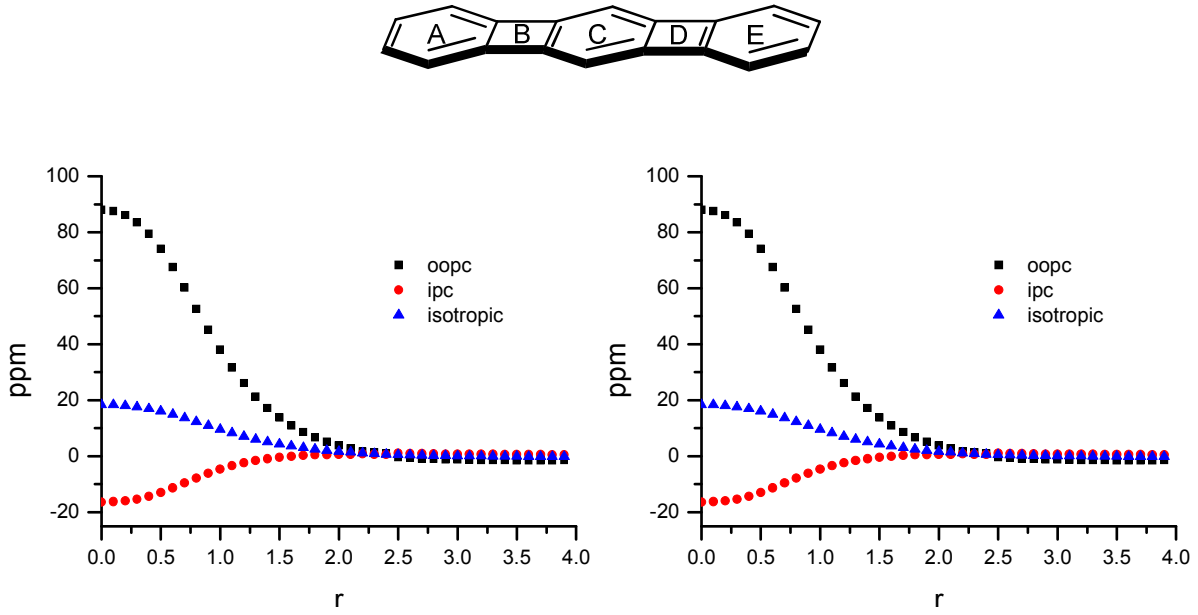

Figure 4.13. NICS-scan above ring B of linear [3]phenylene (left) and its CpCo complex (right).

Inspection of the shape and values of the oopc curve shows that the four-membered ring in the free ligand is strongly paratropic. This picture changes on CpCo complexation. At or close to the ring plane the values are much less positive (12.1@0.0 vs. 88.0@0.0), become negative at greater distance, and reach a minimum of -16.1@1.2. Consequently, the presence of the metal clearly reduces paratropic character. The ipc curve is similar to that of (benzene)Cr(CO)3. Therefore, again, isotropic NICS values are misleading with respect to an assessment of the size of ring current effects.

The two isomeric CpCo complexes of linear [5]phenylene, as depicted next, behave in an analogous manner and engender the same conclusions as above.

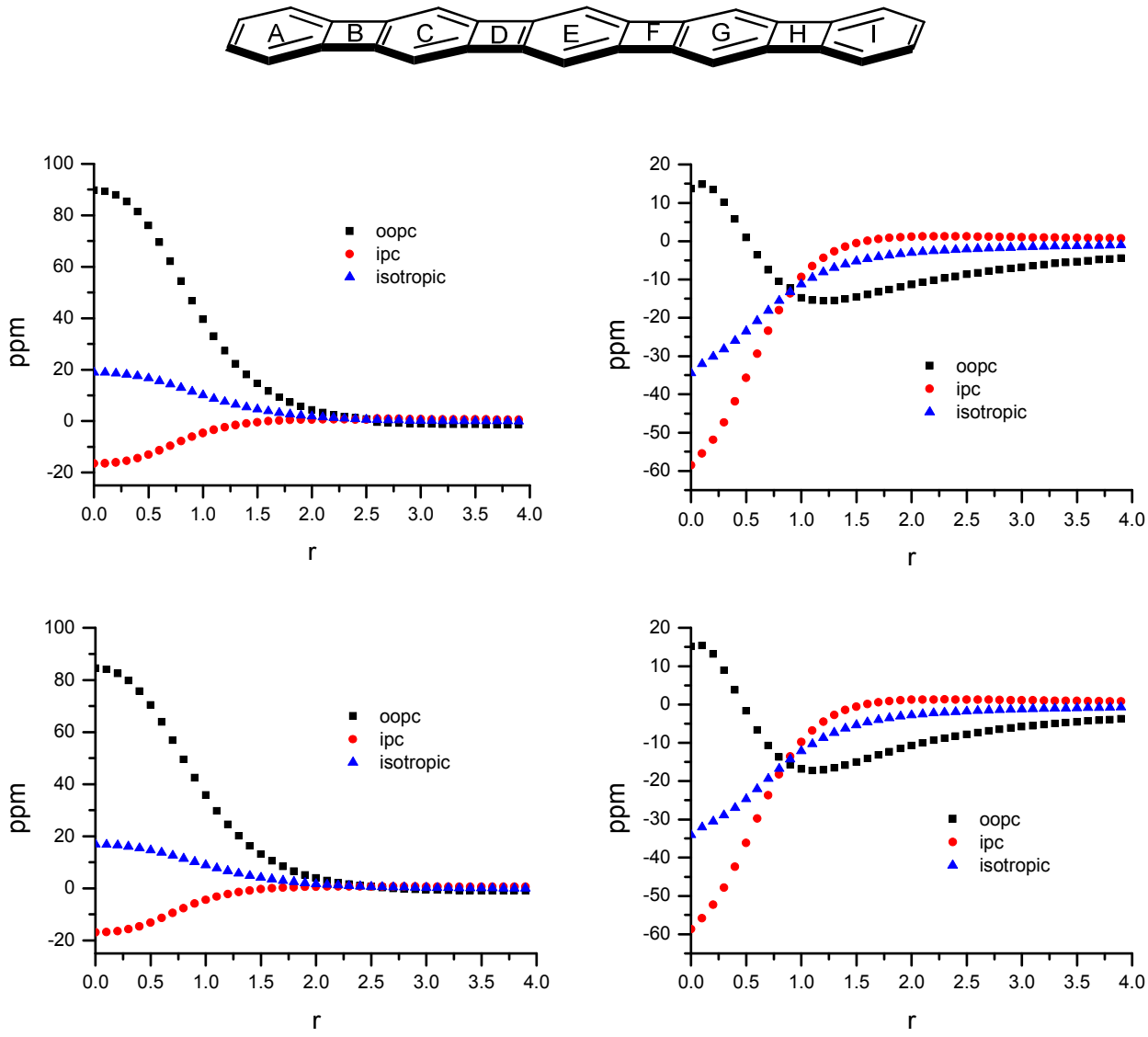

Figure 4.14. NICS-scans of linear [5]phenylene and its CpCo complexes. Top left - ring B of the free ligand. Top right - ring B complexed to CpCo. Bottom left - ring D of the free ligand. Bottom right - ring D complexed to CpCo.

The effect of CpCo complexation is also reflected in the NICS-scan properties of the remaining rings. To illustrate this point, the NICS-scans of the central cyclohexatrienoid ring C of linear [3]phenylene are shown below, first for the free ligand, then for the cyclobutadiene complex.

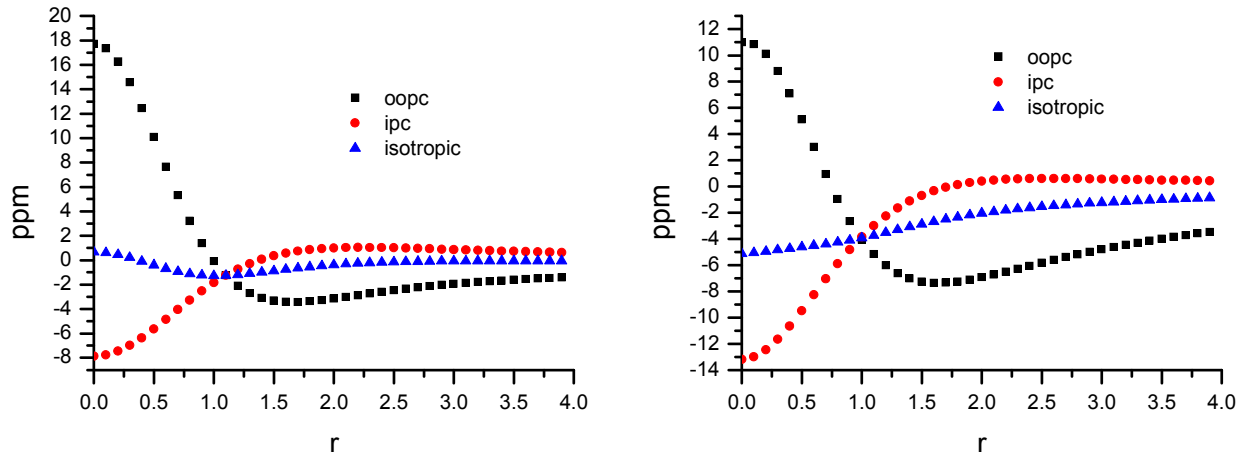

Figure 4.15. NICS-scans of ring C of linear [3]phenylene. Left - as a free ligand. Right: as a CpCo complex of the neighboring cyclobutadiene ring B.

The oopc curve clearly reveals a diminution of paratropism. Thus, at the ring plane the oopc values of the free ligand and of the complex are 17.7 and 11.0 ppm, respectively. Both plots show shallow and relatively distant minima, at –3.4@1.7 and –7.3@1.6, respectively, an indication of larger diamagnetic character of the latter. While the ipc values also become more negative on complexation, this effect is far smaller.
The tables that follow provide an overview of the NICS-scan results over all component rings in linear [3]- and [5]phenylene, complexed and uncomplexed. The diagnostic shape of the oopc curve is designated NM for no minimum, indicating paratropism; and M for minimum, indicating diatropism. Specific values are given at r = 0 Å, r = 1.0 Å, and the minimum (if diamagnetic).

Table 4.16. NICS-scan Details of the oopc for Linear [3]Phenylene and its CpCo Complex at Ring B

Ring	Shape	oopc@0.0	oopc@1.0	Minimum
A	M	7.1	–10.7	–11.8@1.3
A–CpCo	M	–6.5	–22.8	–22.8@1.1
B	NM	88.0	38.1	
B–CpCo	M	12.1	–15.1	–16.1@1.2
C	M	17.7	–0.1	–3.4@1.8
C–CpCo	M	11.6	–1.7	–9.3@1.5
D	NM	88.0	38.1	
D–CpCo	NM	70.4	23.7	
E	M	7.1	–10.7	–11.8@1.3
E–CpCo	M	1.5	–14.8	–15.2@1.2

Table 4.17. NICS-Scan Details of the oopc for Linear [5]Phenylene and its CpCo Complex at Ring B

Ring	Shape	oopc@0.0	oopc@1.0	Minimum
A	M	8.3	–9.7	–10.8@1.3
A–CpCo	M	–6.2	–22.7	–22.8@1.1
B	NM	89.8	39.6	
B–CpCo	M	13.7	–14.8	–15.6@1.2
C	M	17.6	0.0	–3.3@1.7
C–CpCo	M	15.2	–0.9	–8.4@1.5
D	NM	84.6	35.7	
D–CpCo	NM	66.8	22.3	
E	M	16.4	–1.2	–4.1@1.6
E–CpCo	M	14.2	–1.7	–5.3@1.5
F	NM	84.6	35.7	
F–CpCo	NM	80.7	34.0	
G	M	17.6	0.0	–3.3@1.7
G–CpCo	M	16.1	–0.4	–3.2@1.6
H	NM	89.8	39.6	
H–CpCo	NM	86.7	37.8	
I	M	8.3	–9.7	–10.8@1.3
I–CpCo	M	6.4	–10.9	–12.1@1.3

Table 4.18. NICS-scan Details of the oopc for Lnear [5]Phenylene and its CpCo Complex at Ring D

Ring	Shape	oopc@0.0	oopc@1.0	Minimum
A	M	8.3	–9.7	–10.8@1.3
A–CpCo	M	1.9	–15.0	–15.9@1.2
B	NM	89.8	39.6	
B–CpCo	NM	71.7	25.6	
C	M	17.6	0.0	–3.3@1.7
C–CpCo	M	11.0	–12.2	–12.2@1.0
D	NM	84.6	35.7	
D–CpCo	M	15.1	–16.9	–17.3@1.1
E	M	16.4	–1.2	–4.1@1.6
E–CpCo	M	15.1	–16.9	–17.3@1.1
F	NM	84.6	35.7	
F–CpCo	NM	68.5	23.1	
G	M	17.6	0.0	–3.3@1.7
G–CpCo	M	14.8	–1.5	–5.4@1.5
H	NM	89.8	39.6	
H–CpCo	NM	85.0	37.0	
I	M	8.3	–9.7	–10.8@1.3

The data clearly show that on CpCo complexation the paramagnetic ring current contributions decrease (or the diamagnetic ring current contributions increase). The strongest effect is on the complexed cycle, but it occurs for all rings, even the most remote (e.g., I in the linear [5]phenylene complexed at ring B). Thus, upon complexation, the paratropic (and, by inference, antiaromatic) character of the phenylenes decrease.

4.5 Experimental Section for Chapter Three

Angular [3]phenylene **22**,[90] angular [4]phenylene **17**,[111] and [7]heliphene[10] were prepared according to the literature.

$Ni(COD)(PMe_3)_2$:[112]

To a solution of $Ni(COD)_2$ (0.275 g, 1.0 mmol) in dry and vigorously degassed THF (10 mL), PMe_3 (0.20 mL, 0.150 g, 2.0 mmol) was added via syringe in a single portion. After stirring at RT for 24 h, the mixture was transferred using a canula and filtered under Ar to remove unreacted starting material. The solvent was removed on the high vacuum line and the resulting product dried for 3 h. It is extremely air sensitive and must be manipulated under an inert atmosphere at all times. Yellow solid: (0.306 g, 96 %); ^{1}H-NMR (400 MHz, C_6D_6): δ = 4.12 (d, J = 11.2 Hz, 4 H), 2.38 (br t, J = 5.2 Hz, 4 H), 2.25 (t, J = 5.2 Hz, 4 H), 1.02 (d, J = 3.2 Hz, 18 H) ppm; ^{31}P-NMR (162 MHz, C_6D_6): δ = –9.46 (s) ppm.

Adducts of diphenylacetylene **88** to angular [3]phenylene **22** – compounds **89** and **90**:

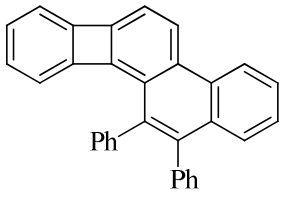

89

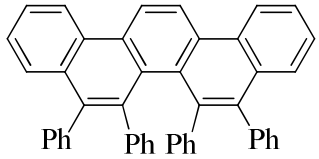

90

In a glove box, an Ace pressure tube was charged with angular [3]phenylene **22** (0.014 g, 0.06 mmol), diphenylacetylene **88** (0.098 g, 0.055 mmol), THF (5 mL) and $Ni(COD)(PMe_3)_2$ (70 μL, 0.08 M in THF, 0.006 mmol). The reaction vessel was tightly sealed, removed from the glovebox, and heated to 75–80 °C (oil bath) for 23 h. After cooling to RT, the solvent was removed by rotary evaporation and the residue purified by flash chromatography on silica gel, using gradient elution (10:1 and then 8:1 hexane/CH_2Cl_2). After a small amount of angular [3]phenylene **22** (0.001 g), the monoadduct **89** (0.004 g, 20 %) eluted to give a yellow solid, m.p. 195–196 °C; ^{1}H-NMR (500 MHz, $CDCl_3$): δ = 8.53 (d, J = 8.4 Hz, 1 H), 8.31 (d, J = 8.0 Hz, 1 H), 7.55 (ddd, J = 1.6, 6.4, 8.0 Hz, 1 H), 7.40–7.32 (m, 2 H), 7.25–7.15 (m, 6 H), 7.15–7.11 (m, 2 H), 7.08 (d, J = 6.5 Hz, 2 H), 7.04 (d, J = 8.0 Hz, 1 H), 6.48 (t, J = 7.2 Hz, 1 H), 6.43 (d, J = 7.0 Hz, 1 H), 6.24 (t, J = 7.5 Hz, 1 H), 4.01 (d, J = 7.0 Hz, 1 H) ppm; ^{13}C-NMR (100 MHz, $CDCl_3$):, δ = 152.5, 151.01, 150.96, 149.5, 139.9, 138.83, 138.79, 134.2, 132.0, 131.2,

130.83, 130.75, 128.2, 128.0, 127.7, 127.6, 127.5, 126.8, 126.6, 126.5, 126.4, 125.0, 123.5, 122.3, 117.9, 116.4, 115.6 ppm, one peak in the region δ = 128–126 ppm is presumed to be accidentally isochronous; IR (KBr): $\tilde{\nu}$ = 3060, 1490, 1481, 1442, 1415, 1159, 1072, 755, 734, 698 cm^{-1}; UV-Vis (CH_3CN): λ_{max} (log ε) 233 (4.42), 265 (4.50), 278 (sh), 294 (sh), 306 (4.47), 318 (4.49), 329 (sh), 380 (3.44), 399 (3.66), 420 (3.66) nm; MS (70 eV): *m/z* (%): 405 [M^++1] (35), 404 [M^+] (100), 326 (13); HRMS (EI): calcd for $C_{32}H_{20}$: 404.1565; found: 404.1571. Elemental analysis calcd for $C_{32}H_{20}$: C 95.02, H 4.98; found: 94.79, 4.60.

Subsequent elution furnished 5,6,7,8-tetraphenylpicene (**90**) (0.009 g, 59 %) as a white solid, m.p. 325–327 °C; the molecule exhibits hindered rotation of the 6,7-phenyl groups on the NMR time scale, ^{1}H-NMR (400 MHz, $CDCl_3$): δ = 8.91 (s, 2 H), 8.85 (d, *J* = 8.4 Hz, 2 H), 7.69 (ddd, *J* = 2.8, 5.2, 8.0 Hz, 2 H), 7.50–7.44 (m, 4 H), 7.44–7.32 (m, 4 H), 7.20 (tt, *J* = 1.6, 7.2 Hz, 2 H), 6.96 (dt, *J* = 0.8, 7.6 Hz, 2 H), 6.89 (tt, *J* = 0.9, 7.6 Hz, 2 H), 6.62 (br s, 4 H), 6.17 (d, *J* = 7.6 Hz, 2 H), 6.07 (br s, 4 H) ppm; ^{13}C-NMR (125 MHz, $CDCl_3$): δ = 140.3, 140.1, 137.7, 136.7, 133.5, 132.5, 132.4, 130.6, 130.0, 129.5, 129.2, 128.3, 127.7, 126.9, 126.4, 126.3, 126.2, 125.6, 125.4, 122.8, 121.3 ppm; IR (KBr): $\tilde{\nu}$ = 3051, 2922, 1599, 1490, 1467, 1442, 1263, 1072, 1027, 758, 702, 630 cm^{-1}; UV-Vis (CH_2Cl_2): λ_{max} (log ε) 266 (4.61), 307 (4.74), 352 (4.17), 366 (4.14) nm; MS (70 eV): *m/z* (%): 583 [M^++1] (52), 582 [M^+] (100), 505 (24), 504 (9), 426 (7); HRMS (EI): calcd for $C_{46}H_{30}$: 582.2348; found: 582.2336.

1,2,7,8-Tetraphenylbenzo[*c*]chrysene (**91**):

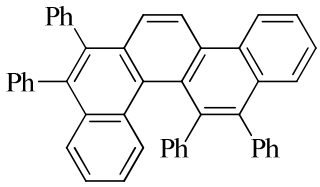

In a glovebox, an Ace pressure tube was charged with **88** (0.020 g, 0.050 mmol), diphenylacetylene **88** (0.026 mg, 0.148 mmol), Ni(COD)(PMe_3)$_2$ (62 μL of a 0.08 M solution in THF), and THF (5 mL). The reaction vessel was sealed, removed from the glovebox, and heated to 85 °C for 39 h. After removal of the solvent, the residue was purified by flash chromatography on silica gel (eluting with 8:1 hexane/CH_2Cl_2), producing a white solid (0.023 g), which was found to consist of starting material (**88**, 1.8 mg), **90** (0.001 g, 6 %), and **91**. Further purification by chromatography afforded pure **91** (0.017 g, 74 %) as a white solid, m.p. 273–274 °C; the 1,2-phenyl groups of **91** exhibit hindered rotation on the NMR timescale, ^{1}H-NMR (500 MHz, $CDCl_3$): δ = 8.80 (d, *J* = 8.0 Hz, 1 H), 8.69 (d, *J* = 9.5 Hz, 1 H), 8.30–8.22 (m, 1 H), 8.01 (d, *J* = 7.5 Hz, 1 H), 7.80–7.47 (m, 2 H), 7.70 (ddd, *J* = 1.0, 7.0, 8.5 Hz, 1 H), 7.62 (dt, *J* = 1.5, 7.5 Hz, 1 H), 7.53 (ddd, *J* = 1.5, 7.0, 8.5 Hz, 1 H), 7.38–7.32 (m, 2 H), 7.30 (td, *J* = 1.5, 7.5 Hz, 1 H), 7.29–7.22 (m, 6 H), 7.22–7.17 (m, 2 H), 7.17–7.10 (m, 2 H), 7.10–6.95 (m, 3 H), 6.80–6.40 (m, 3 H), 6.35 (d, *J* = 7.0 Hz, 1 H), 6.23–5.95 (br s, 1 H) ppm; ^{13}C-NMR (100 MHz, $CDCl_3$): δ = 141.8, 140.0, 139.5, 139.4, 137.8, 137.7, 137.5, 135.7, 132.3, 132.2, 131.6, 131.4, 131.13, 131.07, 130.9, 130.8, 130.7, 130.5, 129.6, 129.5, 128.8, 128.2, 127.7, 127.5, 127.4, 127.3, 127.0, 126.53, 126.47, 126.4, 126.0, 125.6, 125.3, 125.2, 125.1,

124.3, 123.1, 120.8 ppm, due to extensive signal overlap, four peaks are presumed to be isochronous in the regions δ = 132–130 and 128–125 ppm; IR (KBr): $\tilde{\nu}$ = 3058, 1601, 1489, 1442, 1263, 1073, 773, 762, 736, 699, 628 cm^{-1}; UV-Vis (CH_2Cl_2): λ_{max} (log ε) 250 (4.87), 313 (5.11), 340 (sh) nm; MS(EI) *m/z* (%) 583 (M^++1, 72), 582 (M^+, 100), 505 (24), 391 (13); HRMS (EI): calcd for $C_{46}H_{30}$: 582.2348; found: 582.2341. Elemental analysis calcd for $C_{46}H_{30}$: C, 89.33, H 5.00; found: 89.14, 4.93.

Ni(PhC≡CPh)(PMe_3)$_2$ (**92**):[91]

In a glove box, PMe_3 (203 μL, 0.152 g, 2.0 mmol) was mixed with a suspension of Ni(COD)$_2$ (0.275 g, 1.0 mmol) in hexane (15 mL). Diphenylacetylene **88** (0.178 g, 1.0 mmol) was then added in one portion, resulting in an immediate color change from yellow to red. The mixture was stirred at room temperature for 19.5 h, during which the color gradually turning returning to yellow. Upon concentration (to ~5 mL), a yellow precipitate formed, collected by filtration under nitrogen. The resulting powder **92** (0.370 g, 95 %) was dried under vacuum, providing a yellow solid; ^{1}H-NMR (500 MHz, C_6D_6): δ = 7.51 (d, *J* = 7.5 Hz, 4 H), 7.17 (t, *J* = 7.5 Hz, 4 H), 7.02 (t, *J* = 7.5 Hz, 2 H), 1.01 (s, 18 H) ppm; ^{13}C-NMR (125 MHz, C_6D_6): δ = 140.6, 128.7, 127.9, 19.6 (d, $J_{C\text{-}P}$ = 18.8 Hz) ppm; ^{31}P-NMR (162 MHz, C_6D_6): δ = –12.82 (br s) ppm.

Adducts of 3-hexyne to angular [3]phenylene **22** – compounds **104** and **105**:

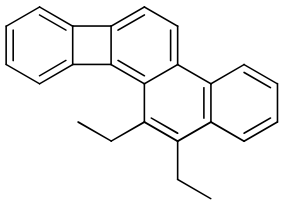

104

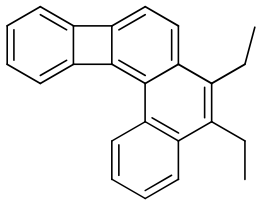

105

In a glovebox, **22** (0.014 mg, 0.060 mmol), 3-hexyne **103** (5.7 μL, 0.004 g, 0.050 mmol), Ni(COD)(PMe_3)$_2$ (0.002 g, 0.005 mmol), and THF (5 mL) were added to an Ace pressure tube. The reaction vessel was sealed and the mixture stirred at 75 °C for 14 h. Flash chromatography on silica gel gave a first fraction that was recrystallized from CH_2Cl_2 to provide pure **104** (7.0 mg, 45 %) as a yellow solid, m.p. 169–170 °C; ^{1}H-NMR (500 MHz, $CDCl_3$): δ = 8.43 (d, *J* = 7.0 Hz, 1 H), 8.21 (d, *J* = 7.5 Hz, 1 H), 7.95 (d, *J* = 7.0 Hz, 1 H), 7.52 (dt, *J* = 1.0, 7.0 Hz, 1 H), 7.48 (dt, *J* = 1.0, 7.0 Hz, 1 H), 6.97 (d, *J* = 7.5 Hz, 1 H), 6.73–6.62 (m, 3 H), 6.55 (d, *J* = 5.5 Hz, 1 H), 3.07 (q, *J* = 7.5 Hz, 2 H), 2.99 (q, *J* = 7.5 Hz, 2 H), 1.33 (t, *J* = 7.5 Hz, 3 H), 1.30 (t, *J* = 7.5 Hz, 3 H) ppm ; ^{13}C-NMR (125 MHz, $CDCl_3$): δ = 153.0, 151.6, 150.4, 147.1, 136.0, 133.0, 131.29, 131.27, 130.7, 128.2, 127.9, 126.7, 126.3, 125.9, 124.6, 123.9, 122.8, 117.9, 115.9, 115.6, 23.2, 21.4, 16.4, 14.9 ppm; IR (KBr): $\tilde{\nu}$ = 3045, 2960, 1600, 1481, 1414, 1261, 1197, 1159, 758, 740 cm^{-1}; UV-Vis (CH_2Cl_2): λ_{max} (log ε) 266 (4.63), 299 (sh), 309 (4.60), 320 (4.62), 331 (4.52), 380 (3.56), 399 (3.74), 419 (3.71) nm; MS (70 eV): *m*/*z* (%): 309 [M^++1] (26), 308 [M^+] (100), 293 [M^+–15] (8), 278 [M^+–30] (21); HRMS (EI): calcd for $C_{24}H_{20}$: 308.1565; found: 308.1666.

A second fraction was **105** (0.002 g, 11 %), isolated as a yellow solid, m.p. 120–122 °C; ^{1}H-NMR (400 MHz, $CDCl_3$): δ = 8.30 (d, J = 7.2 Hz, 1 H), 7.97 (d, J = 7.6 Hz, 1 H), 7.61 (d, J = 8.0 Hz, 1 H), 7.61–7.49 (m, 2 H), 7.00 (d, J = 8.0 Hz, 1 H), 6.99 (d, J = 7.2 Hz, 1 H), 6.74 (quint, J = 7.6 Hz, 2 H), 6.58 (d, J = 6.4 Hz, 1 H); 3.07 (q, J = 7.6 Hz, 2 H), 3.02 (q, J = 7.6 Hz, 2 H), 1.32 (t, J = 7.6 Hz, 3 H), 1.31 (t, J = 7.6 Hz, 3 H) ppm; ^{13}C-NMR (125 MHz, $CDCl_3$): δ = 152.5, 151.9, 148.9, 147.2, 135.6, 134.5, 132.4, 131.8, 128.8, 128.3, 127.9, 127.3, 125.9, 125.2, 125.1, 125.0, 124.1, 117.9, 116.5, 116.0, 22.13, 22.05, 14.9, 14.6 ppm; IR (KBr): $\tilde{\nu}$ = 3063, 2958, 2925, 1490, 1442, 1417, 1262, 1147, 1099, 822, 762, 730 cm^{-1}; UV-Vis (CH_2Cl_2): λ_{max} (log ε) 281 (4.34), 291 (4.48), 303 (4.60), 313 (sh), 369 (3.46), 389 (3.73), 410 (3.77) nm; MS (70 eV): m/z (%): 309 [M^++1] (28), 308 [M^+] (100), 293 [M^+–15] (13), 278 [M^+–30] (21), 226 (22), 149 (29); HRMS (EI): calcd for $C_{24}H_{20}$: 308.1565; found: 308.1664.

Adducts of 1,4-dimethoxy-2-butyne to angular [3]phenylene **22** – compounds **107** and **108**:

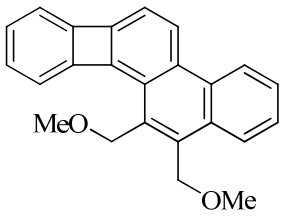

107

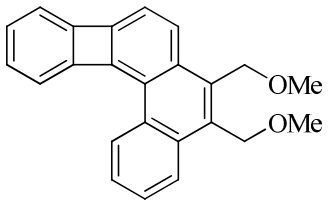

108

In a glovebox, **22** (0.011 g, 0.050 mmol), 1,4-dimethoxybut-2-yne **106** (0.034 g, 0.30 mmol), Ni(COD)(PMe_3)$_2$ (63 μL of a 0.08 M solution in THF), and THF (5 mL) were added to an Ace pressure tube. The reaction vessel was sealed and the mixture stirred at 75 °C for 16.5 h. The ^{1}H-NMR spectrum of the crude indicated the formation of **107** and **108** in the ratio of 6:1. Flash chromatography on silica gel gave first **107** (0.012 g, 68 %) as a yellow solid, m.p. 150–151 °C; ^{1}H-NMR (400 MHz, $CDCl_3$): δ = 8.41 (dd, J = 3.2, 6.4 Hz, 1 H), 8.19 (d, J = 8.0 Hz, 1 H), 8.10 (dd, J = 3.6, 6.4 Hz, 1 H), 7.54 (dd, J = 3.6, 6.4 Hz, 2 H), 7.00 (d, J = 8.0 Hz, 1 H), 6.76 (t, J = 6.4 Hz, 1 H), 6.74–6.65 (m, 2 H), 6.56 (d, J = 6.0 Hz, 1 H), 4.93 (s, 2 H), 4.88 (s, 2 H), 3.53 (s, 3 H), 3.45 (s, 3 H) ppm; ^{13}C-NMR (100 MHz, $CDCl_3$): δ = 152.7, 151.3, 150.9, 148.4, 133.6, 131.8, 131.6, 130.9, 129.6, 128.3, 128.2, 127.2, 127.0, 125.9, 125.5, 123.8, 122.5, 118.3, 116.6, 116.1, 67.7, 67.5, 58.4, 57.5 ppm; IR (KBr): $\tilde{\nu}$ = 3072, 2927, 1485, 1446, 1417, 1376, 1185, 1097, 956, 898, 821, 743, 730 cm^{-1}; MS (70 eV): m/z (%): 341 [M^++1] (16), 340 [M^+] (100), 308 [M^+–38] (26), 293 (34), 280 (15), 265 (44); HRMS (EI): calcd for $C_{24}H_{20}O_2$: 340.1463; found: 340.1466.

Further elution provided **108** (0.002 g, 9 %) as a yellow solid, m.p. 156–157 °C; ^{1}H-NMR (400 MHz, $CDCl_3$): δ = 8.31–8.24 (m, 1 H), 8.13–8.06 (m, 1 H), 7.75 (d, J = 8.0 Hz, 1 H), 7.63–7.56 (m, 2 H), 7.02 (d, J = 8.0 Hz, 1 H), 6.99 (d, J = 6.4 Hz, 1 H), 6.81–6.70 (m, 2 H), 6.60 (d, J = 6.4 Hz, 1 H), 4.93 (s, 2 H), 4.87 (s, 2 H), 3.53 (s, 3 H), 3.51 (s, 3 H) ppm; ^{13}C-NMR (125 MHz, $CDCl_3$): δ = 152.3, 151.7, 150.5, 147.0, 132.7, 132.2,

131.6, 131.5, 129.7, 128.5, 128.2, 127.6, 126.8, 126.6, 125.64, 125.55, 125.2, 118.1, 116.8, 116.5, 68.04, 68.01, 58.38, 58.35 ppm; IR (KBr): $\tilde{\nu}$ = 2925, 1498, 1415, 1379, 1262, 1187, 1095, 1061, 940, 930, 814, 750, 734, 717 cm^{-1}; UV-Vis (CH_3CN): λ_{max} (log ε) 237 (4.58), 287 (4.62), 298 (4.72), 314 (sh), 371 (3.57), 387 (3.80), 407 (3.86) nm; MS (70 eV): *m*/*z* (%): 341 [M^++1] (16), 340 [M^+] (56), 308 [M^+–MeOH] (8), 293 (27), 279 (17), 265 (24); HRMS (EI): calcd for $C_{24}H_{20}O_2$: 340.1463; found: 340.1456.

Optimized cycloaddition reaction between **22** and **88**:

In a glovebox, a round bottom flask was charged with **22** (0.058 g, 0.257 mmol) and $Ni(COD)(PMe_3)_2$ (0.008 g, 0.034 mmol). Both reagents were then dissolved in THF (100 mL). A reflux condenser fitted with a vacuum line adapter was attached to the flask. The assembly was sealed, removed from the glovebox, connected to the vacuum line, flushed with Ar, and the glass stopper quickly replaced with a septum under a purge of Ar. A solution of diphenylacetylene **88** (0.093 g, 0.521 mmol) in THF (20 mL) was taken up in a gas-tight syringe and slowly added over 13 h via syringe pump to the boiling mixture of **22**/$Ni(COD)(PMe_3)_2$. Upon complete addition of the diphenylacetylene solution, the reaction mixture was stirred at reflux for an extra 6 h. After this time, mixture was cooled to RT, and the solvent removed by rotary evaporation to give a yellow residue. The crude product was passed through a plug of silica gel, eluting with a mixture of hexanes/CH_2Cl_2 (10:1), to afford a yellow solid. Analysis of the product by ^{1}H-NMR (using the solvent peak of $CDCl_3$ as the internal standard) revealed the presence of **89** and **90** in a 13:87 ratio.

Adducts of diphenylacetylene **88** to angular [4]phenylene **17** – compounds **130**–**134**:

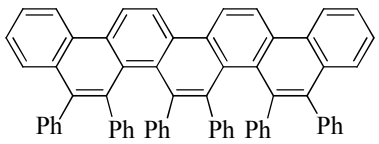

130

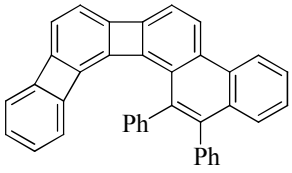

131

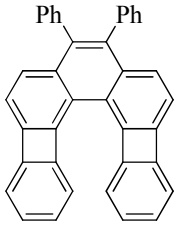

132

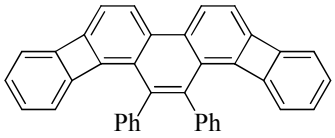

133

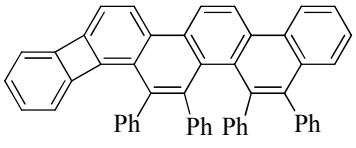

134

In a glovebox, angular [4]phenylene **17** (0.036 g, 0.12 mmol), diphenylacetylene **88** (0.018 g, 0.10 mmol), and $Ni(COD)(PMe_3)_2$ (125 μL of a 0.08 M solution in THF) were added to an Ace pressure tube and dissolved in THF (6 mL). The reaction vessel was sealed, removed from the glovebox, and stirred at 75 °C for 5 h. Flash chromatography

on silica gel gave starting material (0.013 g of **17**), as well as a yellow residue. Further purification of the latter by preparative TLC afforded (in order of elution) **132**, **131**, **133**, **134**, and **139**. Compound **130** (0.008 g, 28 %) was obtained as a white solid, m.p. 360–363 °C (decomp); the phenyl groups located on the central benzene ring of **130** exhibit hindered rotation on the NMR timescale, ^{1}H-NMR (500 MHz, $CDCl_3$): δ = 9.04 (d, J = 9.0 Hz, 2 H), 8.95 (d, J = 9.0 Hz, 2 H), 8.81 (d, J = 8.5 Hz, 2 H), 7.65 (ddd, J = 1.5, 6.5, 8.0 Hz, 2 H), 7.42–7.36 (m, 4 H), 7.34 (dd, J = 1.0, 8.5 Hz, 2 H), 7.21 (tt, J = 1.5, 7.5 Hz, 2 H), 7.16 (d, J = 7.5 Hz, 2 H), 6.98 (dd, J = 0.5, 8.0 Hz, 2 H), 6.93 (tt, J = 1.0, 8.5 Hz, 2 H), 6.81 (tt, J = 1.0, 7.0 Hz, 2 H), 6.76 (t, J = 7.5 Hz, 4 H), 6.56 (t, J = 7.0 Hz, 4 H), 6.33 (d, J = 7.0 Hz, 4 H), 6.14 (d, J = 7.5 Hz, 2 H), 5.95 (d, J = 7.0 Hz, 4 H) ppm; ^{13}C-NMR (125 MHz, $CDCl_3$): δ = 140.58, 140.57, 140.3, 139.4, 137.5, 137.4, 134.5, 134.1, 133.6, 132.7, 132.4, 130.9, 130.8, 130.1, 129.4, 129.2, 128.2, 127.6, 126.8, 126.3, 126.22, 126.19, 125.9, 125.7, 125.4, 125.0, 122.7, 121.4, 121.2 ppm; IR (KBr): $\tilde{\nu}$ = 3052, 2923, 1600, 1491, 1440, 1261, 1076, 1029, 809, 783, 759, 747, 700, 631 cm^{-1}; UV-Vis (CH_2Cl_2): λ_{max} (log ε) 248 (4.98), 306 (sh), 329 (5.20), 388 (4.63) nm; MS(FAB): *m/z* (%): 836 [M^++2] (18), 835 [M^++1] (42), 834 [M^+] (54), 757 (8); HRMS (FAB): calcd for $C_{66}H_{42}$: 834.3287; found: 834.3280.

Compound **131** (0.003g, 6%) was isolated as yellow solid, m.p. 251–253 °C (decomp); ^{1}H-NMR (500 MHz, $CDCl_3$): δ = 8.80 (d, J = 8.0 Hz, 1 H), 7.75 (dt, J = 1.0, 8.0 Hz, 1 H), 7.52 (dt, J = 1.0, 8.0 Hz, 1 H), 7.46 (d, J = 8.0 Hz, 1 H), 7.37 (d, J = 6.5 Hz, 1 H), 7.26–7.21 (m, 5 H), 7.21–7.16 (m, 2 H), 7.16–7.11 (m, 5 H), 7.09 (t, J = 7.5 Hz, 1 H), 7.05 (d, J = 8.0 Hz, 1 H), 6.99 (d, J = 7.0 Hz, 1 H), 6.19 (d, J = 6.0 Hz, 1 H), 6.14 (d, J = 6.0 Hz, 1 H) ppm; ^{13}C-NMR (125 MHz, $CDCl_3$): δ = 150.2, 149.2, 149.1, 149.0, 148.5, 144.4, 139.4, 139.2, 138.2, 137.1, 136.7, 135.1, 132.71, 132.68, 130.92, 130.88, 129.9, 128.98, 128.96, 128.3, 127.64, 127.60, 127.4, 126.54, 126.52, 126.1, 125.3, 124.5, 119.5, 118.4, 117.2, 113.8, 112.9 ppm, one peak is presumed to be accidentally isochronous in the region between δ = 130–124 ppm ; IR (KBr): $\tilde{\nu}$ = 3023, 2921, 1602, 1478, 1371, 1262, 1026, 809, 795, 748, 725, 695 cm^{-1}; UV-Vis (CH_2Cl_2): λ_{max} (log ε) 252 (4.73), 285 (4.56), 320 (4.53), 335 (4.62), 353 (4.37), 370 (4.32), 410 (3.76), 431 (3.72) nm; MS (FAB): *m*/*z* (%): 479 [M^++1] (27), 478 [M^+] (70), 300 (100); HRMS (FAB): calcd for $C_{38}H_{22}$: 478.1722; found: 478.1718.

Molecule **132** (0.002 g, 5 %) was acquired as a yellow solid; ^{1}H-NMR (500 MHz, $CDCl_3$): δ = 7.26–7.21 (m, 2 H), 7.16–7.09 (m, 6 H), 6.95–6.90 (m, 2 H), 6.76 (d, J = 8.0 Hz, 2 H), 6.73 (d, J = 7.5 Hz, 2 H), 6.71 (t, J = 7.5 Hz, 2 H), 6.65 (t, J = 7.0 Hz, 2 H), 6.58 (d, J = 6.5 Hz, 2 H), 6.48 (d, J = 6.5 Hz, 2 H) ppm; ^{13}C-NMR (125 MHz, $CDCl_3$): δ = 151.6, 151.0, 149.7, 149.0, 139.1, 137.2, 131.0, 130.3, 128.3, 128.1, 127.7, 127.5, 127.3, 126.4, 121.6, 116.8, 116.3 ppm; UV-Vis (CH_2Cl_2): λ_{max} (log ε) 254 (4.76), 294 (sh), 300 (4.65), 322 (sh), 338 (3.92), 376 (4.00) nm; MS (FAB): *m*/*z* (%): 479 [M^++1] (50), 478 [M^+] (86), 391 (100); HRMS (FAB): calcd for $C_{38}H_{22}$: 478.1722; found: 478.1723.

Adduct **133** (0.017 g, 33 %) was isolated as a red crystalline solid, m.p. 290–291 °C; ^{1}H-NMR (500 MHz, $CDCl_3$): δ = 8.00 (d, J = 8.0 Hz, 2 H), 7.20–7.13 (m, 6 H), 7.08–7.02 (m, 4 H), 6.90 (d, J = 8.0 Hz, 2 H), 6.48 (t, J = 7.0 Hz, 2 H), 6.42 (d, J = 7.0 Hz, 2 H), 6.23 (t, J = 7.0 Hz, 2 H), 3.93 (d, J = 7.0 Hz, 2 H) ppm; ^{13}C-NMR (100 MHz, $CDCl_3$): δ = 152.2, 150.9, 150.6, 149.6, 139.2, 135.9, 131.5, 130.9, 128.2, 127.8, 127.7, 126.6, 125.0, 123.2, 118.1, 116.6, 115.7 ppm; IR (KBr): $\tilde{\nu}$ = 3057, 1489, 1441, 1412, 1273,

1161, 810, 738, 709, 690, 623 cm^{-1}; UV-Vis (CH_2Cl_2): λ_{max} (log ε) 271 (4.74), 285 (4.69), 345 (4.60), 353 (4.54), 414 (4.83), 432 (3.81), 460 (3.63) nm; MS (70 eV): *m*/*z* (%): 479 [M^++1] (46), 478 [M^+] (100), 400 (10); HRMS (EI): calcd for $C_{38}H_{22}$: 478.1722; found: 478.1719.

Compound **134** (0.009 g, 27 %) was obtained as a yellow solid, m.p. 178–180 °C; the phenyl groups of this molecule located at the bay regions of the phenanthrene subunit are static while the others exhibit hindered rotation on the NMR time scale, ^{1}H-NMR (400 MHz, $CDCl_3$): δ = 8.80 (d, *J* = 8.8 Hz, 1 H), 8.79 (d, *J* = 8.8 Hz, 1 H), 8.63 (d, *J* = 9.2 Hz, 1 H), 8.34 (d, *J* = 8.0 Hz, 1 H), 7.70–7.58 (m, 1 H), 7.48–7.32 (m, 4 H), 7.27–7.21 (m, 2 H), 7.21–7.10 (m, 2 H), 7.06 (d, *J* = 8.0 Hz, 1 H), 7.02–6.91 (m, 3 H), 6.84 (t, *J* = 7.4 Hz, 1 H), 6.73 (br s, 2 H), 6.55 (t, *J* = 7.6 Hz, 2 H), 6.50–6.38 (m, 3 H), 6.30–6.10 (m, 4 H), 5.90 (d, *J* = 7.6 Hz, 2 H), 4.10 (d, *J* = 6.8 Hz, 1 H) ppm; ^{13}C-NMR (125 MHz, $CDCl_3$): δ = 152.7, 151.0, 150.9, 149.4, 140.3, 140.0, 139.9, 139.6, 137.3, 137.1, 133.9, 133.5, 133.0, 132.5, 132.4, 131.7, 130.9, 130.6, 130.5, 130.4, 129.9, 129.5, 129.1, 128.3, 128.2, 128.1, 127.7, 127.5, 127.2, 126.9, 126.8, 126.32, 126.27, 126.1, 125.62, 125.56, 125.4, 125.3, 123.9, 122.6, 121.6, 120.9, 118.0, 116.2, 115.4 ppm, three peaks are presumed to be accidentally isochronous in the region δ = 128–125 ppm; IR (KBr): $\tilde{\nu}$ = 2964, 1262, 1096, 1022, 801, 701 cm^{-1}; UV-Vis (CH_2Cl_2): λ_{max} (log ε) 267 (5.01), 303 (4.97), 335 (4.89), 361 (sh), 379 (4.64), 427 (4.02), 456 (3.77) nm ; MS(FAB): *m/z* (%): 658 [M^++2] (22), 657 [M^++2] (67), 656 [M^+] 1(00), 579 (12), 502 (7); HRMS (FAB): calcd for $C_{52}H_{32}$: 656.2504; found: 656.2492.

Cycloaddition reaction between [7]heliphene **142** and diphenylacetylene **88**:

In a glovebox, a round bottom flask was charged with **142** (0.008 g, 0.152 mmol) and Ni(COD)(PMe_3)$_2$ (0.001 g, 0.003 mmol). The mixture was then dissolved in THF (25 mL). A reflux condenser fitted with a vacuum line adapter was attached to the flask. The assembly was sealed, removed from the glovebox, connected to the vacuum line, flushed with Ar, and the glass stopper quickly replaced with a septum under a purge of Ar. A solution of diphenylacetylene **88** (0.016 g, 3.00 mmol) in THF (10 mL) was taken up in a gas-tight syringe and slowly added over 12 h via syringe pump to the boiling mixture of **142**/Ni(COD)(PMe_3)$_2$. Upon complete addition of the diphenylacetylene solution, the reaction mixture was stirred at reflux for an extra 12 h. After this time, it was cooled to RT, and the solvent removed by rotary evaporation to give an orange residue. The crude product was chromatographed on silica gel (2.5 x 16.5 cm), eluting first with hexane/CH_2Cl_2 (10:1, then 5:1). The first product collected was diphenylacetylene **88** (0.005 g), followed by a yellow band. Analysis of the isolated yellow solid (0.002 g) revealed a large mixture of products; MS(FAB): *m/z* (%): 532 (70), 664 (25), 700 (13), 732 (16), 911 (21), 1056 (11), 1234 (4), 1412 (5).

4.6 Computational Details for Chapter Three

All geometries of intermediates and transition states were optimized fully without symmetry constraints using the Gaussian 03 program.[100] The DFT computations were carried out using the B3LYP functional as implemented in Gaussian. The nickel atom was described by a double-zeta basis set (LANL2DZ),[113] and the 6-31G(d) basis set[114]

was used for the other elements. Frequency calculations were performed to confirm the nature of the stationary points and to obtain zero-point energies (ZPE). The connectivity between stationary points was established by intrinsic reaction coordinate calculations (IRC). The Chemcraft program[102] was used to draw the calculated structures.

4.7 References

1) Harvey, R. G. *Polycyclic Aromatic Hydrocarbons*; Wiley-VCH: New York, 1997.
2) (a) *Chem. Rev.* **2001**, *101,* 1115–1566, Special Issue: Aromaticity. (b) *Chem. Rev.* **2005**, *105*, 3343–3397, Special Issue: Delocalization-Pi and Sigma.
3) (a) Cyranski, M. K.; Krygowski, T. M.; Katritzky, A. R; Schleyer, P. von R. *J. Org. Chem*. **2002**, *67*, 1333. (b) Stanger, A. *Chem. Commun.* **2009**, 1939.
4) (a) Minkin, V. I.; Glukhovtsev, M. N.; Simkin, B. Ya. *Aromaticity and Antiaromaticity: Electronic and Structural Aspects;* Wiley: New York, 1994; pp 63–74. (b) Garratt, P. J. *Aromaticity*; Wiley: New York, 1986; pp 30–34, 93–95.
5) (a) Wu, J.; Müllen, K. In *Carbon Rich Compounds: Molecules to Materials*; Haley, M. M.; Tykwinski, R. R., Eds.; Wiley-VCH: Weinheim, 2006; Chapter 3, pp 90–139. (b) Wu, J.; Pisula, W.; Müllen, K. *Chem. Rev.* **2007**, *107*, 718. (c) *Handbook of Organic Electronics and Photonics*; Nalwa, H. S., Ed.; American Scientific, 2008.
6) Miljanić, O. Š.; Vollhardt, K. P. C. In *Carbon Rich Compounds: Molecules to Materials*; Haley, M. M.; Tykwinski, R. R., Eds.; Wiley-VCH: Weinheim, 2006; Chapter 4, pp 140–197.
7) (a) Shepherd, M. K. *Cyclobutarenes. The Chemistry of Benzocyclobutene, Biphenylene, and Related Compounds*; Elsevier: Amsterdam, 1991. (b) Toda, F.; Garratt, P. J. *Chem. Rev.* **1992**, *92*, 1685.
8) (a) Diercks, R.; Vollhardt, K. P. C. *J. Am. Chem. Soc.* **1986**, *108*, 3150. (b) Mohler, D. L.; Vollhardt, K. P. C.; Wolff, S. *Angew. Chem., Int. Ed. Engl.* **1990**, *29*, 1151. (c) Mohler, D. L.; Vollhardt, K. P. C.; Wolff, S. *Angew. Chem., Int. Ed. Engl.* **1995**, *34*, 563.
9) (a) Holmes, D.; Kumaraswamy, S.; Matzger, A. J.; Vollhardt, K. P. C. *Chem. Eur. J.* **1999**, *5*, 3399. (b) Dosche, C.; Kumke, M. U.; Ariese, F.; Bader, A. N.; Gooijer, C.; Dosa, P. I.; Han, S.; Miljanic, O. Š.; Vollhardt, K. P. C.; Puchta, R.; van Eikema Hommes, N. J. R. *Phys. Chem. Chem. Phys.* **2003**, *5*, 4563. (c) Wagner, H.-U.; Szeimies, G.; Chandrasekhar, J.; Schleyer, P. von R.; Pople, J. A.; Binkley, J. S. *J. Am. Chem. Soc.* **1978**, *100*, 1210.
10) Han, S.; Bond, A. D.; Disch, R. L.; Holmes, D.; Schulman, J. M.; Teat, S. J.; Vollhardt, K. P. C.; Whitener, G. D. *Angew. Chem. Int. Ed.* **2002**, *41*, 3223.
11) Jackman, L. M.; Sondheimer, F.; Amiel, Y.; Ben-Efraim, D. A.; Gaoni, Y.; Wolovsky, R.; Bothner-By, A. A. *J. Am. Chem. Soc*. **1962**, *84*, 4307.
12) Untch, K. G.; Wysocki, D. C. *J. Am. Chem. Soc*. **1967**, *89*, 6386.
13) (a) Chen, Z.; Wannere, S. C.; Corminboeuf, C.; Puchta, R.; Schleyer, P. von R. *Chem. Rev.* **2005**, *105*, 3842 and the references therein. (b) Steinmann, S. N.; Jana, D. F.; Wu, J. I.-C.; Schleyer, P. v. R.; Mo, Y.; Corminboeuf, C. *Angew. Chem. Int. Ed.* **2009**, *48*, 9828.
14) Schleyer, P. v. R.; Manoharan, M.; Wang, Z.-X.; Kiran, B.; Jiao, H.; Puchta, R.; van Eikema Hommes, N. J. R. *Org. Lett.* **2001**, *3*, 2465.

15)Schulman, J. M.; Disch, R. L.; Jiao, H.; Schleyer, P. v. R. *J. Phys. Chem. A* **1998**, *102*, 8051.
16)Jeany, H.; Mason, K. G.; Sketchley, J. M. *Tetrahedron Lett.* **1970**, *11*, 485.
17)Brown**,** F. C.; Choi, N.; Coulston**,** K. J.; Eastwood, F. W.; Wiersum, U. E.; Jenneskens, L. W. *Tetrahedron Lett.* **1994**, *35*, 4405.
18)(a) Linear [3]phenylene: Dosa, P. I.; Schleifenbaum, A.; Vollhardt, K. P. C. *Org. Lett.* **2001**, *3*, 1017. (b) Angular [3]phenylene: Matzger, A. J.; Vollhardt, K. P. C. *Chem. Commun.* **1997**, 1415. (c) Angular [4]phenylene: Dosa, P. I.; Gu, Z.; Hager, D.; Karney, W. L.; Vollhardt, K. P. C. *Chem. Commun.* **2009**, 1967.
19)Perthuisot, C.; Edelbach, B. L.; Zubris, D. L.; Simhai, N.; Iverson, C. N.; Müller, C.; Satoh, T.; Jones, W. D. *J. Mol. Catal., A* **2002**, *189*, 157.
20)Dosche, C.; Löhmannsröben, H.-G.; Bieser, A.; Dosa, P. I.; Han, S.; Iwamoto, M.; Schleifenbaum, A.; Vollhardt, K. P. C. *Phys. Chem. Chem. Phys.* **2002**, *4*, 2156.
21)(a) Deniz, A. A.; Peters, K. S.; Snyder G. J. *Science* **1999**, *286,* 1119. (b) Fattahi, A.; Lis, L.; Tian, Z.; Kass, P. S. *Angew. Chem. Int. Ed.* **2006**, *45*, 4984. (c) Bally, T. *Angew. Chem. Int. Ed.* **2006**, *45*, 6616.
22)Anslyn, E.; Dougherty, D. *Modern Physical Organic Chemistry*; University Science Books: Palo Alto, 2006.
23)Crabtree, R. H. *The Organometallic Chemistry of the Transition Metals*; *4th Ed*.; Wiley-VCH: New York, 2005.
24)Mestdagh, H. *Postdoctoral Research Report*, University of California, Berkeley, **1986**.
25)Hirthammer, M.; Vollhardt, K. P. C. *J. Am. Chem. Soc.* **1986**, *108*, 2481.
26)Blanco, L.; Helson, H. E.; Hirthammer, M.; Mestdagh, H.; Spyroudis, S.; Vollhardt, K. P. C. *Angew. Chem.*, *Int. Ed. Engl.* **1987**, *26*, 1246.
27)Berris, B. C.; Hovakeemian, G. H.; Lai, Y.-H., Mestdagh, H.; Vollhardt, K. P. C. *J. Am. Chem. Soc.* **1985**, *107*, 5670.
28)Dosa, P. I. *The Chemistry of Angular and Linear [N]Phenylenes*; Ph.D. Thesis, University of California, Berkeley, **2002**.
29)Diercks, R.; Eaton, B. E.; Gürtzgen, S.; Jalisatgi, S.; Matzger, A. J.; Radde, R. H.; Vollhardt, K. P. C. *J. Am. Chem. Soc.* **1998**, *120*, 8247.
30)(a) Nambu, M.; Siegel, J. S. *J. Am. Chem. Soc.* **1988**, *110*, 3675. (b) Nambu, M.; Hardcastle, K.; Baldridge, K. K.; Siegel, J. S. *J. Am. Chem. Soc.* **1992**, *114*, 369.
31)Nambu, M.; Mohler, D. L.; Hardcastle, K.; Baldridge, K. K.; Siegel, J. S. *J. Am. Chem. Soc.* **1993**, *115*, 6138.
32)Kumaraswamy, S.; Jalisatgi, S. S.; Matzger, A. J.; Miljanić, O. Š.; Vollhardt, K. P. C. *Angew. Chem. Int. Ed.* **2004**, *43*, 3711.
33)(a) Eisch, J. J.; Piotrowski, A. M.; Han, K. I.; Krüger, C.; Tsay, Y. H. *Organometallics* **1985**, *4*, 224. (b) Schwager, H.; Spyroudis, S.; Vollhardt, K. P. C. *J. Organometallic Chem.* **1990**, *382*, 191.
34)Albright, T. A.; Hofmann, P.; Hoffmann, R.; Lillya, C. P.; Dobosh, P. A. *J. Am. Chem. Soc.* **1983**, *105*, 3397.
35)Dötz, K. H.; Jahr, H. C.; *Chem. Rec.* **2005**, *4*, 61.
36)Gridnev, I. D. *Coord. Chem. Rev.* **2008**, *252*, 1798.
37)Eickmeier, C.; Holmes, D.; Junga, H.; Matzger, A. J.; Scherhag, F.; Shim, M.; Vollhardt, K. P. C. *Angew. Chem., Int. Ed. Engl.* **1999**, *38*, 800.

38) Großmann, T. N. *Haptotropism in Linear Phenylene Complexes*; Diplomarbeit Thesis, University of California, Berkeley, **2004**.
39) Dinculear photothermal haptotropic systems: Tsuchiya, K.; Ideta, K.; Mogi, K.; Sunada, Y.; Nagashima, H. *Dalton Trans.* **2008**, 2708, and the references therein.
40) Additive assisted photothermal haptotropic systems: (a) Jahr, H. C.; Nieger, M.; Dötz, H. K. *Chem. Eur. J.* **2005**, 11, 5333. d) Herbert, D. E.; Tanabe, M.; Bourke, S. C.; Lough, A. J.; Manners, I. *J. Am. Chem. Soc.* **2008**, *130*, 4166; e) leong, N. S.; Manners, I. *J. Organomet. Chem.* **2008**, *693*, 802, and references therein.
41) (a) Zhu, G.; Tanski, T. M.; Churchill, D. G.; Janak, K. E.; G. Parkin, G*. J. Am. Chem. Soc.* **2002**, *124*, 13658. (b) Zhu, G.; Pang, G.; Parkin, G*. J. Am. Chem. Soc.* **2008**, *130*, 1564.
42) Selected reviews of photobased devices and molecular switches: (a) Balzani, V.; Credi, A.; Venturi, M. *Chem. Soc. Rev.* **2009**, *38*, 1542. (b) Kay, E. R.; Leigh, D. A.; Zerbetto, F. *Angew. Chem. Int. Ed.* **2007**, *46*, 72. (c) *Photochromism, Molecules and Systems*; Dürr, H.; Bouas-Laurent, H., Eds.; Elsevier: Amsterdam, 2003. (d) Feringa, B. *Molecular Switches*; Wiley-VCH: Weinheim, 2001.
43) (a) a) *Photofunctional Transition Metal Complexes*; Yam, V. W. W., Ed.; Springer, Berlin, 2007. b) Coppens, P.; Novozhilova, I.; Kovalevsky, A. *Chem. Rev.* **2002**, *102*, 861. c) Gütlich, P.; Garcia, Y.; Woike, T. *Coord. Chem. Rev.* **2001**, *219–221*, 839.
44) (a) Lambert, J. B.; Mazozola, E. P. *Nuclear Magnetic Resonance Spectroscopy: An Introduction to Princples, Applications, and Experimental Methods*; Pearson Education: Upper Saddle River, 2004 (b) Berger, S.; Braun, S. *200 and More NMR Experiments: A Practical Course*; Wiley-VCH: Weinheim, 2004. (c) Friebolin, H. *Basic One- and Two-Dimensional NMR Spectroscopy*, 4th edition; Wiley-VCH: Weinheim, 2005.
45) (a) Schulman, J. M.; Disch, R. L. *J. Phys. Chem. A* **2003**, *107*, 5223. (b) Schulman, J. M.; Disch, R. L. *J. Am. Chem. Soc.* **1996**, *118*, 8470 and the references cited therein.
46) (a) Bursten, B. E.; Fenske, R. F. *Inorg. Chem.* **1979**, *18*, 1760. (b) Chinn, J. W. Jr.; Hall, M. B. *Inorg. Chem.* **1983**, *22*, 2759. (c) Datta, A.; Pati, S. K. *J. Am. Chem. Soc.* **2005**, *127*, 3496.
47) Ooloba, K. *Haptotropic Shifts in the Linear [N]-Phenylene (N=3, 4, and 5) and Angular [3]-Phenylene Cyclopentadienylcobalt Complexes*; Ph.D. Thesis, University of Houston, **2008**.
48) Hillard III, R. L.; Vollhardt, K. P. C. *J. Am. Chem. Soc.,* **1977**, *99*, 4058.
49) Berris, B. C.; Lai, Y-H.; Vollhardt, K. P. C*. J. Chem. Soc., Chem. Commun.* **1982**, 953.
50) (a) Rausch, M. D.; Genetti, R. A.; *J. Org. Chem.* **1970**, *35*, 3888. (b) Hart, W. P.; Rausch, D. M.; *J. Organometallic. Chem.* **1988**, *355*, 455.
51) Duclos, R. I.; Vollhardt, K. P. C.; Yee, J. L. S. *J. Organomet. Chem.* **1979**, *174*, 109.
52) (a) Myers, A. G.; Sogi, M.; Lewis, M. A.; Arvedson, S. P. *J. Org. Chem.* **2004**, *69*, 2516. (b) Wolfart, V.; Ramming, M.; Gleiter, R.; Nuber, B.; Pritzkow, H.; Rominger, F. *Eur. J. Inorg. Chem.* **1999**, 499. (c) Mitchell, R. H.; Chen, Y.; Khalifa, N.; Zhou, P. *J. Am. Chem. Soc.* **1998**, *120*, 1785. (d) McGlinchey, M. J.; Burns, R. C.; Hofer, R.; Top, S.; Jaouen, G. *Organometallics* **1986**, *5*, 104.
53) Feixas, F.; Jiménez-Halla, J. O. C.; Matito, E.; Poater, J.; Solà, M. *Pol. J. Chem.*

2007, *81*, 783.
54)(a)Stanger, A. *J. Org. Chem.* **2006**, *71*, 883. (b) Stanger, A. *Chem. Eur. J.* **2006**, *12*, 2745. (c) Tsipis, A. C. *Phys. Chem. Chem. Phys.* **2009**, *11*, 8244. (d) Stanger, A. *Chem. Commun.* **2009**, 1939.
55)For very recent literature compilations of theoretical (and experimental) treatments of haptotropism in arene metal complexes, see: a) Joistgen, O; Pfletschinger, A.; Ciupka, J.; Dolg, M.; Nieger, M.; Schnakenburg, G.; Fröhlich, R.; Kataeva, O.; Dötz, K. H. *Organometallics* **2009**, *28*, 3473; b) Pfletschinger, A.; Dolg, N. *J. Organomet. Chem.* **2009**, *694*, 3338; c) Jiménez-Halla, J. O. C.; Robles, J.; Solà, M. *Organometallics* **2008**, *27*, 5230; d) Kirillov, E.; Kahlal, S.; Roisnel, T.; Georgelin, T.; Saillard, J.-Y.; Carpentier, J.-F. *Organometallics* **2008**, *27*, 387 and references therein.
56)Jiménez-Halla, J. O. C.; Robles, J.; Solà, M. *J. Phys. Chem. A.* **2008**, *112*, 1202.
57)Oprunenko, Y.; Gloriozov, I.; Lyssenko, K.; Malyugina, S.; Mityuk, D.; Mstislavsky, V.; Günther, H.; von Firks, G.; Ebener, M. *J. Organomet. Chem.* **2002**, *656*, 27.
58)Müller, J.; Gaede, P. E.; Qiao, K. *J. Organomet. Chem.* **1994**, *480*, 213.
59)Bianchini, C.; Caulton, K. G.; Chardon, C.; Doublet, M. L.; Eisenstein, O.; Jackson, S. A.; Johnson, T. J.; Meli, A.; Peruzzini, M.; Streib, W. E., Vacca, A.; Vizzat, F. *Organometallics* **1994**, *13*, 2010.
60)(a) De Boer, E.; Van Willigen, H. V. *Prog. Nuc. Mag. Res. Spec.* **1967**, *2,* 111. (b) Memory, J. D.; Wilson, N. K. *NMR of Aromatic Compounds*; Wiley-VCH: New York, 1982.
61)(a) Poli, R. *Chem. Rev.* **1996**, *96*, 2135 and the references cited therein. (b) Schröder, D.; Shaik, S.; Schwartz, H. *Acc. Chem. Res.* **2000**, *33*, 139. (c) Harvey, J. N.; Poli, R.; Smith, K. M. *Coord. Chem. Rev.* **2003**, 237, 347 and the references cited therein.
62)For computational examples of 16 electron triplet Cp cobalt species influencing cobalt-mediated reactions, see: (a) Siegbahn, P. E. M. *J. Am. Chem. Soc.* **1996**, *118*, 1487. (b) Poli, R.; Smith, K. M. *Eur. J. Inorg. Chem.* **1999**, 877. (c) Carreón-Macedo, J.-L.; Harvey, J. N. *J. Am. Chem. Soc.* **2004**, *126*, 5789. (d) Petit, A.; Richard, P.; Cacelli, I.; Poli, R. *Chem. Eur. J.* **2006**, *12*, 813. (e) Aubert, C.; Betschmann, P.; Eichberg, M. J.; Gandon, V.; Geny, A.; Heckrodt, T. J.; Lehmann, J.; Malacria, M.; Masjost, B.; Paredes, E.; Vollhardt, K. P. C.; Whitener, G. D. *Chem. Eur. J.* **2007**, *13*, 7443. (f) Gandon, V.; Agenet, N.; Vollhardt, K. P. C.; Malacria, M.; Aubert, C. *J. Am. Chem. Soc.* **2009**, *131*, 3007.
63)Illustrative examples: (a) Olson, W. L.; Stacy, A. M.; Dahl, L. F. *J. Am. Chem. Soc.* **1986**, *108*, 7646. (b) Wadepohl, H.; Galm, W.; Pritzkow, H.; Wolf, A. *Chem. Eur. J.* **1996**, *2*, 1453. (c) Knijnenburg, W.; Hetterscheid, D.; Kooistra, T. M.; Budzelaar, P. H. M. *Eur. J. Inorg. Chem.* **2004**, 1204.
64)Benito-Garagorri, D.; Bernskoetter, W. H.; Lobkovsky, E.; Chirik, P. J. *Organometallics* **2009**, *28*, 4807.
65)Fox, J. P.; Ramdhanie B.; Zareba, A. A.; Czernuszewicz, R. S.; Goldberg, D. P. *Inorg. Chem.* **2004**, *43*, 6600.
66)Guennic, B. L.; Floyd, T.; Galan, B. R.; Autschbach, J.; Keister, J. B. *Inorg. Chem.* **2009**, *48*, 5504.
67)Cremer, C.; Burger, P. *J. Am. Chem. Soc.* **2003**, *125*, 7664.

68)Atkins, P.; de Paula, J. P. *Physical Chemistry*, 8th Edition; Oxford University Press, Oxford, 2006.
69)Butters, T.; Toda, F.; Winters, W. *Angew. Chem., Int. Ed. Engl.* **1980**, *19*, 926.
70)Mann, B. E.; Taylor, B. F. *^{13}C Data for Organometallic Compounds*; Academic, London, 1981.
71)For a review on triple decker arene complexes and closely related *syn* dinuclear systems, see: (a) Beck, V.; O'Hare, D. *J. Organomet. Chem*. **2004**, *698*, 3920, and the references therein. For a review of trinuclear CpCo(arene) complexes, see: (b) Wadepohl, H. *Angew. Chem., Int. Ed. Engl.* **1992**, *31*, 247 and the references therein.
72)Jonas, K.; Koepe, G.; Schieferstein, L.; Mynott, R.; Krüger, C.; Tsay Y.-H. *Angew. Chem., Int. Ed. Engl.* **1983**, *22*, 620; *Angew. Chem. Suppl.* **1983**, 920.
73)Müller, J.; Gaede, P. E.; Qiao. K. *Angew. Chem.*, *Int. Ed. Engl.* **1993**, *32*, 1697.
74)Schneider, J. J.; Wolf, D.; Janiak, C.; Heinemann, O.; Rust, J.; Krüger, C. *Chem. Eur. J.* **1998**, *4*, 1982.
75)Schneider, J. J.; Denninger, U.; Heinemann, O.; Krüger, C. *Angew. Chem.*, *Int. Ed. Engl.* **1995**, *34*, 592.
76)Budzelaar, P. H. M.; Moonen, N. N. P.; de Gelder, R.; Smits, J. M. M.; Gal, A. W. *Chem. Eur. J.* **2000**, *6*, 2740.
77)Albright, T. A.; Dosa, P. I.; Großmann, T. N.; Oluwakemi, O.; Padilla, R.; Paubelle, R.; Timofeeva, T.; Vollhardt, K. P. C. *Angew. Chem. Int. Ed.* **2009**, *48*, 9853.
78)Schaub, T.; Radius, U. *Chem. Eur. J.* **2005**, *11*, 5024.
79)Edelbach, B. L.; Lachicotte, R. J.; Jones, W. D. *Organometallics* **1999**, *18*, 4660.
80)(a) Edelbach, B. L.; Lachicotte, R. J.; Jones, W. D. *Organometallics* **1999**, *18*, 4040. (b) Müller, C.; Lachicotte, R. J.; Jones, W. D. *Organometallics* **2002**, *21*, 1975.
81)Martin, R. H. *Angew. Chem.*, *Int. Ed. Engl.* **1974**, *13*, 649.
82)Mallory, F.B.; Butler, K. E.; Evans, A.C.; Mallory, C.W. *Tetrahedron Lett.* **1996**, *37*, 7176.
83)Selected Reviews: (a) Amemiya, R.; Yamaguchi, M. *Chem. Rec.* **2008**, *8*, 116. (b) Rulíšek, L.; Exner, O.; Cwiklik, L.; Jungwirth, P.; Starý, I.; Pospíšil, L.; Havlas, Z. *J. Phys. Chem. C.* **2007**, *111*, 14948. (c) Hopf, H. *Classics in Hydrocarbon Chemistry*, Wiley-VCH, Weinheim, 2000, pp 321–330. (d) Vögtle, F. *Fascinating Molecules in Organic Chemistry*, Wiley, New York, 1992, pp 156–180. (e) Meurer, K. P.; F. Vögtle, *Top. Curr. Chem.* **1985**, *127*, 1. (f) Laarhoven, W. H.; Prinsen, W. J. *Top. Curr. Chem.* **1984**, *125*, 63.
84)(a) Mallory, F.B.; Butler, K. E.; Mallory, C.W; Bérubé, A.; Luzik, E. D.; Brondyke, E. J.; Hiremath, R.; Ngo, P.; Carroll, P. J.; *Tetrahedron* **2001**, *57,* 3715. (b) Mallory, F. B.; Butler, K. E.; Evans, A. C.; Brondyke, E. J.; Mallory, C. W.; Yang, C.; Ellenstein, A. *J. Am. Chem. Soc.* **1997**, *119*, 2119.
85)(a) Mitsuhashi, R.; Suzuki, Y.; Yamanari, Y.; Mitamura, H.; Kambe, T.; Ikeda, N.; Okamoto, H.; Fujiwara, A.; Yamaji, M.; Kawasaki, N.; Maniwa, Y.; Kubozono, Y. *Nature* **2010**, *464*, 74. (b) Okamoto, H.; Kawasaki, N.; Kaji, Y.; Kubozono, Y.; Fujiwara, A.; Yamaji, M.; *J. Am. Chem. Soc.* **2008**, *130*, 10470. (c) Tian, Y. H.; Park, G.; Kertesz, M. *Chem. Mater.* **2008**, *20*, 3266.
86)Recent reviews of acenes in electronic applications: (a)Yamashita, Y. *Sci. Technol. Adv. Mater.* **2009**, *10*, 024313. (b) Würthner, F.; Schmidt, R. *ChemPhysChem.*

2006, *7*, 793. (c) Bendikov, M.; Wudl, F. *Chem. Rev.* **2004**, *104*, 4891.
87) NICS-based comparison of phenacene and acene properties: Portella, G.; Poater, P.; Bofill, J. M.; Alemany, P.; Solà, M. *J. Org. Chem.* **2005**, *70*, 2509 and the references therein.
88) Mallory, F. B.; Mallory, C. W. *Org*. *React*. **1984**, *30*, 1.
89) Gu, Z. *Nickel-Catalyzed Cycloaddition Reaction of [N]Phenylenes and Alkynes*; Postdoctoral Report, University of California, Berkeley, **2008**
90) Preferential displacement of COD by π ligands from $Ni(COD)(PMe_3)_2$ is well documented. See, e.g. Karsch, H. H.; Leithe, A. W.; Reisky, M.; Witt, E. *Organometallics* **1999**, *18*, 90.
91) (a) Bochmann, M.; Hawkins, I.; Hursthouse, M. B.; Short, R. L. *J. Chem. Soc.*, *Dalton Trans.* **1990**, 1213. (b) Poerschke, K. R.; Mynott, R.; Angermund, K.; Krüger, C. *Z. Naturforsch.* **1990**, *40B*, 199. See also: (c) Bartik, T.; Happ, B.; Iglewsky, M.; Bandmann, H.; Boese, R.; Heimbach, P.; Hoffmann, T.; Wenschuh, E. *Organometallics* **1992**, *11*, 1235.
92) For Ni-phosphine migrations along polycyclic benzenoid ligands, see, e.g. Stanger, A.; Vollhardt, K. P. C. *Organometallics* **1992**, *11*, 317.
93) Edelbach, B. L.; Vicic, D. A.; Lachicotte, R. J.; Jones, W. D. *Organometallics* **1998**, *17*, 4784.
94) (a) Feiken, N.; Pregosin, P. S.; Trabesinger, G.; Scalone, M. *Organometallics* **1997**, *16*, 537. (b) Feiken, N.; Pregosin, P. S.; Trabesinger, G.; Albinati, A.; Evoli, G. L. *Organometallics* **1997**, *16*, 5756. (c) Geldbach, T. J.; Pregosin, P. S. *Eur. J. Inorg. Chem.* **2002**, 1907.
95) Cheng, T.-Y.; Szalda, D. J.; Hanson, J. C.; Muckerman, J. T.; Bullock, R. M. *Organometallics* **2008**, *27,* 3785.
96) (a) Grimme, S.; Harren, J.; Sobanski, A.; Vögtle, F. *Eur. J. Org. Chem.* **1998**, *8*, 1491. (b) Dias, J. *J. Chem. Inf. Model.* **2005**, *45*, 562.
97) Still, W. C.; Mitra, A.; Kahn, M. *J. Org. Chem.* **1978**, *43*, 2923.
98) (a) Leonard, J.; Lygo, B.; Procter, G. *Advanced Practical Organic Chemistry*, 2nd ed.; CRC Press: Boca Raton 1998. (b) Errington, R. J. *Advanced Practical Inorganic Chemistry and Metalorganic Chemistry*; Chapman and Hill: London 1997
99) Jonas, K.; Deffense, E.; Habermann, D. *Angew. Chem.*, *Int. Ed. Engl.* **1983**, *22*, 716.
100) Gaussian 03, Revision B.03, M. J. Frisch, G. W. Trucks, H. B. Schlegel, G. E. Scuseria, M. A. Robb, J. R. Cheeseman, J. A. Montgomery, Jr., T. Vreven, K. N. Kudin, J. C. Burant, J. M. Millam, S. S. Iyengar, J. Tomasi, V. Barone, B. Mennucci, M. Cossi, G. Scalmani, N. Rega, G. A. Petersson, H. Nakatsuji, M. Hada, M. Ehara, K. Toyota, R. Fukuda, J. Hasegawa, M. Ishida, T. Nakajima, Y. Honda, O. Kitao, H. Nakai, M. Klene, X. Li, J. E. Knox, H. P. Hratchian, J. B. Cross, C. Adamo, J. Jaramillo, R. Gomperts, R. E. Stratmann, O. Yazyev, A. J. Austin, R. Cammi, C. Pomelli, J. W. Ochterski, P. Y. Ayala, K. Morokuma, G. A. Voth, P. Salvador, J. J. Dannenberg, V. G. Zakrzewski, S. Dapprich, A. D. Daniels, M. C. Strain, O. Farkas, D. K. Malick, A. D. Rabuck, K. Raghavachari, J. B. Foresman, J. V. Ortiz, Q. Cui, A. G. Baboul, S. Clifford, J. Cioslowski, B. B. Stefanov, G. Liu, A. Liashenko, P. Piskorz, I. Komaromi, R. L. Martin, D. J. Fox, T. Keith, M. A. Al-Laham, C. Y. Peng, A. Nanayakkara, M. Challacombe, P. M. W. Gill, B. Johnson, W. Chen, M. W. Wong, C. Gonzalez, J. A. Pople, Gaussian, Inc., Pittsburgh PA,

2003.
101) www.gaussian.com
102) www.chemcraftprog.com
103) Becke, A. D. *J. Chem. Phys.* **1993**, *98*, 5648.
104) Lee, C.; Yang, W.; Parr, G. R. *Phys. Rev. B* **1988**, *37*, 785.
105) Binkley, J. S.; Pople, J. A.; Hehre, W. J. *J. Am. Chem. Soc.* **1980**, *102*, 939 for hydrogen, and Gordon, M. S.; Binkley, J. S.; Pople, J. A.; Pietro, W. J.; Hehre, W. J. *J. Am. Chem. Soc.* **1983**, *104*, 2797.
106) Hay, P. J.; Wadt, W. R. *J. Chem. Phys.* **1985**, *82*, 270.
107) Hehre, W. J.; Ditchfield, R.; Pople, J. A. *J. Chem. Phys. B* **1972**, *56*, 2257.
108) Curtiss, L. A.; McGrath, M. P.; Blaudeau, J.-P.; Davis, N. E.; Binning, R. C. Jr.; Radom, L. *J. Chem. Phys.* **1995**, *103*, 6104.
109) A. W. Ehlers, M. Böhme, S. Dapprich, A. Gobbi, A. Höllwarth, V. Jonas, K. F. Köhler, R. Stegmann, A. Veldkamp, G. Frenking, *Chem. Phys. Lett.* **1993**, *208*, 111.
110) QST is a synchronous transit approach to the quadratic region around the transition state structure. For details, see: (a) J. B. Foresman, A. Frisch in *Exploring Chemistry with Electronic Structure Methods: A Guide to Using Gaussian*; Gaussian, Inc.: Pittsburgh, PA, USA, 1996; (b) H. B. Schlegel in *Ab Initio Methods in Quantum Chemistry,* Part I; Wiley: Chichester, 1987.
111) Gu, Z. *The Improvement of Total Synthesis of Angular [4]Phenylene and Its Flash Vacuum Pyrolysis (FVP) Study*; Postdoctoral Report, University of California, Berkeley, **2008.**
112) Schwager, H. Postdoctoral Research Report, University of California, Berkeley, **1987.**
113) Küchle, W.; Dolg, M.; Stoll, H.; Preuss, H. *Mol. Phys.* **1991**, *74***,** 1245.
114) (a) Hariharan, P. C.; Pople, J. A. *Theor. Chim. Acta* **1973**, *28*, 213. (b) Francl, M. M.; Petro, W. J.; Hehre, W. J.; Binkley, J. S.; Gordon, M. S.; DeFrees, D. J.; Pople, J. A. *J. Chem. Phys*. **1982**, *77*, 3654. (c) Rassolov, V.; Pople, J. A.; Ratner, M.; Windus*,* T. L. *J. Chem. Phys.* **1998**, *109*, 1223.